PREDICTIVE MODELING OF METAL-CATALYZED POLYOLEFIN PROCESSES

Neeraj Prasad Khare

Dissertation submitted to the Faculty of the Virginia Polytechnic Institute and State University in partial fulfillment of the requirements for the degree of

DOCTOR OF PHILOSOPHY

in

Chemical Engineering

10:00 AM

November 14, 2003

143-B Randolph Hall

Blacksburg, VA

Dr. Y. A. Liu, Chairman (Chemical Engineering)

Dr. Richey M. Davis (Chemical Engineering)

Dr. Donald G. Baird (Chemical Engineering)

Dr. James E. McGrath (Chemistry)

Dr. Slimane Adjerid (Mathematics)

Keywords: Ziegler-Natta, metallocene, polymerization kinetics, model, simulation, reactor, polyethylene, polypropylene, physical properties, phase equilibrium.

Predictive Modeling of Metal-Catalyzed Polyolefin Processes

Neeraj Prasad Khare

Abstract

This dissertation describes the essential modeling components and techniques for building comprehensive polymer process models for metal-catalyzed polyolefin processes. The significance of this work is that it presents a comprehensive approach to polymer process modeling applied to large-scale commercial processes. Most researchers focus only on polymerization mechanisms and reaction kinetics, and neglect physical properties and phase equilibrium. Both physical properties and phase equilibrium play key roles in the accuracy and robustness of a model.

This work presents the fundamental principles and practical guidelines used to develop and validate both steady-state and dynamic simulation models for two large-scale commercial processes involving the Ziegler-Natta polymerization to produce high-density polyethylene (HDPE) and polypropylene (PP). It also provides a model for the solution polymerization of ethylene using a metallocene catalyst. Existing modeling efforts do not include physical properties or phase equilibrium in their calculations. These omissions undermine the accuracy and predictive power of the models.

The forward chapters of the dissertation discuss the fundamental concepts we consider in polymer process modeling. These include physical and thermodynamic properties, phase equilibrium, and polymerization kinetics. The later chapters provide the modeling applications described above.

Table of Contents

List of Figures

List of Tables

Chapter 1 Introduction

The focus of this work is the modeling of processes involving the polymerization of olefins using Ziegler-Natta and metallocene catalysts. Modeling entails fundamental chemical engineering concepts, including mass and energy balances, physical properties, thermodynamics (phase equilibrium), and polymerization kinetics.

Simulation models play a key role in the development and operation of polymerization processes. We can use a model to plan and optimize grade-change operations, to debottleneck existing processes, or to design new products. We can also use a model for scaleup calculations, or for designing a process retrofit. Companies can save manpower, raw material, and energy resources by using simulations instead of experimenting on a trial-and-error basis when trying to tackle any one of these tasks.

The significance of this work is that it presents a comprehensive approach to polymer process modeling applied to large-scale commercial processes. Most researchers focus only on polymerization mechanisms and reaction kinetics, and neglect physical properties and phase equilibrium. Both physical properties and phase equilibrium play key roles in the accuracy and robustness of a model. This work presents the fundamental principles and practical guidelines used to develop and validate both steady-state and dynamic simulation models for two large-scale commercial processes involving the Ziegler-Natta polymerization to produce high-density polyethylene (HDPE) and polypropylene (PP). It also provides a model for the solution polymerization of ethylene using a metallocene catalyst. Existing modeling efforts do not include physical properties or phase equilibrium in their calculations. These omissions undermine the accuracy and predictive power of the models.

Section 1.1 discusses the essential components of a polymer process model. A robust model must consider physical and thermodynamic properties in addition to polymerization kinetics. Section 1.2 gives a general flowchart for model development.

We use this flowchart in each of our modeling applications. Section 1.3 outlines the remaining content of the dissertation.

1.1 Essential Components of a Polymer Process Model

Figure 1-1 shows the basic inputs and outputs of a polymer process model. Each input is essential to developing a comprehensive model for a polymerization process.

We use fundamental mass and energy balances for each unit operation in the model. These may include reactors, flash vessels, heat exchangers, compressors, and pumps. These balances are the most basic requirements of any process model.

We must include physical properties, such as density, to properly model vessel sizing and volumetric throughput. Density also affects the reactor residence time, which is an important variable that affects the polymerization phenomena.

We also consider phase equilibrium for vessels containing multiple phases. Equilibrium calculations are important to obtain correct phase compositions, which affect the reaction kinetics. They are also important in downstream separation units, which typically recycle material to the reactor.

Finally, we need polymerization kinetics to properly model the synthesis of the polymer, and particularly, the change in polymer properties with changes in reactor conditions. The polymerization kinetics represent the heart of a polymer process model.
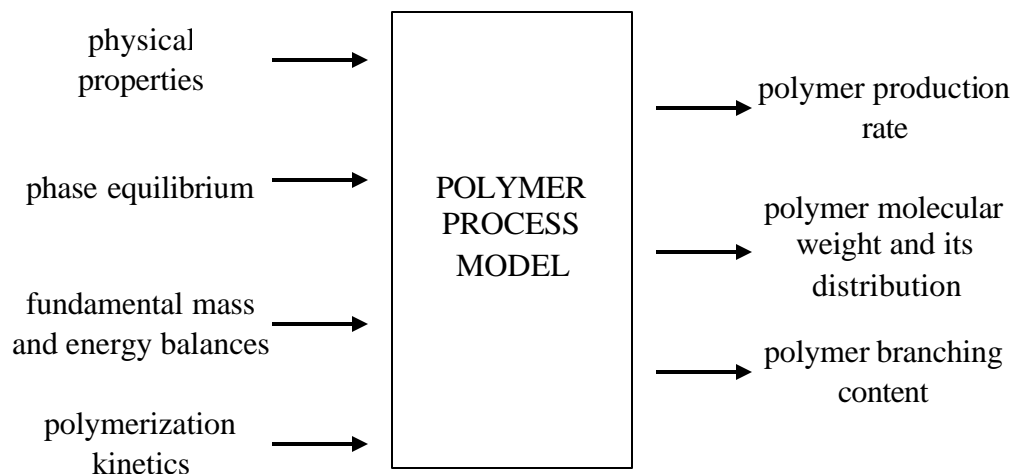
Figure 1-1. The basic inputs and outputs of a polymer process model.

1.2 Flowchart for Developing a Polymer Process Model

Figure 1-2 shows the general flowchart that we use for developing and applying a polymer process model. We begin by choosing appropriate models for physical properties and phase equilibrium. We use heuristics set forth by Bokis et al.[1], for example, to choose appropriate models.

Next, we determine unary and binary-interaction parameters for the property models. We can use published values as long as they were determined under conditions that are close to those of the modeled process. Alternatively, we can regress experimental data to determine the parameter values. Finally, we validate the predictions by comparing them to experimental data. This ensures that the model will have accurate physical-property and phase-equilibrium predictions. If necessary, we can use plant data to adjust the binary-interaction parameters to more closely match the phase-equilibrium behavior of the process. Note that we do not need a process model to complete the tasks up to this point.

---

[1] Bokis, C. P.; Orbey, H.; Chen, C.-C. Properly Model Polymer Processes. *Chemical Engineering Progress* **1999**, *95*, 39.

Next, we establish a reaction mechanism that is appropriate for the specific polymerization. Once we have a set of elementary steps, we obtain nominal kinetic parameters from the open literature. If possible, we include temperature dependence to the kinetics, since most reaction rates change significantly with small variations in temperature.

We build a flowsheet model that contains the relevant unit operations, using fundamental mass and energy balances. In our applications, these can include reactors and subsequent separation/recycle flash units, heat exchangers, mixers, compressors, and pumps.

We develop an iterative methodology for adjusting the kinetic parameters to match the polymerization phenomena in the plant data. This is a key step because the reactions are usually highly coupled, and changing the value of one parameter typically affects several properties simultaneously. As a result, it is very difficult to establish a set of kinetic parameters that match plant data without using a carefully developed methodology.

If we are performing dynamic modeling, we incorporate the control scheme. We also adjust the control parameters to match dynamic plant data, if available.

Once we build and validate the process model, we can apply it to a variety of areas. We can debottleneck an existing process, propose a process retrofit, or design a new polymer grade.

STEP 1: Choose appropriate models for physical properties and phase equilibrium

STEP 2: Regress pure-component and mixture data to determine unary and binary-interaction parameters for property models, or obtain established values from the open literature.

STEP 3: Validate property predictions using literature or plant data. Use plant data to adjust binary-interaction parameters for phase-equilibrium modeling, if necessary.

STEP 4: Choose appropriate reaction mechanism with nominal kinetic parameters from the open literature.

STEP 5: Build flowsheet model using fundamental principles for unit operations.

STEP 6: Use iterative methodology to adjust kinetic parameters to match plant data.

STEP 7: Incorporate control scheme for dynamic modeling.

STEP 8: Model application.

Figure 1-2. Flowchart for developing and utilizing a polymer process model.

1.3 Organization of the Dissertation

The dissertation contains two general parts. The forward chapters discuss the fundamental concepts we consider in polymer process modeling. The later chapters provide the modeling applications.

Chapter 2 deals with physical and thermodynamic properties, and phase equilibrium. We discuss the importance of each property and its role in model predictions. Chapter 3 covers polymerization kinetics. We focus on Ziegler-Natta and metallocene mechanisms individually. We also describe the conversion of the mechanisms to algebraic rate expressions for use in a model.

Chapter 4 describes the modeling of an industrial slurry high-density polyethylene (HDPE) process using a Ziegler-Natta catalyst. Chapter 5 discusses our modeling of a gas-phase polypropylene process using a Ziegler-Natta catalyst. Chapter 6 details a model for the solution polymerization of ethylene using a constrained-geometry catalyst.

Chapter 2 Physical Properties and Phase Equilibrium for Polymer Systems

2.1 Introduction

In this section, we describe the various physical properties that are necessary for comprehensive modeling of polymer synthesis processes. We also present the thermodynamic models that we use in this project work.

Physical-property modeling is essential to chemical process simulation, and cannot be ignored when performing design calculations. The main physical properties we are concerned with include density, vapor pressure, heat capacity, enthalpy, heat of vaporization, and heat of polymerization. These properties impact phase equilibrium, equipment sizing, and energy requirements, among other variables associated with process modeling and design.

In polymerization engineering, we are concerned with mixtures of polymeric and non-polymeric species; these mixtures can exist in multiple phases. There are several fundamental aspects of polymer systems that require different treatment than that for conventional, low-molecular-weight systems. First, polymers are essentially non-volatile. Also, unlike conventional species, polymers can experience change in molecular structure (chain length), and potentially their composition[1]. From a thermodynamic standpoint, mixing high-molecular-weight polymers with smaller species involves an entropy of mixing, which has a significant effect on phase behavior. Thermodynamic models must account for these differences in order to accurately describe the phase behavior and thermodynamic properties of polymeric systems.

In this project work, we use equations of state (EOS) for phase-equilibrium calculations. Specifically, we use the Sanchez-Lacombe (SL) and the perturbed-chain statistical associating fluid theory (PC-SAFT) EOS.

The primary thermodynamic properties we are concerned with include enthalpy, entropy, Gibbs free energy, and fugacity. We must often consider these properties when building a rigorous polymer process model. We use fugacity coefficients to correct for ideal phase-equilibrium behavior. We use enthalpy to perform energy balances. Entropy is useful for pump and turbine efficiency calculations. We usually obtain it from enthalpy and Gibbs energy.

An accurate description of phase behavior is critical to modeling polymer reactors and post-reactor devolatilization. During synthesis, polymers can be in liquid or solid form. As a liquid, polymer can reside as dissolved in a solvent, creating a single liquid phase, or remain as a separate liquid phase. In any of these cases, the reaction kinetics require accurate concentration predictions for the reacting phase. Many monomers reside in the vapor phase, and their solubility in the reacting phase is important. Post-reactor devolatilization involves the removal of unreacted monomer, solvent, or other light components from the polymer before downstream processing. This is the case whether the polymer is a liquid or solid.

Rigorous considerations require energy balances for each unit operation. Polymerizations tend to be highly exothermic, and accurate enthalpy predictions are essential for the design and optimization of polymer reactors. In some cases, inadequate cooling can lead to decomposition and reactor runaway. We can use thermodynamic models or empirical correlations to compute the enthalpies used in energy balances.

The remainder of this chapter is organized as follows. Section 2.2 covers physical properties. Section 2.2.2 describes segment-based calculations commonly used for polymeric systems. Section 2.2.3 discusses pure-component properties, and Section 2.2.4 deals with mixture properties. We cover phase equilibrium in Section 2.3. Section 2.3.3 describes the relevant EOS mentioned earlier. Section 2.3.5 describes the use of EOS property methods, which combine various physical-property and thermodynamic models for comprehensive model predictions. We provide equations and derivations for thermodynamic properties, as well as model constants, in Section 2.4.

2.2 Physical Properties

2.2.1 Introduction

This section describes the various physical properties required for comprehensive modeling of polymer synthesis processes. Accurate density calculations allow models to properly consider equipment sizing and process throughput, as well as phase volumes and residence times for reactors. Vapor pressure is important for phase-equilibrium calculations. Heat of vaporization is important for proper heat-balance calculations. Some reaction systems rely on the vaporization of a solvent to remove the heat of polymerization. Heat of polymerization and enthalpy are used in energy balances, which are important for determining required heating and cooling duties.

2.2.2 Species vs. Segment-Based Accounting

There are two types of accounting systems commonly used for modeling physical properties and phase equilibrium for polymeric systems. Species-based calculations consider polymer chains as single molecules, and segment-based accounting treats every polymer repeat unit (segment) as an individual molecule. The segment-based approach has the advantage of being able to characterize polymer molecules by the chemical properties of the segments, or monomer units, which comprise them. This facilitates the consideration of the effect of segment composition on the thermodynamic properties. Note that the use of the segment-based approach does not exclude the consideration of chain length, which is important for modeling many physical properties and phase-equilibrium behavior.

Figure 2-1 illustrates the segment-based approach for a polymer chain containing different segment types dissolved in a solvent medium. The interactions between the various segment types and the solvent molecules can be very different, affecting the physical properties and phase behavior of such a system.
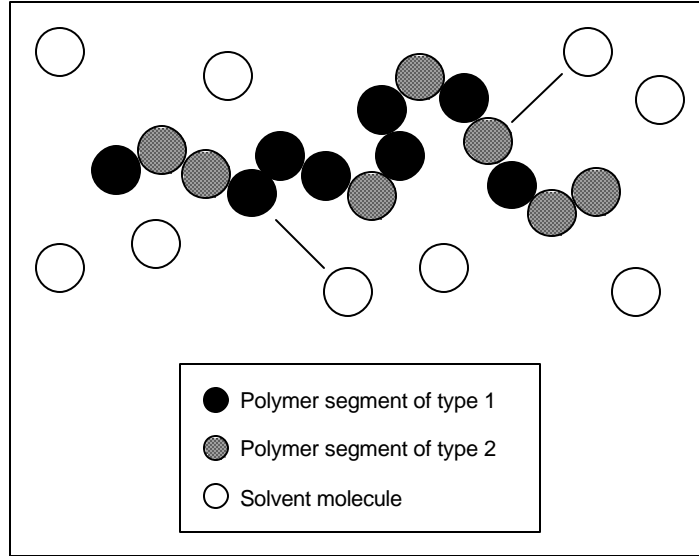
Figure 2-1. Illustrating a segment-based consideration of polymer chains in a mixture. This approach permits the consideration of interactions between each segment type and other species.

The mole fraction of polymer chains is often not useful. Consider a mixture of 1 g polyethylene, of molecular weight 50,000, dissolved in 20 g *n*-hexane, of molecular weight 86. The mole fraction of polymer is

$$x_{\text{polymer}} = \frac{\text{moles polymer}}{\text{moles solvent} + \text{moles polymer}} = \frac{1/50,000}{20/86 + 1/50,000} = 8.6\text{E}-5 \qquad (1)$$

where *x* is the real mole fraction. While this seems like a vanishing amount of polymer, we now consider the mass fraction of polymer in the mixture:

$$m_{\text{polymer}} = \frac{\text{mass polymer}}{\text{mass solvent} + \text{mass polymer}} = \frac{1}{20+1} = 0.048 \qquad (2)$$

where *m* is mass fraction. Although the mole fraction of polymer is tiny, the polymer occupies about 5% of the mass of the mixture. In terms of physical and thermodynamic properties, it is more meaningful to consider mass fractions than mole fractions.

Let us now consider the same mixture and apply the segment-based accounting. The ethylene segments have a molecular weight of 28, giving the polymer a degree of

polymerization of 1,786 (= 50,000/28). We assume that each solvent molecule is a single segment. The mole fraction of polymer segments is then

$$X_{\text{polymer}} = \frac{\text{moles polymer segments}}{\text{moles solvent} + \text{moles polymer segments}} = \frac{\frac{1}{50,000} \times 1786}{\frac{20}{86} + \frac{1}{50,000} \times 1786} = 0.133 \quad (3)$$

where X is segment-based mole fraction. The segment mole fraction is more representative of the amount of polymer in the system than is the mole fraction of whole polymer chains. Note that this segment fraction would be equal to the total polymer mass fraction in the event that the segment molecular weight was the same as that for the solvent species.

The general expression for converting between real and segment-based mole fraction is

$$X_I = \frac{x_i r_{i,I}}{\sum_i \sum_I x_i r_{i,I}} \quad (4)$$

where subscript I refers to polymer segments, subscript i refers to species, and $r_{i,I}$ is the number of segment type I in species i.

The segment approach is useful for the consideration of binary interactions between the different types of segments in the polymer and the solvent species. This accommodates EOS that utilize binary interaction parameters to correlate phase-equilibrium data. It also facilitates modeling polymer properties such as copolymer composition and isotacticity.

2.2.3 Pure-Component Properties

2.2.3.1 Introduction

There are many physical properties that we must consider to properly model polymer processes. Pure-component properties include density, vapor pressure, enthalpy, heat of vaporization, heat capacity, and heat of polymerization. These properties often form the basis for characterizing mixture properties, e.g., computing a mixture property by using a

11

mixing rule in conjunction with the pure-component properties and mixture composition. In this section, we describe these properties, their modeling importance, and relevant models.

2.2.3.2 Liquid Density

Since many polymerizations occur in the liquid phase, liquid density is important for phase-volume and residence-time calculations for reactors. It is also important for accurate phase concentrations, on which the reaction kinetics rely. In process retrofit and design, it is essential for modeling volumetric throughput. Density is also commonly used as a factor for quality control for polymers. When using an equation of state for phase-equilibrium calculations, we use the EOS to compute liquid density.

2.2.3.3 Vapor Density

Vapor density is important for equipment sizing for reactor overhead units and other operations. We typically use an equation of state to compute the vapor-phase density for both pure components and mixtures. Since polymers are essentially nonvolatile, the vapor phase in any given portion of a polymer process contains only conventional species. This allows more flexibility when choosing an EOS for vapor-phase calculations.

We describe the relevant equations of state in Section 2.3.3, and the EOS approach to property prediction in Section 2.3.5. Vapor-phase nonideality is typically small compared to liquid non-ideality. However, the ideal-gas law is only appropriate for the few systems where pressure is close to atmospheric and the species are non-associating.

2.2.3.4 Vapor Pressure

An important pure-component property for modeling phase equilibrium is vapor pressure. When using an equation of state for phase-equilibrium calculations, we can use it to compute the vapor pressure of each species.

2.2.3.5 Ideal-Gas Enthalpy

Enthalpy is used for computing energy balances for unit operations. It is important for non-isothermal systems, where the energy balance determines the system temperature. Enthalpy is particularly essential in polymerization reactors, where a balance must often be struck between the exothermic heat of polymerization and the energy removed using a heat jacket. Some reactors rely on the heat absorbed by vaporization of a solvent to remove some of the heat of polymerization.

The ideal gas is a hypothetical state often used as a reference point for calculating thermodynamic properties such as enthalpy. It represents the enthalpy of a pure species at conditions of standard temperature and pressure (298 K and 1 atm, STP). We compute its value using

$$H_i^{\text{ig}} = \Delta H_{\text{f},i}\left(T^{\text{ref}}\right) + \int_{T^{\text{ref}}}^{T} C_{\text{p},i}^{\text{ig}} dT \tag{5}$$

where $\Delta H_{\text{f},i}(T^{\text{ref}})$ is the heat of formation of species i at a reference temperature (usually 298 K), and $C_{\text{p},i}$ is the heat capacity for species i, as a function of temperature. We can obtain experimental values for the heats of formation from standard data references. Note that the ideal-gas enthalpy is independent of pressure.

Typically, we use an empirical expression to represent the temperature dependence of the ideal-gas heat capacity on temperature. A common form is the DIPPR model:

$$c_{\text{p},i}^{\text{ig}} = A_i + B_i\left(\frac{C_i/T}{\sinh\left(C_i/T\right)}\right)^2 + D_i\left(\frac{E_i/T}{\cosh\left(E_i/T\right)}\right)^2 \tag{6}$$

where A_i through E_i are adjustable parameters. Integrating eq (6) gives:

$$\int_{298\text{K}}^{T} c_{\text{p},i}^{\text{ig}} dT = A_i T + B_i \coth\frac{C_i}{T} - D_i \tanh\frac{E_i}{T}\bigg|_{298\text{K}}^{T} \tag{7}$$

2.2.3.6 Vapor Enthalpy

13

Since polymer species are nonvolatile, we only need to consider the vapor enthalpy for conventional species. We use equations of state to compute vapor enthalpy. We represent the vapor enthalpy as a sum of ideal-gas and residual contributions

$$H^V = H^{ig} + H^{res,V} \qquad (8)$$

where $H^{res,V}$ is the residual enthalpy for the vapor phase, computed using the equation of state. The ideal-gas enthalpy for a mixture is the sum of the pure-component contributions, weighted by mole fraction in the vapor phase

$$H^{ig} = \sum_i y_i H_i^{ig} \qquad (9)$$

where H_i^{ig} is the ideal-gas enthalpy for species i. We compute its value as described in the previous section. See Section 2.4 for the expression for the residual contribution.

2.2.3.7 Liquid Enthalpy

For an equation of state, the computation of liquid enthalpy is analogous to that for the vapor phase

$$H^L = H^{ig} + H^{res,L} \qquad (10)$$

where $H^{res,L}$ is the residual enthalpy for the liquid phase, computed using the equation of state. The ideal-gas enthalpy for a mixture is the sum of the pure-component contributions, weighted by mole fraction in the liquid phase

$$H^{ig} = \sum_i x_i H_i^{ig} \qquad (11)$$

The expression for the pure-component ideal-gas enthalpy is given in eq (5).

2.2.3.8 Heat of Vaporization

Accurate calculations for the heat of vaporization are important for reactors, flash vessels, and other unit operations that involve vapor and liquid in equilibrium. Heat of vaporization is particularly important for non-isothermal modeling of reactors where vaporization of the solvent removes the heat of polymerization, such as in the slurry HDPE process.

When using an equation of state for phase-equilibrium calculations, we do not need to compute the heat of vaporization directly because the EOS computes the vapor and liquid enthalpies for each phase.

2.2.3.9 Heat Capacity

Although heat capacity is not always used directly in enthalpy calculations, experimental data are usually in this form. When using an EOS for thermodynamic calculations, we obtain the heat capacity by differentiating enthalpy with respect to temperature:

$$C_p = \left(\frac{\partial H}{\partial T} \right)_P \tag{12}$$

Since we compute enthalpy using ideal-gas and residual contributions, we can break the right-hand side of eq (12) into two parts:

$$C_p = \left(\frac{\partial H^{ig}}{\partial T} \right)_P + \left(\frac{\partial H^{res}}{\partial T} \right)_P = C_p^{ig} + \Delta C_p \tag{13}$$

where C_p is the constant pressure heat capacity, C_p^{ig} is the ideal-gas contribution and ΔC_p is the residual contribution. Recall that the ideal gas is a hypothetical state at the system temperature and near zero pressure, and that a common modeling approach considers the ideal gas as the reference state for each component.

We can use a simple polynomial for the temperature dependence of the ideal-gas heat capacity

$$C_{p,i}^{ig} = A_i + B_i T + C_i T^2 + D_i T^3 \tag{14}$$

where A_i, B_i, C_i, and D_i are adjustable parameters corresponding to species i.

Table 2-1 gives the required parameters for the ideal-gas heat capacity model.

Table 2-1. Required parameters for the ideal-gas heat capacity model.

description	parameter	units
parameter	A_i	J/mol-K
parameter	B_i	J/mol-K^2
parameter	C_i	J/mol-K^3
parameter	D_i	J/mol-K^4
temperature	T	K

We can use polynomials to model the heat capacity for polymer. For example,

$$C_{p,L} = A + BT + CT^2 + DT^3 \tag{15}$$

where *A*, *B*, *C*, and *D* are adjustable parameters determined using experimental heat-capacity data.

2.2.3.10 Heat of Polymerization

Many polymerizations are highly exothermic, and we must account for this when computing reactor energy balances. These polymerizations require careful temperature control to avoid thermal decomposition and reactor runaway. The rigorous method for computing the heat of polymerization is to take the difference between the enthalpy, per segment, of polymer and the enthalpy of pure monomer at their physical states in the reactor[2]. Figure 2-2 illustrates this computation. We use an equation of state to compute each transition along the path.

---

[2] Leonard, J. Heats and Entropies of Polymerization, Ceiling Temperatures, Equilibrium Monomer Concentrations, and Polymerizability of Heterocyclic Compounds. In *Polymer Handbook*; Brandrup, J., Immergut, E. H., Grulke, E. A., Eds.; Wiley & Sons: New York, 1999; p II/363.

ideal-gas monomer ——————— ideal-gas polymer

gas monomer - - - - - - -▶ solid polymer
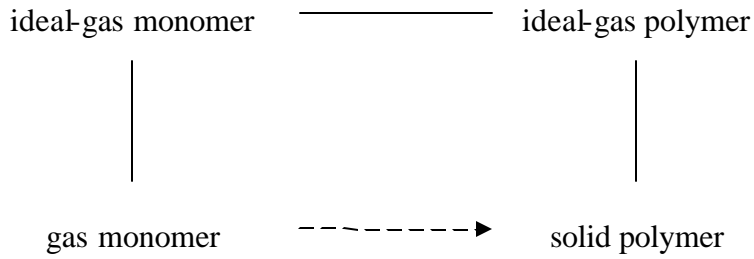
Figure 2-2. Pathway for computing the heat of polymerization for the EOS approach[2].

For ethylene, the reaction is

$$C_2H_{4(g)} \rightarrow \frac{1}{n}(C_2H_4)_{n(s)}$$
(16)

where n is the number of ethylene segments in the polymer[2].

2.2. 4 Mixture Properties

2.2.4.1 Introduction

In Section 2.2.3, we provided the major pure-component properties that we are concerned with. In some cases, the effect of mixing is negligible, and in others it is not. Here, we show how to compute physical properties of mixtures.

2.2.4.2 Mixture Density (Molar Volume)

We model the liquid mixture molar volume using Amagat's law:

$$v^L = \sum_i x_i v_i^L$$
(17)

This assumes no excess volume of mixing. This is generally acceptable for the applications that require an external correlation for liquid density. When using an EOS for physical-property and phase-equilibrium calculations, we use the EOS to compute the mixture molar volume.

2.2.4.3 Mixture Enthalpy

In the previous sections, we describe how to compute the pure-component enthalpies for vapor and liquid. Here, we explain how to compute enthalpy for a mixture, either vapor or liquid.

2.2.4.3.1 Vapor Mixture Enthalpy

Eq (18) gives the vapor mixture enthalpy:

$$h^V = \sum_i y_i h_i^{ig} + \int_\infty^{v^V} \left[P - T \left(\frac{\partial P}{\partial T} \right)_{v^V} \right] dv^V \tag{18}$$

where y_i is the vapor mole fraction of species i, h_i^{ig} is the ideal-gas (pure-component) enthalpy, for species i, at the temperature of the system, and v^V is the molar volume of the mixture, computed using the EOS.

We ignore the polymer contribution to the ideal-gas enthalpy because the vapor-phase mole fraction for polymer is always nearly zero. As in the pure-component case, we compute the value of the integral in eq (18) by inserting an expression for pressure furnished by a pressure-explicit equation of state.

2.2.4.3.2 Liquid Mixture Enthalpy

The liquid calculation is similar to that for the vapor approach. The only difference is that we use the liquid molar volume in place of the vapor molar volume:

$$h^L = \sum_i x_i h_i^{ig} + \int_\infty^{v^L} \left[P - T \left(\frac{\partial P}{\partial T} \right)_{v^L} \right] dv^L \tag{19}$$

where v^L is the liquid molar volume of the mixture.

2.3 Phase Equilibrium

2.3.1 Introduction

The purpose of this section is to discuss phase equilibrium for polymeric systems. We first give a brief overview of the fundamentals of phase equilibrium. We then discuss the EOS approach. We end the section by describing treatment for solid polymer.

The fundamental criterion for phase equilibrium is the isofugacity relation for each species in each phase. For a system where two phases are in equilibrium:

$$f_i^{\,a} = f_i^{\,b} \tag{20}$$

where $f_i^{\,a}$ and $f_i^{\,b}$ are the fugacities for species i in phases $\boldsymbol{a}$ and $\boldsymbol{b}$, respectively. A key aspect of modeling phase equilibrium is the formulation of fugacity expressions that accurately describe the behavior for each phase.

2.3.2 VLE: The Ideal Case

The simplest relationship for VLE is Raoult's law:

$$y_i P = x_i P_i^{\,s} \tag{21}$$

where $P_i^{\,s}$ is the vapor pressure of species i. This relation states that, in the absence of molecular interactions, the partial pressure of a component in the vapor phase relates to the liquid mole fraction times the saturation pressure of that component. In other words, the vapor partial pressure for a species is directly proportional to its liquid mole fraction, with its saturation pressure as the constant. This relation is somewhat accurate only for mixtures of non-associating species at conditions close to STP.

2.3.3 Equations of State

2.3.3.1 Basis

19

EOS relate the molar volume of each species to temperature and pressure. They are applicable to both vapor and liquid phases. They are applicable over wide ranges of temperature and pressure, are consistent in the critical region, and provide unified prediction of thermodynamic properties. They do not generally perform well for highly non-ideal mixtures (polar and other associating systems). In the following sections, we give detailed descriptions of the SL and PC-SAFT EOS.

The simplest EOS is the ideal-gas law:

$$Pv = RT \tag{22}$$

where P is pressure, v is molar volume, R is the gas constant, and T is temperature. This EOS assumes no interaction between molecules, and does not consider the finite volume of the molecules. It is only useful for predicting vapor-phase molar volume as a function of temperature and pressure for non-associating species at conditions near STP. It does not apply to polymer species. There exist more complex EOS models designed specifically for polymeric mixtures over wide ranges of temperature and pressure. These include the Sanchez-Lacombe[3] (SL) and the perturbed-chain statistical associating fluid theory[4] (PC-SAFT) EOS. We describe these models later in this chapter.

We can use an EOS to compute both the vapor and liquid properties simultaneously. We define the fugacity of each phase as follows:

$$f_i^V = y_i \Phi_i^V P \qquad f_i^L = x_i \Phi_i^L P \tag{23}$$

where y_i and x_i are the mole fractions of species i in the vapor and liquid phases, respectively, and Φ_i^V and Φ_i^L are the fugacity coefficients for species i in the vapor and liquid phases, respectively. The fugacity coefficients account for the nonideality of the phase behavior of mixtures.

The resulting phase-equilibrium relation for the EOS approach is

[3] Sanchez, I. C.; Lacombe, R. H.; Statistical Thermodynamics of Polymer Solutions. *Macromolecules* **1978**, *11*, 1145.

[4] Gross, J.; Sadowski, G.; Perturbed-Chain SAFT: An Equation of State Based on a Perturbation Theory for Chain Molecules. *Industrial and Engineering Chemistry Research* **2001**, *40*, 1244.

$$y_i \Phi_i^{\mathrm{V}} = x_i \Phi_i^{\mathrm{L}} \tag{24}$$

In the next section, we describe the EOS used in this work.

2.3.3.2 Models

2.3.3.2.1 Sanchez-Lacombe Model

The Sanchez-Lacombe (SL) EOS is a lattice model developed using statistical mechanics[5,6,7]. It can be used to predict thermodynamic properties and phase behavior of both polymeric and nonpolymeric systems.

Using an approach similar to that of Flory[8] and Huggins[9] for polymer solutions, Sanchez and Lacombe begin by considering chain-like fluids in a lattice. Unlike the Flory-Huggins theory, they include empty sites in the lattice as well, allowing the model to account for compressibility effects. Figure 2-3 illustrates a representative lattice as considered using the SL model. The total number of lattice sites is

$$N_{\mathrm{tot}} = N_0 + rN \tag{25}$$

where N_0 is the number of empty sites, N is the number of molecules, and r is the number of sites occupied by each molecule.

[5] Sanchez, I. C.; Lacombe, R. H. An Elementary Molecular Theory of Classical Fluids. Pure Fluids. *Journal of Physical Chemistry* **1976**, *80*, 2352.

[6] Lacombe, R. H.; Sanchez, I. C. Statistical Thermodynamics of Fluid Mixtures. *Journal of Physical Chemistry* **1976**, *80*, 2568.

[7] Sanchez, I. C.; Lacombe, R. H.; Statistical Thermodynamics of Polymer Solutions. *Macromolecules* **1978**, *11*, 1145.

[8] Flory, P. J. Thermodynamics of High-Polymer Solutions. *Journal of Chemical Physics* **1941**, *9*, 660.

[9] Huggins, M. L. Solutions of Long-Chain Compounds. *Journal of Chemical Physics* **1941**, *9*, 440.
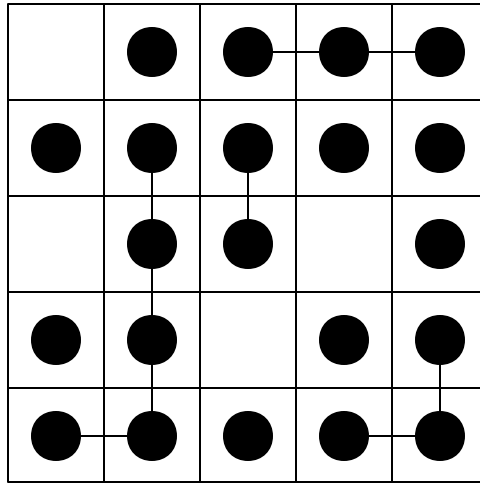
Figure 2-3. Lattice considered in the Sanchez-Lacombe equation of state. Connected dots represent chemical species on a fixed-volume lattice.

Each lattice site has a constant volume. We can represent the total volume of the lattice as

$$V = v^* \left(N_0 + rN \right) \tag{26}$$

where v^* is the site volume.

The lattice energy is based on the interactions between nearest neighbors. Only molecules have non-zero interaction; holes do not participate.

Using statistical mechanics, Sanchez and Lacombe relate the Gibbs free energy to the number of possible configurations of a fluid and holes in the lattice. Assuming a random distribution of molecules in the lattice, they use an expression for combinatorial entropy that is analogous to that in the Flory-Huggins theory.

Upon minimizing their resulting expression for the Gibbs free energy, they obtain the equation of state:

$$\overline{r}^2 + \overline{P} + \overline{T}\left[\ln\left(1 - \overline{r}\right) + \left(1 - \frac{1}{r}\right)\overline{r}\right] = 0 \tag{27}$$

where $\overline{r}$, $\overline{P}$, and $\overline{T}$ are reduced density, pressure, and temperature, respectively. We relate the reduced properties to their corresponding absolute variables with

$$\overline{r} = \frac{r}{r^*} \quad \overline{P} = \frac{P}{P^*} \quad \overline{T} = \frac{T}{T^*} \tag{28}$$

where r^*, P^*, and T^* are scale factors that completely characterize each pure fluid. They relate to lattice variables:

$$r^* = \frac{M}{m^*} \quad P^* = \frac{e^*}{n^*} \quad T^* = \frac{e^*}{R} \tag{29}$$

Here, e^* is the characteristic interaction energy per mole of segments, n^* is the mass-based volume of empty lattice sites, r is the number of lattice sites a fluid molecule occupies, and k is Boltzmann's constant.

We extend the EOS to fluid mixtures by applying mixing rules to the lattice variables, as follows:

$$e_{\text{mix}}^* = \frac{1}{n_{\text{mix}}^*}\sum_i\sum_j f_i f_j e_{ij}^* n_{ij}^* \quad n_{\text{mix}}^* = \sum_i\sum_j f_i f_j n_{ij}^* \quad \frac{1}{r_{\text{mix}}} = \sum_j \frac{f_j}{r_j} \tag{30}$$

where e_{mix}^*, n_{mix}^*, and r_{mix} are mixture parameters, e_{ij}^* and n_{ij}^* are cross parameters for components i and j, and f_i, the volume fraction of component i, is

$$f_i = \frac{\dfrac{m_i}{r_i^* n_i^*}}{\displaystyle\sum_j \dfrac{m_j}{r_j^* n_j^*}} \tag{31}$$

and m_i is the weight fraction of component i. We compute cross parameters using

$$n_{ij}^* = \frac{1}{2}\left(n_{ii}^* + n_{jj}^*\right)\left(1 - h_{ij}\right) \quad e_{ij}^* = \left(1 - k_{ij}\right)\sqrt{e_{ii}^* e_{jj}^*} \tag{32}$$

where h_{ij} and k_{ij} are binary interaction parameters.

The SL EOS is applicable to non-polar systems, although Sanchez and Panayiotou[10] recently modified the SL model to consider associating species (hydrogen bonding). It is better at predicting liquid density that simple cubic EOS, although it tends to overpredict the critical point. In this region, the cubic EOS do a better job[1].

The SL EOS has been successfully applied to polymer-liquid systems, polymer-vapor systems, and supercritical polymer systems. Additionally, vapor-pressure, enthalpy, and mixing-volume predictions are found to be accurate for polymer-solvent systems[11].

Table 2-2 summarizes the parameters used in the SL EOS. We require three pure-component parameters for each pure fluid. There are two optional binary-interaction parameters. Sanchez and Lacombe provide pure-component parameters for several common low-molecular weight fluids[5] and polymer species[7].

Table 2-2. Parameters used in the Sanchez-Lacombe equation of state.

description	parameter	units
characteristic temperature	T^*	temperature
characteristic pressure	P^*	pressure
characteristic density	r^*	mass density
binary interaction parameter	h_{ij}	--
binary interaction parameter	k_{ij}	--

We regress the parameters for low-molecular-weight components using vapor-pressure data; for polymer species, we use liquid-volume data. Due to the over-prediction of the critical point, Sanchez and Lacombe recommend that we omit data points within 15 to 20 °C of the critical point. We can regress the values for binary-interaction parameters using

[10] Sanchez, I. C.; Panayiotou, C. G. Equation of State Thermodynamics of Polymer and Related Solutions. In *Models for Thermodynamic and Phase Equilibria Calculations*; S. I. Sandler, Ed., Marcel Dekker: New York, 1994.
[11] Prausnitz, J. M.; Lichtenthaler, R. N.; de Azevedo, E. G. *Molecular Thermodynamics of Fluid-Phase Equilibria*; Prentice Hall: New Jersey, 1999, Chapter 8.

binary phase-equilibrium data for the components of interest, in order to improve model performance. In the absence of such data, we set the binary parameters to zero.

2.3.3.2.2 Perturbed-Chain Statistical Associating Fluid Theory (PC-SAFT) Model

The perturbed-chain statistical associating fluid theory (PC-SAFT) model represents the latest modification to the SAFT equation of state (EOS). We begin our description with the original developments of by Chapman et al.[12], the modification and application of the SAFT theory to fluid mixtures for engineering applications by Huang and Radosz[13,14], and finally, the recent adaptations by Gross and Sadowski[4], resulting in the PC-SAFT model.

Using perturbation theory, which states that molecular interactions can be divided into attractive and repulsive contributions, Chapman et al.[12] express the residual Helmholtz energy as a sum of the following contributions:

1. Short-range repulsions (molecular volume).
2. Long-range dispersion (attractive) forces.
3. Chemical bonding (molecular structure, chains).
4. Association/solvation (hydrogen bonding).

Model development in terms of the Helmholtz energy is useful because we can derive most thermodynamic properties using differentiated forms of the Helmholtz energy. The expression for the molar residual Helmholtz energy for the SAFT EOS is

$$a_{\text{SAFT}}^{\text{res}} = a_{\text{SAFT}}^{\text{hs}} + a_{\text{SAFT}}^{\text{hc}} + a_{\text{SAFT}}^{\text{disp}} + a_{\text{SAFT}}^{\text{assoc}} \tag{33}$$

where $a_{\text{SAFT}}^{\text{hs}}$, $a_{\text{SAFT}}^{\text{hc}}$, $a_{\text{SAFT}}^{\text{disp}}$, $a_{\text{SAFT}}^{\text{assoc}}$ are the hard-sphere, hard-chain, dispersion, and association contributions, respectively. The use of hard-sphere chains allows the PC-SAFT EOS to account for the connectivity of segments that comprise the chains when

---

[12] Chapman, W. G.; Gubbins, K. E.; Jackson, G.; Radosz, M. New Reference Equation of State for Associating Liquids. *Industrial and Engineering Chemistry Research* **1990**, *29*, 1709.

[13] Huang, S. H.; Radosz, M. Equation of State for Small, Large, Polydisperse, and Associating Molecules. *Industrial and Engineering Chemistry Research* **1990**, *29*, 2284.

[14] Huang, S. H.; Radosz, M. Equation of State for Small, Large, Polydisperse, and Associating Molecules: Extension to Fluid Mixtures. *Industrial and Engineering Chemistry Research* **1991**, *30*, 1994.

considering the attractions between species, resulting in a realistic description of the
thermodynamic behavior of mixtures of chain-like molecules.

Figure 2-4 gives a physical description of the considerations in the SAFT EOS[15]. The
SAFT model uses spherical segments of equal size as a reference fluid (top left).
Intermolecular attraction (dispersion forces) occurs between each individual molecule
and segment. Consideration is then made for chain connectivity (molecular structure).
Finally, association forces account for hydrogen bonding and polar effects.

Begin with a hard-sphere fluid   Add attractive forces between molecules

Add associative forces between molecules   Form chains with hard-sphere segments
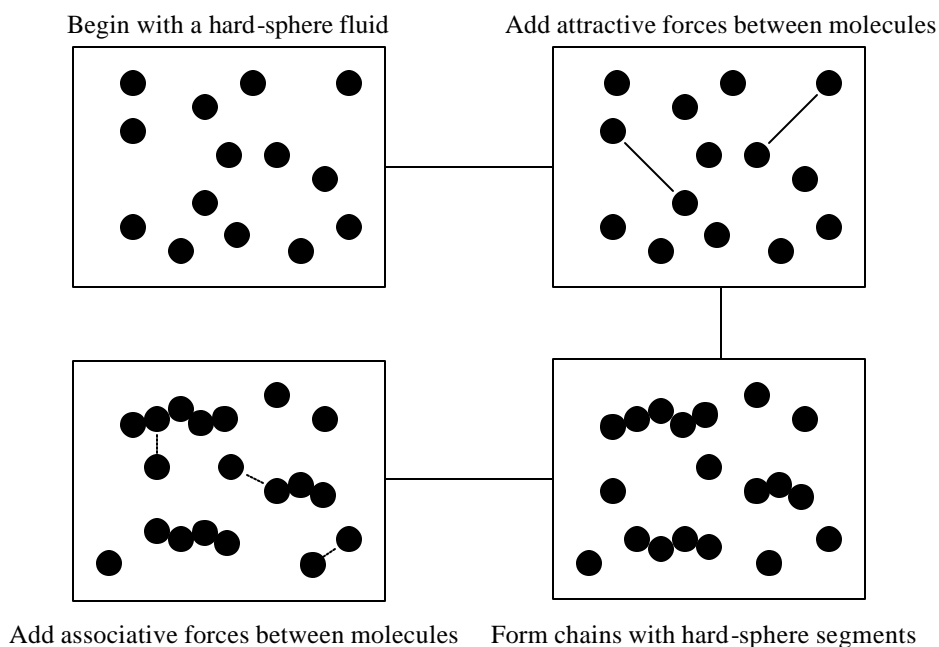
Figure 2-4. A physical description of the attractive and repulsive considerations of the SAFT EOS[15].

Chapman et al. used a hard-sphere contribution to the residual Helmholtz energy
developed by Carnahan and Starling[16], the perturbation theory of Wertheim[17,18] for the

[15] Prausnitz, J. M.; Lichtenthaler, R. N.; de Azevedo, E. G. *Molecular Thermodynamics of Fluid-Phase Equilibria*;
Prentice Hall: New Jersey, 1999, Chapter 7.
[16] Carnahan, N. F.; Starling, K. E. Equation of State for Nonattracting Rigid Spheres. *Journal of Chemical Physics*
1969, *51*, 635.
[17] Wertheim, M. S. Fluids with Highly Directional Attractive Forces. I. Statistical Thermodynamics. *Journal of
Statistical Physics* **1984**, *35*, 19.

chain and association contributions, and an expression presented by Cotterman et al.[19] for the dispersion term. Huang and Radosz modified the model by using a dispersion term based on work by Alder et al.[20] and Chen et al.[21]. They used the same sphere, chain, and association terms as in the original SAFT model. While other modifications have appeared in the literature, the form by Huang and Radosz is the most widely used, as it is one of the most successful versions[4].

Gross and Sadowski recently modified the SAFT model by using hard chains instead of hard spheres as the reference fluid for the dispersion term. Figure 2-5 compares the physical significance of this consideration between the SAFT and PC-SAFT models. In the SAFT model, attractive interactions occur between individual molecules and chain segments, while the PC-SAFT considers interactions between entire molecules. This approach provides a more realistic description of the thermodynamic behavior of chain-like fluid mixtures.

SAFT   PC-SAFT
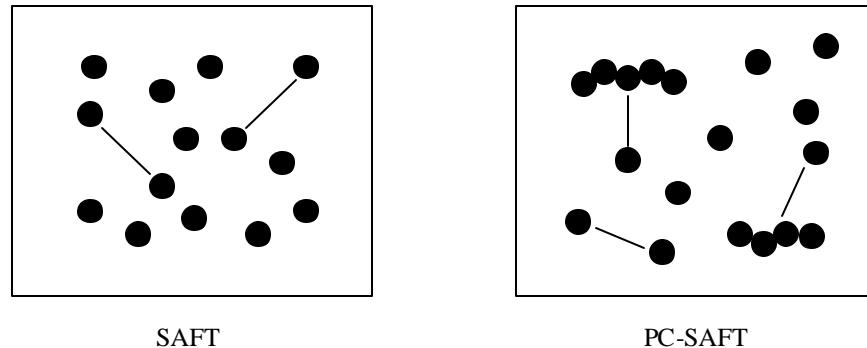
Figure 2-5. Comparing the intermolecular (attractive) forces as modeled by the SAFT and PC-SAFT EOS.

[18] Wertheim, M. S. Fluids with Highly Directional Attractive Forces. II. Thermodynamic Perturbation Theory and Integral Equations. *Journal of Statistical Physics* **1984**, *35*, 35.

[19] Cotterman, R. L.; Schwartz, B. J.; Prausnitz, J. M. Molecular Thermodynamics for Fluids at Low and High Densities. *AIChE Journal* **1986**, *32*, 1787.

[20] Alder, B. J.; Young, D. A.; Mark, M. A. Molecular Dynamics. X. Corrections to the Theory for the Square Well Fluid. *Journal of Chemical Physics* **1972**, *56*, 3013.

[21] Chen, S. S.; Kreglewski, A. *Ber. Bunsen-Ges. Phys. Chem.* **1977**, *81*, 1048.

Gross and Sadowski developed the dispersion term for a hard-chain reference fluid using the perturbation theory of Barker and Henderson[22]. The PC-SAFT model contains the same hard-sphere and hard-chain terms as the SAFT EOS. While Gross and Sadowski do not discuss the implementation of an association term, they plan to deal with it in a future publication. Therefore, the application of the PC-SAFT EOS is currently limited to non-associating mixtures, such as hydrocarbons. In non-associating systems, dispersion forces dominate the attractive contribution, while the association forces dominate for polar substances. Upon consideration of association, we will be able to extend the application of the EOS to systems containing alcohols and water, etc.

The PC-SAFT provides excellent prediction of thermodynamic properties and phase equilibrium for of small molecules, chain-like polymers, and their mixtures. Predictions for vapor-liquid equilibrium were substantially improved over those using the SAFT EOS by Huang and Radosz. While the PC-SAFT slightly overpredicts the critical point, its predictions are improved over those of the SAFT model. The PC-SAFT also performs better than the SAFT for VLE calculations of hydrocarbon systems and polymer solutions at both low and high pressures. Phase-equilibrium predictions for binary mixtures of small molecules were better than those by the Peng-Robinson EOS. It also performed well for high-pressure liquid-liquid equilibrium for polyethylene mixtures[4].

The equation of state for the PC-SAFT EOS is

$$z = z^{id} + z^{hs} + z^{hc} + z^{disp} \tag{34}$$

where z^{id} is the ideal-gas compressibility, equal to unity, z^{hs} is the hard-sphere contribution, z^{hc} is the hard-chain contribution, and z^{disp} is the dispersion contribution.

For the hard-sphere contribution:

$$z^{hs} = \frac{z_3}{(1-z_3)} + \frac{3z_1 z_2}{z_0 (1-z_3)^2} + \frac{3z_2^3 - z_3 z_2^3}{z_0 (1-z_3)^3} \tag{35}$$

[22] Barker, J. A.; Henderson, D. Perturbation Theory and Equation of State for Fluids. II. Successful Theory of Liquids. *Journal of Chemical Physics* **1967**, *47*, 4714.

$$z_n = \frac{pr}{6} \sum_i x_i m_i d_i^{\ n} \qquad n = 0,1,2,3 \tag{36}$$

$$d_i = s_i \left[1 - 0.12 \exp\left(-\frac{3e_i}{kT} \right) \right] \tag{37}$$

where r is the total number density of molecules (Å^{-3}), x_i is the mole fraction of component i, m_i is the number of segments per chain for component i, s_i is the segment diameter (Å) for component i, e_i/k is the segment energy parameter for component i (K) with e_i as the segment depth of pair potential and k is Boltzmann's constant, and T is temperature.

For the hard-chain contribution

$$z^{hc} = \sum_i x_i (1 - m_i) r \frac{\partial \ln g_{ii}^{hs}}{\partial r} \tag{38}$$

$$r \frac{\partial \ln g_{ii}^{hs}}{\partial r} = \frac{z_3}{(1 - z_3)^2} + \frac{d_i}{2} \left(\frac{3z_2}{(1 - z_3)^2} + \frac{6z_2 z_3}{(1 - z_3)^3} \right) + \left(\frac{d_i}{2} \right)^2 \left(\frac{4z_2^{\ 2}}{(1 - z_3)^3} + \frac{6z_2^{\ 2} z_3}{(1 - z_3)^4} \right) \tag{39}$$

where g_{ii}^{hs} is the radial-pair distribution function for segments of component i.

For the dispersion contribution:

$$z^{disp} = -2pr \left(\frac{\partial hI_1}{\partial h} \right) \langle m^2 es^3 \rangle - pr \overline{m} \left[C_1 \left(\frac{\partial hI_2}{\partial h} \right) + C_2 hI_2 \right] \langle m^2 e^2 s^3 \rangle \tag{40}$$

$$I_1 = \sum_{i=0}^{6} a_i (m) h^i \tag{41}$$

$$I_2 = \sum_{i=0}^{6} b_i(m)\boldsymbol{h}^i \tag{42}$$

$$a_i(m) = a_{0i} + \frac{m-1}{m}a_{1i} + \frac{m-1}{m}\frac{m-2}{m}a_{2i} \tag{43}$$

$$b_i(m) = b_{0i} + \frac{m-1}{m}b_{1i} + \frac{m-1}{m}\frac{m-2}{m}b_{2i} \tag{44}$$

$$\boldsymbol{h} = \boldsymbol{z}_3 = \frac{\boldsymbol{p}}{6}\sum_i x_i m_i d_i^3 \tag{45}$$

$$\bar{m} = \sum_i x_i m_i \tag{46}$$

We refer the reader to Section 2.4 for the values for constants a_{ji} and b_{ji} appearing in eqs (43) and (44).

We compute the molar density using

$$\hat{\boldsymbol{r}} = \boldsymbol{r}\frac{10^{30}\left(\overset{\text{o}}{\text{A}}/\text{m}\right)^3}{N_A} \tag{47}$$

where N_A is Avogadro's number.

Finally, the compressibility relates to the system pressure as follows:

$$z = \frac{P}{\boldsymbol{r}\text{R}T} \tag{48}$$

where R is the gas constant and P is pressure.

Table 2-3 lists the required parameters for the PC-SAFT model. We need three pure-component parameters for each pure fluid. There is also an optional binary-interaction parameter, which we can adjust to match experimental data for binary mixtures. The parameter s is a characteristic diameter for the segments of a given species. The parameter e is a segment energy parameter. The parameter m serves as a characteristic chain length. For polymer species, we use r, the ratio of m and the number average molecular weight

$$r = \frac{m}{M_n} \qquad (49)$$

in place of segment number m. This is more convenient because the polymer molecular weight is often unknown until after the polymer is produced. Finally, the binary-interaction parameter is k_{ij}.

Gross and Sadowski[4,23] provide pure-component and binary-interaction parameters for many species. We can regress pure-component parameters using vapor-pressure data. We use liquid-density data for polymer species. We can use phase-equilibrium data to fit binary-interaction parameters.

Table 2-3. Parameters for the PC-SAFT model.

description	parameter	units
segments per chain for species i	m_i	--
segment diameter for species i	s_i	length (Å)
segment energy for species i	e_i/k	temperature (K)
binary interaction parameter	k_{ij}	--

[23] Gross, J.; Sadowski, G. Modeling Polymer Systems Using the Perturbed-Chain Statistical Associating Fluid Theory Equation of State. *Industrial and Engineering Chemistry Research* **2002**, *41*, 1084.

2.3.4 Considering Solid Polymer in Phase Behavior

Many polymer synthesis processes contain polymer in solid form. In high-density polyethylene slurry systems, polymer exists as a solid dispersed in the liquid phase. In gas-phase polypropylene processes, the reactor contains gaseous monomer and solid polymer. In both of these cases, the polymer is essentially inert and does not interact thermodynamically with the other components. There are several options for dealing with the phase behavior of such systems.

The most straightforward case would consider the solubility of light gases in the solid polymer, using Henry's law. However, Henry's law is only applicable when an activity-coefficient model is used for phase-equilibrium calculations. Also, many commercial simulators require that the reacting phase participate in phase-equilibrium calculations.

For slurry systems, we can approximate the solid polymer as dissolved in the liquid phase. We apply this technique in the modeling project for a slurry high-density polyethylene (HDPE) process[24]. Figure 2-6 compares the actual reactor to this modeling assumption.

---

[24] Khare, N. P.; Seavey, K. C.; Liu, Y. A.; Ramanathan, S.; Lingard, S.; Chen, C.-C. Steady-State and Dynamic Modeling of Commercial Slurry High-Density Polyethylene (HDPE) Processes. *Industrial and Engineering Chemistry Research* **2002**, *41*, 5601.
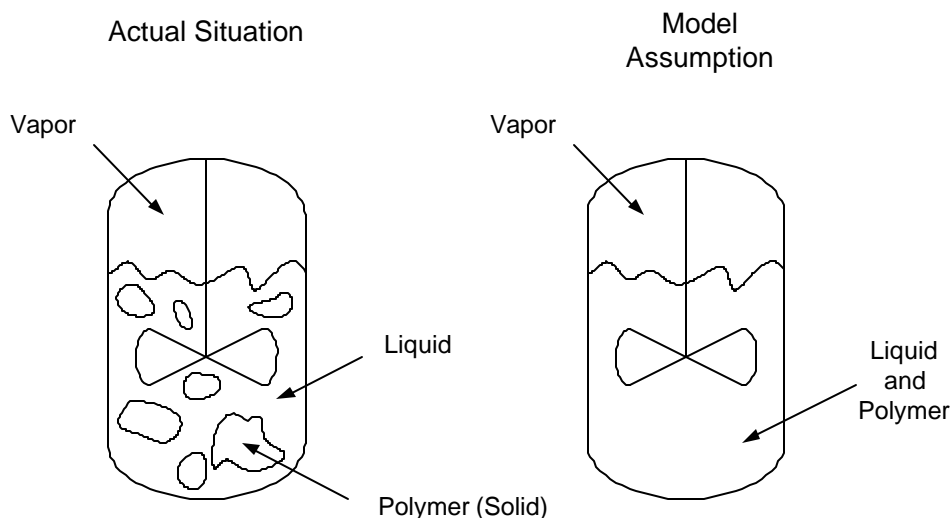
Figure 2-6. Comparing the actual situation in a slurry system with a modeling assumption where the polymer is dissolved in the liquid solvent.

For gas-phase processes, we can model the solid polymer as a pseudo-liquid. We regress pure-component parameters for the equation of state using density data for solid polymer. We vary interaction parameters to adjust the amount of gases that dissolve into the polymer. We use this technique in the modeling example for gas-phase polymerization of polypropylene (see Chapter 5).

2.3.5 Property Methods

In this section, we combine the models described earlier in the chapter to create property method packages for physical property/phase equilibrium calculations. We usually use the model for some physical and thermodynamic properties in addition to VLE calculations.

We compute the fugacity coefficients for the vapor and liquid phases using an equation of state. The fugacity coefficient for each phase depends on temperature and pressure, as well as the density and composition of the particular phase:

$$\Phi_i^{\text{V}} = \Phi_i^{\text{V}}\left(T, P, \boldsymbol{r}^{\text{V}}, y_i\right) \tag{50}$$

$$\Phi_i^{\text{L}} = \Phi_i^{\text{L}}\left(T, P, \mathbf{r}^{\text{L}}, x_i\right) \tag{51}$$

where $\mathbf{r}^{\text{V}}$ and $\mathbf{r}^{\text{L}}$ and the molar densities of the vapor and liquid phases, respectively. There are several ways to compute the fugacity coefficients using thermodynamic relations. We provide these expressions in Section 2.4.

We also use the EOS to compute the molar enthalpy (h), entropy (s) and Gibbs free energy (g) departures. These properties are important when using energy balances for non-isothermal modeling, or when predicting liquid phase separation. We represent each of these properties as sums of ideal-gas and EOS (residual) contributions:

$$
\begin{aligned}
h &= h^{\text{ig}} + h^{\text{res}} \\
s &= s^{\text{ig}} + s^{\text{res}} \\
g &= g^{\text{ig}} + g^{\text{res}}
\end{aligned}
\tag{52}
$$

where the *ig* and *res* superscripts refer to the ideal-gas and residual contributions, respectively. We use lower-case letters to represent molar quantities, and capital letters for total properties. We compute a total property by multiplying the molar property by the total number of moles in the phase of interest:

$$
\begin{aligned}
H &= n_{\text{T}} h \\
S &= n_{\text{T}} s \\
G &= n_{\text{T}} g
\end{aligned}
\tag{53}
$$

We provide expressions for computing residual properties in Section 2.4. We use eqs (52) to compute properties of each phase individually, and then use molar averages to determine the property of the entire system.

We discuss computing mixture enthalpy in Section 2.2.4.3. We compute the ideal-gas entropy in a similar fashion:

$$s_{\text{V}}^{\text{ig}} = \sum_i y_i s_i^{\text{ig}} \tag{54}$$

$$s_{\text{L}}^{\text{ig}} = \sum_i x_i s_i^{\text{ig}} \tag{55}$$

For the pure-component contributions, we use

$$s_i^{\text{ig}} = \Delta s_{\text{f},i}\left(T^{\text{ref}}\right) + \int_{T^{\text{ref}}}^{T} \frac{C_{\text{p},i}}{T}\,\mathrm{d}T \tag{56}$$

where $\Delta s_{\text{f},i}(T^{\text{ref}})$ is the entropy of formation at a reference temperature, taken as 25 °C. There are no established methods for estimating the standard entropy of formation, nor are experimental techniques possible. We determine its value using the heat of formation and Gibbs energy of formation for each species:

$$\Delta s_{\text{f},i}\left(T^{\text{ref}}\right) = \frac{\Delta h_{\text{f},i}\left(T^{\text{ref}}\right) - \Delta g_{\text{f},i}\left(T^{\text{ref}}\right)}{T^{\text{ref}}} \tag{57}$$

The enthalpy and Gibbs free energies are experimentally determined, and available in the open literature. We use the same polynomial for the heat capacity as that used for enthalpy calculations (see Section 2.2.3).

We compute the Gibbs free energy using its relationship to the enthalpy and entropy:

$$g^{\text{ig}} = h^{\text{ig}} - Ts^{\text{ig}} \tag{58}$$

In the EOS approach, the heat of vaporization of a species is the difference between its pure-component enthalpies in the vapor and liquid:

$$\Delta h_i^{\text{vap}} = h_i^{\text{L}} - h_i^{\text{V}} \tag{59}$$

We therefore do not need a separate model for heat of vaporization.

We determine the pure-component vapor pressure for a species by applying eq (24) and determining the pressure that yields the same value for the vapor and liquid fugacity coefficients:

$$\Phi_i^{\text{V}}\left(T, P_i^{\text{sat}}\right) = \Phi_i^{\text{L}}\left(T, P_i^{\text{sat}}\right) \tag{60}$$

where P_i^{sat} is the vapor pressure for species i.

Tables 2-4 and 2-5 summarize the properties and their sources for the EOS approach to thermodynamic modeling.

Table 2-4. Properties and model sources for the vapor phase in the equation-of-state approach.

Vapor Phase		
Property	Required Sub-Property	Method for Conventional and Polymer Species
fugacity coefficient	--	EOS
enthalpy	standard enthalpy of formation	literature value
	ideal-gas heat capacity	empirical correlation
	residual enthalpy	EOS
entropy	standard enthalpy of formation	literature value
	standard Gibbs energy of formation	literature value
	ideal-gas heat capacity	empirical correlation
	residual entropy	EOS
Gibbs free energy	standard enthalpy of formation	literature value
	standard Gibbs energy of formation	literature value
	ideal-gas heat capacity	empirical correlation
	residual Gibbs free energy	EOS
molar volume	--	EOS

Table 2-5. Properties and model sources for the liquid phase in the equation-of-state approach.

Liquid Phase		
Property	Required Sub-Property	Method for Conventional and Polymer Species
fugacity coefficient	--	EOS
enthalpy	standard enthalpy of formation	literature value
	ideal-gas heat capacity	empirical correlation
	residual enthalpy	EOS
entropy	standard enthalpy of formation	literature value
	standard Gibbs energy of formation	literature value
	ideal-gas heat capacity	empirical correlation
	residual entropy	EOS
Gibbs free energy	standard enthalpy of formation	literature value
	standard Gibbs energy of formation	literature value

	ideal-gas heat capacity	empirical correlation
	residual Gibbs free energy	EOS
molar volume	--	EOS

Symbols

English Symbols

a_i	calculated parameter in the PC-SAFT equation of state
a_{0i}	parameter in the PC-SAFT equation of state
a_{1i}	parameter in the PC-SAFT equation of state
a_{2i}	parameter in the PC-SAFT equation of state
a^{res}	molar residual Helmholtz energy
$a_{\text{SAFT}}^{\text{res}}$	molar residual Helmholtz energy in the SAFT equation of state
$a_{\text{SAFT}}^{\text{hs}}$	hard-sphere contribution to the molar residual Helmholtz energy in the SAFT equation of state
$a_{\text{SAFT}}^{\text{hc}}$	hard-chain contribution to the molar residual Helmholtz energy in the SAFT equation of state
$a_{\text{SAFT}}^{\text{disp}}$	dispersion contribution to the molar residual Helmholtz energy in the SAFT equation of state
$a_{\text{SAFT}}^{\text{assoc}}$	association contribution to the molar residual Helmholtz energy in the SAFT equation of state
A_i	parameter in heat-capacity correlation
A^{res}	residual Helmholtz energy
b_i	calculated parameter in the PC-SAFT equation of state
b_{0i}	parameter in the PC-SAFT equation of state
b_{1i}	parameter in the PC-SAFT equation of state
b_{2i}	parameter in the PC-SAFT equation of state
B_i	parameter in heat-capacity correlation
C_1	calculated parameter in the PC-SAFT equation of state
C_i	parameter in heat-capacity correlation

C_{p}	heat capacity
$C_{\mathrm{p},i}$	heat capacity of species i
$C_{\mathrm{p,L}}$	liquid heat capacity
$c_{\mathrm{p},i}^{\mathrm{ig}}$	ideal-gas heat capacity
ΔC_{p}	residual contribution to heat capacity, computed with equation of state
d_i	calculated parameter in the PC-SAFT equation of state
D_i	parameter in heat-capacity correlation
E_i	parameter in heat-capacity correlation
EOS	equation of state
$f_i^{\boldsymbol{a}}$	fugacity of species i in phase $\boldsymbol{a}$
g	molar Gibbs free energy
g^{ig}	molar ideal-gas Gibbs free energy
g^{res}	molar residual Gibbs free energy
g_{ii}^{hs}	radial-pair distribution function for segments of species i in the PC-SAFT equation of state
$\Delta g_{\mathrm{f},i}$	molar Gibbs free energy of mixing
G	Gibbs free energy
G^{res}	residual Gibbs free energy
h	molar enthalpy
H	enthalpy
h_i	molar enthalpy of species i
h_i^{ig}	molar ideal-gas enthalpy of species i
h^{ig}	molar ideal-gas enthalpy
h^{res}	residual molar enthalpy
H^{ig}	ideal-gas enthalpy
H_i^{ig}	ideal-gas enthalpy of species i
H^{res}	residual enthalpy
$H^{\mathrm{res,L}}$	liquid residual enthalpy
$H^{\mathrm{res,V}}$	vapor residual enthalpy

Δh_i^{vap}	enthalpy of vaporization of species i
h_i^{L}	molar liquid enthalpy of species i
h_i^{V}	molar vapor enthalpy of species i
H^{L}	liquid molar enthalpy
H^{V}	vapor molar enthalpy
HDPE	high-density polyethylene
$\Delta H_{\text{f},i}$	enthalpy of formation of species i
k	Boltzmann's constant
k_{ij}	binary interaction parameter
I_1	calculated parameter in the PC-SAFT equation of state
I_2	calculated parameter in the PC-SAFT equation of state
m	characteristic chain length in the PC-SAFT equation of state
$\overline{m}$	calculated parameter in the PC-SAFT equation of state
m_i	mass fraction of species i; number of segments per chain of species i; number of segments per chain of species i in the PC-SAFT equation of state
M_{n}	number-average molecular weight
n_{T}	total number of moles
N	number of molecules
N_0	number of empty lattice sites
N_{A}	Avogadro's number
N_{tot}	total number of lattice sites
P	pressure
P^*	characteristic pressure in the Sanchez-Lacombe equation of state
$\overline{P}$	reduced pressure in the Sanchez-Lacombe equation of state
$P_{\text{c},i}$	critical pressure of component i
P_i^{s}	vapor pressure for component i
PC-SAFT	Perturbed-Chain Statistical Associating Fluid Theory equation of state
r	number of lattice sites occupied by each molecule
R	gas constant

$r_{i,I}$	degree of polymerization of polymer i, segment type I
r_{mix}	mixture parameter in the Sanchez-Lacombe equation of state
s	molar entropy
s^{ig}	molar ideal-gas entropy
s^{res}	molar residual entropy
s_i^{ig}	molar ideal-gas entropy of species i
s_L^{ig}	liquid molar ideal-gas entropy
s_V^{ig}	vapor molar ideal-gas entropy
S	entropy
SAFT	Statistical Associating Fluid Theory equation of state
SL	Sanchez-Lacombe equation of state
STP	standard temperature and pressure
T	temperature
T^*	characteristic temperature in the Sanchez-Lacombe equation of state
T^{ref}	reference temperature
$T_{c,i}$	critical temperature of component i
$\overline{T}$	reduced temperature in the Sanchez-Lacombe equation of state
v^*	volume of each lattice site
$\boldsymbol{n}_{ij}^*$	cross parameter in the Sanchez-Lacombe equation of state
$\boldsymbol{n}_{mix}^*$	mixture parameter in the Sanchez-Lacombe equation of state
v^L	liquid molar volume
v_i^L	liquid molar volume of species i
v^V	vapor molar volume
V	volume
$\overline{v}_i$	mixture molar volume
VLE	vapor-liquid equilibrium
x_i	liquid mole fraction of i
X_i	segment-based mole fraction of species i
y_i	vapor mole fraction of i

z	compressibility factor
z^{id}	ideal compressibility contribution, equal to unity
z^{hs}	hard-sphere contribution to compressibility
z^{hc}	hard-chain contribution to compressibility
z^{disp}	dispersion contribution to compressibility

Greek Symbols

$\boldsymbol{f}_i$	volume fraction of species i
$\boldsymbol{r}$	molar density
$\boldsymbol{r}^V$	molar vapor density
$\boldsymbol{r}^L$	molar liquid density
$\boldsymbol{r}^*$	characteristic molar density in the Sanchez-Lacombe equation of state
$\boldsymbol{r}_{c,i}$	critical molar density of species i
$\overline{\boldsymbol{r}}$	reduced density in the Sanchez-Lacombe equation of state
$\boldsymbol{h}$	calculated parameter in the PC-SAFT equation of state
Φ_i	fugacity coefficient of species i
Φ_i^L	liquid fugacity coefficient of species i
Φ_i^V	vapor fugacity coefficient of species i
$\boldsymbol{e}^*$	characteristic interaction energy per mole of segments in the Sanchez-Lacombe equation of state
$\boldsymbol{e}_{ij}^*$	cross parameter in the Sanchez-Lacombe equation of state
$\boldsymbol{e}_{mix}^*$	mixture parameter in the Sanchez-Lacombe equation of state
$\boldsymbol{h}_{ij}$	binary interaction parameter in the Sanchez-Lacombe equation of state
$\boldsymbol{e}_i$	segment energy parameter in the PC-SAFT equation of state
$\boldsymbol{p}$	Pi
$\boldsymbol{s}_i$	characteristic segment diameter in the PC-SAFT equation of state
$\boldsymbol{z}_n$	calculated parameter in the PC-SAFT equation of state

2.4 Appendices

2.4.1 Residual Thermodynamic Properties from the Equation-of-State Approach

Here, we provide expressions for computing the residual thermodynamic properties of mixtures using the equation of state approach described in the beginning of the chapter. The properties we consider here are fugacity, enthalpy, entropy, Gibbs free energy, and Helmholtz energy. There are two different forms for each equation, corresponding to the type of EOS used, namely, pressure- or volume-explicit forms. Pressure-explicit EOS give pressure as a function of temperature and molar volume, while volume-explicit EOS give molar volume in terms of pressure and temperature.

There are several equivalent relations for computing the various thermodynamic properties. A particularly useful approach is the use of the residual Helmholtz energy, from which we can derive all other thermodynamic properties.

In the EOS approach, we use the same equations for both the vapor and liquid phases. While each phase shares the same temperature and pressure, they have independent densities and compositions.

The residual molar Helmholtz energy is

$$a^{\text{res}} = RT \int_0^r (z-1) \frac{dr}{r} \tag{61}$$

where z is the mixture compressibility:

$$z = \frac{Pv}{RT} \tag{62}$$

We use the EOS to compute the values for the fugacity coefficients as follows:

$$RT \ln \Phi_i = \frac{\partial}{\partial n_i}\left(n_{\mathrm{T}} a^{\mathrm{res}}\right) - RT \ln z$$

$$= a^{\mathrm{res}} + n_{\mathrm{T}} \frac{\partial a^{\mathrm{res}}}{\partial n_i} - RT \ln z \tag{63}$$

$$= a^{\mathrm{res}} + \frac{\partial a^{\mathrm{res}}}{\partial x_i} - \sum_j x_j \left(\frac{\partial a^{\mathrm{res}}}{\partial x_j}\right) + RT(z - 1 - \ln z)$$

where n_i is the number of moles of species i in the mixture.

We use these equations for both vapor and liquid calculations. The only difference between the two cases is that the mixing rules used for the EOS are based on the composition of the specific phase of interest.

Alternatively, we can use equivalent expressions for the fugacity coefficient[25]. For a pressure-explicit EOS:

$$RT \ln \Phi_i = \int_V^\infty \left[\left(\frac{\partial P}{\partial n_i}\right)_{T,V,n_j} - \frac{RT}{V}\right] dV - RT \ln z \tag{64}$$

For a volume-explicit EOS:

$$RT \ln \Phi_i = \int_0^P \left[\overline{v}_i - \frac{RT}{P}\right] dP \tag{65}$$

In terms of the residual Helmholtz energy, the expressions for the residual enthalpy, entropy, and Gibbs free energy are

$$H^{\mathrm{res}} = RT(z - 1) + A^{\mathrm{res}} - T\frac{\partial A^{\mathrm{res}}}{\partial T} \tag{66}$$

$$S^{\mathrm{res}} = R \ln z - \frac{\partial A^{\mathrm{res}}}{\partial T} \tag{67}$$

$$G^{\mathrm{res}} = H^{\mathrm{res}} - TS^{\mathrm{res}} \tag{68}$$

---

[25] Prausnitz, J. M.; Lichtenthaler, R. N.; de Azevedo, E. G. *Molecular Thermodynamics of Fluid-Phase Equilibria*; Prentice Hall: New Jersey, 1999, Chapter 3.

Using a pressure-explicit EOS, we can use alternative expressions:

$$H^{\text{res}} = \int_V^\infty \left[P - T\left(\frac{\partial P}{\partial T}\right)_{V,n_\text{T}} \right] \mathrm{d}V \tag{69}$$

$$S^{\text{res}} = \int_V^\infty \left[\frac{n_\text{T}\text{R}}{P} - \left(\frac{\partial P}{\partial T}\right)_{V,n_\text{T}} \right] \mathrm{d}V + \text{R}\sum_i n_i \ln\left(\frac{V}{n_i \text{R} T}\right) \tag{70}$$

$$G^{\text{res}} = \int_V^\infty \left[P - \frac{n_\text{T}RT}{V} \right] \mathrm{d}V - \text{R}T\sum_i n_i \ln\left(\frac{V}{n_i \text{R} T}\right) \tag{71}$$

For a volume-explicit EOS, we have

$$H^{\text{res}} = \int_0^P \left[V - T\left(\frac{\partial V}{\partial T}\right)_{P,n_\text{T}} \right] \mathrm{d}P \tag{72}$$

$$S^{\text{res}} = \int_0^P \left[\frac{n_\text{T}\text{R}}{P} - \left(\frac{\partial V}{\partial T}\right)_{P,n_\text{T}} \right] \mathrm{d}P - \text{R}\sum_i n_i \ln\left(y_i P \right) \tag{73}$$

$$G^{\text{res}} = \int_0^P \left[V - \frac{n_\text{T}RT}{P} \right] \mathrm{d}P + \text{R}T\sum_i n_i \ln\left(y_i P \right) \tag{74}$$

2.4.2 Model Constants for the PC-SAFT EOS

Table 2-6 lists the constants for the parameters $a_{j,i}$ and $b_{j,i}$ that appear in eqs (43) and (44)

.

Table 2-6. Model constants for eqs (43) and (44) in the PC-SAFT EOS[4].

i	$a_{0,i}$	$a_{1,i}$	$a_{2,i}$	$b_{0,i}$	$b_{1,i}$	$b_{2,i}$
0	0.9105631445	-0.3084016918	-0.0906148351	0.7240946941	-0.5755498075	0.0976883116
1	0.6361281449	0.1860531159	0.4527842806	2.2382791861	0.6995095521	-0.2557574982
2	2.6861347891	-2.5030047259	0.5962700728	-4.0025849485	3.8925673390	-9.1558561530
3	-26.547362491	21.419793629	-1.7241829131	-21.003576815	-17.215471648	20.642075974
4	97.759208784	-65.255885330	-4.1302112531	26.855641363	192.67226447	-38.804430052
5	-159.59154087	83.318680481	13.776631870	206.55133841	-161.82646165	93.626774077
6	91.297774084	-33.746922930	-8.6728470368	-355.60235612	-165.20769346	-29.666905585

Chapter 3 Polymerization Kinetics

3.1 Introduction

The purpose of this chapter is to describe the reaction mechanisms for Ziegler-Natta and metallocene catalyzed polymerizations. Each type involves a unique set of elementary reactions that affects the properties of the corresponding polymer product. We also describe the method of moments, which is a useful mathematical treatment for developing rate expressions for reactor modeling.

The structure of this chapter is as follows. We begin by providing the notation used for polymer species throughout the chapter. We follow this with a description of the method of moments. Finally, we give individual sections that discuss the mechanisms and rate expressions for Ziegler-Natta and metallocene systems.

3.2 Notation for Polymer Species

There potentially are a number of different types of polymer species that we may choose to use in a given reaction model, depending on the number and type of polymer properties we wish to track. Table 3-1 gives the different species we consider in this work. The three basic types of polymer molecules include live chains, dead chains, and dead chains with terminal double bonds. Live chains are those that are capable of further growth by addition of monomer. For catalyzed systems, live chains are those that are attached to active catalyst sites. Dead chains are no longer able to add monomer, although they can participate in other reactions. Tracking dead chains with terminal double bonds is important for metallocene systems, where these molecules are incorporated into growing chains to yield long-chain branches. Just trace amounts of these branches can have a large effect on the flow properties of the resulting polymer.

Table 3-1. Polymer species used in the development of polymerization kinetics.

polymeric species	description

$P_{n,i}$	live chain of length n, attached to catalyst site type i
D_n	dead chain of length n
$D_n^=$	dead chain of length n with a terminal double bond

The most basic polymer property is chain length. We use a subscripted n to represent the number of segments in a given polymer chain. The reaction rates for copolymerization kinetics can depend on the last monomer added to the growing chain. Finally, we designate a dead polymer chain with a terminal double bond with a superscripted =.

3.3 Mathematical Treatment of Polymerization Kinetics

We use the *method of moments* to rewrite the kinetic equations for each polymerization mechanism in terms of the leading moments of the molecular-weight distribution of the polymer. This is also known as the population-balance method. This treatment is a statistical technique that enables us to track various polymer chain properties without the need to include the very large number of equations and unknowns required to account for chains of every possible length. Common properties we can model include chain-length distributions, type and frequency of chain branching, and content of terminal double bonds.

3.3.1 Leading Moments of the Molecular Weight Distribution

The moments are averages of the concentrations of polymer molecules that are weighted by their chain lengths. The moment expression for live polymer chains is

$$\boldsymbol{l}_{i,j} = \sum_{n=1}^{\infty} n^i \left[P_{n,j} \right] \tag{1}$$

where $\boldsymbol{l}_{i,j}$ is the ith moment of the molecular weight distribution of live chains attached to catalyst site type j, and $\left[P_{n,j} \right]$ is the molar concentration of the corresponding live polymer chains. We write a similar expression for dead chains:

$$\boldsymbol{m}_i = \sum_{n=2}^{\infty} n^i \left[\mathrm{D}_n \right] \tag{2}$$

where $\boldsymbol{m}_i$ is the ith moment of the molecular weight distribution of dead chains and $[\mathrm{D}_n]$ is the molar concentration of the corresponding dead chains. Finally, for dead chains with terminal double bonds, we have

$$\boldsymbol{m}_i^{=} = \sum_{n=2}^{\infty} n^i \left[\mathrm{D}_n^{=} \right] \tag{3}$$

the notation for which is analogous to that in eq (2).

The three leading moments, namely, the zeroth, first, and second, are sufficient for describing the molecular weight distribution of most commercial polymers.

3.3.2 Polymer Properties in Terms of Moment Expressions

We can deduce a variety of common polymer properties using the moment expressions given in the previous section. The number-average degree of polymerization is

$$DPN = \frac{\boldsymbol{l}_1 + \boldsymbol{m}_1 + \boldsymbol{m}_1^{=}}{\boldsymbol{l}_0 + \boldsymbol{m}_0 + \boldsymbol{m}_0^{=}} \tag{4}$$

The weight-average degree of polymerization is

$$DPW = \frac{\boldsymbol{l}_2 + \boldsymbol{m}_2 + \boldsymbol{m}_2^{=}}{\boldsymbol{l}_1 + \boldsymbol{m}_1 + \boldsymbol{m}_1^{=}} \tag{5}$$

The number-average molecular weight is

$$M_{\mathrm{n}} = M_{\mathrm{seg}} \times \frac{\boldsymbol{l}_1 + \boldsymbol{m}_1 + \boldsymbol{m}_1^{=}}{\boldsymbol{l}_0 + \boldsymbol{m}_0 + \boldsymbol{m}_0^{=}} \tag{6}$$

where M_{seg} is the molecular weight of the segments that comprise the chains. The weight-average molecular weight is

$$M_{\mathrm{w}} = M_{\mathrm{seg}} \times \frac{\boldsymbol{l}_2 + \boldsymbol{m}_2 + \boldsymbol{m}_2^{=}}{\boldsymbol{l}_1 + \boldsymbol{m}_1 + \boldsymbol{m}_1^{=}} \tag{7}$$

The polydispersity index is

$$PDI = \frac{M_w}{M_n} = \frac{\left(l_2 + m_2 + \bar{\bar{m}}_2\right)\left(l_0 + m_0 + \bar{\bar{m}}_0\right)}{\left(l_1 + m_1 + \bar{\bar{m}}_1\right)^2} \tag{8}$$

The number of long-chain branches per 1000 carbon atoms is

$$LCB/1000Cs = 500 \times \frac{[LCB]}{l_1 + m_1 + \bar{\bar{m}}_1} \tag{9}$$

The number of long-chain branches per polymer chain is

$$LCB/mol = \frac{[LCB]}{l_0 + m_0 + \bar{\bar{m}}_0} \tag{10}$$

3.4 Ziegler-Natta Polymerization

3.4.1 Catalyst Chemistry

The patent definition of a Ziegler-Natta catalyst is the combination of a transition-metal salt whose metal is from groups IV to VII of the Periodic Table, and a metal alkyl whose metal is from groups I to III of the Table[26]. The most common catalyst system is titanium tetrachloride, $TiCl_4$, with triethyl aluminum, $Al(C_2H_5)_3$, and it is used for polyethylene production. There exist some Ziegler-Natta catalysts that do not require activation by a cocatalyst.

Various catalyst-cocatalyst combinations yield behavior that can be markedly different. They can vary in activity, stability, ability to polymerize specific monomers and incorporate comonomers, ability to control tacticity, and their effects on the molecular-weight distribution of the polymer, among other properties[26].

Figure 3-1 illustrates a proposed scheme for the activation of $TiCl_4$ by $Al(C_2H_5)_3$[26]. The catalyst and cocatalyst undergo several elementary reactions before forming a complex

---

[26] Boor, J. *Ziegler-Natta Catalysts and Polymerizations*, Academic Press: New York, 1979.

capable of polymerization. The role of the cocatalyst is to alkylate the transition-metal salt to yield an active catalyst site.

$$TiCl_4 + Al(C_2H_5)_3 \rightarrow (C_2H_5)TiCl_3 + Al(C_2H_5)2Cl$$
$$TiCl_4 + Al(C_2H_5)2Cl \rightarrow (C_2H_5)TiCl_3 + Al(C_2H_5)Cl_2$$
$$TiCl_4 + Al(C_2H_5)Cl_2 \rightarrow (C_2H_5)TiCl_3 + AlCl_3$$
$$(C_2H_5)TiCl_3 \rightarrow TiCl_3 + (C_2H_5)\bullet$$
$$2(C_2H_5)\bullet \rightarrow ethylene + ethane$$
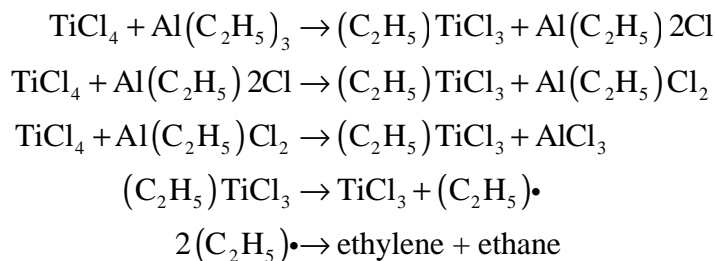
Figure 3-1. An example of a mechanism of catalyst activation by cocatalyst[26].

During chain growth, the double bonds in monomer molecules coordinate to the active catalyst sites. As a result, the monomer units added at early times are farther down the chain extending from the catalyst site, relative to monomer added more recently. Figure 3-2 shows the generally accepted addition mechanism, according to Cossee[27].
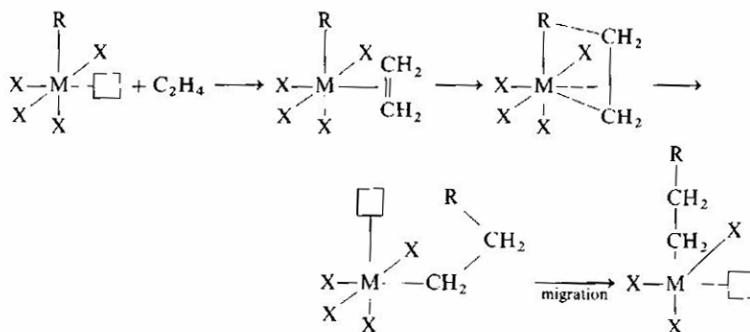
Figure 3-2. Mechanism for ethylene addition to a growing chain for a Ziegler-Natta catalyst, derived by Cossee. The ethylene double bond coordinates to the catalyst site (M) and upon addition the empty site migrates back to its original position. X represents the ligands of the transition metal, and is typically Cl. R is either the alkyl from the metal alkyl (e.g., $Al(C_2H_5)_3$), or the growing polymer chain. Taken from Boor[26], p. 329.

---

[27] Cossee, P. Ziegler-Natta Catalysis I. Mechanism of Polymerization of *a*-Olefins with Ziegler-Natta Catalysts. *Journal of Catalysis* **1964**, *3*, 80.

There are two existing theories that explain the ability for Ziegler-Natta catalysts to produce polydisperse polymers. The first is diffusive and the second is kinetic. The diffusive theory involves the assumption that mass-transfer limitations affect the ability of the monomer molecules to reach some of the active sites on the catalyst particle, due to the presence of pores or other structural effects that hinder transport to the sites. As a result, different sites polymerize monomer at different rates, leading to a polydisperse polymer product[28].

The kinetic theory involves the assumption that there exist different catalyst site types, each with its own relative reactivity, due to variations in the local chemical composition of each site type. An example is the presence of different ligands on the active transition metal. Experimentation has provided compelling evidence that this second theory is a more accurate description of the physical reality[28,29,30]. These site types tend to produce chains that differ in both length and comonomer composition. More specifically, the sites that produce longer chains tend to incorporate less comonomer[26]. We therefore develop our kinetic equations based on the kinetic theory, rather than the mass-transfer theory.

Ziegler-Natta catalysts are used in soluble, colloidal, and heterogeneous forms. Each one has its own advantages, depending on the application[26]. Supported versions are used in gas-phase and slurry processes, while soluble catalysts are used in solution processes. Although the supported types tend to have higher activity than the non-supported ones, likely due to an increase in the number of catalyst sites that are active, the catalytic mechanism is the same[30].

[28] Xie, T.; McAuley, K. B.; Hsu, J. C. C.; Bacon, D. W. Gas Phase Ethylene Polymerization: Production Processes, Polymer Properties, and Reactor Modeling. *Industrial and Engineering Chemistry Research* **1994**, *33*, 449.
[29] de Carvalho, A. B.; Gloor, P. E.; Hamielec, A. E. A Kinetic Mathematical Model for Heterogeneous Ziegler-Natta Copolymerization. *Polymer* **1989**, *30*, 280.
[30] Peacock, A. J. *Handbook of Polyethylene*, Marcel Dekker: New York, 2000, pp. 1-10, 43-66.

3.4.2 Kinetic Mechanism for Polymerization

Here, we describe each of the reactions understood to take place for Ziegler-Natta polymerizations. Not all reactions may be applicable in every process. For example, chain transfer to hydrogen occurs only when hydrogen is added as a chain-transfer agent. A general kinetic scheme for polymerizations using Ziegler-Natta catalysts includes the following elementary reactions[28,31]:

1. Catalyst activation.
2. Chain initiation.
3. Chain propagation.
4. Chain transfer.
5. Catalyst deactivation.
6. Reversible catalyst site inhibition.

3.4.2.1 Catalyst Activation

There are four ways for the catalyst to become activated[28]: spontaneously, by cocatalyst, by monomer, and by hydrogen. If the modeled process uses a cocatalyst, and no specific information about the susceptibility of the catalyst to activate upon reaction with either monomer or hydrogen exists, a first approach should utilize only the activation by cocatalyst, since this is the primary activation path. It is important to minimize the model complexity unless there exists sufficient information to do otherwise. We denote the catalyst species and corresponding reaction constants with a subscripted i, referring to the individual site types.

The reactions for activation are:

$$\mathrm{CAT}_i + \mathrm{COCAT} \xrightarrow{k_{\mathrm{ac},i}} \mathrm{P}_{0,i} \tag{11}$$

$$\mathrm{CAT}_i + \mathrm{M} \xrightarrow{k_{\mathrm{am},i}} \mathrm{P}_{0,i} \tag{12}$$

---
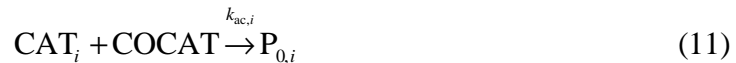
[31] McAuley, K. B.; MacGregor, J. F.; Hamielec, A. E. A Kinetic Model for Industrial Gas-Phase Ethylene Polymerization. *AIChE Journal* **1990**, *36*, 837.

$$\text{CAT}_i + \text{H}_2 \xrightarrow{k_{\text{ah},i}} \text{P}_{0,i} \tag{13}$$

$$\text{CAT}_i \xrightarrow{k_{\text{asp},i}} \text{P}_{0,i} \tag{14}$$

3.4.2.2 Chain Initiation

Chain initiation involves the addition of the first monomer unit to an active catalyst site. The reaction is

$$\text{P}_{0,i} + \text{M} \xrightarrow{k_{\text{ini}i}} \text{P}_{1,i} \tag{15}$$

3.4.2.3 Chain Propagation

This step is the addition of monomer species to the growing chains. Since the monomer units add to the chain at the catalyst site, we segregate chains based on the site type of the catalyst they are attached to:

$$\text{P}_{n,i} + \text{M} \xrightarrow{k_{\text{p},i}} \text{P}_{n+1,i} \tag{16}$$
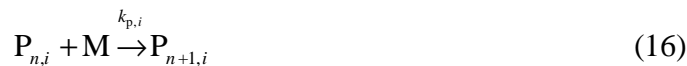
3.4.2.4 Chain Transfer to Monomer

Instead of adding to a growing chain, a monomer molecule can cause a live chain to detach from the catalyst site during insertion:

$$\text{P}_{n,i} + \text{M} \xrightarrow{k_{\text{tm},i}} \text{D}_n + \text{P}_{1,i} \tag{17}$$

3.4.2.5 Chain Transfer to Solvent

Similarly, a solvent species can also create a dead chain, leaving a live chain with a single segment. Note that we do not account for the compositional effect of the solvent on the polymer properties. This is reasonable because the fraction of solvent that participates in chain growth relative to monomer is vanishingly small, and the solvent is typically a light hydrocarbon similar to the monomer.

$$P_{n,i} + S \xrightarrow{k_{ts,i}} D_n + P_{1,i} \tag{18}$$

3.4.2.6 Chain Transfer to Transfer Agent

Some processes use a transfer agent for molecular-weight control. Hydrogen is the most common species chosen[32]. Hydrogen reacts with the catalyst site to disengage the polymer chain

$$P_{n,i} + H_2 \xrightarrow{k_{th,i}} D_n + P_{0,i} \tag{19}$$

This produces an empty live site, unlike the previous chain-transfer reactions that produce an initiated site.

3.4.2.7 Chain Transfer to Cocatalyst

Cocatalyst has been known to act as a chain transfer agent in Ziegler-Natta systems:

$$P_{n,i} + COCAT \xrightarrow{k_{tc,i}} D_n + P_{1,i} \tag{20}$$

3.4.2.8 Spontaneous Chain Transfer

A growing chain can spontaneously detach from the catalyst site.

$$P_{n,i} \xrightarrow{k_{tsp,i}} D_n + P_{0,i} \tag{21}$$

---

[32] Vandenberg, E. J. Process for Polymerizing Olefins Wherein Hydrogen Is Utilized as a Molecular Weight Control Agent. U.S. Patent 3,051,690, 1962.

3.4.2.9 Catalyst Deactivation

We consider the possible deactivation of catalyst by monomer, cocatalyst, and transfer agent, as well as spontaneous deactivation.

$$P_{n,i} + M \xrightarrow{k_{dm,i}} D_n \tag{22}$$

$$P_{n,i} + COCAT \xrightarrow{k_{dc,i}} D_n \tag{23}$$

$$P_{n,i} + H_2 \xrightarrow{k_{dh,i}} D_n \tag{24}$$

$$P_{n,i} \xrightarrow{k_{dsp,i}} D_n \tag{25}$$

3.4.2.10 Reversible Catalyst Site Inhibition

Some species are known to inhibit catalyst sites. This inhibition is reversible. We write reactions for a general poison.

$$P_{n,i} + X \xrightarrow{k_{finh i}} D_n + ICAT_i \tag{26}$$

$$CAT_i + X \xrightarrow{k_{finh,i}} ICAT_i \tag{27}$$

$$ICAT_i \xrightarrow{k_{rinh i}} CAT_i + X \tag{28}$$
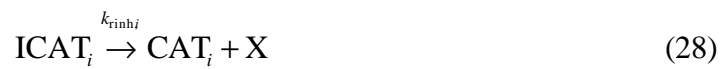
3.4.3 Development of Rate Expressions

We use the reactions provided in the previous section and the method of moments to develop rate expressions for each participating species. We directly apply these rate expressions in reactor models.

3.4.3.1 Unactivated Catalyst

For the unactivated catalyst sites:

$$R_{CAT_i} = -k_{ac,i}\left[CAT_i\right]\left[COCAT\right] - k_{am,i}\left[CAT_i\right]\left[M\right] - k_{ah,i}\left[CAT_i\right]\left[H_2\right]$$
$$-k_{asp,i}\left[CAT_i\right] - k_{finh,i}\left[CAT_i\right]\left[X\right] + k_{rinh,i}\left[ICAT_i\right]$$

(29)

3.4.3.2 Inhibited Catalyst

For the inhibited catalyst sites:

$$R_{ICAT_i} = k_{finh,i}\left[CAT_i\right]\sum_{n=1}^{\infty}\left[P_{n,i}\right] + k_{finh,i}\left[CAT_i\right]\left[X\right] - k_{rinh,i}\left[ICAT_i\right]$$
$$= k_{finh,i}\left[CAT_i\right]\boldsymbol{\lambda}_{0,i} + k_{finh,i}\left[CAT_i\right]\left[X\right] - k_{rinh,i}\left[ICAT_i\right]$$

(30)

3.4.3.3 Cocatalyst

For the cocatalyst species:

$$R_{COCAT} = -\left[COCAT\right]\sum_{i}k_{ac,i}\left[CAT_i\right] - \left[COCAT\right]\sum_{i}k_{tc,i}\sum_{n=1}^{\infty}\left[P_{n,i}\right]$$

$$-\left[COCAT\right]\sum_{i}k_{dc,i}\sum_{n=1}^{\infty}\left[P_{n,i}\right]$$

$$= -\left[COCAT\right]\sum_{i}k_{ac,i}\left[CAT_i\right] - \left[COCAT\right]\sum_{i}k_{tc,i}\boldsymbol{\lambda}_{0,i}$$

$$-\left[COCAT\right]\sum_{i}k_{dc,i}\boldsymbol{\lambda}_{0,i}$$

(31)

3.4.3.4 Empty Active Catalyst Sites

For active catalyst sites that have not yet polymerized monomer:

$$
\begin{aligned}
R_{\mathrm{P}_{0,i}} &= k_{\mathrm{ac},i}\left[\mathrm{CAT}_i\right]\left[\mathrm{COCAT}\right] + k_{\mathrm{am},i}\left[\mathrm{CAT}_i\right]\left[\mathrm{M}\right] + k_{\mathrm{ah},i}\left[\mathrm{CAT}_i\right]\left[\mathrm{H}_2\right] \\
&\quad + k_{\mathrm{asp},i}\left[\mathrm{CAT}_i\right] - k_{\mathrm{ini},i}\left[\mathrm{M}\right]\left[\mathrm{P}_{0,i}\right] + k_{\mathrm{th},i}\left[\mathrm{H}_2\right]\sum_{n=1}^{\infty}\left[\mathrm{P}_{n,i}\right] + k_{\mathrm{tsp},i}\sum_{n=1}^{\infty}\left[\mathrm{P}_{n,i}\right] \\
&= k_{\mathrm{ac},i}\left[\mathrm{CAT}_i\right]\left[\mathrm{COCAT}\right] + k_{\mathrm{am},i}\left[\mathrm{CAT}_i\right]\left[\mathrm{M}\right] + k_{\mathrm{ah},i}\left[\mathrm{CAT}_i\right]\left[\mathrm{H}_2\right] \\
&\quad + k_{\mathrm{asp},i}\left[\mathrm{CAT}_i\right] - k_{\mathrm{ini},i}\left[\mathrm{M}\right]\left[\mathrm{P}_{0,i}\right] + k_{\mathrm{th},i}\left[\mathrm{H}_2\right]\boldsymbol{\lambda}_{0,i} + k_{\mathrm{tsp},i}\boldsymbol{\lambda}_{0,i}
\end{aligned}
\tag{32}
$$

3.4.3.5 Monomer

For the monomer species:

$$
\begin{aligned}
R_{\mathrm{M}} &= -\left[\mathrm{M}\right]\sum_i k_{\mathrm{am},i}\left[\mathrm{CAT}_i\right] - \left[\mathrm{M}\right]\sum_i k_{\mathrm{ini},i}\left[\mathrm{P}_{0,i}\right] - \left[\mathrm{M}\right]\sum_i k_{\mathrm{p},i}\sum_{n=1}^{\infty}\left[\mathrm{P}_{n,i}\right] \\
&\quad -\left[\mathrm{M}\right]\sum_i k_{\mathrm{tm},i}\sum_{n=1}^{\infty}\left[\mathrm{P}_{n,i}\right] - \left[\mathrm{M}\right]\sum_i k_{\mathrm{dm},i}\sum_{n=1}^{\infty}\left[\mathrm{P}_{n,i}\right] \\
&= -\left[\mathrm{M}\right]\sum_i k_{\mathrm{am},i}\left[\mathrm{CAT}_i\right] - \left[\mathrm{M}\right]\sum_i k_{\mathrm{ini},i}\left[\mathrm{P}_{0,i}\right] - \left[\mathrm{M}\right]\sum_i k_{\mathrm{p},i}\boldsymbol{\lambda}_{0,i} \\
&\quad -\left[\mathrm{M}\right]\sum_i k_{\mathrm{tm},i}\boldsymbol{\lambda}_{0,i} - \left[\mathrm{M}\right]\sum_i k_{\mathrm{dm},i}\boldsymbol{\lambda}_{0,i}
\end{aligned}
\tag{33}
$$

3.4.3.6 Solvent

For the solvent species:

$$
\begin{aligned}
R_{\mathrm{S}} &= -\left[\mathrm{S}\right]\sum_i k_{\mathrm{ts},i}\sum_{n=1}^{\infty}\left[\mathrm{P}_{n,i}\right] \\
&= -\left[\mathrm{S}\right]\sum_i k_{\mathrm{ts},i}\boldsymbol{\lambda}_{0,i}
\end{aligned}
\tag{34}
$$

3.4.3.7 Chain-Transfer Agent (Hydrogen)

For the chain-transfer agent:

$$R_{\mathrm{H_2}} = -[\mathrm{H_2}]\sum_i k_{\mathrm{ah},i}[\mathrm{CAT}_i] - [\mathrm{H_2}]\sum_i k_{\mathrm{th},i}\sum_{n=1}^{\infty}[\mathrm{P}_{n,i}] - [\mathrm{H_2}]\sum_i k_{\mathrm{dh},i}\sum_{n=1}^{\infty}[\mathrm{P}_{n,i}]$$

$$= -[\mathrm{H_2}]\sum_i k_{\mathrm{ah},i}[\mathrm{CAT}_i] - [\mathrm{H_2}]\sum_i k_{\mathrm{th},i}\mathbf{I}_{0,i} - [\mathrm{H_2}]\sum_i k_{\mathrm{dh},i}\mathbf{I}_{0,i} \qquad (35)$$

3.4.3.8 Inhibitor/Poison

For the catalyst inhibitor or poison:

$$R_{\mathrm{X}} = -[\mathrm{X}]\sum_i k_{\mathrm{finh},i}\sum_{n=1}^{\infty}[P_{n,i}] - [\mathrm{X}]\sum_i k_{\mathrm{finh},i}[\mathrm{CAT}_i] + \sum_i k_{\mathrm{rinh},i}[\mathrm{ICAT}_i]$$

$$= -[\mathrm{X}]\sum_i k_{\mathrm{finh},i}\mathbf{I}_{0,i} - [\mathrm{X}]\sum_i k_{\mathrm{finh},i}[\mathrm{CAT}_i] + \sum_i k_{\mathrm{rinh},i}[\mathrm{ICAT}_i] \qquad (36)$$

If the poison is hydrogen, we add these reactions to the expression for chain-transfer agent, and replace the concentration of X with that for hydrogen.

3.4.3.9 Live Polymer Chains

For live polymer chains:

$$R_{\mathrm{P}_{n,j}} = \left(k_{\mathrm{ini},i}[\mathrm{M}][\mathrm{P}_{0,i}] + k_{\mathrm{tm},i}[\mathrm{M}][\mathrm{P}_{n,i}] + k_{\mathrm{ts},i}[\mathrm{S}][\mathrm{P}_{n,i}] + k_{\mathrm{tc},i}[\mathrm{COCAT}][\mathrm{P}_{n,i}]\right)_{n=1}$$

$$-k_{\mathrm{p},i}[\mathrm{M}][\mathrm{P}_{n,i}] + k_{\mathrm{p},i}[\mathrm{M}][\mathrm{P}_{n-1,i}] - k_{\mathrm{tm},i}[\mathrm{M}][\mathrm{P}_{n,i}] - k_{\mathrm{ts},i}[\mathrm{S}][\mathrm{P}_{n,i}]$$

$$-k_{\mathrm{th},i}[\mathrm{H_2}][\mathrm{P}_{n,i}] - k_{\mathrm{tc},i}[\mathrm{COCAT}][\mathrm{P}_{n,i}] - k_{\mathrm{tsp},i}[\mathrm{P}_{n,i}] - k_{\mathrm{dm},i}[\mathrm{M}][\mathrm{P}_{n,i}] \qquad (37)$$

$$-k_{\mathrm{dc},i}[\mathrm{COCAT}][\mathrm{P}_{n,i}] - k_{\mathrm{dh},i}[\mathrm{H_2}][\mathrm{P}_{n,i}] - k_{\mathrm{dsp},i}[\mathrm{P}_{n,i}] - k_{\mathrm{finh},i}[\mathrm{X}][\mathrm{P}_{n,i}]$$

We apply the moment definitions provided in Section 3.3 to obtain a general expression for the ith live moment of polymer chains:

$$R_{\mathbf{I}_{i,j}} = k_{\mathrm{ini},j}[\mathrm{M}][P_{0,j}] + k_{\mathrm{tm},j}[\mathrm{M}]\mathbf{I}_{0,j} + k_{\mathrm{ts},j}[\mathrm{S}]\mathbf{I}_{0,j} + k_{\mathrm{tc},j}[\mathrm{COCAT}]\mathbf{I}_{0,j}$$

$$+k_{\mathrm{p},j}[\mathrm{M}]\left(\sum_{k=0}^{l}\binom{l}{k}\mathbf{I}_{k,j} - \mathbf{I}_{l,j}\right) - k_{\mathrm{tm},j}[\mathrm{M}]\mathbf{I}_{i,j} - k_{\mathrm{ts},j}[\mathrm{S}]\mathbf{I}_{i,j}$$

$$-k_{\mathrm{th},j}[\mathrm{H_2}]\mathbf{I}_{i,j} - k_{\mathrm{tc},j}[\mathrm{COCAT}]\mathbf{I}_{i,j} - k_{\mathrm{tsp},j}\mathbf{I}_{i,j} - k_{\mathrm{dm},j}[\mathrm{M}]\mathbf{I}_{i,j} \qquad (38)$$

$$-k_{\mathrm{dc},j}[\mathrm{COCAT}]\mathbf{I}_{i,j} - k_{\mathrm{dh},j}[\mathrm{H_2}]\mathbf{I}_{i,j} - k_{\mathrm{dsp},j}\mathbf{I}_{i,j} - k_{\mathrm{finh},j}[\mathrm{X}]\mathbf{I}_{i,j}$$

We now determine expressions for the three leading moments of the live chains.

3.4.3.9.1 Zeroth Live Moment

$$R_{I_{0,i}} = k_{\text{ini},i}[\text{M}][\text{P}_{0,i}] - k_{\text{th},i}[\text{H}_2]\boldsymbol{I}_{0,i} - k_{\text{tsp},i}\boldsymbol{I}_{0,i} - k_{\text{dm},i}[\text{M}]\boldsymbol{I}_{0,i}$$
$$- k_{\text{dc},i}[\text{COCAT}]\boldsymbol{I}_{0,i} - k_{\text{dh},i}[\text{H}_2]\boldsymbol{I}_{0,i} - k_{\text{dsp},i}\boldsymbol{I}_{0,i} - k_{\text{finh},i}[\text{X}]\boldsymbol{I}_{0,i}$$

(39)

3.4.3.9.2 First Live Moment

$$R_{I_{1,i}} = k_{\text{ini},i}[\text{M}][\text{P}_{0i}] + \left(k_{\text{tm}i}[\text{M}]\boldsymbol{I}_{0,i} + k_{\text{ts},i}[\text{S}]\boldsymbol{I}_{0,i} + k_{\text{tc},i}[\text{COCAT}]\right)\left(\boldsymbol{I}_{0,i} - \boldsymbol{I}_{1,i}\right)$$
$$+ k_{\text{p},i}[\text{M}]\boldsymbol{I}_{0,i} - k_{\text{th},i}[\text{H}_2]\boldsymbol{I}_{1,i} - k_{\text{tsp},i}\boldsymbol{I}_{1,i} - k_{\text{dm},i}[\text{M}]\boldsymbol{I}_{1,i} - k_{\text{dc},i}[\text{COCAT}]\boldsymbol{I}_{1,i}$$
$$- k_{\text{dh},i}[\text{H}_2]\boldsymbol{I}_{1,i} - k_{\text{dsp},i}\boldsymbol{I}_{1,i} - k_{\text{finh},i}[\text{X}]\boldsymbol{I}_{1,i}$$

(40)

3.4.3.9.3 Second Live Moment

$$R_{I_{2,i}} = k_{\text{ini},i}[\text{M}][\text{P}_{0i}] + \left(k_{\text{tm},i}[\text{M}] + k_{\text{ts},i}[\text{S}] + k_{\text{tc},i}[\text{COCAT}]\right)\left(\boldsymbol{I}_{0,i} - \boldsymbol{I}_{2,i}\right)$$
$$+ k_{\text{p},i}[\text{M}]\left(\boldsymbol{I}_{0,i} + 2\boldsymbol{I}_{1,i}\right) - k_{\text{th},i}[\text{H}_2]\boldsymbol{I}_{2,i} - k_{\text{tsp},i}\boldsymbol{I}_{2,i} - k_{\text{dm},i}[\text{M}]\boldsymbol{I}_{2,i} - k_{\text{dc},i}[\text{COCAT}]\boldsymbol{I}_{2,i}$$
$$- k_{\text{dh},i}[\text{H}_2]\boldsymbol{I}_{2,i} - k_{\text{dsp},i}\boldsymbol{I}_{2,i} - k_{\text{finh},i}[\text{X}]\boldsymbol{I}_{2,i}$$

(41)

3.4.3.10 Dead Polymer Chains

$$R_{D_n} = [\text{M}]\sum_i k_{\text{tm},i}\sum_{n=1}^{\infty}[\text{P}_{n,i}] + [\text{S}]\sum_i k_{\text{ts},i}\sum_{n=1}^{\infty}[\text{P}_{n,i}] + [\text{H}_2]\sum_i k_{\text{th},i}\sum_{n=1}^{\infty}[\text{P}_{n,i}]$$

$$+ [\text{COCAT}]\sum_i k_{\text{tc},i}\sum_{n=1}^{\infty}[\text{P}_{n,i}] + [\text{M}]\sum_i k_{\text{dm},i}\sum_{n=1}^{\infty}[\text{P}_{n,i}] + [\text{COCAT}]\sum_i k_{\text{dc},i}\sum_{n=1}^{\infty}[\text{P}_{n,i}]$$

(42)

$$+ [\text{H}_2]\sum_i k_{\text{dh},i}\sum_{n=1}^{\infty}[\text{P}_{n,i}] + \sum_i k_{\text{dsp},i}\sum_{n=1}^{\infty}[\text{P}_{n,i}] + [\text{X}]\sum_i k_{\text{finh}i}\sum_{n=1}^{\infty}[\text{P}_{n,i}]$$

In terms of moment expressions, this becomes

$$R_{m_i} = [\text{M}]\sum_j k_{\text{tm},j}\boldsymbol{I}_{i,j} + [\text{S}]\sum_j k_{\text{ts},j}\boldsymbol{I}_{i,j} + [\text{H}_2]\sum_j k_{\text{th},j}\boldsymbol{I}_{i,j}$$

$$+ [\text{COCAT}]\sum_j k_{\text{tc},j}\boldsymbol{I}_{i,j} + [\text{M}]\sum_j k_{\text{dm},j}\boldsymbol{I}_{i,j} + [\text{COCAT}]\sum_j k_{\text{dc},j}\boldsymbol{I}_{i,j}$$

(43)

$$+ [\text{H}_2]\sum_j k_{\text{dh},j}\boldsymbol{I}_{i,j} + \sum_j k_{\text{dsp},j}\boldsymbol{I}_{i,j} + [\text{X}]\sum_j k_{\text{finh},j}\boldsymbol{I}_{i,j}$$

$$R_{m_0} = [\text{M}]\sum_i k_{\text{tm},i}\boldsymbol{I}_{0,i} + [\text{S}]\sum_i k_{\text{ts},i}\boldsymbol{I}_{0,i} + [\text{H}_2]\sum_i k_{\text{th},i}\boldsymbol{I}_{0,i}$$

$$+ [\text{COCAT}]\sum_i k_{\text{tc},i}\boldsymbol{I}_{0,i} + [\text{M}]\sum_i k_{\text{dm},i}\boldsymbol{I}_{0,i} + [\text{COCAT}]\sum_i k_{\text{dc},i}\boldsymbol{I}_{0,i} \qquad (44)$$

$$+ [\text{H}_2]\sum_i k_{\text{dh},i}\boldsymbol{I}_{0,i} + \sum_i k_{\text{dsp},i}\boldsymbol{I}_{0,i} + [\text{X}]\sum_i k_{\text{finh},i}\boldsymbol{I}_{0,i}$$

$$R_{m_1} = [\text{M}]\sum_i k_{\text{tm},i}\boldsymbol{I}_{1,i} + [\text{S}]\sum_i k_{\text{ts},i}\boldsymbol{I}_{1,i} + [\text{H}_2]\sum_i k_{\text{th},i}\boldsymbol{I}_{1,i}$$

$$+ [\text{COCAT}]\sum_i k_{\text{tc},i}\boldsymbol{I}_{1,i} + [\text{M}]\sum_i k_{\text{dm},i}\boldsymbol{I}_{1,i} + [\text{COCAT}]\sum_i k_{\text{dc},i}\boldsymbol{I}_{1,i} \qquad (45)$$

$$+ [\text{H}_2]\sum_i k_{\text{dh},i}\boldsymbol{I}_{1,i} + \sum_i k_{\text{dsp},i}\boldsymbol{I}_{1,i} + [\text{X}]\sum_i k_{\text{finh},i}\boldsymbol{I}_{1,i}$$

$$R_{m_2} = [\text{M}]\sum_i k_{\text{tm},i}\boldsymbol{I}_{2,i} + [\text{S}]\sum_i k_{\text{ts},i}\boldsymbol{I}_{2,i} + [\text{H}_2]\sum_i k_{\text{th},i}\boldsymbol{I}_{2,i}$$

$$+ [\text{COCAT}]\sum_i k_{\text{tc},i}\boldsymbol{I}_{2,i} + [\text{M}]\sum_i k_{\text{dm},i}\boldsymbol{I}_{2,i} + [\text{COCAT}]\sum_i k_{\text{dc},i}\boldsymbol{I}_{2,i} \qquad (46)$$

$$+ [\text{H}_2]\sum_i k_{\text{dh},i}\boldsymbol{I}_{2,i} + \sum_i k_{\text{dsp},i}\boldsymbol{I}_{2,i} + [\text{X}]\sum_i k_{\text{finh},i}\boldsymbol{I}_{2,i}$$

3.5 Metallocene Catalyzed Polymerizations

3.5.1 Catalyst Chemistry

Metallocene catalysts are defined as organometallic compounds that contain either one or two cyclopentadienyl rings or substituted cyclopentadienyl rings, which are bonded to a

central transition-metal atom. Figure 3-3 gives the general structure[33]. The transition metal, M, is from group IV of the Periodic Table. The transition-metal substituents, R, are hydrocarbyl, alkylidene, or halogen radicals. The cyclopentadienyl ring substituents, S, are hydrogen or hydrocarbyl radicals. The bridge, B, is an alkylene or alkyl radical[33]. A bridge is only present in constrained-geometry metallocenes, described in the next paragraph. The most commonly used transition metals are zirconium (Zr), titanium (Ti), and hafnium (Hf). As with Ziegler-Natta systems, changing the chemical environment of the transition-metal atom can lead to changes in the behavior of metallocene catalysts[34].
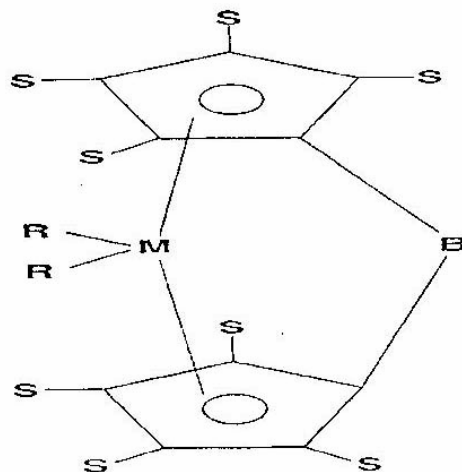
Figure 3-3. The general structure for a metallocene catalyst[33].

Constrained-geometry metallocenes have the face of the transition-metal more open for both the addition of *a*-olefins and polymer chains with terminal double bonds. The constrained cyclic structure is due to the use of a heteroatom bonding the cyclopentadienyl units to open the face of the transition-metal atom. This corresponds to the bridge atom (B) in Figure 3-3. This type of catalyst is able to incorporate polymer chains with terminal double bonds, creating long-chain branches[33]. These are substantially linear polymers, where the number of LCBs per chain is in the range of 0.01

---

[33] Hamielec, A. E.; Soares, J. B. P. Polymerization Reaction Engineering – Metallocene Catalysts. *Progress in Polymer Science* **1996**, *21*, 651.
[34] Soares, J. B. P.; Hamielec, A. E. Metallocene/Aluminoxane Catalysts for Olefin Polymerization. A Review. *Polymer Reaction Engineering* **1995**, *3*, 131.

– 3. The presence of a few long-chain branches can affect the rheology of the polymer product to a large extent.

Metallocene catalysts require activation by an aluminum-alkyl cocatalyst. The predominating cocatalyst for metallocene activation is methylaluminoxane. When this cocatalyst is used, metallocene catalysts have a much higher activity than traditional Ziegler-Natta catalysts. The aluminoxane is understood to be involved in site activation by alkylation of the metallocene, prevention of site deactivation, and impurity scavenging[33]. The structure of the methylaluminoxane is not known with certainty. The cocatalyst concentration affects the productivity of the polymerization and the molecular weight of the polymer[34].

Metallocenes are used in both soluble and insoluble (supported) forms. The soluble forms are useful in solution polymerizations for systems that produce long-chain branches, since the macromonomers can diffuse easily to the active sites. The supported forms were primarily developed so that metallocene catalysts could replace their Ziegler-Natta counterparts without the need to build new polymerization plants, since supported Ziegler-Natta catalysts were almost exclusively used because of their stability and activity compared with the soluble types[33].

3.5.2 Kinetic Mechanism for Polymerization

Several authors have recently presented kinetic mechanisms for metallocene-catalyzed polymerization[35,36,37]. Here, we provide a general reaction set that includes reactions corresponding to all types of metallocenes. They may not all be applicable to every system. For example, metallocenes that do not have a constrained geometry may not incorporate polymer chains with terminal double bonds to form long-chain branches.

[35] Beigzadeh, D.; Soares, J. B. P. Study of Long-Chain Branching in Ethylene Polymerization. *Polymer Reaction Engineering* **1997**, *5*, 141.

[36] Wang, W.-J.; Yan, D.; Zhu, S.; Hamielec, A. E. Kinetics of Long-Chain Branching in Continuous Solution Polymerization of Ethylene Using Constrained Geometry Metallocene. *Macromolecules* **1998**, *31*, 8677.

[37] Yiannoulakis, H.; Yiagopoulos, A.; Pladis, P.; Kiparissides, C. Comprehensive Dynamic Model for the Calculation of the Molecular Weight and Long Chain Branching Distributions in Metallocene-Catalyzed Ethylene Polymerization Reactors. *Macromolecules* **2000**, *33*, 2757.

The reaction set for systems catalyzed by constrained-geometry metallocenes is very similar to that for Ziegler-Natta catalysts. We consider cases where multiple catalyst types are used. As a result, the kinetic mechanism appears similar to that for Ziegler-Natta catalysts with multiple site types.

Unlike the Ziegler-Natta kinetics, here we track separately chains that have terminal double bonds and those that do not. The concentration of chains containing these bonds is important for modeling constrained-geometry catalysts, since they allow the insertion of dead chains with terminal double bonds into growing chains, creating long-chain branches. The reaction set is as follows.

3.5.2.1 Catalyst Activation by Cocatalyst

Methylaluminoxane (MAO) is used as cocatalyst species for many metallocene catalysts. The activation step is

$$CAT_i + COCAT \xrightarrow{k_{ac,i}} P_{0,i} \tag{47}$$

where CAT_i is catalyst type i, COCAT is the cocatalyst species, $P_{0,i}$ represents an active site for catalyst type i that is capable of polymerization, and $k_{ac,i}$ is the rate constant for catalyst activation for catalyst type i.

3.5.2.2 Spontaneous Catalyst Activation

We include a spontaneous activation step for non-MAO systems that use ion-exchange resins to activate the metallocene:

$$CAT_i \xrightarrow{k_{asp,i}} P_{0,i} \tag{48}$$

where $k_{asp,i}$ is the rate constant for spontaneous activation of catalyst type i.

3.5.2.3 Chain Initiation

The active sites react with monomer to initiate chain growth. This reaction is

$$P_{0,i} + M \xrightarrow{k_{\text{ini},i}} P_{1,i} \tag{49}$$

where M is the monomer, $P_{1,i}$ is a polymer chain attached to catalyst type i containing one monomer segment, and $k_{\text{ini},i}$ is the rate constant for chain initiation for catalyst type i.

3.5.2.4 Chain Propagation

As with Ziegler-Natta catalysts, the addition of monomer species involves a complexation of the double-bond of the monomer at the catalyst site[33]. The reaction is

$$P_{n,i} + M \xrightarrow{k_{p,i}} P_{n+1,i} \tag{50}$$

where $P_{n,i}$ is a polymer chain attached to catalyst type i, and $k_{p,i}$ is the rate constant for propagation for catalyst type i.

3.5.2.5 Chain Transfer to Agent (Hydrogen)

Hydrogen is almost exclusively used as a chain-transfer agent[32]. Metallocene catalysts require only trace amounts of hydrogen to achieve chain transfer, compared to Ziegler-Natta catalysts. In this modeling work, we consider chain transfer to hydrogen only. The modeler can easily modify the reaction set to use a different species. The reaction is

$$P_{n,i} + H_2 \xrightarrow{k_{\text{th},i}} D_n + P_{0,i} \tag{51}$$

where D_n is a dead chain containing n segments, and $k_{\text{th},i}$ is the rate constant for chain transfer to hydrogen for catalyst type i.

3.5.2.6 Chain Transfer to Monomer

This reaction is analogous to that for hydrogen given above. The reaction is

$$P_{n,i} + M \xrightarrow{k_{\text{tm},i}} D_n^= + P_{1,i} \tag{52}$$

where $D_n^=$ is a dead polymer chain detached from the catalyst, and contains a terminal double bond, and $k_{tm,i}$ is the rate constant for chain transfer to monomer for catalyst type i.

3.5.2.7 Chain Transfer to Solvent

This reaction is similar to chain transfer to monomer. Since most solvents are hydrocarbons, we consider an initiated active site to form as a result:

$$P_{n,i} + S \xrightarrow{k_{ts,i}} D_n^= + P_{1,i} \tag{53}$$

where $k_{ts,i}$ is the rate constant for chain transfer to solvent for catalyst type i.

3.5.2.8 Chain Transfer to Cocatalyst

As with Ziegler-Natta catalysts, we can expect the cocatalyst to cause chain transfer to occur:

$$P_{n,i} + COCAT \xrightarrow{k_{tc,i}} D_n^= + P_{1,i} \tag{54}$$

where $k_{tc,i}$ is the rate constant for chain transfer to cocatalyst for catalyst type i.

3.5.2.9 Spontaneous Chain Transfer (*b*-Hydride Elimination)

We also include a reaction where *b*-hydride elimination occurs, detaching the polymer chain from the active site and leaving it with a terminal double bond. The catalyst site remains active for reinitiation and polymerization. This reaction is important in the incorporation of long-chain branches, as well as the control of molecular weight. When supported on inorganic species, metallocene catalysts become much less susceptible to *b*-hydride elimination, and hydrogen must be used to control molecular weight[34]. The reaction is

$$P_{n,i} \xrightarrow{k_{b,i}} D_n^= + P_{0,i} \tag{55}$$

where $k_{b,i}$ is the rate constant for spontaneous chain transfer for catalyst type i.

3.5.2.10 Long-Chain Branching (Terminal Double Bond)

A live chain can react with a chain containing a terminal double bond to form a single chain with a long branch:

$$P_{n,i} + D_m^= \xrightarrow{k_{tdb,i}} P_{n+m,i} \tag{56}$$
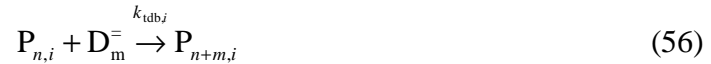
where $k_{tdb,i}$ is the rate constant for incorporation of polymer chains with terminal double bonds for catalyst type i. Constrained-geometry metallocene catalysts are able to utilize this reaction to produce polymer with long-chain branches at moderate reactor conditions.

3.5.2.11 Reversible Catalyst Site Inhibition

We consider the reversible inhibition of catalyst sites by a poison. As with Ziegler-Natta catalysts, hydrogen is known to reversibly inhibit metallocene catalysts as well[33]. The forward reaction inhibits the catalyst site:

$$CAT_i + X \xrightarrow{k_{finh,i}} ICAT_i \tag{57}$$

where X represents a poison, such as hydrogen, $ICAT_i$ is the inhibited catalyst of type i, and $k_{finh,i}$ is the rate constant for inhibition of catalyst type i. The reverse inhibition reaction frees the catalyst site for initiation and propagation:

$$ICAT_i \xrightarrow{k_{rinh,i}} CAT_i + X \tag{58}$$

where $k_{rinh,i}$ is the rate constant for reverse inhibition for catalyst type i.

3.5.2.12 Spontaneous Catalyst Deactivation

We can also consider catalyst deactivation:

$$P_{0,i} \xrightarrow{k_{dsp,i}} CAT_i \tag{59}$$

where $k_{\text{dsp},i}$ is the rate constant for the spontaneous deactivation of catalyst type i. The catalyst can react with cocatalyst to form an active site again.

3.5.3 Development of Rate Expressions

3.5.3.1 Unactivated Catalyst

$$
\begin{aligned}
R_{\text{CAT}_i} = &-k_{\text{ac},i}\left[\text{CAT}_i\right]\left[\text{COCAT}\right] - k_{\text{am},i}\left[\text{CAT}_i\right]\left[\text{M}\right] \\
&-k_{\text{asp},i}\left[\text{CAT}_i\right] - k_{\text{finh},i}\left[\text{CAT}_i\right]\left[\text{X}\right] + k_{\text{rinh},i}\left[\text{ICAT}_i\right]
\end{aligned}
\tag{60}
$$

3.5.3.2 Inhibited Catalyst

$$
R_{\text{ICAT}_i} = k_{\text{finh},i}\left[\text{CAT}_i\right]\left[\text{X}\right] - k_{\text{rinh}i}\left[\text{ICAT}_i\right]
\tag{61}
$$

3.5.3.3 Deactivated Catalyst

$$
R_{\text{DCAT}_i} = k_{\text{ds},i}\boldsymbol{l}_{0,i} + k_{\text{dp},i}\left[\text{X}\right]\boldsymbol{l}_{0,i}
\tag{62}
$$

3.5.3.4 Cocatalyst

$$
R_{\text{COCAT}} = -\left[\text{COCAT}\right]\sum_i k_{\text{ac},i}\left[\text{CAT}_i\right] - \left[\text{COCAT}\right]\sum_i k_{\text{tc},i}\boldsymbol{l}_{0,i}
\tag{63}
$$

3.5.3.5 Empty Active Catalyst Sites

We recast the rate expression for active sites by recognizing the zeroth live moment in some of its terms:

$$
\begin{aligned}
R_{\text{P}_{0,i}} = &\, k_{\text{ac},i}\left[\text{CAT}_i\right]\left[\text{COCAT}\right] + k_{\text{am},i}\left[\text{CAT}_i\right]\left[\text{M}\right] + k_{\text{asp}i}\left[\text{CAT}_i\right] \\
&-k_{\text{ini},i}\left[\text{M}\right]\left[\text{P}_{0,i}\right] + k_{\text{th},i}\left[\text{H}_2\right]\boldsymbol{l}_{0,i} + k_{\boldsymbol{b},i}\boldsymbol{l}_{0,i}
\end{aligned}
\tag{64}
$$

34.5.3.6 Monomer

The rate expression for monomer becomes

$$R_{\mathrm{M}} = -[\mathrm{M}]\sum_i k_{\mathrm{ini},i}\left[\mathrm{P}_{0,i}\right] - [\mathrm{M}]\sum_i \left(k_{\mathrm{p},i}\mathbf{1}_{0,i}\right) - [\mathrm{M}]\sum_i \left(k_{\mathrm{tm},i}\mathbf{1}_{0,i}\right) \tag{65}$$

3.5.3.7 Solvent

The rate expression for solvent is

$$R_{\mathrm{S}} = -[\mathrm{S}]\sum_i k_{\mathrm{ts},i}\mathbf{1}_{0,i} \tag{66}$$

3.5.3.8 Chain-Transfer Agent (Hydrogen)

The rate expression for hydrogen becomes

$$R_{\mathrm{H}_2} = -[\mathrm{H}_2]\sum_i k_{\mathrm{th},i}\mathbf{1}_{0,i} \tag{67}$$

3.5.3.9 Inhibitor/Poison

$$R_{\mathrm{X}} = -[\mathrm{X}]\sum_i k_{\mathrm{finh},i}\left[\mathrm{CAT}_i\right] + \sum_i k_{\mathrm{rinh},i}\left[\mathrm{ICAT}_i\right] - [\mathrm{X}]\sum_i k_{\mathrm{dp},i}\mathbf{1}_{0,i} \tag{68}$$

3.5.3.10 Live Polymer Chains

The general expression for live polymer chains is

$$R_{l_{i,j}} = k_{\text{ini},j}[\text{M}][\text{P}_{0,j}] + \left(k_{\text{tm},j}[\text{M}] + k_{\text{ts},j}[\text{S}] + k_{\text{tc},j}[\text{COCAT}]\right)l_{0,j}$$
$$+k_{\text{p},j}[\text{M}]\left(\sum_{k=0}^{l}\binom{l}{k}l_{k,j} - l_{l,j}\right) - k_{\text{tdb},j}l_{i,j}m_0^{=} + k_{\text{tdb},j}\sum_{k=0}^{l}\binom{l}{k}m_k^{=}l_{l-k,j} \qquad (69)$$
$$-\left(k_{\text{th},j}[\text{H}_2] + k_{\text{ts},j}[\text{S}] + k_{\text{tc},j}[\text{COCAT}] + k_{\text{tm},j}[\text{M}] + k_{b,j} + k_{\text{dsp},j} + k_{\text{dp},j}[\text{X}]\right)l_{i,j}$$

3.5.3.10.1 Zeroth Live Moment

For the zeroth live moment:

$$R_{l_{0,i}} = k_{\text{ini},i}[\text{M}][\text{P}_{0,i}] - \left(k_{\text{th},i}[\text{H}_2] + k_{b,i} + k_{\text{dsp}i} + k_{\text{dp},i}[\text{X}]\right)l_{0,i} \qquad (70)$$

3.5.3.10.2 First Live Moment

For the first live moment:

$$R_{l_{1,i}} = k_{\text{ini},i}[\text{M}][\text{P}_{0,i}] + \left(k_{\text{tm},i}[\text{M}] + k_{\text{ts},i}[\text{S}] + k_{\text{tc},i}[\text{COCAT}]\right)\left(l_{0,i} - l_{1,i}\right)$$
$$+k_{\text{p},i}[\text{M}]l_{0i} + k_{\text{tdb},i}l_{0,i}m_1^{=} - \left(k_{\text{th},i}[\text{H}_2] + k_{b,i} + k_{\text{dsp},i} + k_{\text{dp},i}[\text{X}]\right)l_{1,i} \qquad (71)$$

3.5.3.10.3 Second Live Moment

For the second live moment:

$$R_{l_{2,i}} = k_{\text{ini},i}[\text{M}][\text{P}_{0i}] + \left(k_{\text{tm},i}[\text{M}] + k_{\text{ts},i}[\text{S}] + k_{\text{tc},i}[\text{COCAT}]\right)\left(l_{0,i} - l_{2,i}\right)$$
$$+k_{\text{p},i}[\text{M}]\left(l_{0,i} + 2l_{1,i}\right) + k_{\text{tdb},i}\left(l_{0,i}m_2^{=} + 2l_{1,i}m_1^{=}\right) \qquad (72)$$
$$-\left(k_{\text{th},i}[\text{H}_2] + k_{b,i} + k_{\text{dsp},i} + k_{\text{dp},i}[\text{X}]\right)l_{2,i}$$

3.5.3.11 Dead Polymer Chains

The general expression for dead polymer chains is

$$R_{m_i} = [\text{H}_2]\sum_{j}k_{\text{th},i}l_{i,j} + \sum_{j}k_{\text{dsp},j}l_{i,j} + [\text{X}]\sum_{j}k_{\text{dp},j}l_{i,j} \qquad (73)$$

68

For the zeroth dead moment:

$$R_{m_0} = [H_2] \sum_{i=1}^{ncat} k_{th,i} \mathbf{I}_{0,i} + \sum_{i=1}^{ncat} k_{sd,i} \mathbf{I}_{0,i} + [X] \sum_{i=1}^{ncat} k_{dp,i} \mathbf{I}_{0,i} \qquad (74)$$

3.5.3.11.2 First Dead Moment

For the first dead moment:

$$R_{m_1} = [H_2] \sum_{i} k_{th,i} \mathbf{I}_{1,i} + \sum_{i} k_{dsp,i} \mathbf{I}_{1,i} + [X] \sum_{i} k_{dp,i} \mathbf{I}_{1,i} \qquad (75)$$

3.5.3.11.3 Second Dead Moment

For the second dead moment:

$$R_{m_2} = [H_2] \sum_{i} k_{th,i} \mathbf{I}_{2,i} + \sum_{i} k_{dsp,i} \mathbf{I}_{2,i} + [X] \sum_{i} k_{dp,i} \mathbf{I}_{2,i} \qquad (76)$$

3.5.3.12 Dead Polymer Chains with Terminal Double Bonds

For dead chains with terminal double bonds, we have

$$R_{m_i^=} = [M] \sum_{j} k_{tm,j} \mathbf{I}_{i,j} + [S] \sum_{j} k_{ts,j} \mathbf{I}_{i,j} + [COCAT] \sum_{j} k_{tc,j} \mathbf{I}_{i,j}$$
$$+ \sum_{j} k_{b,j} \mathbf{I}_{i,j} - m_i^= \sum_{j} k_{tdb,j} \mathbf{I}_{0,j} \qquad (77)$$

3.5.3.12.1 Zeroth TDB Moment

For the zeroth TDB dead moment:

$$R_{m_0^=} = [M] \sum_{i} k_{tm,i} \mathbf{I}_{0,i} + [S] \sum_{i} k_{ts,i} \mathbf{I}_{0,i} + [COCAT] \sum_{i} k_{tc,i} \mathbf{I}_{0,i}$$
$$+ \sum_{i} k_{b,i} \mathbf{I}_{0,i} - m_0^= \sum_{i} k_{tdb,i} \mathbf{I}_{0,i} \qquad (78)$$

For the first TDB dead moment:

$$R_{\boldsymbol{m}_1^=} = [\mathrm{M}] \sum_i k_{\mathrm{tm},i} \boldsymbol{l}_{1,i} + [\mathrm{S}] \sum_i k_{\mathrm{ts},i} \boldsymbol{l}_{1,i} + [\mathrm{COCAT}] \sum_i k_{\mathrm{tc},i} \boldsymbol{l}_{1,i}$$
$$+ \sum_i k_{\boldsymbol{b},i} \boldsymbol{l}_{1,i} - \boldsymbol{m}_1^= \sum_i k_{\mathrm{tdb},i} \boldsymbol{l}_{0,i}$$

(79)

3.5.3.12.3 Second TDB Moment

For the second TDB dead moment:

$$R_{\boldsymbol{m}_2^=} = [\mathrm{M}] \sum_i k_{\mathrm{tm},i} \boldsymbol{l}_{2,i} + [\mathrm{S}] \sum_i k_{\mathrm{ts},i} \boldsymbol{l}_{2,i} + [\mathrm{COCAT}] \sum_i k_{\mathrm{tc},i} \boldsymbol{l}_{2,i}$$
$$+ \sum_i k_{\boldsymbol{b},i} \boldsymbol{l}_{2,i} - \boldsymbol{m}_2^= \sum_i k_{\mathrm{tdb},i} \boldsymbol{l}_{0,i}$$

(80)

3.6 Summary

We have presented the kinetic mechanisms and algebraic rate expressions for polyolefin production catalyzed by both Ziegler-Natta and metallocene catalysts. These expressions allow the kinetic models to capture essential polymer properties, including number- and weight-average molecular weight, and frequency of long-chain branching. We apply these formulations in the industrial projects for HDPE and PP production (see the next two sections), as well as in the proposed project for predicting long-chain branching in metallocene-catalyzed ethylene polymerization.

Symbols

English Symbols

$\mathrm{Al(C_2H_5)_3}$	triethyl aluminum cocatalyst
C	carbon atom
CAT_i	catalyst associated with site type i
COCAT	cocatalyst

D_n	dead polymer chain containing n segments
$D_n^=$	dead polymer chain with a terminal double bond
DPN	number-average degree of polymerization
DPW	weight-average degree of polymerization
H_2	hydrogen
$ICAT_i$	inhibited catalyst associated with site type i
$k_{ac,i}$	rate constant for catalyst activation by cocatalyst, for site type i
$k_{ah,i}$	rate constant for catalyst activation by hydrogen, for site type i
$k_{am,i}$	rate constant for catalyst activation by monomer, for site type i
$k_{asp,i}$	rate constant for spontaneous catalyst activation, for site type i
$k_{dc,i}$	rate constant for catalyst deactivation by cocatalyst, for site type i
$k_{dh,i}$	rate constant for catalyst deactivation by hydrogen, for site type i
$k_{dm,i}$	rate constant for catalyst deactivation by monomer, for site type i
$k_{dsp,i}$	rate constant for spontaneous catalyst deactivation, for site type i
$k_{finh,i}$	rate constant for forward catalyst inhibition, for site type i
$k_{ini,i}$	rate constant for catalyst initiation, for site type i
$k_{p,i}$	rate constant for chain propagation, for site type i
$k_{rinh,i}$	rate constant for reverse catalyst inhibition, for site type i
$k_{tc,i}$	rate constant for chain transfer to cocatalyst, for site type i
$k_{tdb,i}$	rate constant for the incorporation of a chain with a terminal double bond, associated with site type i
$k_{th,i}$	rate constant for chain transfer to hydrogen, for site type i
$k_{tm,i}$	rate constant for chain transfer to monomer, for site type i
$k_{ts,i}$	rate constant for chain transfer to solvent, for site type i
$k_{\beta,i}$	rate constant for β-hydride elimination, for site type i
LCB	long-chain branch
M	monomer
M_{seg}	segment molecular weight
MAO	methylaluminoxane
$P_{0,i}$	empty active catalyst site of type i
$P_{1,i}$	initiated catalyst site of type i

$P_{n,i}$ live chain containing n segments, attached to site type i

PDI   polydispersity index

R_{CAT_i} rate of reaction of catalyst site type i

R_{COCAT} rate of reaction of cocatalyst

R_{D_n} rate of reaction of dead chains

$R_{D_n^=}$ rate of reaction of dead chains with terminal double bonds

R_{H_2} rate of reaction of hydrogen

R_{ICAT_i} rate of reaction of inhibited catalyst site type i

R_M rate of reaction of monomer

$R_{P_{0,i}}$ rate of reaction of empty catalyst site type i

$R_{P_{ni}}$ rate of reaction of live polymer chains attached to site type i

R_S rate of reaction of solvent

R_X rate of reaction of poison

$R_{l_{i,j}}$ rate of reaction of ith live moment associated with site type j

R_{m_i} rate of reaction of dead moment associated with site type i

$R_{m_i^=}$ rate of reaction of dead chains with terminal double bonds, associated with site type i

S   solvent

T_iCl_4 titanium tetrachloride catalyst

X   poison

[ ]   molar concentration of species within brackets

Greek Symbols

$l_{i,j}$ i^{th} moment of live chains associated with site type j

m_i i^{th} moment of dead chains

$m_i^=$ i^{th} moment of dead chains with terminal double bonds

Chapter 4 Manuscript for the Slurry Polymerization of High-Density Polyethylene (HDPE) Using a Ziegler-Natta Catalyst

Khare, N. P.; Seavey, K. C.; Liu, Y. A.; Ramanathan, S.; Lingard, S.; Chen, C.-C.

Steady-State and Dynamic Modeling of Commercial Slurry High-Density Polyethylene (HDPE) Processes

Neeraj P. Khare, Kevin C. Seavey, and Y. A. Liu*

Honeywell Center of Excellence in Computer-Aided Design

Department of Chemical Engineering

Virginia Polytechnic Institute and State University

Blacksburg, VA 24061

Sundaram Ramanathan, Simon Lingard, and Chau-Chyun Chen

Aspen Technology, Inc.

10 Canal Park

Cambridge, MA 02141

*Phone: (540) 231-7800; Fax: (540) 231-5022; E-mail: design@vt.edu

To whom correspondence should be addressed.

Abstract

We present the development of both steady-state and dynamic models for a slurry HDPE process using fundamental chemical engineering principles and advanced software tools, ASPEN Polymers Plus and ASPEN Dynamics. Discussion includes thermodynamic properties, phase equilibrium, reaction kinetics, polymer properties, and other modeling issues. We characterize a Ziegler-Natta catalyst by assuming the existence of multiple catalyst-site types and deconvoluting data from gel-permeation chromatography to determine the most probable chain-length distributions and relative amounts of polymer produced at each site type. We validate the model using plant data from two large-scale commercial slurry HDPE processes. Significantly, the model contains a single set of kinetic and thermodynamic parameters that accurately predicts the polymer production rate, molecular weight, polydispersity index, and composition, for several product grades. We illustrate the utility of the dynamic model by simulating a grade change. Finally, we propose a process retrofit that permits an increase in HDPE production rate of up to 20%, while maintaining the product quality.

Keywords: high-density polyethylene (HDPE); Ziegler-Natta; simulation; modeling; polymerization kinetics; deconvolution; slurry

4.1 Introduction

4.1.1 Slurry HDPE Process Technology

The slurry polymerization of HDPE is the oldest and most widely used method of production. Figure 4-1 gives a flowchart for a typical slurry HDPE process. Slurry processes utilize either continuous stirred-tank reactors (CSTRs), as in our case, or loop reactors[1]. The monomers, chain-transfer agent, solvent, and catalyst species enter the reactors for polymerization. The vaporization of the solvent removes a large portion of the highly exothermic heat of polymerization. The resulting slurry undergoes separation, removing unreacted monomer, solvent and oligomeric species from the polymer. Solvent is separated from the oligomer and recycled to the reactor inlets, and the oligomer is processed and packaged. Meanwhile, the polymer undergoes mixing, pelletizing, and packaging.
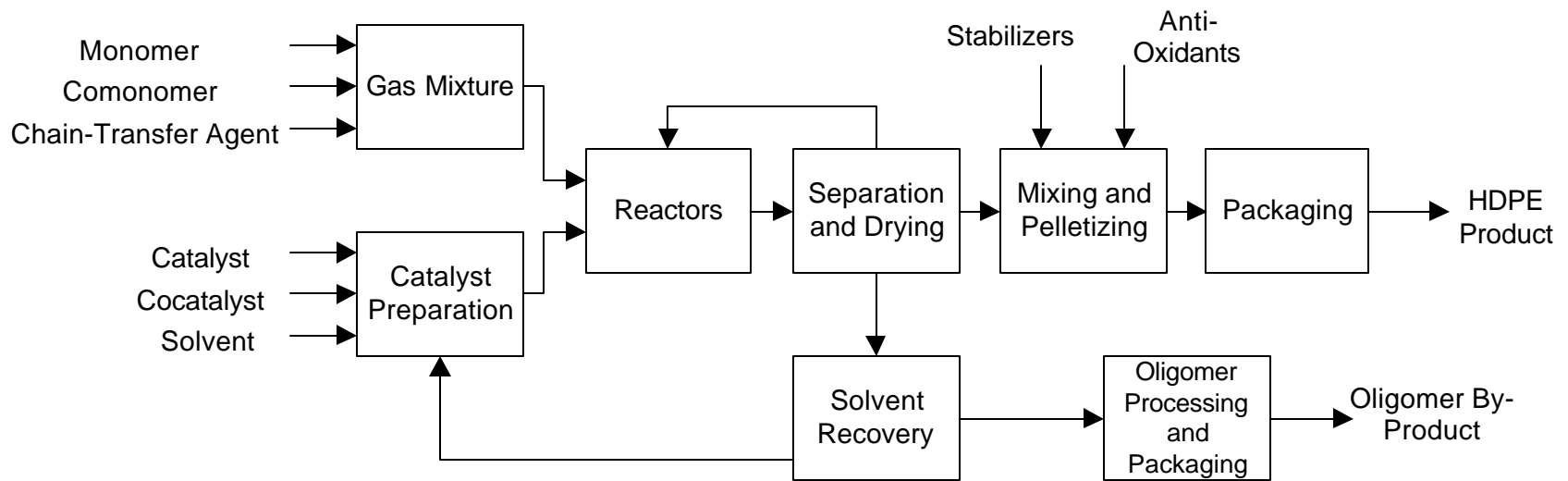
Figure 4-1. Flowchart of the slurry HDPE process.

The reactor temperature remains below the polymer melting point. The polymer crystallizes upon formation, creating a slurry of solid particles in the solvent[1]. The introduction of a comonomer species (typically propylene, 1-butene, or 1-hexene) allows for the adjustment of the polymer properties, due to short-chain branches resulting from the alkyl groups on the comonomer. Increasing the comonomer content decreases the crystallinity of the polymer product and increases the rate of ethylene polymerization[2]. An increase in the comonomer content also decreases the polymer density and melting point[1].

The major advantages of a slurry process include mild operating conditions, high monomer conversion, ease of heat removal, and relative ease of processing. Its disadvantages include long residence times (1 to 2.5 hours per reactor), and limited production rates of polymers that have relatively low densities (lower than 0.940 g/cm^3) due to resin swelling[1].

The Ziegler-Natta catalyst system involves a primary catalyst and a cocatalyst. The primary catalyst is a transition-metal salt, with a metal from groups IV to VIII of the periodic table. The cocatalyst is a base-metal halide or alkyl, with a metal from groups I to III[3]. Our modeled process uses titanium tetrachloride (TiCl$_4$) as the catalyst and triethyl aluminum (Al(C$_2$H$_5$)$_3$) as the cocatalyst.

Ziegler-Natta catalysts produce polymers with broad molecular weight distributions due to chemical properties of the catalyst. Two theories currently exist that explain this heterogeneous behavior[2]. The first is the existence of different site types within the catalyst, each with its own reactivity, caused by differences in the local chemical compositions of the active sites. The second is the presence of transport resistances that affect the rate at which monomer species travel to the active sites. However, at most polymerization conditions, the effect of different catalyst-site types is the dominating factor[4]. We therefore incorporate this catalytic effect by kinetically modeling multiple catalyst-site types. We discuss this approach in Section 4.3.5.

4.1.2 Modeled Processes

We obtained process data for eight grades of HDPE produced in two large-scale slurry polymerization plants (144,000 and 240,000 tons/yr). In this paper, we present modeling methodology and results of modeling these two commercial plants. We refer to these as Plant A and Plant B, respectively. Each plant houses two production trains. One train has a parallel reactor configuration, while the other train has two reactors connected in series, or tandem. In the following sections, we provide more details about each configuration.

4.1.2.1 Parallel Reactor Configuration

Figure 4-2 shows the parallel arrangement, in which two continuous stirred-tank reactors (CSTRs) produce the HDPE. The comonomer for the parallel process is propylene. The slurry streams leaving each reactor are combined and enter a flash unit for the removal of light hydrocarbons. The vapor streams leaving the reactors contain hexane, monomer, and light gases present in the system. These streams are cooled and flashed into vapor and liquid streams, which recycle to the monomer and solvent feed streams, respectively. The vaporization of hexane is the primary means for removal of the heat of polymerization. The polymer slurry leaving the flash unit enters a centrifugal separator that removes hexane from the polymer. This mother liquor returns to the reactor inlets, while the polymer stream travels to the processing and packaging phases of production.

4.1.2.2 Series Reactor Configuration

Figure 4-3 illustrates the series layout, where raw materials feed to the first CSTR, and the slurry product is then pumped to the second CSTR, which also receives fresh monomer, catalyst, and solvent. The comonomer for the series process is 1-butene, and only enters as a feed stream to the second reactor. The vapor outlet from each reactor undergoes cooling and recycles to the reactor inlet. The slurry stream leaving the second reactor enters a flash unit for removal of volatiles. The resulting stream enters a centrifugal separator, which removes and returns hexane to the reactor inlets.
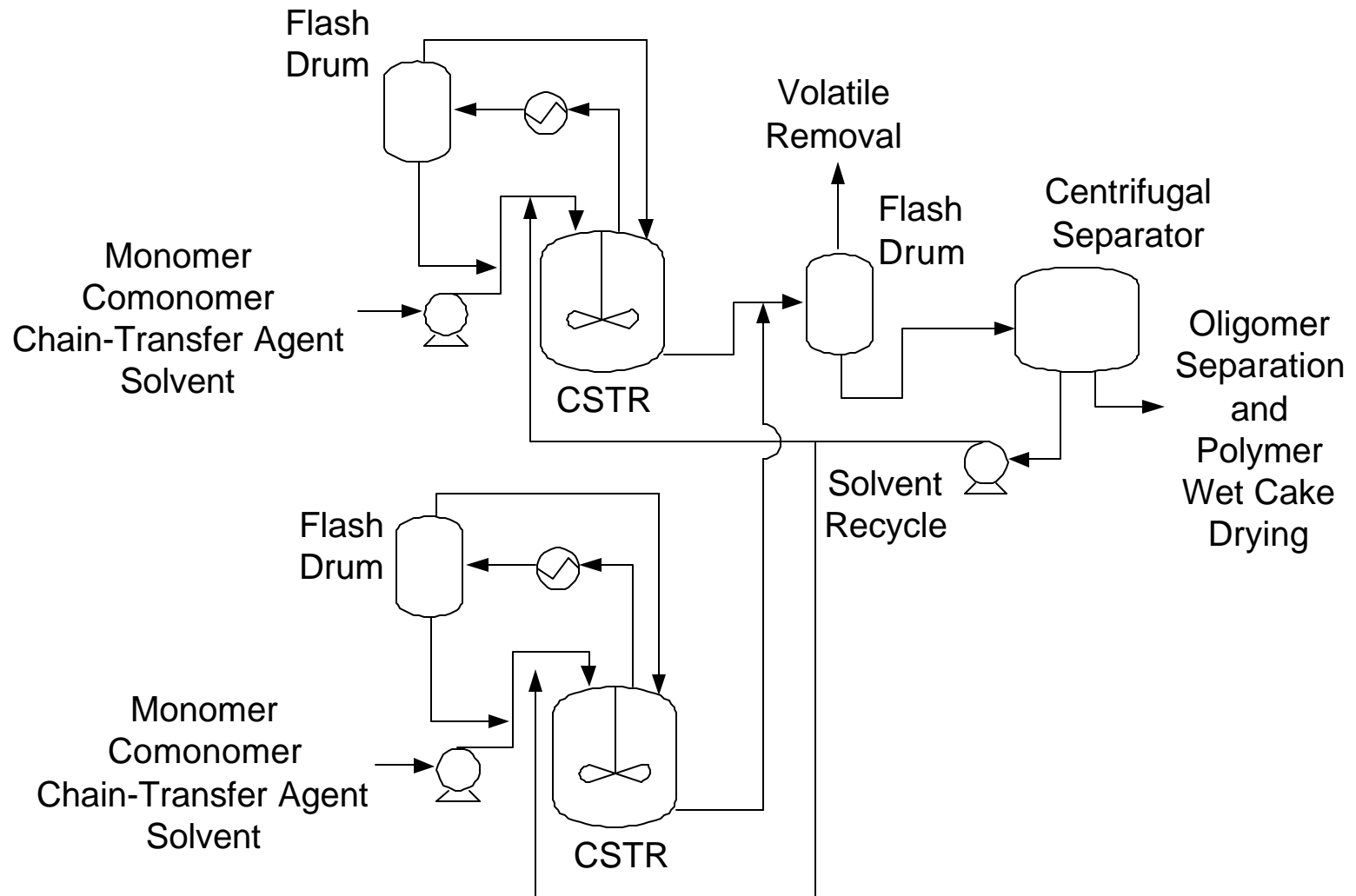
Figure 4-2. Process flow diagram for the parallel reactor configuration.

Figure 4-3. Process flow diagram for the series reactor configuration.

Although the temperatures of both reactors in the series configuration are the same, the hydrogen partial pressures are different, permitting the production of polymers with different average molecular weights in both reactors. This results in a bimodal molecular weight distribution for the final polymer product. We can also vary the amounts of comonomer fed to each reactor, providing a means of producing polymers with a variety of specific properties[1].

4.1.3 Modeling Technology

Our modeling incorporates fundamental chemical engineering principles and advanced software tools for both steady-state and dynamic process simulation. We include mass and energy balances, thermophysical properties, phase equilibrium, polymerization kinetics, and reactor modeling.

We use both ASPEN Polymers Plus and ASPEN Dynamics to simulate the HDPE process. Polymers Plus applies process modeling technology to a wide variety of industrial polymerization processes. It considers the characterization of polymers and tracking of their structural properties throughout the flowsheet, phase equilibrium for polymer systems, polymerization kinetics, and reactor modeling.

Polymers Plus uses a segment-based approach for computing the physical properties of polymer species. By considering a polymer chain as a series of segments, whose structures are well-defined, Polymers Plus can model the polymer properties that commonly vary with time in a synthesis process. This technique permits the modeling of properties such as molecular weight and copolymer composition, and can account for the fact that most polymer products contain an ensemble of molecules having a distribution of chain lengths. It facilitates the use of group-contribution methods for estimation of properties such as heat capacity, density, and melt- and glass-transition temperatures. We can also incorporate subroutines for user-defined correlations for polymer properties such as density and melt index.

Polymers Plus can interface with ASPEN Dynamics to create dynamic models of polymer processes. We incorporate control schemes and track changes in polymer attributes with modifications of process variables like reactor conditions or component feed rates. This integrated software package provides powerful modeling and predictive capabilities to the process design engineer.

4.2 Physical Properties

4.2.1 Introduction

Choosing appropriate property models for thermodynamic calculations can be a challenging endeavor. The phase behavior and thermophysical properties of polymer systems are generally much more complicated than those for conventional mixtures. We can describe the phase behavior of polymer systems by using activity-coefficient models and equations of state. The latter typically give pressure as a function of temperature, molar volume, and composition, while the former provide a correction to the ideal-solution assumption of Raoult's law[5].

Since polymer equations of state do not normally perform as well as simple cubic equations of state for small components[5], we use different property methods for the units and streams that contain polymer and those that do not. In the HDPE process, the polymer exists in the reactors and the subsequent separation units. The vapor recycle contains only monomer, solvent, and other small-molecule components, because the polymer is nonvolatile. We use the Sanchez-Lacombe equation of state for the polymer-containing sections of the plant, and the Chao-Seader method for the non-polymer areas. Table 4-1 lists the portions of the process model for which we use the Sanchez-Lacombe and Chao-Seader methods, respectively. We describe these methods next.

Table 4-1. Unit operations for which we use the Sanchez-Lacombe and the Chao-Seader property methods.

polymer-containing units (Sanchez-Lacombe method)	non-polymer units (Chao-Seader method)
polymer reactors	raw-feed pumps
polymer devolatilizers (flash units)	overhead compressors
polymer recycle pumps	overhead flash units

4.2.2 Sanchez-Lacombe Equation of State for Polymer Systems

We use an equation of state (EOS) developed by Sanchez and Lacombe[6-8] for the polymer-containing portions of the flowsheet. It is based on lattice theory, which states that fluids are mixtures of molecules and holes that are confined to sites in a lattice. The Sanchez-Lacombe EOS provides accurate prediction of the phase behavior and thermodynamic properties of the specific components in our system. It is valid for polymer species as well as conventional components. These predictions include molar volume, fugacity coefficients, heat capacities, and departures for enthalpy, entropy, and Gibbs free energy. The model is

$$\bar{r}^2 + \bar{P} + \bar{T}\left[\ln\left(1 - \bar{r}\right) + \left(1 - \frac{1}{r}\right)\bar{r}\right] = 0 \tag{1}$$

where $\bar{r}$, $\bar{P}$, and $\bar{T}$ are reduced density, pressure, and temperature, respectively. These quantities relate to density, pressure, and temperature:

$$\bar{r} = \frac{r}{r^*} \quad \bar{P} = \frac{P}{P^*} \quad \bar{T} = \frac{T}{T^*} \tag{2}$$

where r^*, P^*, and T^* are scale factors that completely characterize each pure fluid. We typically determine values for these parameters by regressing experimental data for each species (usually, vapor-pressure data for conventional components and liquid-volume

data for polymer species). Alternatively, we can use values published in the open literature, provided that the data used to obtain the parameter values were measured at or near the conditions of the modeled process. The Sanchez-Lacombe EOS also has two binary interaction parameters that we can determine by regressing binary phase data for the components of interest. Refer to Sections 4.2.4 and 4.2.5 for the regressed parameter values and data sources we used.

4.2.3 Chao-Seader, Scatchard-Hildebrand, and Redlich-Kwong Models for Conventional Species

The Chao-Seader correlation provides excellent prediction of the reference-state fugacity coefficients for pure liquid hydrocarbons at our system conditions[9]. Its form is

$$\ln\left(f_i^{liq}\right) = \ln\left(n_i^{(0)}\right) + w_i \ln\left(n_i^{(1)}\right) \tag{3}$$

where $v_i^{(0)}$ and $v_i^{(1)}$ are functions of the system temperature and pressure and the critical temperature and pressure for component i, and w_i is the acentric factor for species i. The Chao-Seader method uses the Redlich-Kwong EOS for vapor-phase fugacities, and the Scatchard-Hildebrand model for liquid activity coefficients[10].

4.2.4 Pure-Component Properties

Table 4-2 lists the primary chemical species that exist in the slurry HDPE process. Impurities can be incorporated if their concentrations are significant. These may include hydrocarbons such as methane and ethane.

Table 4-2. Components used in the slurry HDPE process model.

species	function
titanium tetrachloride	catalyst
triethyl aluminum	cocatalyst
ethylene	monomer
ethylene segment	monomer segment

propylene	comonomer
propylene segment	comonomer segment
1-butene	comonomer
1-butene segment	comonomer segment
high-density polyethylene	polymer
oligomer	wax by-product
hydrogen	chain-transfer agent
n-hexane	solvent
nitrogen	purge gas
methane	impurity
ethane	by-product
propane	impurity
n-butane	impurity

The component list includes segments for the monomer species. As described in Section 4.1.3, Polymers Plus considers polymer species using a segment-based approach, where the macromolecules consist of chains containing segment versions of each monomer species. We write the polymerization reactions in terms of these segments as well.

A comprehensive model for the slurry HDPE process must provide an accurate description of the density, saturation pressure, heat capacity, and heat of vaporization for each species. This is especially important in the reactor because the kinetics depend on accurate phase concentrations, and the heat of polymerization is primarily removed through the vaporization of the solvent, hexane.

4.2.4.1 Sanchez-Lacombe Pure-Component Parameters

Table 4-3 provides pure-component parameters for the Sanchez-Lacombe EOS for relevant species. Note that in Polymers Plus, we must enter the polymer unary parameters for the individual segments that comprise it. We must regress density and heat-capacity data for polyethylene, polypropylene, and poly(1-butene), and use the

resulting parameters for each respective segment species. We choose parameters for the catalyst and cocatalyst such that they remain in the liquid phase.

Table 4-3. Pure-component parameters for the Sanchez-Lacombe EOS. T^*, P^*, and $\mathbf{r}^*$ are characteristic temperature, pressure, and density, respectively.

component	T^*	P^*	r^*
	(K)	(bar)	(kg/m^3)
catalyst	924.87	4000	866.97
cocatalyst	924.87	4000	866.97
hexane	483.13	2900	786
ethylene segment	663.15	4000	896.6
propylene segment	724.3	2800	938.87
1-butene segment	924.87	4000	866.97
ethylene	333	2400	631
propylene	360.43	3100	670.83
1-butene	396.62	2900	671.5
hydrogen	45.89	1000	142.66
nitrogen	140.77	1786.17	922.5
methane	224	2482	500
ethane	315	3273	640
propane	354.33	2800	615.91
butane	412.78	3257.9	755.68

Figure 4-4 compares model predictions with experimental data for hexane saturation pressure. Figures 4-5 to 4-7 compare model predictions to experimental data for density of hexane, hydrogen, and ethylene. Figure 4-8 compares model predictions with data for the heat of vaporization of hexane. Both the Sanchez-Lacombe and Chao-Seader methods accurately describe these properties.
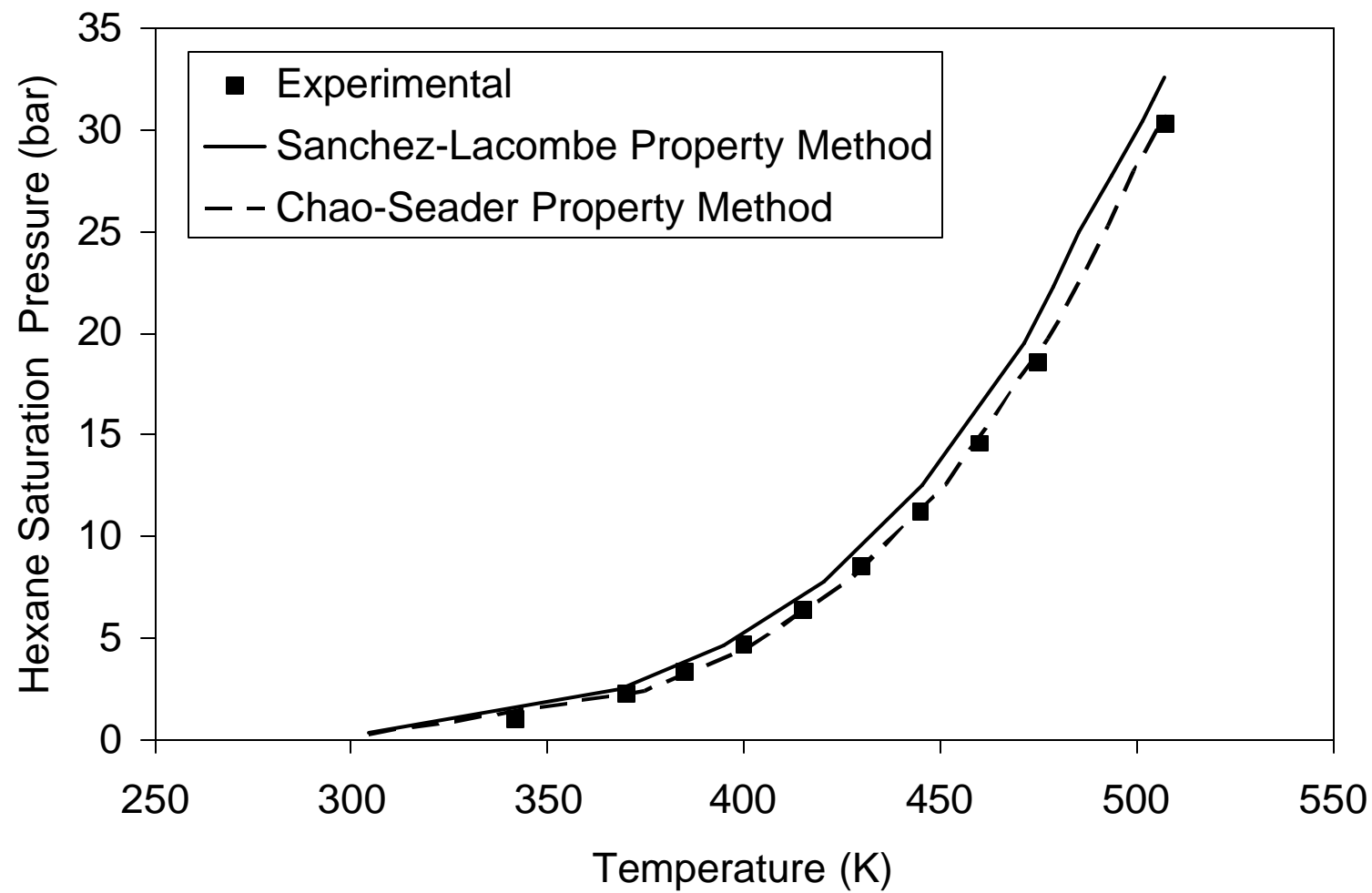
Figure 4-4. Saturation pressure of hexane[11].
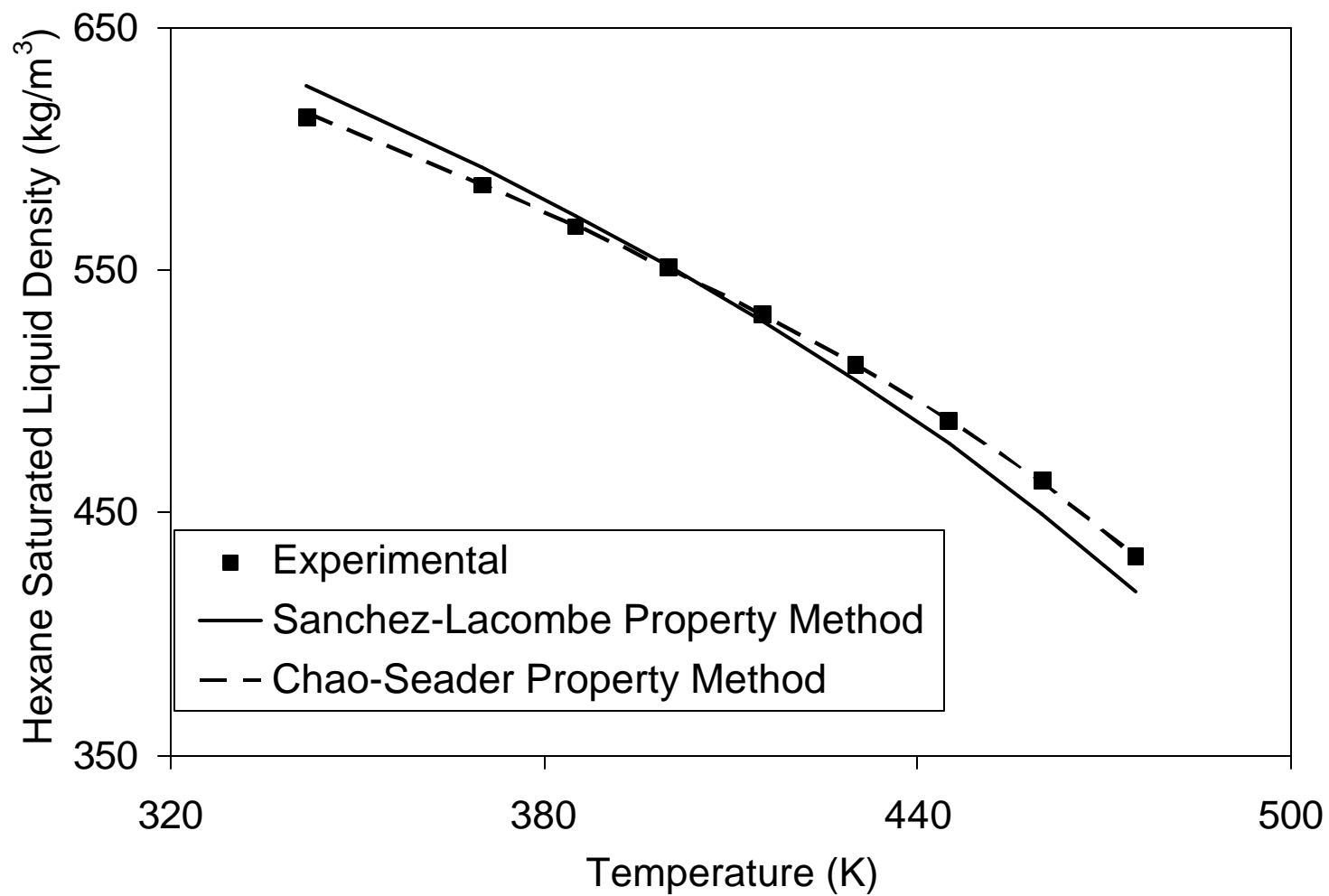
Figure 4-5. Saturated liquid density of hexane[11].
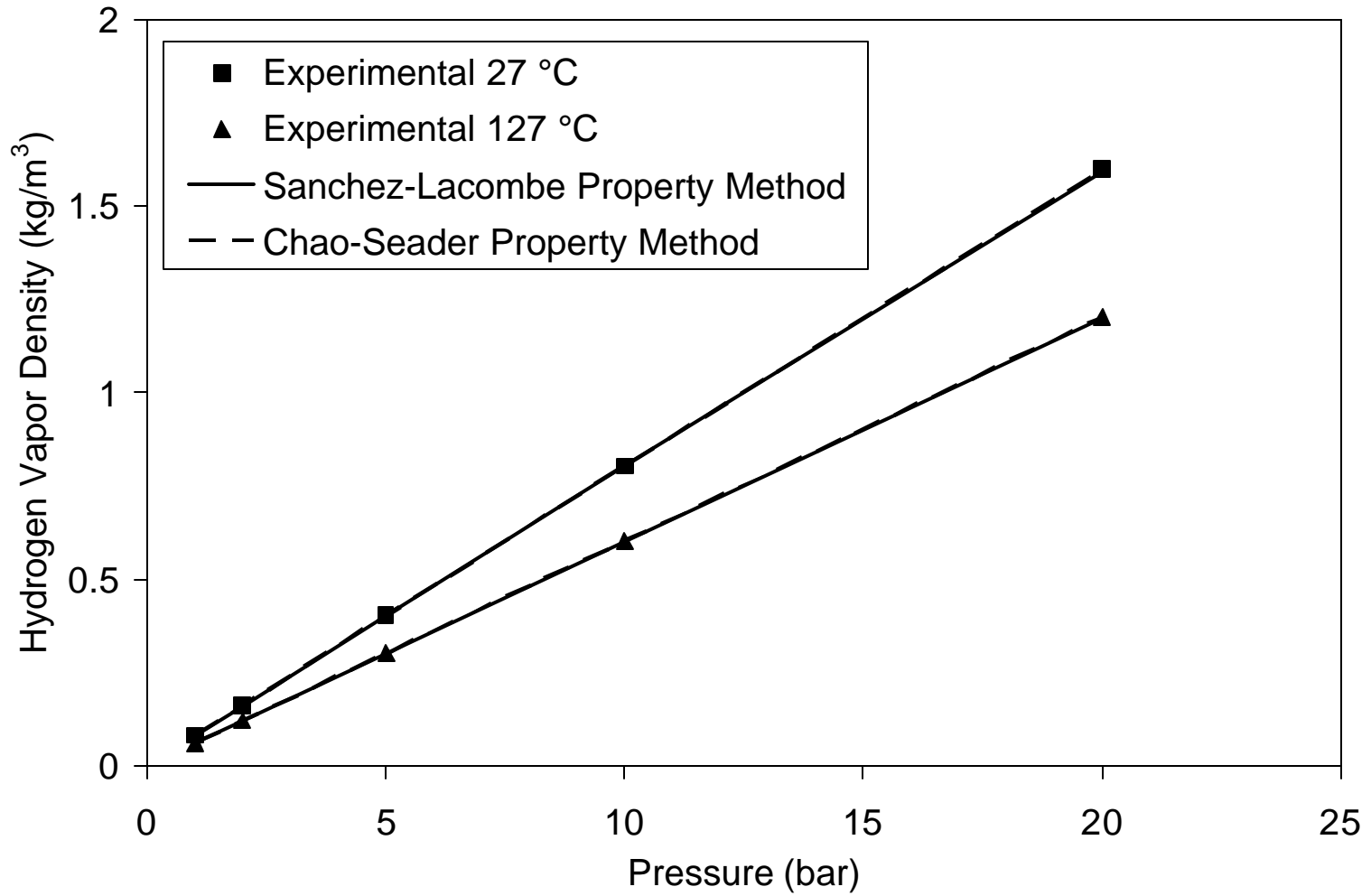
Figure 4-6. Density of hydrogen vapor[11]. The predictions of both property methods are almost identical.
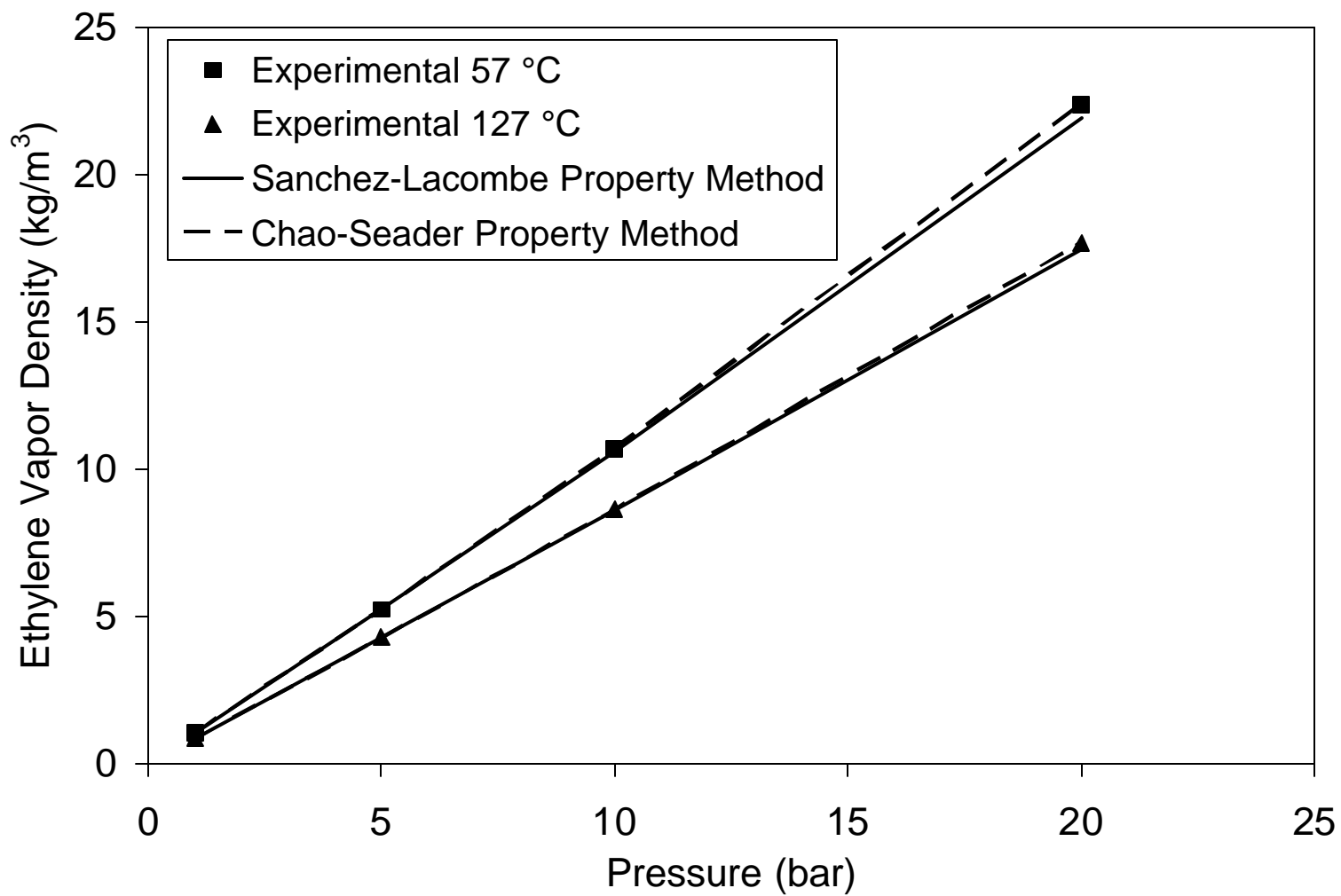
Figure 4-7. Density of ethylene vapor[12].
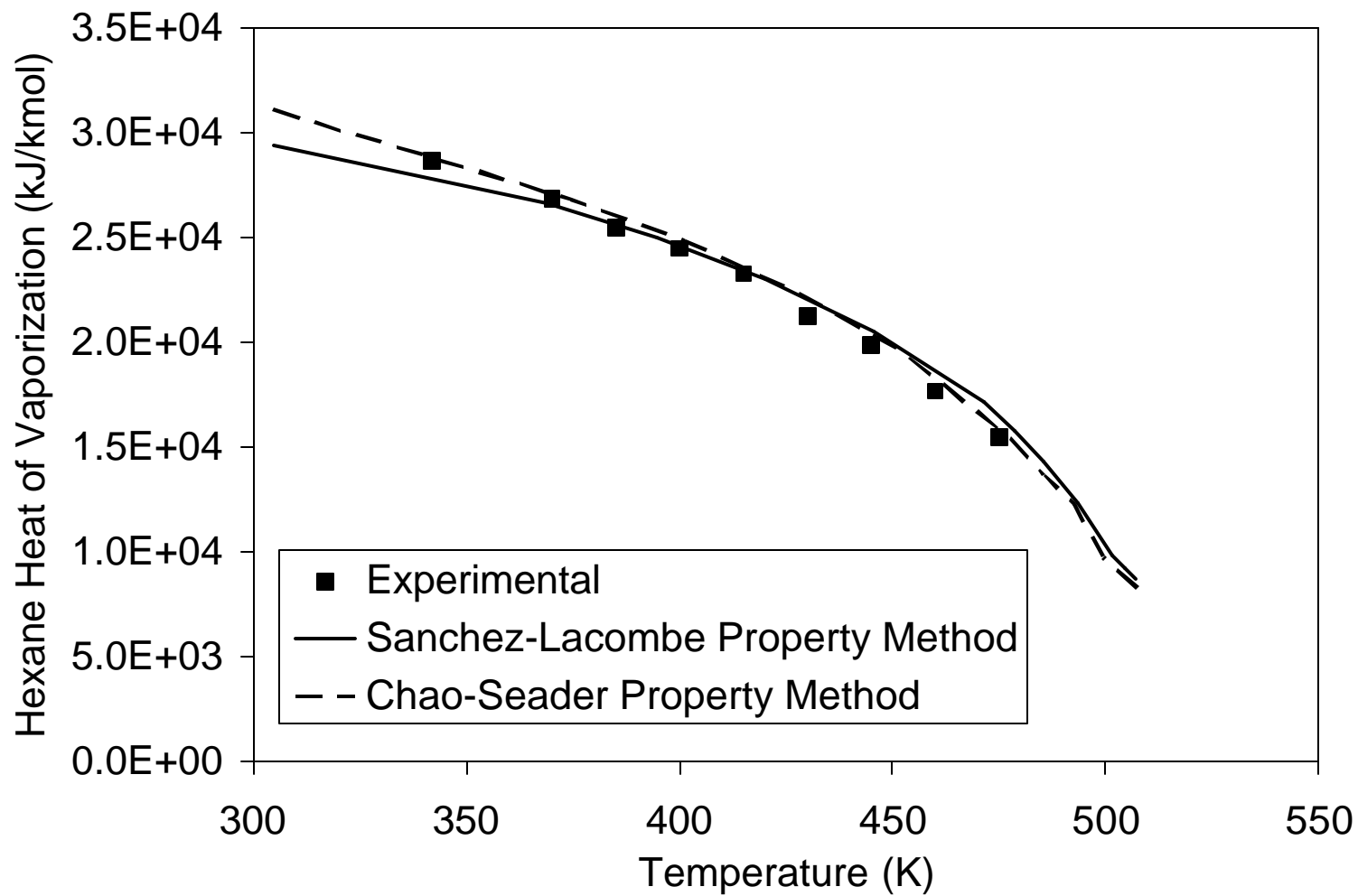
Figure 4-8. Heat of vaporization of hexane[11].

4.2.4.2 Heat Capacity

We can regress heat-capacity data for pure species to determine parameters for the ideal-gas heat capacity model, used in enthalpy predictions:

$$C_p^{ig} = C_1 + C_2 T \qquad (4)$$

Table 4-4 gives the parameters for the major species in the slurry HDPE process.

Table 4-4. Parameters for the ideal-gas heat capacity (eq 4). Values were determined by regressing pure-component data. Units for heat capacity are J/kmol-K.

component	C_1	C_2
HDPE (R-C2h4)	3.51e4	68.22
HDPE (R-C3h6)	4.3205e4	133.58
HDPE (R-C4h8)	8.2932e4	115.29
hexane	1.6321e4	431.71
ethylene	2.3194e4	78.6581
propylene	1.0638e4	178.06
1-butene	4.6593e4	154.94
hydrogen	2.8332e4	1.96

Figures 4-9 to 4-11 compare model predictions to experimental data for the heat capacity of hexane, HDPE, and ethylene. Note that the EOS predictions tend to be less accurate near the critical region, producing small deviations at higher temperatures and pressures.

4.2.5 Mixture Properties

The vapor-liquid equilibrium in the slurry polymerization process is important because the solubilities of the monomer, comonomer, and hydrogen in the hexane directly affect the rates of reaction, and the resulting polymer properties.

Tables 4-5 and 4-6 give values for each of the binary interaction parameters used in the Sanchez-Lacombe model. Unlike that for the unary parameters, we use the HDPE species when specifying binary interaction parameters in Polymers Plus.

Table 4-5. Values for binary interaction parameter h_{ij} for the Sanchez-Lacombe EOS.

	component j		
component i	ethylene	HDPE	hexane
hydrogen	-0.0867	--	0.100705
ethylene	--	-0.1093	0.1476
1-butene	--	--	--
hexane	0.1476	--	--
propylene	--	--	0.14

Table 4-6. Values for binary interaction parameter k_{ij} for the Sanchez-Lacombe EOS.

	component j	
component i	hexane	HDPE
ethylene	0.0248	--
hexane	--	-0.14
methane	0.01951	--
ethane	0.00853	--
propylene	0.02473	-0.14
hydrogen	0.100705	--
butane	-0.002286	--

Figure 4-12 compares model predictions with experimental data for the solubility of hydrogen in hexane. Hydrogen approaches the supercritical state at the conditions used in the HDPE process. Since the Sanchez-Lacombe EOS generally tends to overpredict the critical point, we do not use data near the critical region when determining pure-component parameters. For this reason, as well as the importance of the solubility

prediction of hydrogen in the hexane solvent, we use the solubility data in Figure 4-12 to regress pure-component parameters for hydrogen.
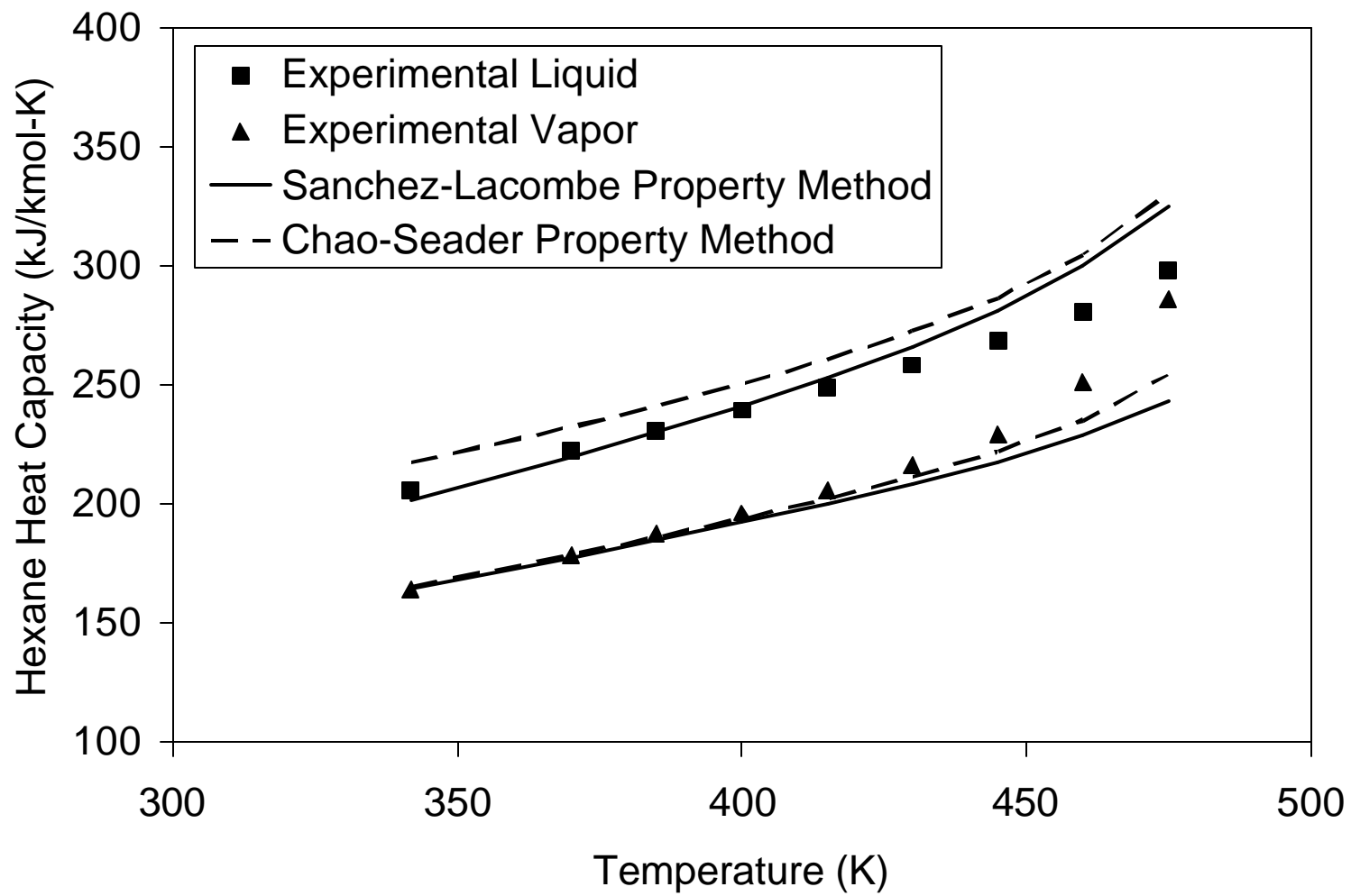
Figure 4-9. Heat capacity of liquid and vapor hexane[11].
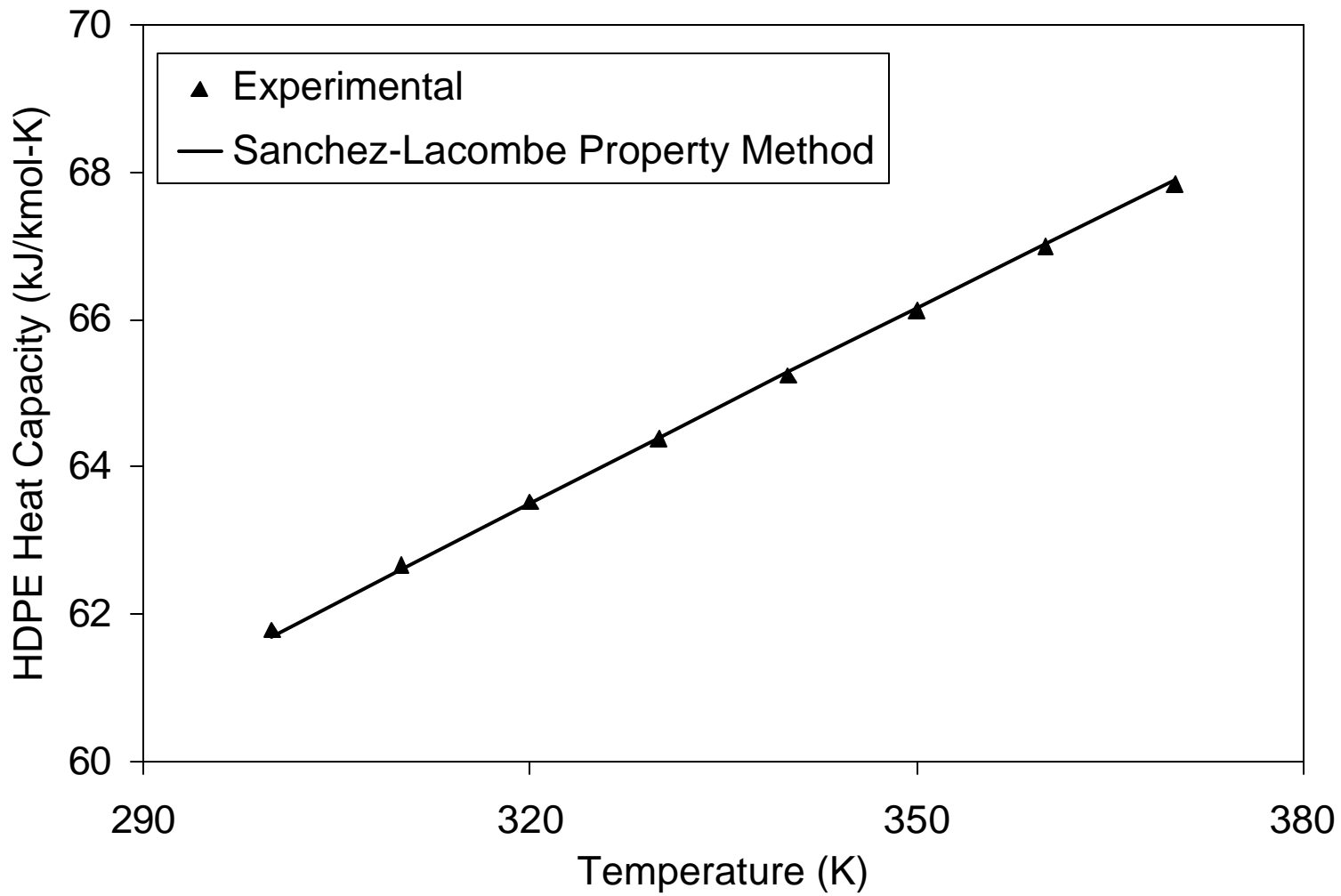
Figure 4-10. Heat capacity of HDPE[13].
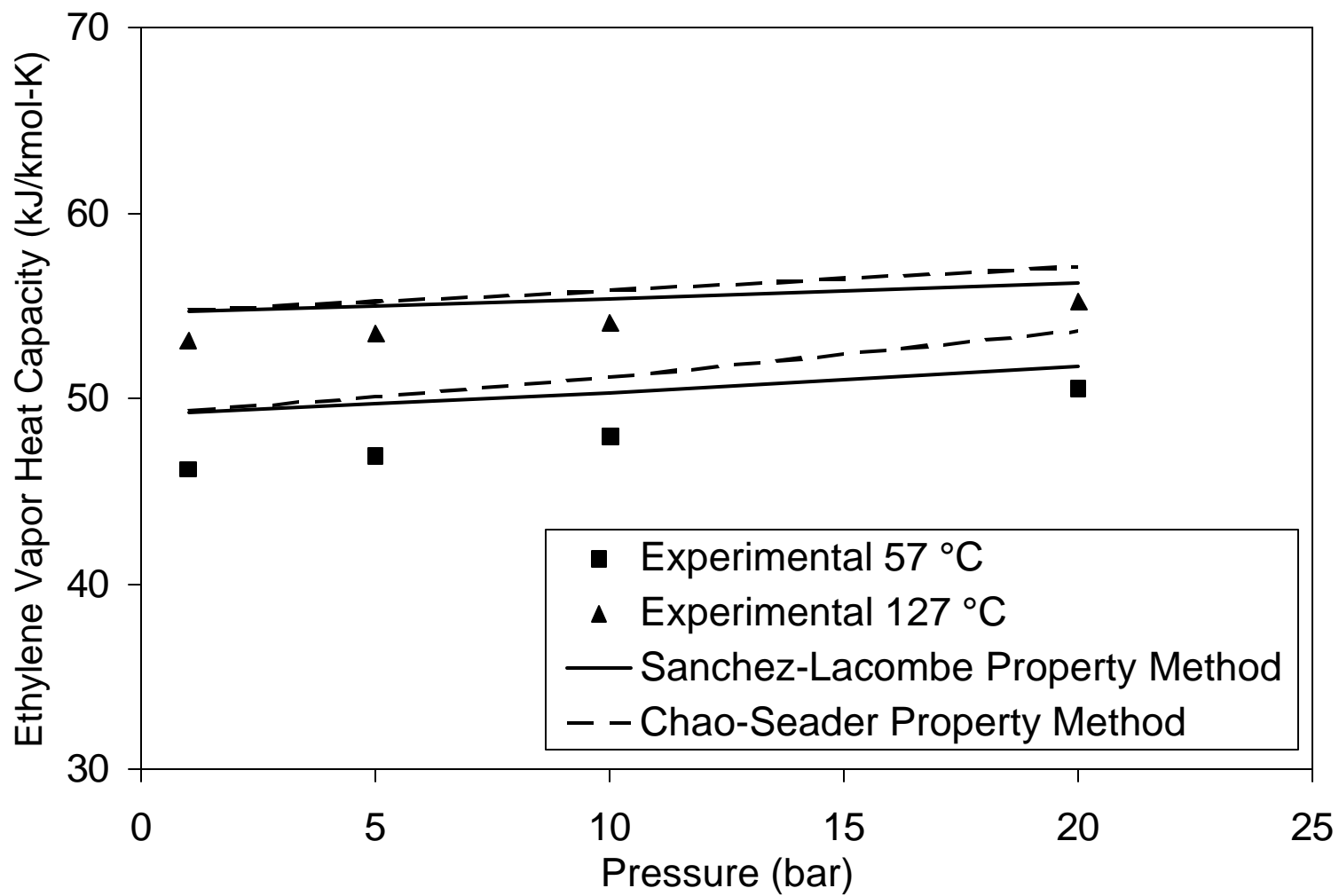
Figure 4-11. Heat capacity of ethylene vapor[12].
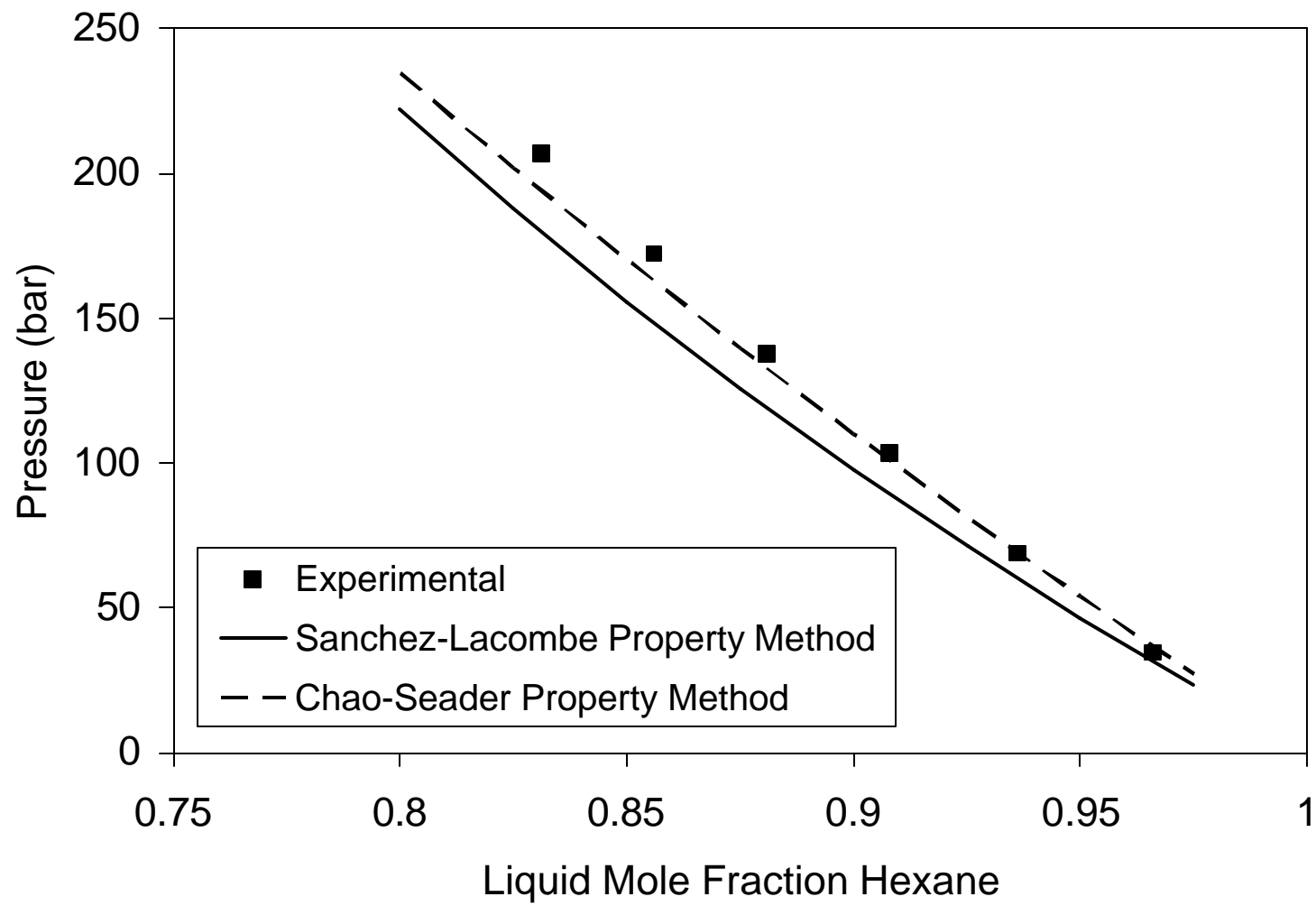
Figure 4-12. Solubility of hydrogen in hexane[14].

4.2.6 Polymer Properties

4.2.6.1 Heat of Polymerization

The heat of ethylene polymerization is the difference between the enthalpy of ethylene and the enthalpy, per segment, of the polymer at the same conditions. The reaction is[15]:

$$C_2H_{4(g)} \rightarrow \frac{1}{n}(C_2H_4)_{n(\text{amorphous})} \qquad \Delta H = -24.3 \text{ kcal/mol} \tag{5}$$
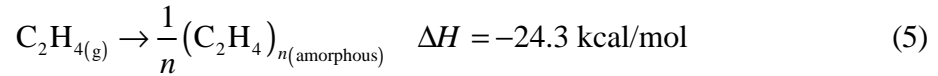
where ΔH is the heat of ethylene polymerization. The difference between the enthalpies of ethylene and HDPE at the reactor conditions represents the heat of polymerization in the model. These enthalpies are computed using the Sanchez-Lacombe EOS. Table 4-7 gives model predictions for the heat of polymerization at representative reactor conditions. These values compare favorably with the literature value given in eq 5.

Table 4-7. Computing the heat of ethylene polymerization using the Sanchez-Lacombe EOS. The results compare favorably with the literature value given in eq 5.

T (°C)	P (bar)	H_{ethylene} (kcal/mol)	H_{HDPE} (kcal/mol)	ΔH_f (kcal/mol)
70	5	12.2	-12.7	-24.9
75	5	12.2	-12.6	-24.8
80	5	12.3	-12.5	-24.8
85	5	12.3	-12.4	-24.7
70	6	12.2	-12.7	-24.9
75	6	12.2	-12.6	-24.8
80	6	12.3	-12.5	-24.8
85	6	12.3	-12.4	-24.7

4.2.6.2 Molecular Weight from Method of Moments

In order to rigorously model a polymer reactor, we would need individual rate expressions for polymer molecules of every chain length. Since polymers commonly contain distributions of chains consisting of up to hundreds of thousands of segments, this would lead to an impractical number of model equations. A useful technique to track the leading moments of the chain-length distribution of the HDPE is the method of moments[16]. The moments are sums of polymer concentrations weighted by chain length. The moment expression for live polymer chains is

$$\boldsymbol{m}_i = \sum_{n=1}^{\infty} n^i \left[P_n \right] \tag{6}$$

where $\boldsymbol{m}_i$ is the ith moment for live chains and $[P_n]$ is the concentration of polymer chains containing n segments. The expression for bulk (live plus dead) chains is

$$\boldsymbol{l}_i = \sum_{n=1}^{\infty} n^i \left(\left[P_n \right] + \left[D_n \right] \right) \tag{7}$$

where $[D_n]$ is the concentration of dead (inactive) polymer chains. The rate expressions involving polymer chains are summed over all n, yielding a small number of closed expressions that are functions of the moments.

Typically, the zeroth, first, and second moments are sufficient for the computation of common polymer properties. Among them is the number-average molecular weight (M_n):

$$M_n = \frac{\boldsymbol{l}_1}{\boldsymbol{l}_0} \tag{8}$$

The weight-average molecular weight (M_w) is

$$M_w = \frac{\boldsymbol{l}_2}{\boldsymbol{l}_1} \tag{9}$$

The polydispersity index (PDI) is

$$PDI = \frac{M_w}{M_n} = \frac{\boldsymbol{l}_2 \boldsymbol{l}_0}{\boldsymbol{l}_1^2} \tag{10}$$

Polymers Plus implements the method of moments approach in tracking polymerization kinetics and polymer properties.

4.2.7 Reactor Phase Equilibrium

As mentioned previously, the polymer forms a crystalline solid within the liquid phase upon formation. Solid polymer is generally considered to be inert, and does not participate in phase equilibrium[5]. A rigorous approach would be to consider only the solubilities of gases that may dissolve in the solid polymer. However, most commercial process simulators do not have reactor models that permit the existence of distinct species that are thermodynamically inert. Alternatively, we can model the polymer as dissolved in the liquid phase. Figure 4-13 compares these physically different situations. In the remainder of this section, we demonstrate that we can make this assumption without undermining the robustness of the reactor model.
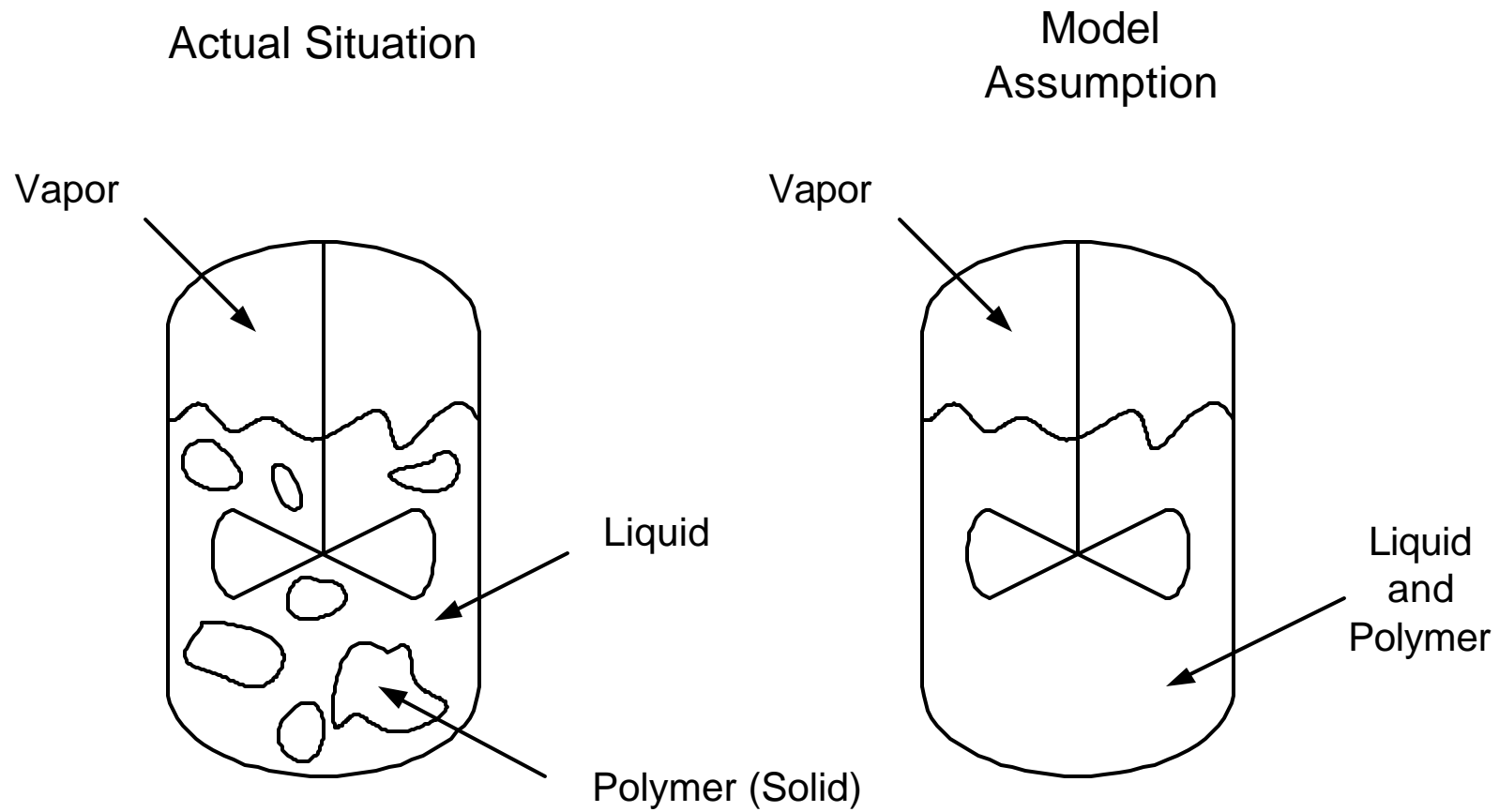
Figure 4-13. Comparing the actual phase behavior in the reactor with the modeling assumption. The actual situation has vapor and liquid phases, with solid polymer dispersed in the liquid phase. Our system considers the polymer as solubilized in the liquid phase.

We justify our simplification by comparing two approaches for modeling the slurry system. The first option is to treat the polymer as residing in a separate liquid phase (vapor-liquid-liquid equilibrium, VLLE), and in the second option, the polymer is dissolved in the solvent (vapor-liquid equilibrium, VLE). We model results for a flash vessel that simulates the phase separation for a mixture of components of mass fractions and conditions that are representative of an industrial slurry HDPE reactor. Table 4-8 gives the species and mass fractions that we use. For the case where HDPE is absent, we normalize the mass fractions of the remaining species to unity. We flash the mixture at 75 °C and 4 bar.

Table 4-8. Representative species and mass fractions used for simulating the phase separation in a slurry HDPE reactor.

component	mass fraction
ethylene	0.25
propylene	0.02
hexane	0.653
hydrogen	0.007
HDPE	0.07

For the two-liquid case, we choose $k_{ij} = 0.5$ and $h_{ij} = 0$ for all polymer/conventional-component pairs to force the polymer into a separate liquid phase. Table 4-9 shows the resulting amounts of species in each liquid phase. The light components do not appreciably dissolve in the polymer phase. We also see that the differences in the total amounts of each species in the liquid phase for each case are relatively small.

Table 4-9. Comparing the liquid compositions for cases where the HDPE has its own liquid phase (VLLE) and when it is dissolved in the diluent (VLE).

species	VLLE case	VLE case

	liquid 1 kg/hr	liquid 2 kg/hr	total liquid kg/hr	liquid kg/hr
hexane	350.8056061	9.81507e-05	350.8057	367.9578
ethylene	5.520240829	0.351363342	5.871604	5.466046
propylene	1.24868794	6.89622e-05	1.248757	1.495278
hydrogen	0.007724188	0.000382869	0.008107	0.014171
HDPE	1.20071e-32	69.99586821	69.99587	70

Table 4-10 compares the vapor-phase predictions for each case. The vapor compositions are approximately the same. Since we use the same pressure in each case, these vapor fractions also represent the relative magnitudes of partial pressures of components in the mixtures.

Table 4-10. Comparing the vapor compositions for the VLE and VLLE cases.

species	vapor mole fraction	
	VLE case	VLLE case
hexane	0.2076432	0.2175847
ethylene	0.54720348	0.53979344
propylene	0.02760584	0.02772536
hydrogen	0.21754748	0.2148965

In the VLLE situation, the reacting phase is the second liquid phase, and in our VLE simplification, it is the single liquid phase. While the compositions of the reacting phases for these two approaches are different, the results are satisfactory. We can reasonably model the slurry HDPE process by considering the polymer as dissolved in the liquid phase (VLE) without compromising the predicted phase behavior of the major components.

4.3 Polymerization Kinetics

4.3.1 Introduction

The reactions and kinetics of Ziegler-Natta polymerization have been studied extensively for different catalyst systems and processes[2, 16-19]. Further, it is generally accepted that Ziegler-Natta catalysts produce polymers with wide molecular weight distributions (MWD) due to the multi-site nature of the catalyst. It is believed that there are several site types on the catalyst, each with its own reactivity. The composite polymer, defined as the sum of the polymer made from all the catalyst sites, has a broad MWD even though the polymer made by each site type has a narrow (most probable) MWD.

In this work, we develop a multi-site kinetic model for the slurry HDPE process. We select a subset of the Ziegler-Natta polymerization reactions that allows the model to describe the observed kinetic phenomena and match the production rate, melt index (MI) and density targets for several grades. Sections 4.3.2 and 4.3.3 describe the reactions for homopolymerization and copolymerization kinetics, respectively. We include additional reactions, described in Section 4.3.4, to account for the production of wax (low molecular weight polymer species) that dissolves in the hexane diluent.

As there are many reactions and kinetic parameters, we develop a detailed methodology to fit the kinetic parameters to data for several grades from both the parallel and series modes of operation. The methodology, described in Section 4.3.5, involves a three-step process to simplify the task of fitting the kinetic parameters. In the first step, we develop a single-site kinetic model and fit the rate constants to match the polymer production rate, comonomer conversion, and polymer M_n for several parallel and series grades. Next, we deconvolute the measured polymer molecular weight distribution into a number of Flory distributions. In the third step, we use the deconvolution results to expand the single-site kinetics to multi-site kinetics. We adjust the kinetic parameters in the multi-site model to fit polymer production rate, comonomer conversion, M_n, and PDI of the polymer for several parallel and series grades.

In the available plant data, the polymerization reactors are at approximately the same temperature. We therefore do not consider the effect of temperature on the polymerization kinetics.

4.3.2 Homopolymerization Kinetic Scheme

We develop a Ziegler-Natta reaction subset to describe the observed phenomena and match targets for several grades in the HDPE slurry process. Table 4-11 lists the homopolymerization reactions that we consider. We describe these reactions in the following sections.

Table 4-11. Reaction subset used in the Ziegler-Natta homopolymerization kinetics.

reaction	description
1	catalyst site activation by cocatalyst
2	chain initiation
3	chain propagation
4	chain transfer to hydrogen
5	chain transfer to monomer
6	reversible catalyst site inhibition
7	spontaneous catalyst site deactivation

4.3.2.1 Catalyst Activation

In Ziegler-Natta systems, an aluminum alkyl cocatalyst, such as triethyl aluminum, is typically used to activate the sites on the catalyst. The cocatalyst is believed to form a complex with the catalyst sites that make them active for polymerization. Equation 11 shows the reaction for site activation by cocatalyst. In this reaction, the transition-metal catalyst (CAT) reacts with the cocatalyst (COCAT) to form vacant sites ($P_{0,i}$) of type i.

$$CAT_i + COCAT \xrightarrow{k_{acti}} P_{0,i} \tag{11}$$

where $k_{act,i}$ is the rate constant for activation of site type i by cocatalyst. The vacant sites are capable of producing polymer chains by reacting with monomer during chain initiation and subsequent propagation.

Typically, Ziegler-Natta catalysts activate almost completely in several minutes, and we therefore choose a relatively high rate constant for site activation. Alternatively, we can determine the rate constants for site activation and deactivation using data for catalyst activity profiles from experiments using laboratory-scale semi-batch reactors.

As typical Ziegler-Natta catalysts are heterogeneous in nature (active metal on a support), the model includes a parameter (max-sites) for the concentration of catalyst sites per unit mass of catalyst. Typical values of the max-sites parameter range from 1.0 E-5 to 1.0 E-3 kg-mol sites per kg of catalyst. This parameter controls the sensitivity of the polymer production rate to changes in catalyst flow rate. Changing the value of this parameter proportionally scales the effects of the site-based reactions (propagation, chain transfer, etc.). We can use it to change the magnitudes of these reactions without changing their values relative to each other. Hence, it changes the polymer production rate but does not affect the polymer molecular weight averages or copolymer composition.

4.3.2.2 Chain Initiation

A monomer molecule reacts with a vacant site to initiate chain growth:

$$P_{0,i} + M \xrightarrow{k_{ini,i}} P_{1,i} \qquad (12)$$

where M is the monomer (ethylene), $P_{1,i}$ is a propagation site of type i with an attached polymer chain containing one segment, and $k_{ini,i}$ is the rate constant for chain initiation at site type i.

It is not possible to determine the rate constants for chain initiation and propagation separately, due to the limited types of data measurements that can be made. Hence, we set the rate constant for ethylene chain initiation equal to the rate constant for propagation

of ethylene monomer on ethylene active segments. Similarly, we set the rate constants for comonomer chain initiation equal to the rate constants for homopropagation of these monomers.

4.3.2.3 Chain Propagation

The polymer chain grows rapidly by the successive addition of monomer molecules at the catalyst site:

$$P_{n,i} + M \xrightarrow{k_{p,i}} P_{n+1,i} \tag{13}$$

where $P_{n,i}$ and $P_{n+1,i}$ are polymer chains of length n and $n+1$ segments, respectively, associated with catalyst-site type i, and $k_{p,i}$ is the rate constant for chain propagation for site type i. In general, a linear increase in the rate constants for propagation yields a linear increase in molecular weight.

4.3.2.4 Chain Transfer

Chain transfer occurs when a monomer or chain-transfer agent disengages a polymer chain from the catalyst, rendering it inactive or dead, and initiates the growth of a new chain. Most slurry HDPE processes use hydrogen as a chain-transfer agent, in order to control the molecular weight of the polymer product. For hydrogen, the reaction is

$$P_{n,i} + H_2 \xrightarrow{k_{th,i}} D_n + P_{0,i} \tag{14}$$

where D_n is a dead polymer chain of length n, and $k_{th,i}$ is the rate constant for chain transfer to hydrogen for site type i.

The chain-transfer reaction to monomer is slightly different, as it produces an initiated chain instead of a vacant catalyst site:

$$P_{n,i} + M \xrightarrow{k_{m,i}} D_n + P_{1,i} \tag{15}$$

where $k_{tm,i}$ is the rate constant for chain transfer to monomer for site type i, and $P_{1,i}$ is an initiated chain associated with site type i.

We adjust the rate constants for chain transfer to hydrogen and to monomer to match the molecular weight of the HDPE produced over several reactors/grades with different H_2/C_2H_4 ratios in the reactor overheads. Note that the reaction with hydrogen produces a vacant catalyst site, while the reaction with monomer produces an initiated catalyst site. Adjusting the rate constant for chain transfer to monomer can disrupt the equilibrium number of inhibited catalyst sites, since the rate of chain initiation competes with that of hydrogen inhibition.

4.3.2.5 Forward and Reverse Catalyst Inhibitions

Some species, such as hydrogen, are known to cause a decrease in the rate of polymerization in some Ziegler-Natta catalyst systems. This rate depression appears to be reversible and disappears upon removal of the hydrogen. Slurry HDPE processes typically operate with two reactors in series to make a polymer product with a bimodal MWD. They do this by making close to 50% of the total polymer in the first reactor with a low average molecular weight, and 50% of the polymer in the second reactor with a high average molecular weight. The catalysts used in these processes exhibit the reaction for reversible site inhibition by hydrogen and it is essential for modeling the production rates in each reactor of the series configuration. We use forward and reverse catalyst inhibitions by hydrogen to represent this behavior. The forward reaction is:

$$\text{CAT}_i + x\text{H}_2 \xrightarrow{k_{finhi}} \text{ICAT}_i \qquad (16)$$

where $k_{finh,i}$ is the rate constant for forward inhibition of catalyst of site type i. The reverse reaction is

$$\text{ICAT}_i \xrightarrow{k_{rinhi}} \text{CAT}_i + x\text{H}_2 \qquad (17)$$

where $k_{rinh,i}$ is the rate constant for reverse inhibition of site type i. We adjust these rate constants to match the production rate of HDPE in each reactor in the series configurations.

4.3.2.6 Spontaneous Catalyst Deactivation

The active sites on the catalyst can undergo spontaneous deactivation to form dead sites that are no longer active:

$$P_{0,i} \xrightarrow{k_{d,i}} CAT_i \tag{18}$$

where $k_{d,i}$ is the rate constant for spontaneous catalyst deactivation for site type i. Increasing this rate constant decreases the production rate of HDPE. Also, if chain-transfer rates are low, catalyst deactivation can affect the number-average molecular weight.

4.3.3 Copolymerization Kinetic Scheme

Comonomers are commonly used to produce HDPE products of varying densities. The introduction of *a*-olefins, such as propylene, 1-butene, and 1-hexene, creates short-chain branching along the polymer backbone, lowering the crystallinity of the polymer.

We assume that the rate of propagation of a monomer (or comonomer) depends only on the active segment (last monomer added to the chain) and the propagating monomer. This is commonly referred to as the terminal model for copolymerization kinetics. For a system with two monomers, we expand the propagation reactions as follows:

$$P_{n,i}^1 + M_1 \xrightarrow{k_{p,i}^{11}} P_{n+1,i}^1 \tag{19}$$

$$P_{n,i}^1 + M_2 \xrightarrow{k_{p,i}^{12}} P_{n+1,i}^2 \tag{20}$$

$$P_{n,i}^2 + M_1 \xrightarrow{k_{p,i}^{21}} P_{n+1,i}^1 \tag{21}$$

$$P_{n,i}^2 + M_2 \xrightarrow{k_{p,i}^{22}} P_{n+1,i}^2 \tag{22}$$

where $P_{n,i}^j$ is a polymer chain of length n, associated with site type i, that has an active segment corresponding to monomer of type j, and $k_{p,i}^{jk}$ is the rate constant for propagation, associated with site type i, for a monomer of type k adding to a chain with an active segment of type j.

For HDPE, the concentration of comonomer segments in the polymer and the concentration of comonomer active segments (i.e. segments attached to an active site) are small. Hence, the homopropagation reaction for ethylene is the primary factor responsible for ethylene conversion, while the propagation reaction for comonomer adding to a chain ending with an ethylene active segment dominates the consumption of comonomer. The concentration of ethylene active segments is very high relative to that of comonomer active segments. As a result, the propagation reactions involving comonomer active segments only provide minor contributions to the conversion of monomer and comonomer, as well as the HDPE production rate.

We expand the reactions for chain initiation and chain transfer to both monomer and hydrogen in a similar fashion, to consider the reaction of these species with the different monomers/active segments on the polymer chains. For chain initiation:

$$P_{0,i} + M_j \xrightarrow{k_{ini,i}^j} P_{1,i}^j \tag{23}$$

where M_j is monomer of type j and $k_{ini,i}^j$ is the rate of chain initiation for monomer j at site type i.

For chain transfer to hydrogen:

$$P_{n,i}^j + H_2 \xrightarrow{k_{th,i}^j} D_n + P_{0,i} \tag{24}$$

111

where $k^j_{th,i}$ is the rate constant for chain transfer to hydrogen associated with a chain ending with a monomer unit of type j at site type i. Similarly, we have the copolymerization reactions for chain transfer to monomer:

$$P^j_{n,i} + M_k \xrightarrow{k^{jk}_{tm,i}} D_n + P^k_{1,i} \tag{25}$$

where $k^{jk}_{tm,i}$ is the rate constant for chain transfer for a monomer of type k reacting with a growing chain ending in a monomer unit of type j at site type i.

4.3.4 Oligomer Production

The slurry HDPE processes produce oligomer, which is a low-molecular-weight polymer species that dissolves in the hexane diluent. Using plant data for the molecular weight of the oligomer, we model its production by reacting stoichiometric amounts of ethylene and hydrogen:

$$x C_2 H_4 + H_2 \rightarrow \text{Oligomer} \tag{26}$$

where x represents the number of ethylene segments in the oligomer. Since we know the amount of oligomer produced, we adjust the extent of this reaction in the model to match its production rate. Specifically, the extent of reaction represents the changes in the number of moles of ethylene due to reaction divided by the stoichiometric coefficient x.

4.3.5 Determination of Kinetic Parameters

4.3.5.1 Introduction

Here, we provide a general methodology for simultaneously fitting the kinetic parameters to plant data for multiple product grades. The fine-tuning of kinetic parameters to match the plant data can be a difficult task. Adjustment of the rate constant for each reaction can affect several simulation variables simultaneously. The methodology assumes no information about the kinetic activity of the catalyst or the number of catalyst sites per mass of catalyst.

As mentioned previously, we do not consider temperature effects on the polymerization kinetics, as all the reactors in the plant were operated at about the same temperature. Since the polymerization reactions are highly coupled, the determination of temperature dependence for each individual reaction would require extensive experimentation. Moreover, there is a scarcity of data in the open literature for the temperature dependence of the reactions for Ziegler-Natta systems.

We divide the procedure into two parts. In the first part, we assume that the catalyst contains a single site type. This simplification only permits us to accurately model the M_n, not the M_w nor the PDI. We adjust the kinetic parameters to match the HDPE production rate in each reactor and the conversions of monomer and comonomer, in addition to the HDPE M_n.

The second part of the procedure involves the introduction of multiple catalyst-site types. We deconvolute the MWD for the polymer product into distributions for each site type. This procedure gives the minimum number of site types that enables us to accurately compute the polymer MWD, as well as the relative rate of propagation and the polymer M_n produced by each site type. The simulation targets include those for the single-site model, as well as the relative amount of polymer produced at each site type, the M_n for HDPE for each site type, the fraction of inhibited catalyst sites as determined in the single-site model, and the PDI of the HDPE product. Table 4-12 summarizes the simulation targets for the single-site and multi-site models.

Table 4-12. Simulation targets for the models for catalysts with single and multiple site types.

model for single-site catalyst	model for multiple-site catalyst
HDPE production in each reactor	HDPE production in each reactor
monomer and comonomer conversions	monomer and comonomer conversions
HDPE M_n	HDPE M_n
	relative production of HDPE by each site type
	M_n of hdpe at each site type
	fraction of inhibited catalyst sites

	HDPE PDI

Section 4.3.5.2 describes the determination of kinetic parameters for the single-site model. We manually iterate between each of the polymer grades until we obtain a set of kinetic parameters that satisfies the simulation targets for each one (Table 12). Section 4.3.5.3 explains the procedure for deconvoluting the MWD of the HDPE to determine the number of catalyst-site types and kinetic behavior for each site. Section 4.3.5.4 details the methodology for using the multi-site model to simultaneously adjust the kinetic parameters to match all of the simulation targets given in Table 4-12.

4.3.5.2 Single-Site Kinetic Model

We begin by modeling the catalyst as containing a single site type. Assuming a single-site catalyst, we can accurately model all of the reaction phenomena except the polymer PDI. The motivation for using this approach is that the consideration of a multi-site catalyst significantly increases the number of kinetic parameters that we must determine, due to the increase in the number of reactions involving catalyst sites. The number of reactions can exceed 60, depending on the number of site types used. The parameter determination is much simpler using a two-step method than trying to establish all of them at once.

We establish a base set of kinetic parameters using sources in the open literature. Table 13 gives their values. We also use an initial concentration of active catalyst sites on the catalyst species of 0.0002 mol sites/mol Ti[20]. We use these numbers as initial values in the model, and then apply an iterative methodology to adjust them to match model predictions with plant data.

Figure 4-14 shows the methodology we use to determine the kinetic parameters for the single-site model to match plant data for multiple product grades (both parallel and series configurations). We step through the algorithm manually. Using the base set of kinetic parameters in Table 4-13, we first adjust the concentration of active sites on the catalyst

species. Only a fraction of the transition-metal sites of the catalyst is available for polymerization. Increasing the active site concentration on the catalyst increases the rates

Table 4-13. Base set of kinetic parameters for the single-site model. We do not consider temperature effects on the polymerization kinetics, and we therefore do not take activation energies into account.

reaction	reactant 1	reactant 2	k^{a}	reference	comments
cat-act	catalyst	cocatalyst	1	17	
chain-ini	catalyst	ethylene	14.6		b
chain-ini	catalyst	Propylene	9.8		b
chain-ini	catalyst	1-butene	9.8		c
propagation	ethylene	ethylene	14.6	18	
propagation	ethylene	propylene	0.81	18	
propagation	propylene	ethylene	41	18	
propagation	propylene	propylene	9.8	18	
propagation	ethylene	1-butene	0.81		c
propagation	1-butene	ethylene	41		c
propagation	1-butene	1-butene	9.8		c
chat-agent	ethylene	hydrogen	0.088	17	
chat-agent	propylene	hydrogen	0.088	17	
chat-agent	1-butene	hydrogen	0.088		c
chat-mon	ethylene	ethylene	0.0021	17	
chat-mon	ethylene	propylene	0.006		d
chat-mon	propylene	ethylene	0.0021		d
chat-mon	propylene	propylene	0.006		d
chat-mon	ethylene	1-butene	0.006	17	
chat-mon	1-butene	ethylene	0.0021	17	
chat-mon	1-butene	1-butene	0.006	17	
fwd site inh	catalyst	hydrogen	2000	17	
rev site inh	catalyst		0.0003	17	
spon-deact	catalyst		0.0001	17	

$^{\mathrm{a}}$ General units are L/mol-s. $^{\mathrm{b}}$ Assumed to be equal to that for homopropagation. $^{\mathrm{c}}$ Assumed to be equal to the analogous rate constant involving propylene. $^{\mathrm{d}}$ Assumed to be equal to the analogous rate constant involving 1-butene.
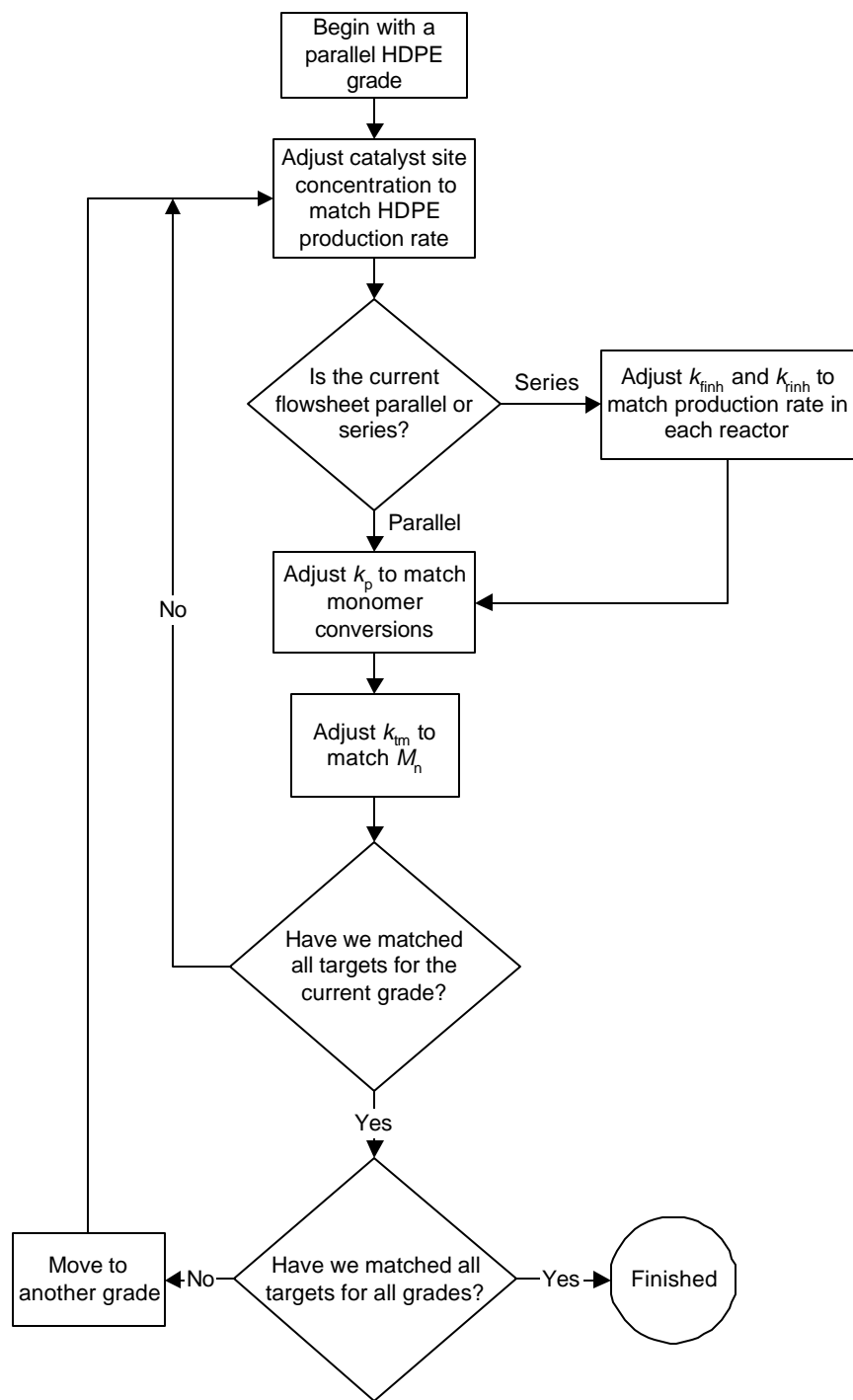
Figure 4-14. Methodology for simultaneously determining the kinetic parameters for a single-site catalyst to match plant data for multiple HDPE grades.

of reaction involving catalyst, such as activation, chain initiation, and chain propagation, while maintaining the relative ratio between them. Thus, we can increase the production rate of the HDPE, while maintaining its comonomer composition and number-average molecular weight.

We adjust the rate constants for chain propagation to match the conversions of monomer and comonomer. The primary reactions affecting monomer and comonomer conversions are those for monomer-monomer and monomer-comonomer propagations, respectively, due to the high monomer concentration relative to that of comonomer. Chain propagation also affects the molecular weight. Adjusting the rate constant for chain transfer to monomer affects the number-average molecular weight of the HDPE, especially when the concentration of chain-transfer agent is low.

For the series grades, we adjust the rate constants for forward and reverse catalyst inhibitions by hydrogen. Note that the series reactors operate at the same temperature. In general, increasing the rate constant for forward site inhibition decreases the polymer production rate in the first reactor, while increasing the production rate in the second reactor. Increasing the rate constant for reverse inhibition affects the relative production rates in both reactors simultaneously, so we can use it to adjust the HDPE production rates in both reactors, while maintaining the same ratio of production in each one.

We iterate between all of the product grades until we obtain a set of single-site kinetic parameters that allows the model to match the plant data (except the PDI) for each grade. The next section describes the use of gel-permeation chromatography (GPC) for obtaining the MWD of the polymer, and a quantification of the multi-site behavior of the catalyst.

4.3.5.3 Deconvolution of Molecular Weight Distribution Data

We can apply a statistical algorithm to deconvolute the polymer MWD to determine a most probable chain-length distribution for each of a determined number of catalyst-site

types. The methodology presented by Soares and Hamielec[4] allows us to determine the minimum number of catalyst-site types that gives an accurate representation of the molecular weight distributions generated by Ziegler-Natta catalysts, as well as the weight fraction and number-average molecular weight of polymer produced by each site type. The consideration of these site types, each with its respective reactivity, enables us to accurately model the broad molecular weight distribution of the HDPE.

Soares and Hamielec use the following expression to represent the most-probable weight chain-length distribution produced by each site type:

$$w_i(n) = t_i^2 n \exp(-t_i n) \tag{27}$$

Here, $w_i(n)$ is the weight fraction of polymer of chain length n produced by site type i. t_i is a fitting parameter for site type i, and represents the inverse of the M_n of polymer produced at that site. The weight chain-length distribution of the entire polymer is a weighted sum of the distributions produced by each site type. The weighting factor is the mass fraction of polymer produced at each site. The expression for the total polymer is

$$W(n) = \sum_{i=1}^{j} m_i w_i(n) \tag{28}$$

where $W(n)$ is the weight fraction of polymer of chain length n, m_i is the mass fraction of polymer produced at site type i, and j is the total number of site types.

We use software produced by Polythink Inc.[21] to deconvolute the GPC data for HDPE. It incorporates the methodology presented by Soares and Hamielec. The program determines the minimum number of site types that accurately describes the MWD, the weight fraction of polymer and its M_n produced at each site type, and the predicted M_n and M_w for the entire distribution.

Table 4-14 shows a representative set of deconvolution results for the parallel rector configuration. Figure 4-15 illustrates the MWD predicted by each site type, as well as a comparison of the prediction for the overall MWD with the experimental curve. The results indicate that a five-site model can describe the molecular weight distribution of

119
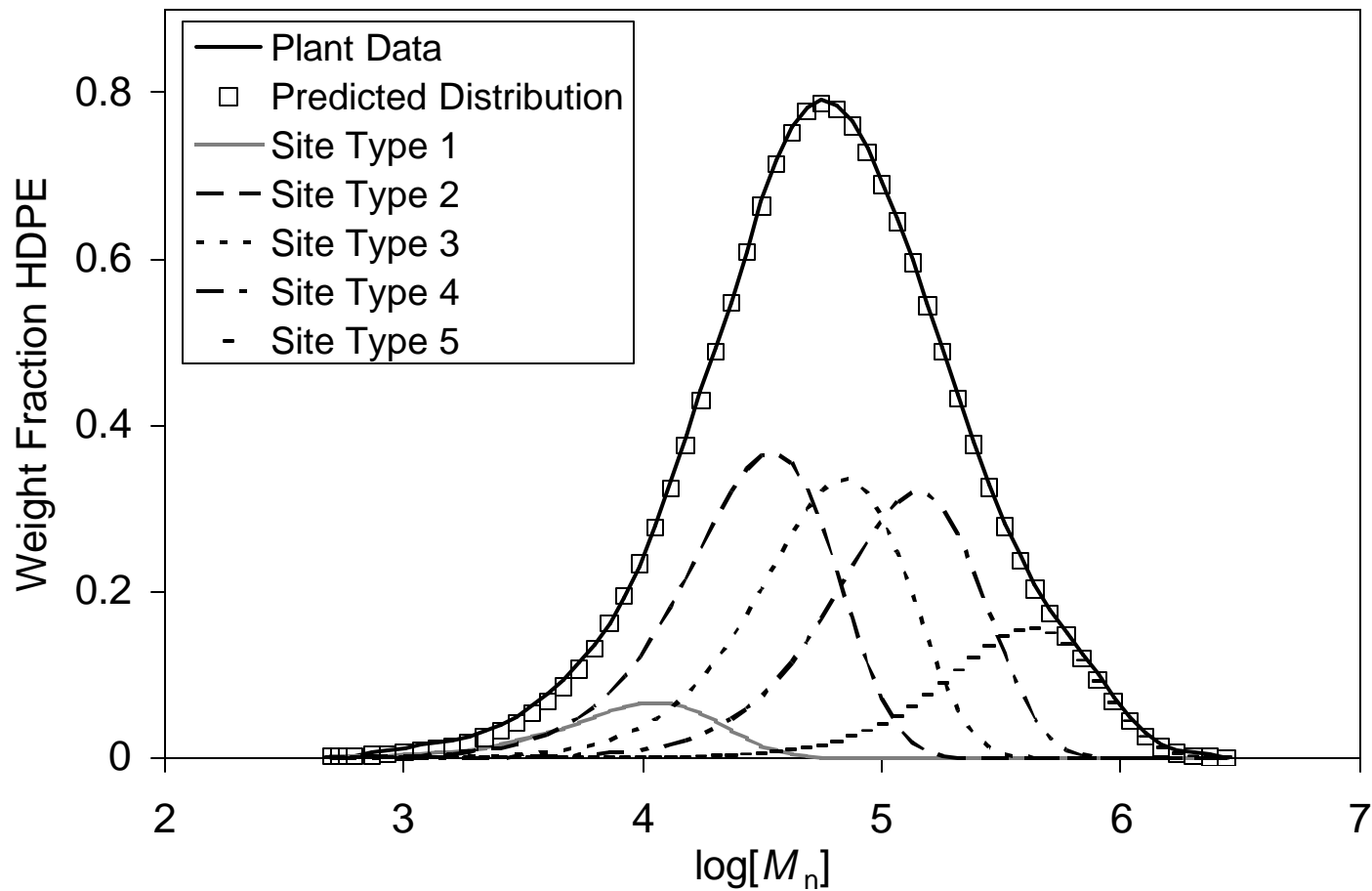
Figure 4-15. GPC Deconvolution results for a representative HDPE sample from the parallel reactor configuration. Five catalyst site types accurately describe the experimental molecular weight distribution.

this particular sample. In the next section, we show how to use these results to determine kinetic parameters for a reaction set considering multiple catalyst-site types.

Table 4-14. Deconvolution results for a representative sample of HDPE produced in the parallel process.

site type	HDPE weight fraction, m_i	t_i (M_n^{-1})	t_i^{-1} (M_n)
1	0.0529	1.76 E-4	5.69 E3
2	0.29538	5.75 E-5	1.74 E4
3	0.26979	2.85 E-5	3.50 E4
4	0.25685	1.41 E-5	7.08 E4
5	0.12504	4.76 E-6	2.10 E5

4.3.5.4 Multi-Site Kinetic Model

Once we establish a set of single-site kinetic parameters that allow the model to match the simulation targets for each grade (see Table 4-12), we introduce multiple site types, the exact number of which is determined by the GPC deconvolution method described in the previous section. It is important to note that the MWD from the second reactor in the series process is not useful for determining kinetic parameters for the site types. The polymer exiting this reactor results from reaction phenomena occurring in both reactors, and there is no reasonable way to decouple these events for the purpose of establishing kinetic parameters for individual reactions.

The transition from the single-site to multi-site catalyst introduces three new criteria for determining the kinetic parameters. These are the weight fraction and M_n of polymer produced at each site type, and the fraction of inhibited catalyst sites. The first two targets result from the MWD deconvolution described in the previous section. The fraction of inhibited sites affects the production rate of polymer, and we must maintain

the fraction that results from the single-site modeling step in order to maintain the correct relative amounts of polymer produced in each reactor for the series grades.

We multiply the rate constant for propagation determined in the single-site model by the weight fraction of polymer produced at site type i, m_i, (see Table 4-14) to obtain the initial values for each propagation rate constant:

$$k_{p,i}^{ij} = n_{st} k_p^{ij} m_i \qquad (29)$$

where n_{st} is the number of site types considered in the model. We must multiply the rate constants by n_{st} (five, in our case) because the concentration of total sites is n_{st} times that of the individual sites. Note that we assume the catalyst contains an equal number of moles of each site type. We adjust the rate constants for chain transfer to hydrogen and to monomer in order to match the number-average molecular weight produced at each site type.

The single-site model yields an equilibrium mole fraction of inhibited catalyst sites. We denote this value as $CISFRAC_{ss}$, where

$$CISFRAC_{ss} = \frac{\text{moles of inhibited catalyst sites}}{\text{total moles of catalyst sites}} \qquad (30)$$

We must maintain this total fraction in the multi-site model in order to preserve the polymer properties computed in the single-site model. We represent the corresponding targets in the multi-site model, $CISFRAC_i$, as the quotient of the single-site value and the number of site types:

$$CISFRAC_i = \frac{\text{moles of inhibited sites of type } i}{\text{total moles of all site types}} = \frac{CISFRAC_{ss}}{n_{st}} \qquad (31)$$

Figure 4-16 shows the iterative scheme for determining kinetic parameters in the multi-site model. It is more complex than that for the single-site model, due to the additional simulation targets. As with the single-site model, we step through the algorithm manually. Beginning iterations with a parallel model, we adjust the rate constants for forward site inhibition to match the inhibited fraction for each site type. If the mass

fraction of polymer produced at each site does not match the target values determined from deconvolution, we adjust the rate constants for propagation. We then adjust the rate constants for chain transfer to hydrogen to match the number-average molecular weights at each site type. If the number-average molecular weight of the total polymer is not correct, we adjust the rate constants for chain transfer to hydrogen for each catalyst-site type, while maintaining their values relative to each other.

For the series grades, we check the PDI produced in each reactor. If, at this point, the kinetics do not match the PDIs in the first reactors for all grades, we hypothesize that at least one of the site types is insensitive to a reactant involving chain transfer, such as hydrogen. We illustrate this using MWDs for representative HDPE. Figure 4-17 compares the MWDs for HDPE produced in reactors that have different hydrogen concentrations.
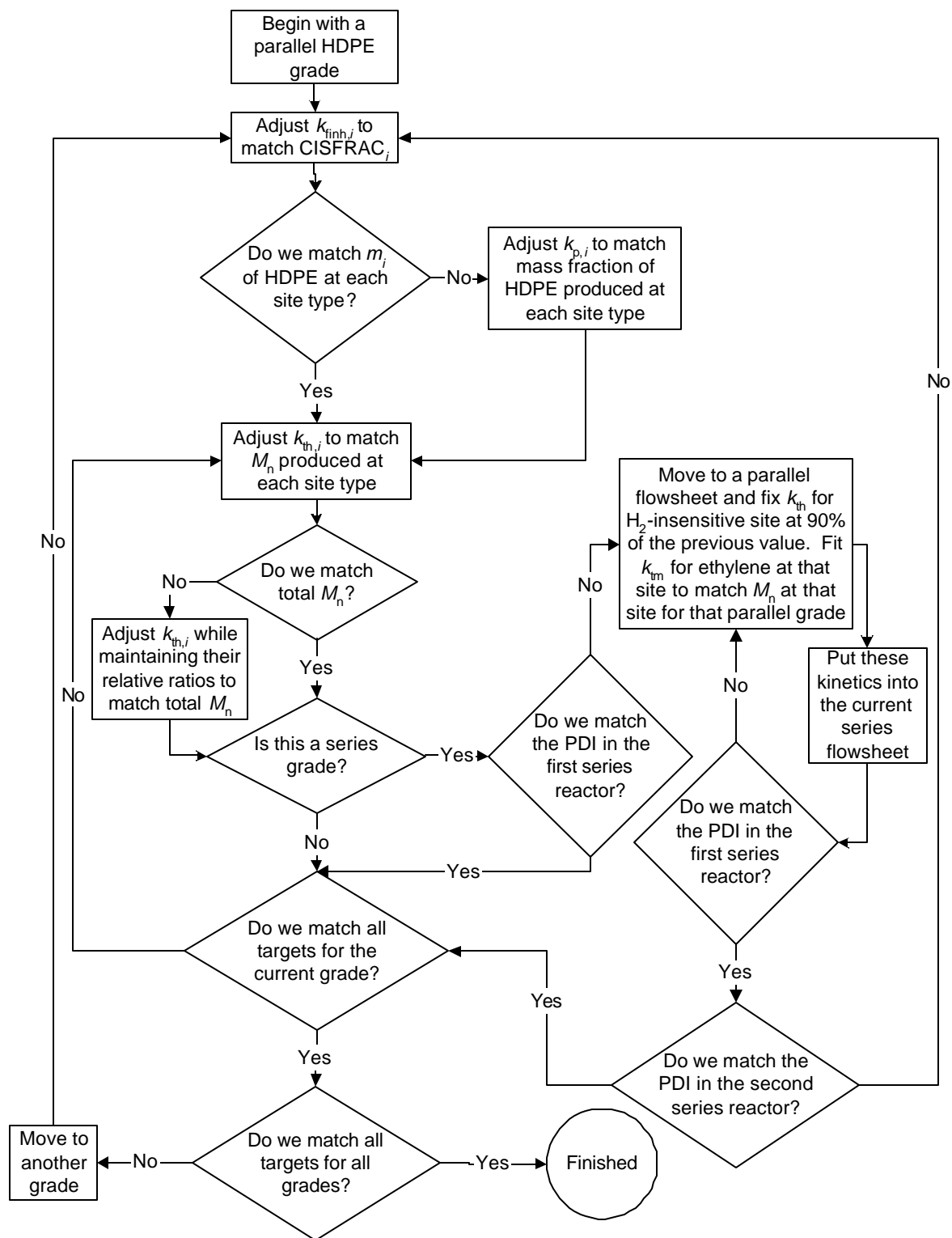
Figure 4-16. Methodology for simultaneously determining the kinetic parameters for a catalyst with multiple site types to match plant data for several HDPE grades.
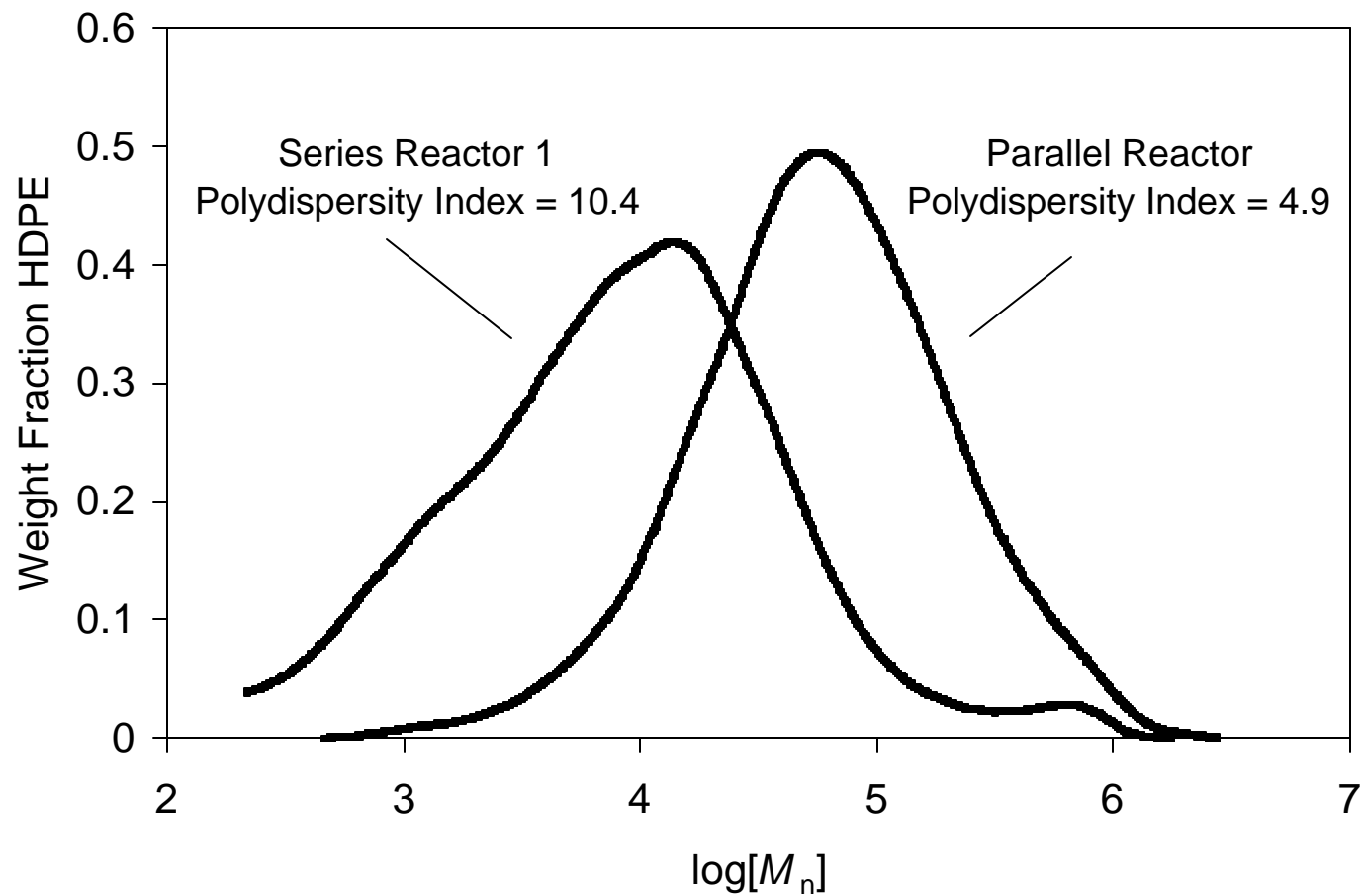
Figure 4-17. Comparing MWDs for two different grades of HDPE. We hypothesize that the Ziegler-Natta site type producing high molecular weight polymer is insensitive to hydrogen concentration.

In this case, the series reactor has a higher hydrogen concentration than the parallel reactor. Since hydrogen limits the molecular weight of the polymer, we expect to see the entire molecular weight distribution shift horizontally to the left as hydrogen concentration increases. However, if a site type is insensitive to hydrogen concentration, a shift does not occur. This is consistent with the behavior appearing in Figure 4-17.

In accordance with this observation, we include steps in the methodology to allow the kinetic model to match the PDI for grades of varying hydrogen concentration. We return to the previous fitted grade in the algorithm, preferably a parallel model. We reduce the rate of chain transfer to hydrogen by 10% for the insensitive site, while increasing the rate of chain transfer to monomer to refit the number-average molecular weight produced at that site. We then place these adjusted kinetics back into the model for the current grade and check the PDI. We repeat this loop until we match the PDI in the first reactor for each grade. We then check the PDI for the second series reactors, and return to the beginning of the algorithm for that grade if it does not match. We repeat this process until we match the data for each reactor in each grade.

Table 4-15 summarizes the model parameters we adjust to match the primary targets for the plant data. In the next section, we compare model predictions to data for eight HDPE grades.

Table 4-15. Simulation targets for each polymer grade and the corresponding model parameters adjusted.

simulation targets	adjusted parameters
monomer conversions (HDPE production rate)	propagation rate constants for monomer and comonomer
HDPE PDI	relative propagation rate constant for each site type, determined using deconvolution of MWD
mass fraction polymer produced at each site type	propagation rate constants for individual sites
M_n produced by each site type	chain-transfer rate constants for individual sites

4.4 Simulation Results

4.4.1 Steady- State Model Validation

We validate the model using plant data from four parallel and four series grades of HDPE, produced in two large-scale commercial plants (144,000 and 240,000 tons/yr). Differences between the processes for each grade include reactor configurations (parallel and series), feed rates for raw materials, and unit-operation conditions. Since we used this same data when developing the kinetic parameters, we can expect that accurate prediction by our model is generally limited to similar process conditions. The utilization of plant data at varying reactor temperatures, for example, would permit the consideration of activation energies in the kinetic expressions, resulting in an expansion of the predictive capabilities of the model.

Figures 4-18 to 4-20 compare the model predictions with data from Plant A for the HDPE produced in each reactor. The model accurately predicts the production rate, M_n, and PDI for each grade. The PDI predictions reflect the validity of the kinetic modeling and parameter determination of the multi-site catalyst.

Figures 4-21 and 4-22 show model validation for the vapor flow in the reactor overhead and the reactor residence times, respectively, for Plant A. The process model provides good agreement with each of these process variables. Accurate prediction of the volumetric flow in the vapor overhead is important due to limitations in equipment capacity. The reactor residence time must be accurate because it affects all of the polymer properties.

Tables 4-16 and 4-17 compare model predictions with data from Plant B[22]. The model provides good agreement with polymer properties and process variables in both the parallel and series configurations.

Table 4-16. Comparing model predictions with data for a parallel grade for Plant B.

	plant data	model prediction
HDPE production rate (kg/hr)	5,096 – 5,148	5,187
ethylene conversion (%)	98 - 99	99.7
propylene conversion (%)	72	75.3
HDPE M_n	14,000 – 16,000	15,975
HDPE PDI	9 - 10	9.63
reactor residence time (hr)	2.2	1.98
H_2/C_2H_4 molar ratio in overhead	0.65 – 0.68	0.643

Table 4-17. Comparing model predictions with data for a series grade for Plant B.

		plant data	model prediction
HDPE production rate (kg/hr)	Total	9,212 – 9,306	9,151
ethylene conversion (%)	Total	98 – 99	97.4
1-butene conversion (%)	Total	89	74.8
HDPE M_n	Reactor 1	--	3,336
	Reactor 2	7,000	6,537
HDPE PDI	Reactor 1	--	10
	Reactor 2	31 - 35	38.9
reactor residence time (hr)	Reactor 1	2.5	2.68
	Reactor 2	1.13	1.17
H_2/C_2H_4 molar ratio in overhead	Reactor 1	6.8 – 7.2	7.25
	Reactor 2	0.08 – 0.09	0.084

Here, we have presented results for a single reactor section for each of the parallel processes (refer to Figure 4-2). Although each parallel process essentially contains two identical process sections that receive the same fresh feeds and operate at the same conditions, identical industrial systems rarely behave in the same way. Therefore, when constructing a robust process model, one should consider both sections on an individual basis.

4.4.2 Dynamic Modeling

4.4.2.1 Introduction

While a steady-state model does not consider changes in the process with time, a dynamic model permits us to vary feed rates or vessel conditions, and to track the resulting process changes as they propagate through the system. A dynamic model can assist in optimizing the time required to carry out a grade change, facilitate the
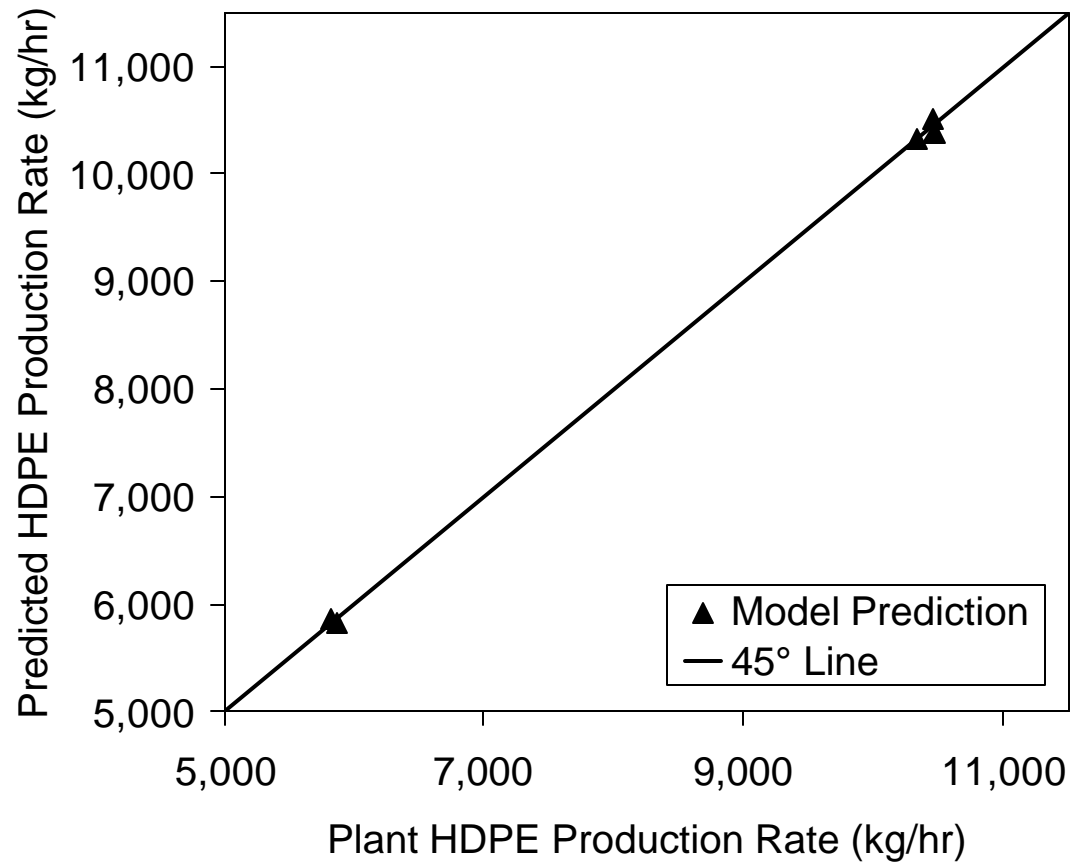
Figure 4-18. Comparing model predictions with plant data for HDPE production rate.
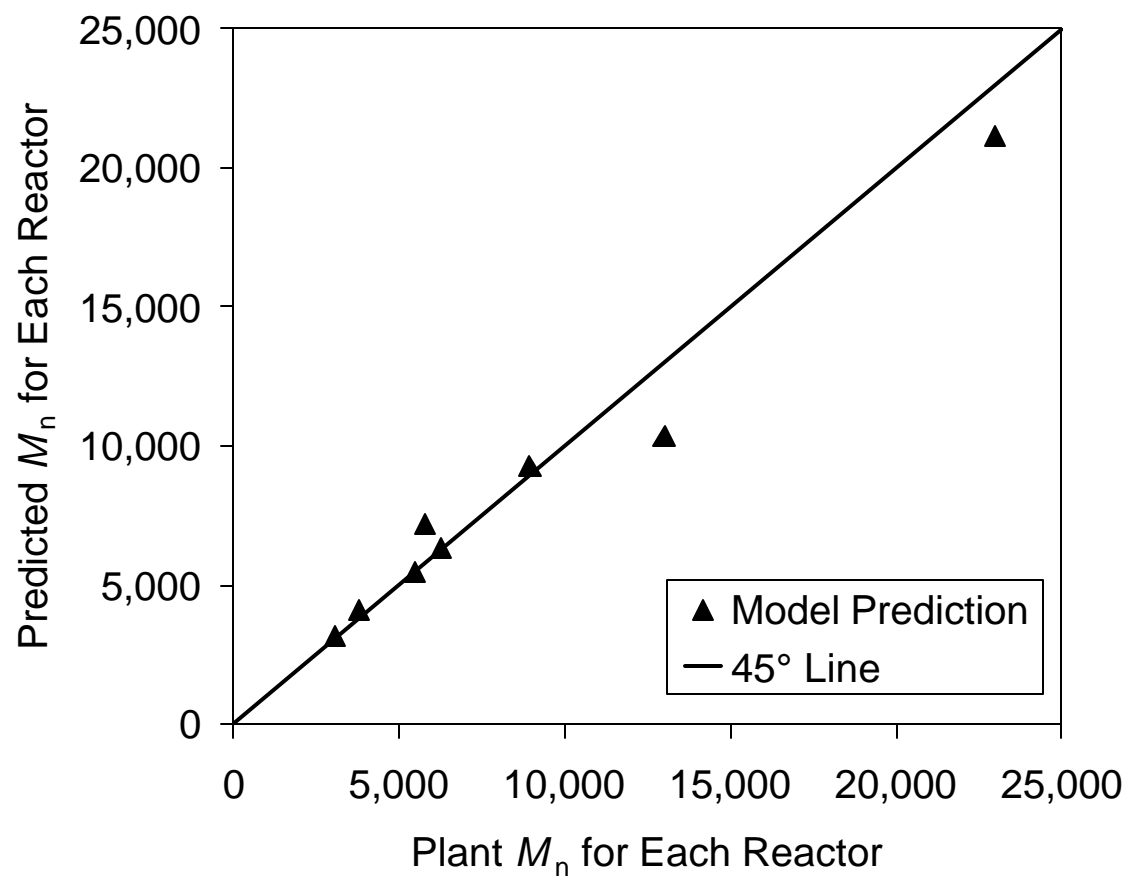
Figure 4-19. Comparing model predictions with plant data for the number-average molecular weight of HDPE for each reactor.
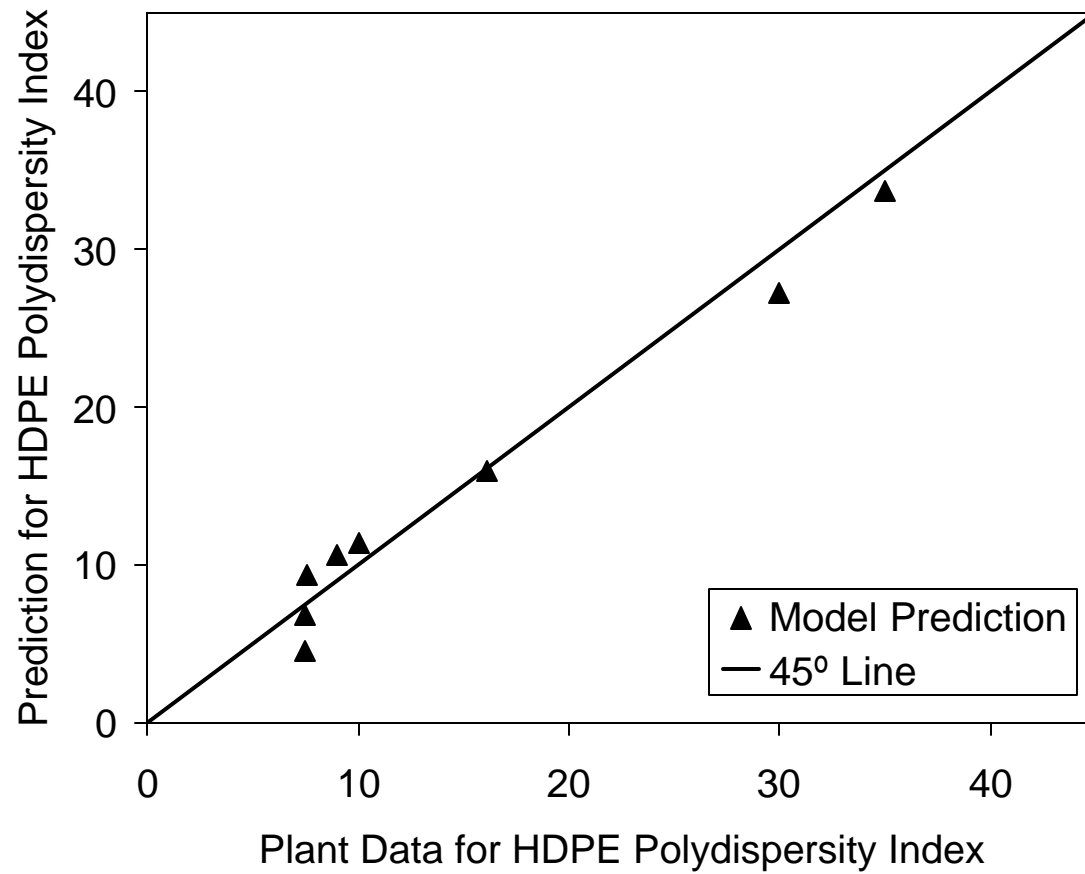
Figure 4-20. Comparing model predictions with plant data for HDPE polydispersity index.
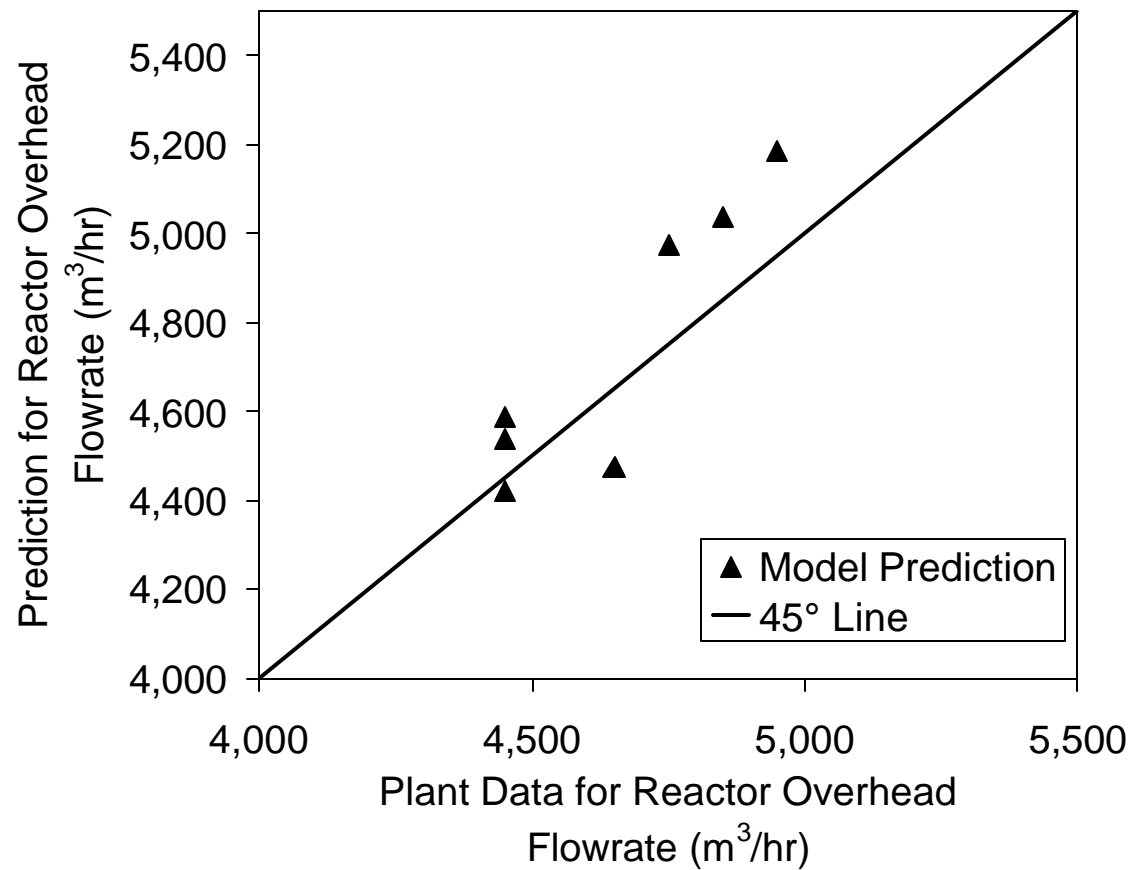
Figure 4-21. Comparing model predictions with plant data for the vapor flow rate in the reactor overhead.
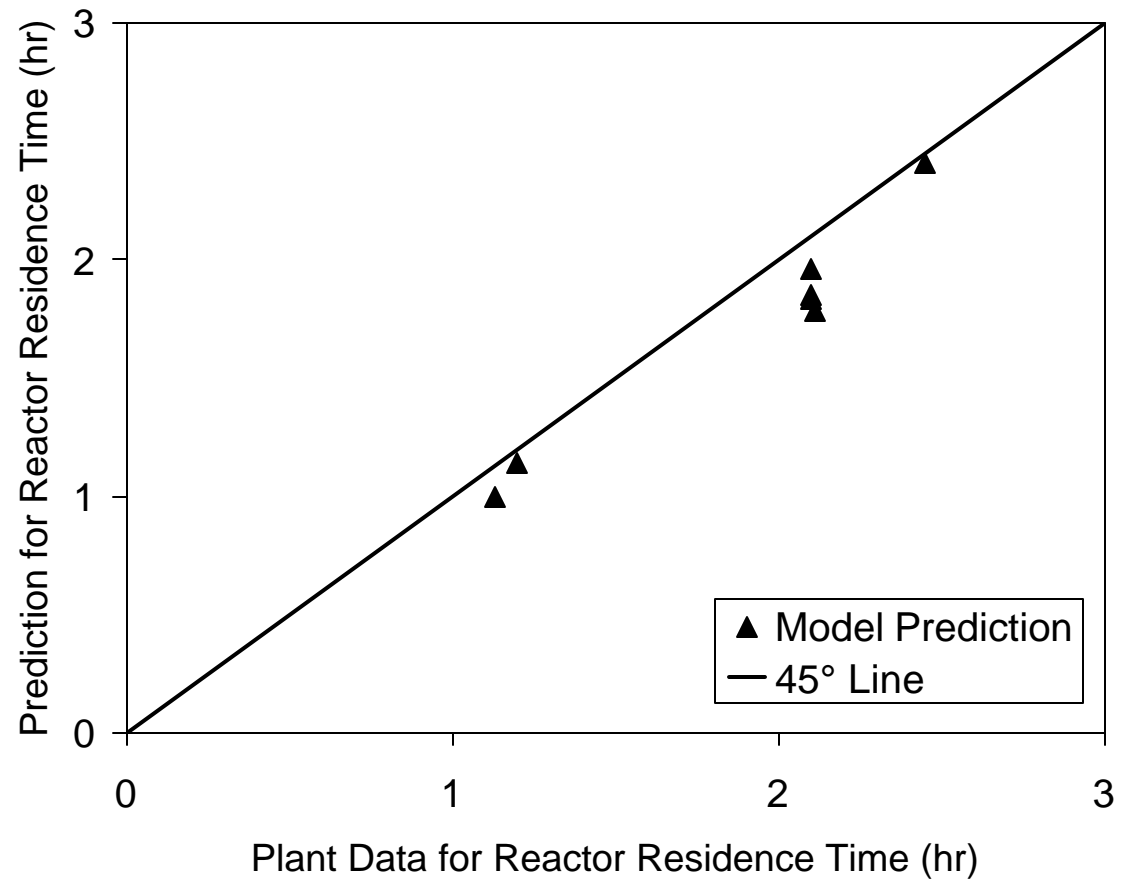
Figure 4-22. Comparing model predictions with plant data for reactor residence time.

development of a new polymer grade, or reveal the time-dependent effects of changing a process variable. Our goal here is to demonstrate the capability and utility of a dynamic model for an industrial slurry HDPE process.

We create the dynamic process model in ASPEN Dynamics by importing the corresponding steady-state model developed in ASPEN Polymers Plus. We include vessel dimensions and geometries to properly account for the liquid levels in each unit.

In the following sections, we illustrate the utility of the dynamic modeling by simulating a grade change for the parallel reactor configuration. Section 4.4.2.2 describes the control scheme for the process. Section 4.4.2.3 gives the feed rates and process variables for the grade change, as well as dynamic results.

4.4.2.2 Control Scheme

Figure 4-23 is a simplified diagram illustrating the control scheme for the parallel configuration. The process includes (1) a reactor temperature controller that adjusts the amount of recycle gas returned to the reactor inlet, (2) a compositional controller that adjusts the hydrogen feed rate and the rate of recycle-gas flare to maintain a constant ratio of hydrogen to ethylene in the recycle-gas stream, and (3) a level controller in the overhead flash unit that adjusts the amount of liquid recycled to the reactor. Table 4-18 summarizes the controlled and manipulated variables.

Table 4-18. Controlled and manipulated variables for the slurry HDPE process.

controlled variables	manipulated variables
reactor temperature	overhead vapor recycle to reactor
overhead H_2/C_2H_4 molar ratio	hydrogen feed rate and overhead flare
liquid level in flash tank	liquid recycle rate to reactor

4.4.2.3 Dynamic Grade Change

Table 4-19 gives the key process modifications for a typical grade change for the parallel configuration. The unit-operation conditions remain the same between the two grades. We assume an instantaneous change in the feed rates in Table 4-19 to the new values. We also change the set point for the H_2/C_2H_4 controller to the new value of 1.54.

Table 4-19. Specifications for the grade change in the parallel configuration.

	grade 1	grade 2
ethylene feed rate (kg/hr)	5,949	5,999
propylene feed rate (kg/hr)	81.7	0
overhead H_2/C_2H_4 molar ratio	0.56	1.54
catalyst feed rate (kg/hr)	0.175	0.386
cocatalyst feed rate (kg/hr)	0.658	0.800

Figure 4-24 shows the dynamic change in the H_2/C_2H_4 ratio in the reactor overhead. The controller initially increases the hydrogen feed rate to achieve the new set point. The rate at which the system reaches the new set point is mainly a function of the value for the
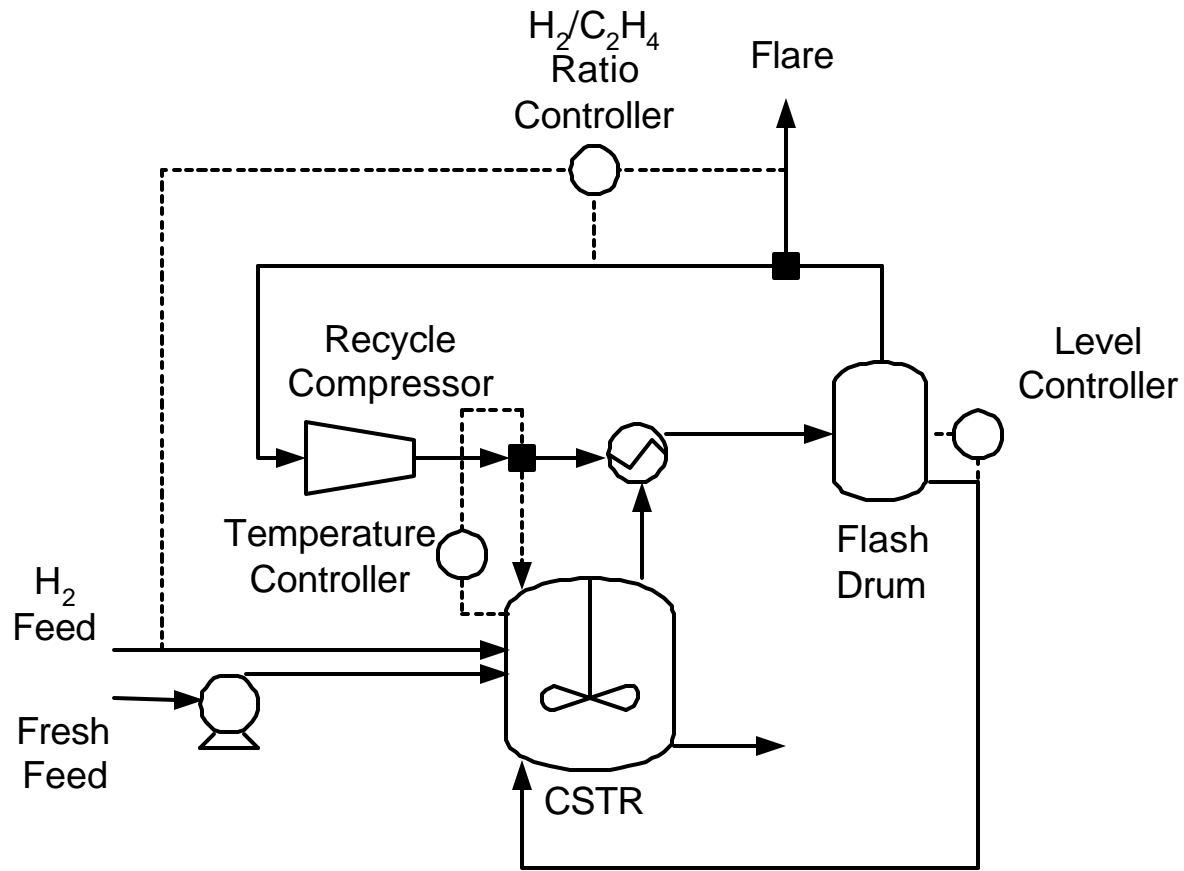
Figure 4-23. Simplified diagram of the control scheme for the parallel reactor configuration.
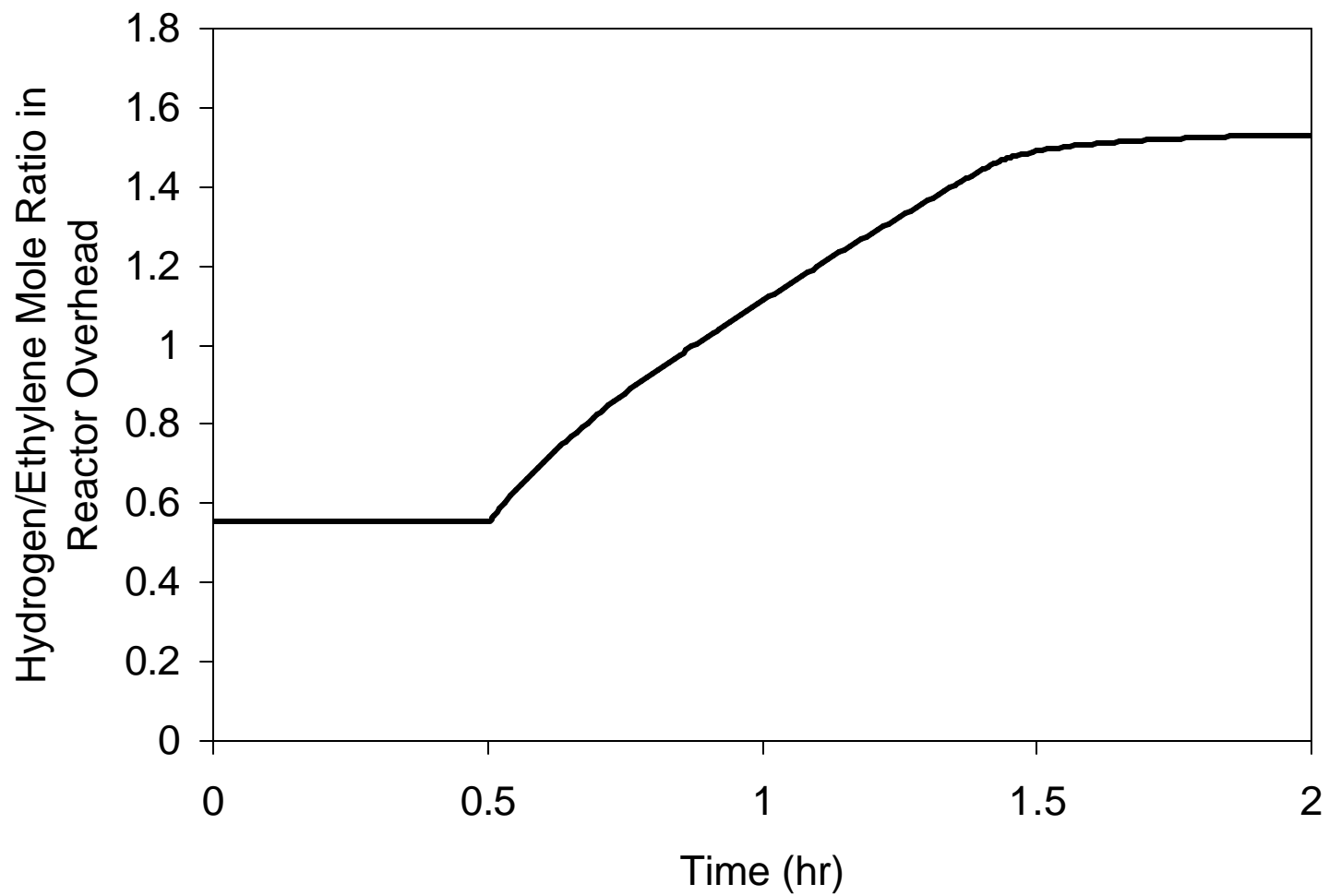
Figure 4-24. Change in the H_2/C_2H_4 overhead ratio during the grade change in the parallel configuration.

proportional gain used for the controller. Figure 4-25 illustrates the effect of the grade change on the production rate of HDPE. The sharp increase is due to the increase in the catalyst feed rate. The production rate then decreases to a value below that for the first grade, due to the large increase in hydrogen concentration, as a result of the higher set point for the H_2/C_2H_4 ratio in the overhead. The hydrogen inhibits the catalyst, effectively reducing the concentration of active sites in the reaction mixture. Figure 4-26 shows the effect of the grade change on the HDPE M_n. The increase in hydrogen and catalyst feed rates decreases the product M_n, due to chain transfer.

4.4.3 Process Retrofit

The purpose of this process retrofit is to increase the production rate of HDPE, while maintaining the same product quality (i.e., polymer attributes). An increase in production requires a corresponding increase in heat removal due to polymerization. If the overhead units are already operating close to capacity, we cannot significantly increase the rate of vapor removed from the reactor to meet its additional heat-transfer requirements. We propose the addition of a pump and a heat exchanger to enable the cooling and recycling of a portion of the slurry product stream to the reactor. We use a single reactor from the parallel configuration to model the retrofit.

Figure 4-27 shows a flowsheet for the retrofit. We increase the feed rates of the monomer, comonomer, and solvent species by the same relative ratios, in order to maintain the same relative concentrations of these components in the reaction mixture. This allows us to preserve the properties of the polymer product.

Table 4-20 summarizes the retrofit results, indicating that we can increase the production rate of HDPE by up to 20% if the overhead units can handle up to a 17% increase in the flow rate of recycle gas. As we increase the feed rate, the HDPE production rate increases, while the molecular weight undergoes an insignificant decrease. The recycle gas flow rate increases, as does the heat duty of the slurry cooler. The slurry recycle flow rate also increases.
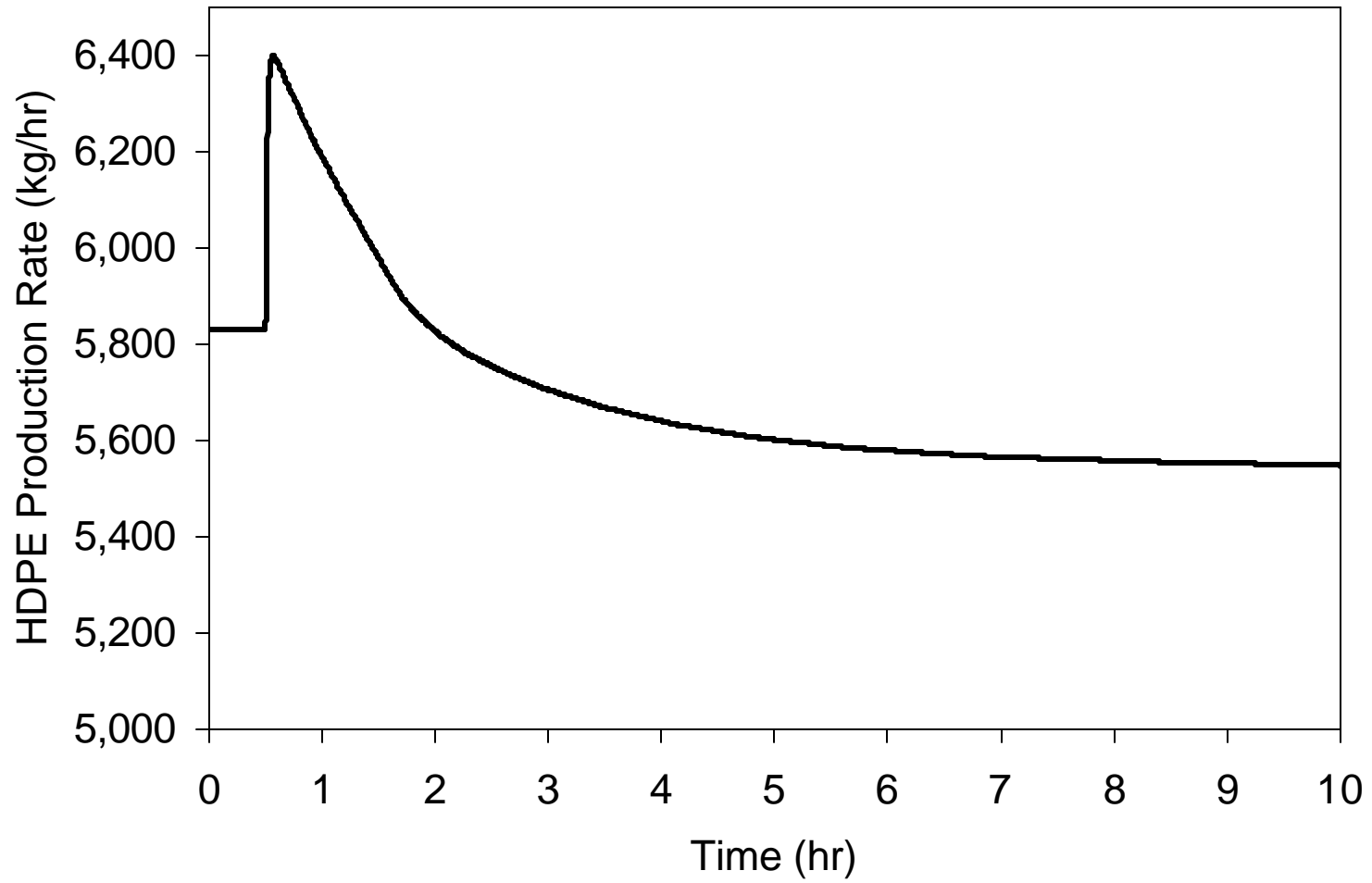
Figure 4-25. Effect of the grade change on the production rate of HDPE in the parallel configuration.
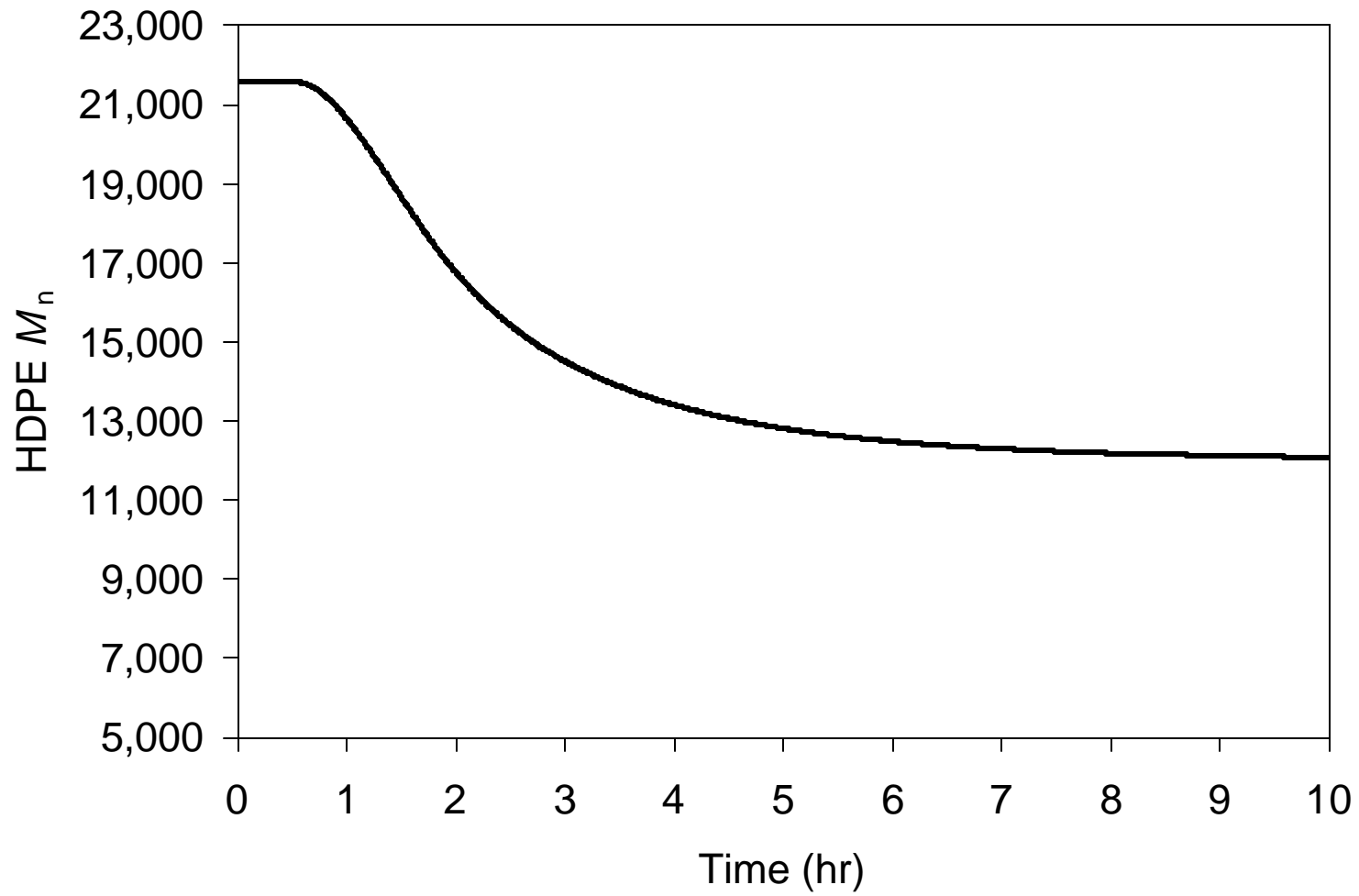
Figure 4-26. Effect of the grade change on the number-average molecular weight of HDPE.
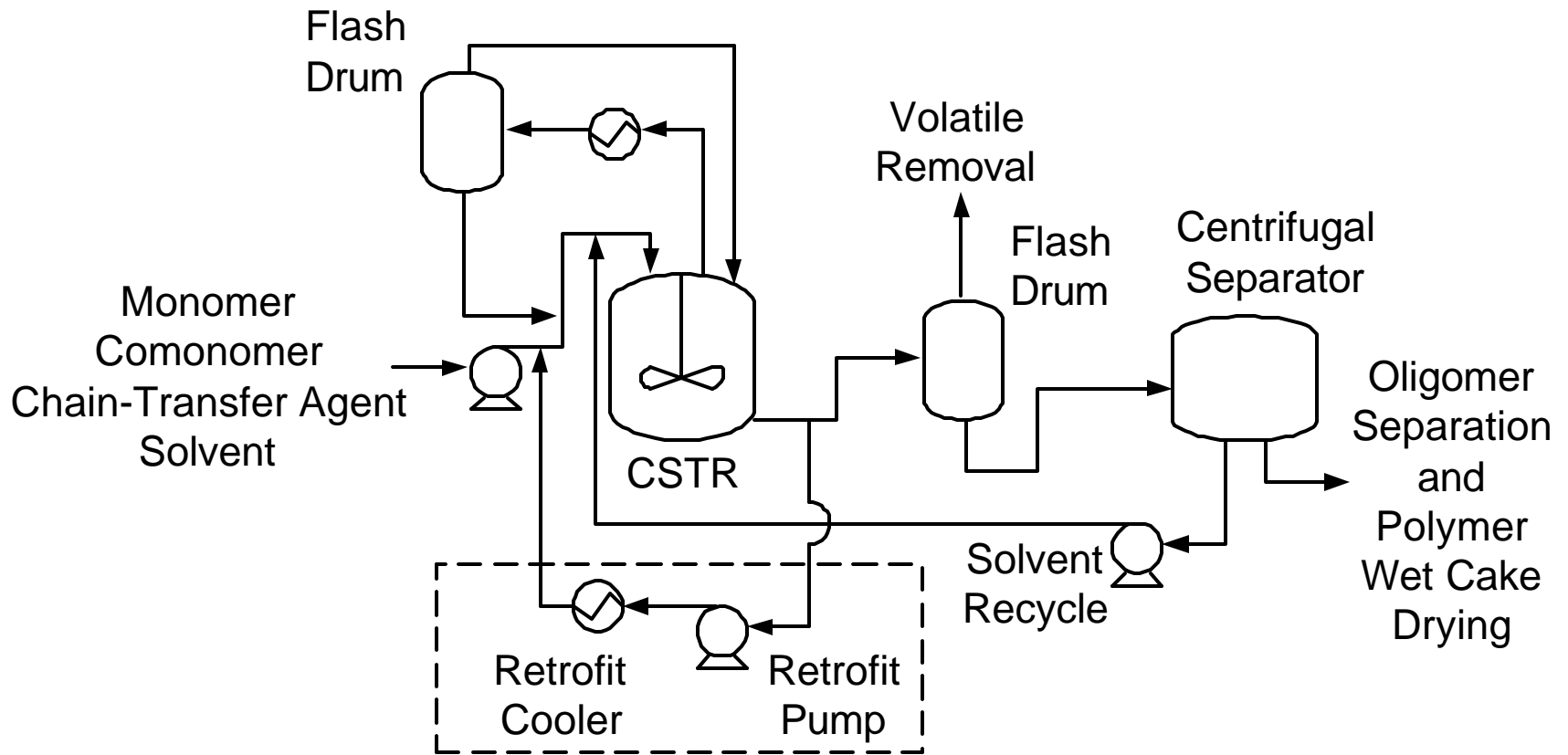
Figure 4-27. Flowsheet for a process retrofit applied to one reactor in the parallel configuration. Increasing the production rate increases the demands for heat removal, thereby necessitating the addition of another pump and cooler to recycle liquid to the reactor.

142

Table 4-20. Comparison of HDPE flow rate and attributes for varying increases in feed rates of raw material for the process retrofit.

% increase in ethylene, propylene, hexane, and mother-liquid feed rates	HDPE production rate (kg/hr)	M_n	PDI	recycle gas flow rate (kg/hr)	heat duty of slurry cooler (kcal/hr)	slurry recycle flow rate (kg/hr)
0 (original model)	5,834	21,148	4.58	24,809	-	-
10	6,426	21,093	4.58	25,622	562,108	23,244
15	6,717	21,037	4.58	28,804	807,327	33,382
20	7,017	20,990	4.58	28,982	1,075,000	44,459

4.5 Conclusions

We have developed both steady-state and dynamic models for a slurry HDPE process with two reactor configurations. We have validated the model using design and operating data from two large-scale commercial HDPE processes. The model uses a single set of kinetic and thermodynamic parameters to accurately predict the production rate, M_n, PDI, monomer conversion, and comonomer composition, as well as trends in these polymer properties with changes in key process variables, for both reactor configurations. We illustrate the utility of the dynamic model by simulating a grade change for the parallel reactor configuration.

The Sanchez-Lacombe EOS provides good prediction of the phase behavior of polymer mixtures. The Chao-Seader property method gives accurate description of the phase behavior of mixtures of light hydrocarbons.

A GPC deconvolution algorithm developed by Soares and Hamielec[4] and implemented by Polythink Inc.[21] accurately describes the polydisperse nature of the HDPE produced using a multiple site-type Ziegler-Natta catalyst. We describe a unimodal molecular weight distribution produced in a parallel reactor and a bimodal molecular weight

distribution produced in the first reactor of a series configuration by assuming that the site type producing the longest chains is insensitive to hydrogen concentration.

We propose a process retrofit that permits an increase in HDPE production rate of up to 20%, while maintaining the same product quality, provided that the overhead units can handle up to a 17% increase in capacity, based on simulation results.

Acknowledgments

Symbols

English Symbols

C_i	constant for ideal-gas heat capacity correlation ($i = 1,2$)
C_p^{ig}	ideal-gas heat capacity (kJ/kmol-K)
C_2H_4	ethylene
CAT_i	inactive catalyst
$CISFRAC_i$	fraction of catalyst-site type i that is inhibited
$CISFRAC_{ss}$	fraction of catalyst sites that are inhibited in the single-site model
COCAT	cocatalyst
CSTR	continuous stirred-tank reactor
D_n	inactive polymer chain containing n segments
$[D_n]$	concentration of inactive polymer chains containing n segments (mol/L)
EOS	equation of state
FC	flow controller
GPC	gel-permeation chromatography
H_2	hydrogen

HDPE	high-density polyethylene
$ICAT_i$	inhibited catalyst of site type i
k	rate constant (L/mol-s)
k_0	pre-exponential factor for the rate constant
$k_{act,i}$	rate constant for activation of catalyst-site type i
$k_{finh,i}$	rate constant for forward hydrogen inhibition of catalyst-site type i
k_{ij}	binary interaction parameter for Sanchez-Lacombe equation of state
$k_{ini,i}$	rate constant for chain initiation for catalyst-site type i
$k^j_{ini,i}$	rate constant for chain initiation of catalyst-site type i by monomer j
k_p	rate constant for chain propagation for the single-site model
$k_{p,i}$	rate constant for chain propagation for catalyst-site type i
$k^{jk}_{p,i}$	rate constant for chain propagation for monomer j adding to segment type k at catalyst-site type i
$k_{rinh,i}$	rate constant for reverse hydrogen inhibition of catalyst-site type i
$k_{th,i}$	rate constant for chain transfer to hydrogen for catalyst-site type i
$k^j_{th,i}$	rate constant for chain transfer to hydrogen for chain ending in segment type j on catalyst-site type i
$k_{tm,i}$	rate constant for chain transfer to monomer for catalyst-site type i
$k^{jk}_{tm,i}$	rate constant for chain transfer to monomer j for chain ending in segment type k on catalyst-site type i
LC	level controller
M	monomer species
m_i	mass fraction of polymer produced at catalyst-site type i
M_i	monomer species of type i
M_n	number-average molecular weight
M_w	weight-average molecular weight
MWD	molecular weight distribution
n	number of monomer segments in a polymer chain
n_{st}	number of catalyst-site types
P	pressure (bar)
$\bar{P}$	reduced pressure in the Sanchez-Lacombe equation of state

P^*	pressure scale factor in the Sanchez-Lacombe equation of state (bar)
$P_{0,i}$	activated catalyst-site of type i
$P_{1,i}$	initiated catalyst-site of type i
PDI	polydispersity index, M_w/M_n
P_n	live polymer chain containing n segments
$[P_n]$	concentration of live polymer chains containing n segments (mol/L)
$P_{n,i}$	live polymer chain containing n segments, attached to catalyst-site type i
$P^j_{n,i}$	live polymer chain containing n segments, ending in segment type j, attached to catalyst-site type i
r	molecular parameter in the Sanchez-Lacombe equation of state
T	temperature (°C)
$\bar{T}$	reduced temperature in the Sanchez-Lacombe equation of state
T^*	temperature scale factor in the Sanchez-Lacombe equation of state (K)
TC	temperature controller
VLE	vapor-liquid equilibrium
VLLE	vapor-liquid-liquid equilibrium
$w_i(n)$	weight fraction of chains of length n produced at catalyst-site type i
$W(n)$	total weight fraction of chains containing n segments
X	stoichiometric coefficient
ΔH	molar enthalpy change

Greek Symbols

$\mathbf{h}_{ij}$	binary interaction parameter for Sanchez-Lacombe equation of state
$\mathbf{l}_i$	i^{th} moment for bulk (live and dead) polymer chains
$\mathbf{m}_i$	i^{th} moment for live polymer chains
$\mathbf{n}_i^{(0)}$	parameter in Chao-Seader fugacity-coefficient model
$\mathbf{n}_i^{(1)}$	parameter in Chao-Seader fugacity-coefficient model
$\mathbf{r}$	density (kg/m^3)
$\bar{\mathbf{r}}$	reduced density in the Sanchez-Lacombe equation of state
$\mathbf{r}^*$	density scale factor in the Sanchez-Lacombe equation of state (kg/m^3)

t_i adjustable parameter for chain-length distribution function

f_i^{liq} liquid fugacity coefficient of species i

w_i acentric factor for species i

Literature Cited

(1) Scheirs, J.; Evens, G. Polyethylene (High Density Preparation). in *Polymeric Materials Encyclopedia*; Salamone, J. C., Ed.; CRC Press: Boca Raton, 1996; 5965.

(2) Xie, T.; McAuley, K. B.; Hsu, J. C. C.; Bacon, D. W. Gas Phase Ethylene Polymerization: Production Processes, Polymer Properties, and Reactor Modeling. *Ind. Eng. Chem. Res.* **1994**, *33*, 449.

(3) Peacock, A. J. *Handbook of Polyethylene: Structures, Properties, and Applications*; Marcel Dekker: New York, 2000.

(4) Soares, J. B. P.; Hamielec, A. E. Deconvolution of Chain-Length Distributions of Linear Polymers Made by Multiple-Site-Type Catalysts. *Polymer* **1995**, *36*, 2257.

(5) Bokis, C. P.; Orbey, H.; Chen, C.-C. Properly Model Polymer Processes. *Chem. Eng. Prog.* **1999**, *95*, 39.

(6) Sanchez, I. C.; Lacombe, R. H. An Elementary Molecular Theory of Classical Fluids. Pure Fluids. *J. Phys. Chem.* **1976**, *80*, 2352.

(7) Lacombe, R. H.; Sanchez, I. C. Statistical Thermodynamics of Fluid Mixtures. *J. Phys. Chem.* **1976**, *80*, 2568.

(8) Sanchez, I. C.; Lacombe, R. H. Statistical Thermodynamics of Polymer Solutions. *Macromolecules* **1978**, *11*, 1145.

(9) Chao, K. C.; Seader, J. D. A General Correlation of Vapor-Liquid Equilibria in Hydrocarbon Mixtures. *AIChE J.* **1961**, *7*, 598.

(10) Reid, R. C.; Prausnitz, J. M.; Poling, B. E. *The Properties of Gases and Liquids*; McGraw-Hill: New York, 1987.

(11) Beaton, C. F.; Hewitt, G. F. *Physical Property Data for the Design Engineer*; Hemisphere Publishing Corp.: New York, 1989.

(12) Sychev, V. V.; Vasserman, A. A.; Golovsky, E. A.; Kozlov, A. D.; Spiridonov, G. A.; Tsymarny, V. A. *Thermodynamic Properties of Ethylene*; Hemisphere Publishing Corp.: Washington, 1987.

(13) Gaur, U.; Wunderlich, B. Heat Capacity and Other Thermodynamic Properties of Linear Macromolecules. II. Polyethylene. *J. Phys. Chem. Ref. Data* **1981**, *10*, 119.

(14) Knapp, H.; Döring, R.; Oellrich, L.; Plöcker, U.; Prausnitz, J. M. *Vapor-Liquid Equilibria for Mixtures of Low Boiling Substances, Chemistry Data Series*; DECHEMA: Frankfurt, 1982; VI.

(15) Leonard, J. Heats and Entropies of Polymerization, Ceiling Temperatures, Equilibrium Monomer Concentrations, and Polymerizability of Heterocyclic Compounds. In *Polymer Handbook*; Brandrup, J., Immergut, E. H., Grulke, E. A., Eds.; Wiley & Sons: New York, 1999; II/363.

(16) Arriola, D. J. Modeling of Addition Polymerization Systems. Ph.D. Dissertation, University of Wisconsin, Madison, WI, 1989.

(17) McAuley, K. B.; MacGregor, J. F.; Hamielec, A. E. A Kinetic Model for Industrial Gas-Phase Ethylene Copolymerization. *AIChE J.* **1990**, *36*, 837.

(18) Cansell, F.; Siove, A.; Fontanille, M. Ethylene-Propylene Copolymerization Initiated with Solubilized Ziegler-Natta Macromolecular Complexes. I. Determination of Kinetic Parameters. *J. Polym. Sci., Part A: Polym. Chem.* **1987**, *25*, 675.

(19) Kissin, Y.V. *Isospecific Polymerization of Olefins with Heterogeneous Ziegler-Natta Catalysts*; Springer-Verlag: New York, 1985.

(20) Nagel, E. J.; Kirillov, V. A.; Ray, W. H. Prediction of Molecular Weight Distributions for High-Density Polyolefins. *Ind. Eng. Chem. Prod. Res. Dev*. **1980**, *19*, 372.

(21) Polythink Inc., 1005 Sydenham Rd., S.W., Calgary, Alberta, Canada T2T 0T3. http://www.polythink.com (accessed August 2002).

(22) Yan, R.; Xu, X.; Khare, J.; Liu, Y. A.; Chen, C.-C. Modeling of a Commercial Slurry HDPE Process Using Polymers Plus. *Proceedings of AspenWorld China 2000*, Beijing, July 2000; 79.

Chapter 5 Manuscript for the Gas-Phase Polymerization of Propylene Using a Ziegler-Natta Catalyst

Steady-State and Dynamic Modeling of Gas-Phase Polypropylene Processes Using Stirred-Bed Reactors

Neeraj P. Khare, Bruce Lucas, Kevin C. Seavey, and Y. A. Liu*

SINOPEC/AspenTech Center of Excellence in Process Systems Engineering

Department of Chemical Engineering

Virginia Polytechnic Institute and State University

Blacksburg, VA 24061

Ashuraj Sirohi, Sundaram Ramanathan, Simon Lingard, Yuhua Song,

and Chau-Chyun Chen

Aspen Technology, Inc.

10 Canal Park

Cambridge, MA 02141

*Phone: (540) 231-7800; Fax: (540) 231-5022; E-mail: design@vt.edu

To whom correspondence should be addressed.

Abstract

This paper presents the development of both steady-state and dynamic models for the continuous gas-phase synthesis of polypropylene using stirred-bed reactors. These include polymerization kinetics, phase equilibrium, residence time, catalyst characterization, and polymer properties. Model development involves fundamental chemical engineering principles and advanced software tools, Polymers Plus and Aspen Dynamics. We characterize a Ziegler-Natta catalyst by assuming the existence of multiple catalyst site types. The model contains a single set of kinetic and thermodynamic parameters that accurately predicts the polymer production rate, molecular weight, polydispersity index, and composition, for both homopolymer and impact copolymer product grades. We demonstrate the utility of the dynamic model by simulating a grade change.

Keywords: polypropylene; Ziegler-Natta; simulation; model; polymerization kinetics; deconvolution; gas-phase; stirred-bed

5.1 Introduction

5.1.1 Gas-Phase Processes Using Stirred-Bed Reactors

Gas-phase polymerization processes are widely used to produce polyolefins. They use either continuous-flow stirred-bed or fluidized-bed reactors. Unlike slurry and solution processes, there is no liquid phase in the reactors, only vapor and solids. This makes the gas-phase process simpler because there is no solvent or liquid monomer to separate from the polymer, purify, and recycle[1].

The first commercial gas-phase processes for polyolefin production appeared in the late 1960s[1]. Amoco developed the first stirred-bed gas-phase reactor for polypropylene manufacture in the 1970s[2-5]. The gas-phase process involves the feeding of liquid monomer into the reactor, which evaporates upon entering. The system involves

mechanical agitation, rather than fluidization. Companies that license polypropylene gas-phase processes include BP Amoco, Dow (Unipol), and Novolen Technology Holdings (Novolen)[6].

Figure 5-1 shows a simplified flowchart for the gas-phase production of polypropylene. Fresh monomer, catalyst and modifiers (chain-transfer agent, etc.) are fed to the reactor section. Traditionally, the resulting polymer powder stream then undergoes catalyst deactivation. However, most of the current-generation high-activity catalyst systems do not require this step. Additional modifiers are then added, depending on the intended use of the product. Finally, the polymer product is pelletized[6].
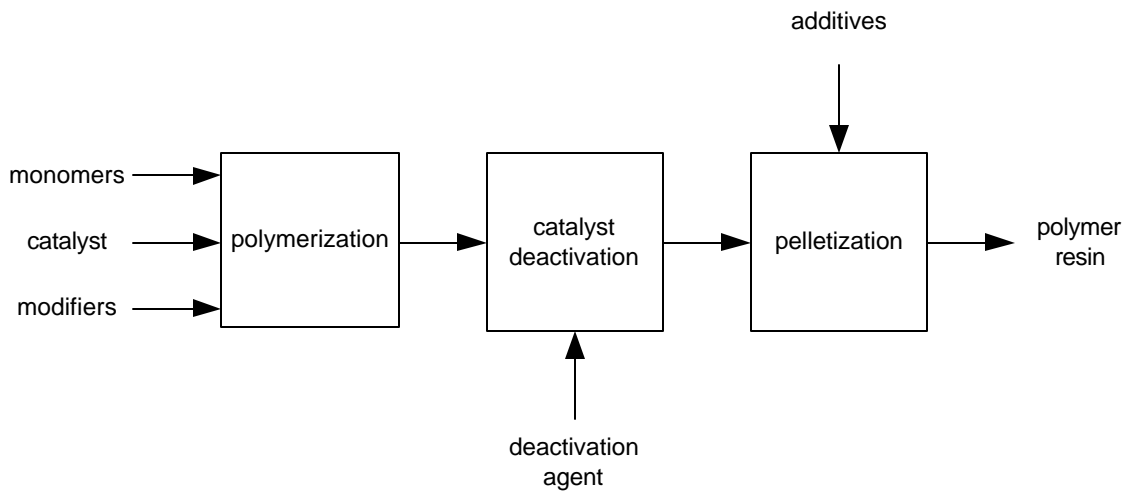
Figure 5-1. Simplified flowchart for the gas-phase polypropylene process[6].

The three general types of polypropylene produced in the gas-phase process are the homopolymer, random copolymer, and impact copolymer. The random copolymer contains small amounts of ethylene comonomer, and the impact copolymer is a mixture of homopolymer and copolymer that contains between 6 and 15 wt % ethylene comonomer[6]. Of these three types, we modeled the homopolymer and impact copolymer processes.

Figure 5-2 shows a simplified diagram of a typical gas-phase process using a stirred-bed reactor. The reactor temperature ranges from 57 to 77 °C and pressure ranges from 19 to 23 bar[7]. Reactor offgas is condensed, flashed, and returned to the reactor. The vapor recycle enters at various points along the bottom of the bed at a low enough flow rate to avoid bed fluidization[7]. The liquid recycle is sprayed at various locations along the top of the reactor[7]. The vaporizing liquid absorbs most of the exothermic heat of polymerization, allowing for 10 to 15% conversion per pass to maintain a constant reactor temperature[7]. The polypropylene process uses a titanium-based catalyst and an aluminum alkyl based cocatalyst[7]. Examples are titanium tetrachloride ($TiCl_4$) and triethyl aluminum [$Al(C_2H_5)_3$], respectively[8]. Fresh propylene enters the process at the overhead flash unit. Ethylene also enters here, for copolymerization grades[7]. Fresh hydrogen, used for molecular weight control, enters at the vapor recycle stream[7]. A small portion of the vapor recycle stream is vented to remove propane and ethane that accumulate in the recycle loop[7]. Tacticity control agents are commonly used to increase the isotactic content of the polypropylene[9].

The reactor is horizontal and cylindrical, and contains several zones that are sometimes separated by weirs[7]. The polymer exists as a powder, since the reactor temperature remains well below the polypropylene melting point of 157 °C[10]. Paddles connected to a rotating shaft mildly agitate the powder[7].
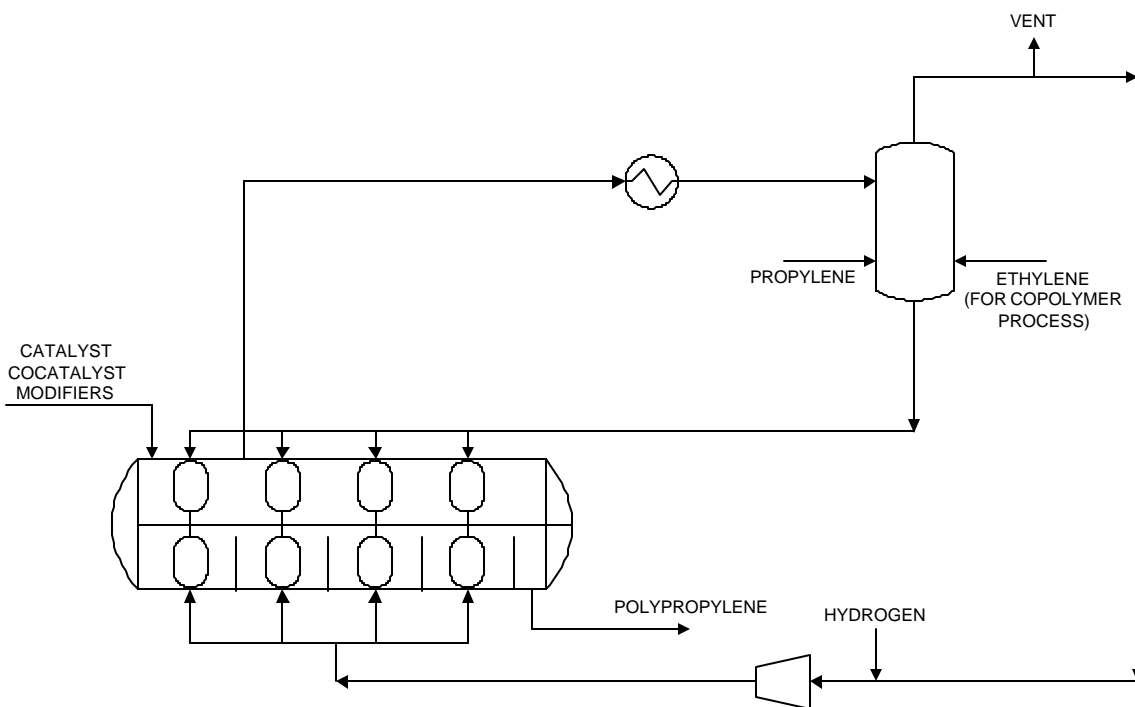
Figure 5-2. An example of a gas-phase polypropylene process using a stirred-bed reactor[7].

5.1.2 Modeled Process

We model a gas-phase polypropylene process using stirred-bed reactors based on publicly available process patents[2-5] and research articles[1,6,7,11]. We validate the model using data from a commercial plant for four product grades.

5.1.3 Modeling Technology

The model incorporates fundamental chemical engineering principles and advanced software tools for both steady-state and dynamic process simulation. Modeling considerations include mass and energy balances, physical properties, phase equilibrium, polymerization kinetics, and reactor modeling. We use Polymers Plus and Aspen Dynamics to simulate the polypropylene process. Polymers Plus is a layered product built on top of Aspen Plus for polymer process simulation. It applies process modeling technology to a wide variety of polymerization processes. Aspen Dynamics converts

steady-state process models to dynamic models that consider time-dependent effects and control schemes.

Polymers Plus includes the characterization of polymers and tracking of their structural properties throughout the flowsheet, phase equilibrium for polymer systems, polymerization kinetics, and reactor modeling. It uses a segment-based approach for computing the physical properties of polymer species. By considering a polymer chain as a series of segments, whose structures are well-defined, Polymers Plus can model the polymer properties that commonly vary with time and location (reactor 1 or reactor 2) in a synthesis process. This technique permits the modeling of properties such as molecular weight and copolymer composition, and can account for the fact that most polymer products contain an ensemble of molecules having a distribution of chain lengths. It facilitates the use of group-contribution methods for estimation of properties such as heat capacity, density, and melt- and glass-transition temperatures. We can also incorporate subroutines for user-defined correlations for polymer properties such as density and melt flow rate.

We export the steady-state model to Aspen Dynamics and incorporate appropriate control schemes to simulate a polymer grade change. The successful development and validation of the model illustrates the powerful modeling and predictive capabilities of this integrated software package.

5.1.4 Modeling Methodology

Proper consideration of the polymerization mechanism and kinetics is essential to any polymer synthesis model. However, a robust model must also accurately account for physical properties and phase equilibrium. Figure 5-3 gives a flowchart for the procedure we follow for developing and validating the polypropylene process model. We first choose physical property and thermodynamic models that permit accurate description of the density, enthalpy, phase-equilibrium behavior, and other properties for each species in

the system. Accurate density modeling permits proper consideration for equipment sizing and capacity. Enthalpy predictions allow for accurate heat-balance computation. Phase-equilibrium is important for predicting the monomer and hydrogen concentrations in the polymer phase and for the overhead condensers that partially liquefy the propylene mixture before returning to the reactor. Section 5.2 describes the perturbed-chain statistical associating fluid theory equation of state (PC-SAFT EOS), which we use for modeling these properties.

Next, we establish pure-component and binary-interaction parameters for the physical-property and thermodynamic models. There are two ways to accomplish this. The simplest way is to obtain values from the open literature. If we take this approach, we must make sure that the parameters were determined using experimental data that are close to the conditions in the modeled process. If this is not the case, or parameters are not available from the open literature, we must obtain values by regressing experimental data. We must then validate the property predictions by comparing them to experimental or plant data. Sections 5.2.3 and 5.2.4 give the parameter values and sources we used, as well as validation plots.

Section 5.3 discusses the modeling of the horizontal stirred-bed reactor. In Section 5.4, we establish the polymerization kinetics for the Ziegler-Natta-catalyzed system. We obtain a nominal set of kinetic parameters from the open literature.

We construct the process model by considering fundamental mass and energy balances for all of the relevant unit operations. In addition to the reactors, we include heat exchangers, flash vessels, pumps, and compressors for the recycle system.

After considering flow rates and compositions for fresh-feed streams, as well as conditions for unit operations, we use the process model to adjust kinetic parameters to match the plant data for process targets. These include polymer molecular weight, composition, production rate, and monomer conversions. We establish the kinetics for a Ziegler-Natta catalyst with multiple site types by deconvoluting gel-permeation

156

chromatography (GPC) data for the polymer. Since many of the reactions in the polymerization mechanism are coupled, we must use iterative techniques to obtain a final set of kinetic parameters that allow the model to match plant data. Finally, we validate the model by comparing predictions with data for four polymer grades produced in a commercial gas-phase polymerization plant.

STEP 1: Choose appropriate
models for physical properties
and phase equilibrium

STEP 2: Regress pure-component and mixture
data to determine unary and binary-interaction
parameters for property models, or obtain
established values from the open literature

STEP 3: Validate property predictions using
literature or plant data. Use plant data to adjust
binary-interaction parameters for phase-
equilibrium modeling, if necessary

STEP 4: Choose appropriate reaction
mechanism with nominal kinetic
parameters from the open literature

STEP 5: Build flowsheet
model using fundamental
principles for unit operations

STEP 6: Use iterative
methodology to adjust kinetic
parameters to match plant data

STEP 7: Incorporate control
scheme for dynamic modeling

STEP 8: Model application

Figure 5-3. Procedure for developing the polypropylene process model.

158

5.2 Physical Properties and Thermodynamic Modeling

5.2.1 Introduction

We use the PC-SAFT EOS to model the physical and thermodynamic properties for the polypropylene process. EOS are appropriate for systems at moderate to high pressures. Reactor pressures for the gas-phase polypropylene process range from 20 to 30 bar. Equations of state also provide unified property prediction across the vapor-liquid transition. The PC-SAFT model was designed specifically for polymer systems, and is suitable for the modeled process.

In the next section, we give more details about the PC-SAFT EOS. We then discuss pure-component and mixture properties, respectively, in Sections 5.2.3 and 5.2.4.

5.2.2 PC-SAFT EOS

Gross and Sadowski[12] recently developed the PC-SAFT EOS, which is an extension of the well known SAFT EOS[13-15]. As with other EOS based on perturbation theory, the PC-SAFT model expresses the residual Helmholtz energy as a sum of two contributions:

$$a^{\text{res}} = a^{\text{ref}} + a^{\text{pert}} \tag{1}$$

where a^{res} is the molar residual Helmholtz energy, and a^{ref} and a^{pert} are the reference and perturbation contributions, respectively. The reference term considers a fluid consisting of hard-sphere chains as a reference for the perturbation theory, and the perturbation term incorporates the attractive forces between the chains. The primary difference between the PC-SAFT and the SAFT models is in the perturbation term. The SAFT model uses hard spheres, not hard-sphere chains, as a reference fluid for the perturbation contribution. The use of hard-sphere chains allows the PC-SAFT EOS to account for the connectivity of segments that comprise the chains when considering the attractions between species, resulting in a more realistic description of the thermodynamic behavior of mixtures of chain-like molecules. The PC-SAFT EOS is valid for both small

molecules and chain-like polymers. Gross and Sadowski illustrate that the PC-SAFT predictions for VLE are superior to those of the SAFT model. It also performs better than the Peng-Robinson EOS for binary mixtures of small molecules[12].

The resulting equation of state expresses the compressibility as follows:

$$z = z^{id} + z^{ref} + z^{pert} \tag{2}$$

where z^{id} is the ideal contribution to compressibility, with a value of unity, and z^{ref} and z^{pert} are the reference and perturbation contributions that correspond to those described above.

The PC-SAFT EOS requires three pure-component parameters for each pure species. It has an optional binary interaction parameter that we can use to correlate phase-equilibrium behavior. We provide the parameters used in the model in the following sections.

5.2.3 Pure-Component Properties

Table 5-1 lists the components we include in the model. As described in section 5.1.3, we use a segment-based approach for the polymer species. We must therefore consider segment species corresponding to each type of monomer that comprises the polymer.

Table 5-1. Components Used in the Model.

species	function
titanium tetrachloride	catalyst
triethyl aluminum	cocatalyst
propylene	monomer
propylene segment	monomer segment
ethylene	comonomer
ethylene segment	comonomer segment
polypropylene	polymer
hydrogen	chain-transfer agent

tacticity control agent	tacticity control agent
ethane	impurity
propane	impurity

5.2.3.1 PC-SAFT Pure-Component Parameters

Table 5-2 lists the pure-component parameters for the PC-SAFT model, and the corresponding sources for parameters or experimental data. The parameter s is a characteristic diameter for the segments of a given species. The parameter e is a segment energy parameter. The parameter m serves as a characteristic chain length. For polymer species, we use r, the ratio of m and the number average molecular weight

$$r = \frac{m}{M_n} \tag{3}$$

in place of segment number m. This is more convenient because the polymer molecular weight is often unknown until after the polymer is produced.

Generally, we regress data along the saturation curve to obtain pure-component parameters for conventional species. For polymer species, which are essentially nonvolatile, we use data for liquid density[18] and liquid heat capacity[19]. Since ethylene is near the supercritical state ($T_c = 9.25$ °C, $P_c = 50.4$ bar)[20], we use data from in the supercritical region to obtain pure-component parameters.

Table 5-2. Pure-component parameters for the PC-SAFT EOS.

species	m (-)	s (Å)	e/k_B (K)	r (mol/g)	reference
hydrogen	8.29E-1	2.97	12.5	--	16
ethylene	1.56	3.43	179	--	17
ethane	1.61	3.52	191	--	12
propylene	1.96	3.54	207	--	12

propane	2.00	3.62	208	--	12
polypropylene	--	4.15	299	2.53E-2	18
polyethylene	--	4.022	252	2.63E-2	12
tacticity control agent	25.0	2.67	199	--	a
catalyst	25.0	2.67	199	--	a
cocatalyst	25.0	2.67	199	--	a

[a] We choose parameters for the tacticity control agent, catalyst, and cocatalyst so that they remain in the liquid phase.

5.2.3.2 Heat Capacity

We compute the heat capacity for each species by summing the ideal-gas and EOS contributions:

$$C_p(T,P) = C_p^{ig}(T) + \Delta C_p(T,P) \tag{4}$$

where $C_p^{ig}(T)$ is the ideal-gas term, evaluated at the system temperature, and $\Delta C_p(T,P)$ is the departure term, evaluated by the EOS at the system temperature and pressure. Since we use an ideal-gas as a reference state for all species, we consider a hypothetical ideal-gas heat capacity for the nonvolatile species, such as polymer and catalyst. We compute the ideal-gas heat capacity using a polynomial:

$$C_p^{ig}(T) = A + BT + CT^2 + DT^3 \tag{5}$$

where A, B, C, and D are adjustable parameters. Table 5-3 lists the parameters we use for each species. We neglect the heat capacity of the catalyst and cocatalyst, since they are only present in trace amounts.

Table 5-3. Parameters for the ideal-gas heat-capacity model.

species	A	B	C	D	reference
	(J/kmol-K)	(J/kmol-K^2)	(J/kmol-K^3)	(J/kmol-K^4)	
hydrogen	2.71E4	9.27	-1.38E-2	7.65E-6	21
ethylene	3.81E3	156	-8.34E-2	1.76E-5	21
ethane	5.41E3	178	-6.93E-2	8.71E-6	21

propylene	3.71E3	235	-1.16E-1	2.21E-5	21
propane	-4.22E3	306	-1.59E-1	3.22E-5	21
polypropylene	4.30E4	153	2.39E-5	0	19
polyethylene	3.51E4	68.2	0	0	22

Figure 5-4 compares our model predictions with experimental data for heat capacity of propylene and ethylene. The fit is excellent.

Figure 5-4. Comparing experimental data with PC-SAFT predictions for heat capacity of superheated propylene and ethylene vapor. Data are from Beaton and Hewitt[23].

5.2.3.3 Density

Accurate density predictions are important for modeling equipment capacity and throughput. Incorrect densities can lead to inaccurate reactor residence times, which

affect most polymer properties. The PC-SAFT EOS gives an excellent description of the vapor and liquid densities of the species in the PP process.

Figure 5-5 shows the saturated liquid density for propylene. Figure 5-6 shows the superheated vapor density for propylene and ethylene. We include comparisons for the ideal gas law to illustrate that, at the reactor conditions, the ideal gas law is not capable of accurately describing the density of superheated propylene. The density error can be more than 25%, thus negatively impacting the residence-time calculations. Figure 5-7 shows the density for polypropylene. The PC-SAFT EOS represents the densities for each species well.
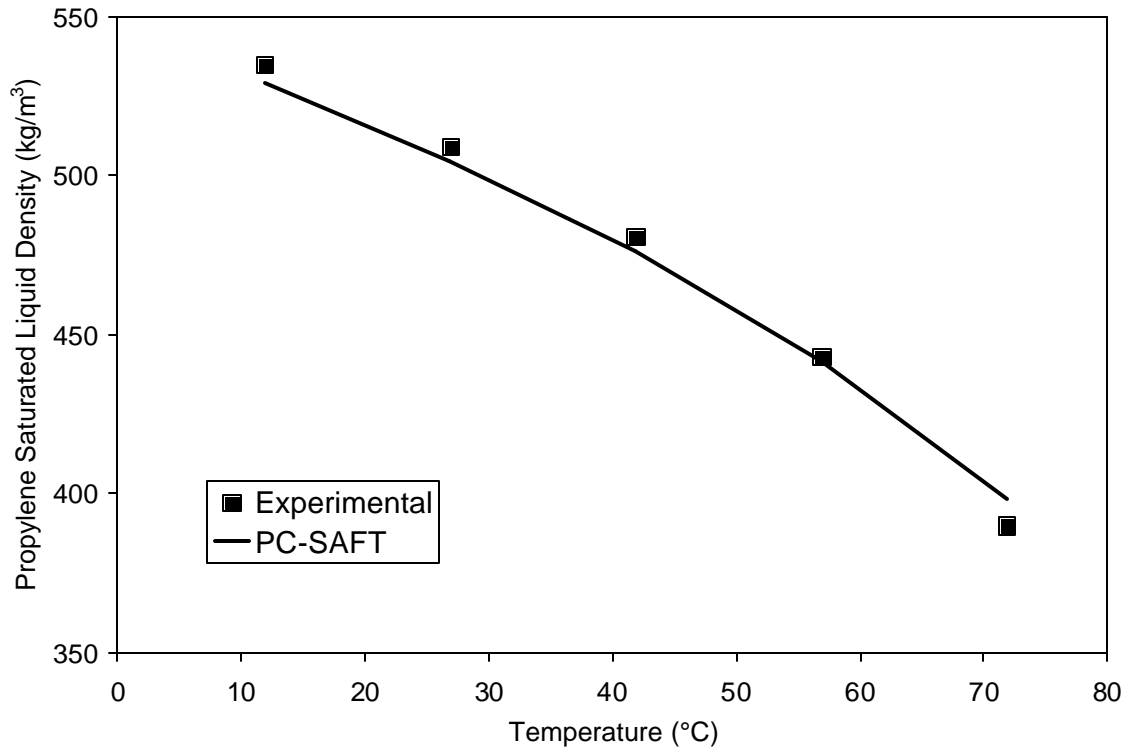
Figure 5-5. Comparing experimental data with PC-SAFT predictions for saturated liquid density of propylene. Data are from Beaton and Hewitt[23].
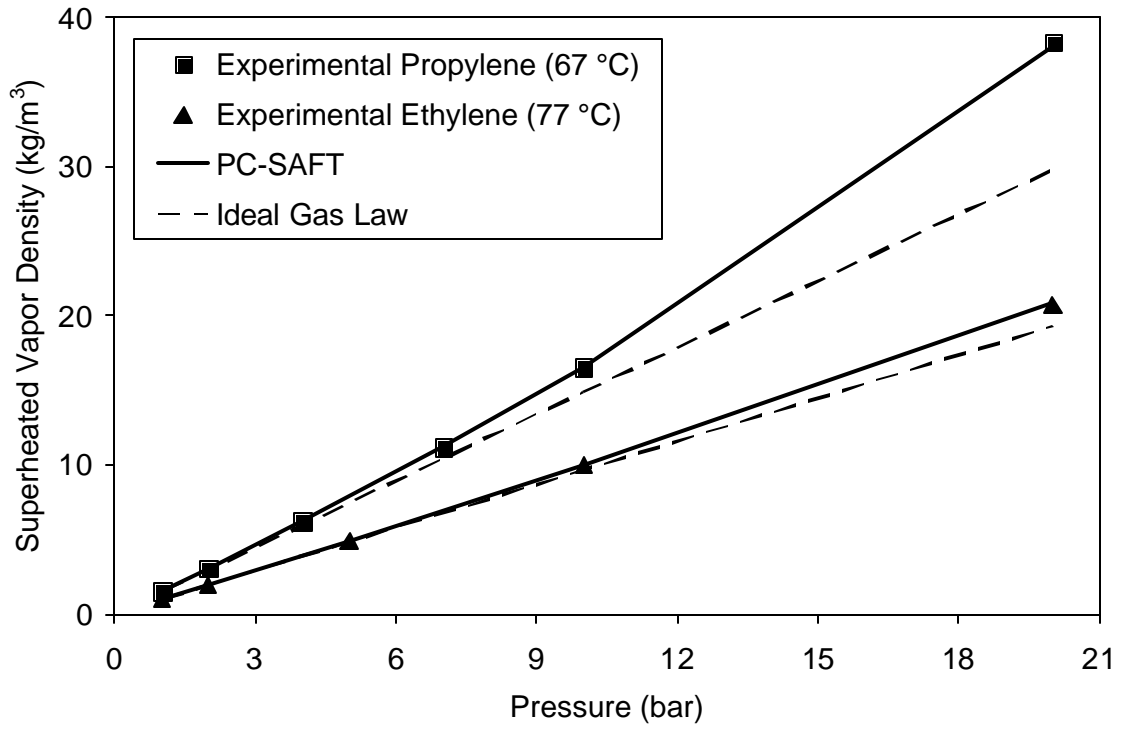
Figure 5-6. Comparing experimental data with PC-SAFT predictions for superheated vapor density of propylene and ethylene. The ideal gas law is unable to describe the propylene density at reactor conditions. Data are from Beaton and Hewitt[23].
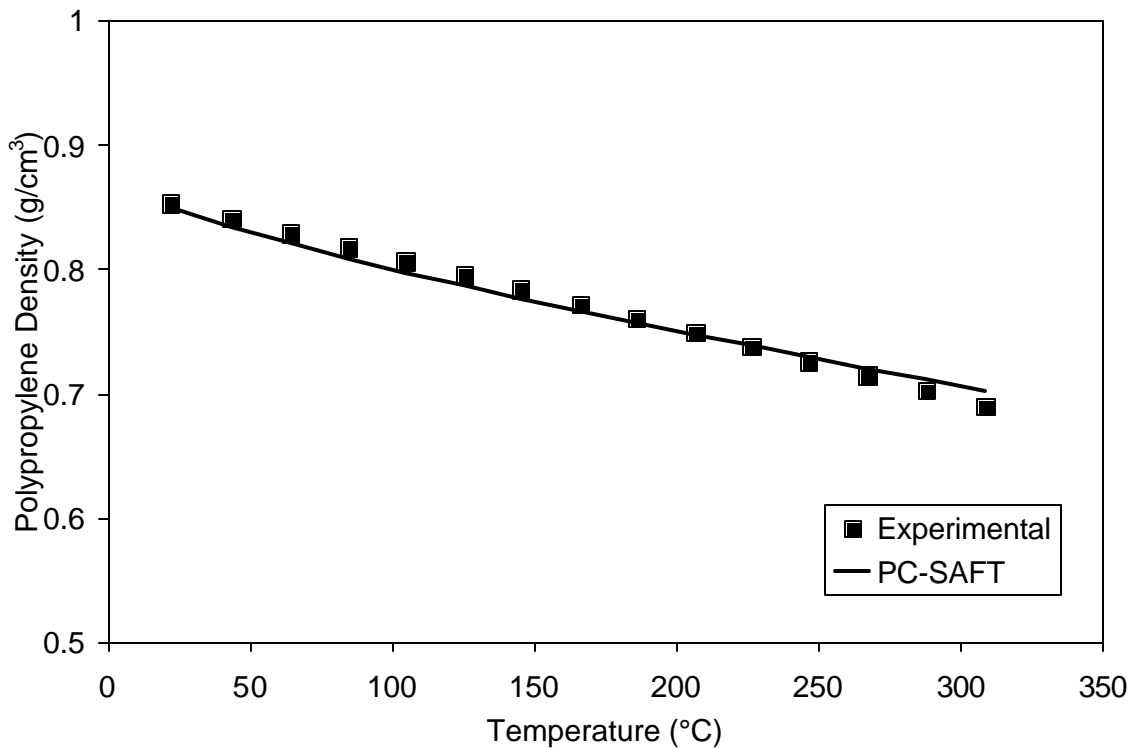
Figure 5-7. Comparing experimental data with PC-SAFT predictions for polypropylene density. Data are from Zoller[18].

5.2.3.4 Vapor Pressure

An accurate prediction of the vapor pressure is important for the overhead flash vessel. The amount of liquid propylene that recycles to the reactor dictates the conversion per pass, since the vaporization of the propylene absorbs most of the heat of polymerization. Figure 5-8 shows the vapor pressure for propylene. The PC-SAFT EOS prediction agrees well with experimental data.
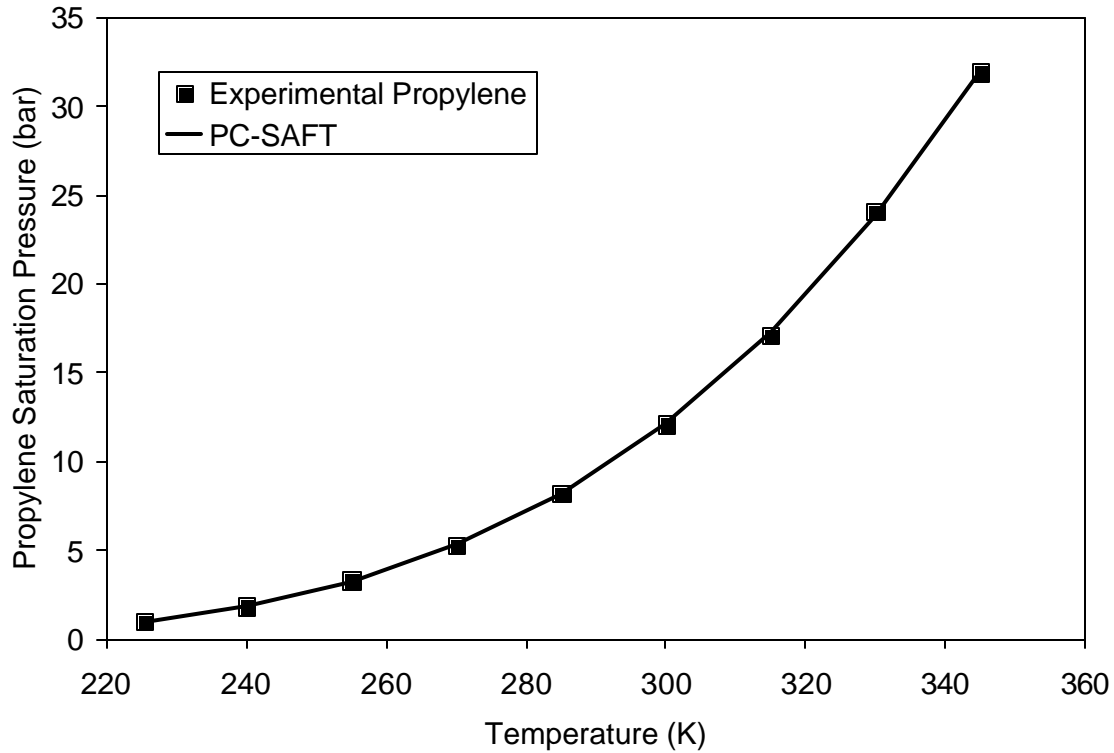
Figure 5-8. Comparing experimental data with PC-SAFT predictions for propylene vapor pressure. Data are from Beaton and Hewitt[23].

5.2.3.5 Heat of Vaporization

The reaction mixture remains at a constant temperature due to the evaporation of the liquid propylene mixture fed to the reactor. We require accurate modeling for the heat of vaporization for the major components for accurate heat balance. We compute the heat of vaporization by taking the difference between calculated values for the pure-component enthalpy of vapor and liquid, at a given temperature and pressure:

$$\Delta H_i^{\mathrm{vap}}(T, P) = H_i^{\mathrm{v}}(T, P) - H_i^{1}(T, P) \tag{6}$$

Figure 5-9 shows the heat of vaporization for propylene and ethylene. The PC-SAFT EOS accurately predicts the experimental values.
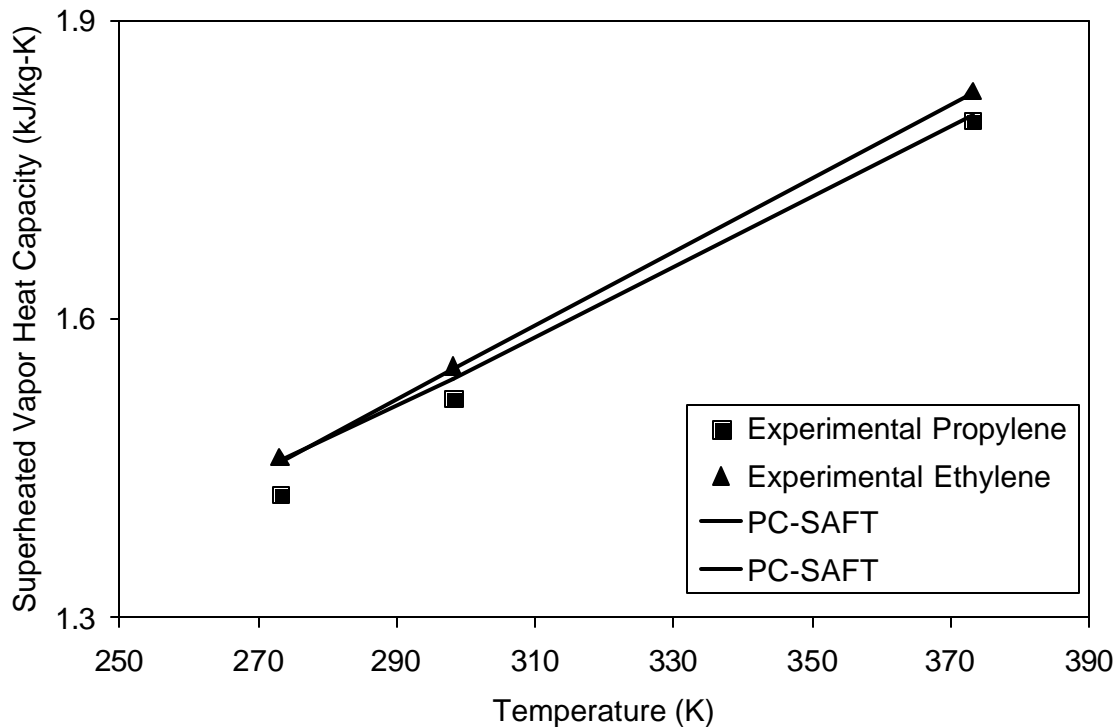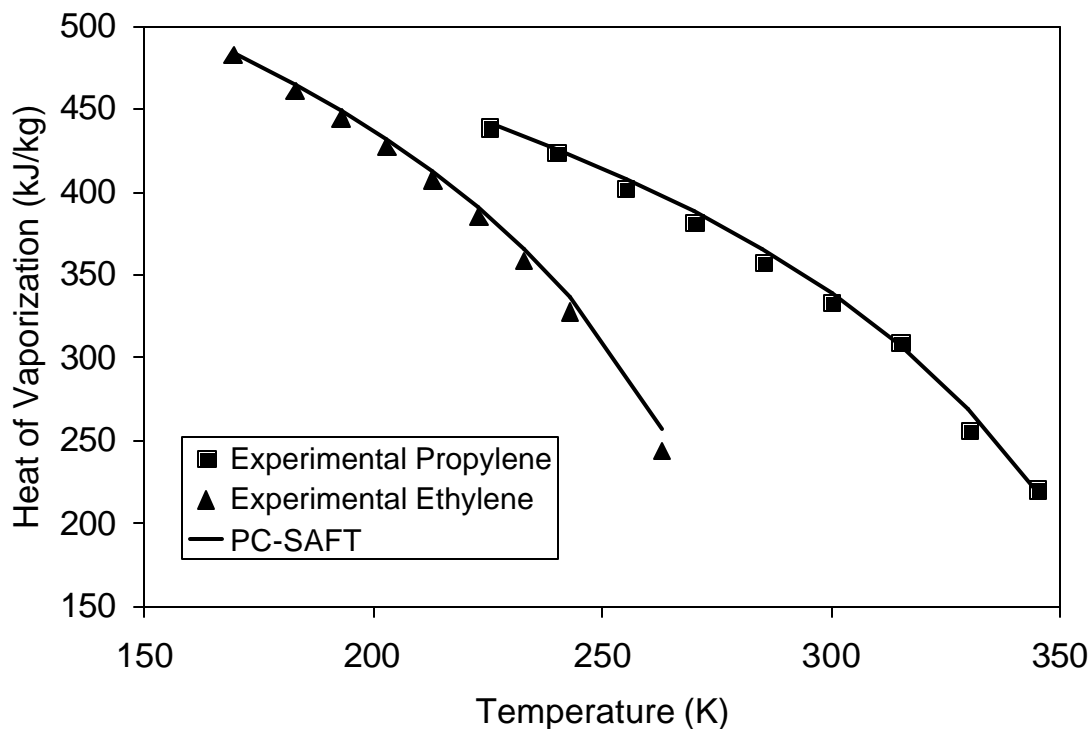
Figure 5-9. Comparing experimental data with PC-SAFT predictions for the heat of vaporization for propylene and ethylene. Data are from Beaton and Hewitt[23].

5.2.4 Mixture Properties

VLE predictions are important in the overhead condensers for recycle to the reactors. Inaccurate solubility predictions can cause trace components, such as hydrogen, to either build up or disappear from the recycle loop. In general, we initially do not use binary-interaction parameters for the PC-SAFT EOS. Data from the open literature tends to be too scarce to yield accurate values. If necessary, we can use plant data to regress binary interaction parameters between key species.

Figures 5-10 and 5-11 show the solubilities of ethylene and hydrogen in propylene, respectively. The PC-SAFT EOS performs well in both cases.
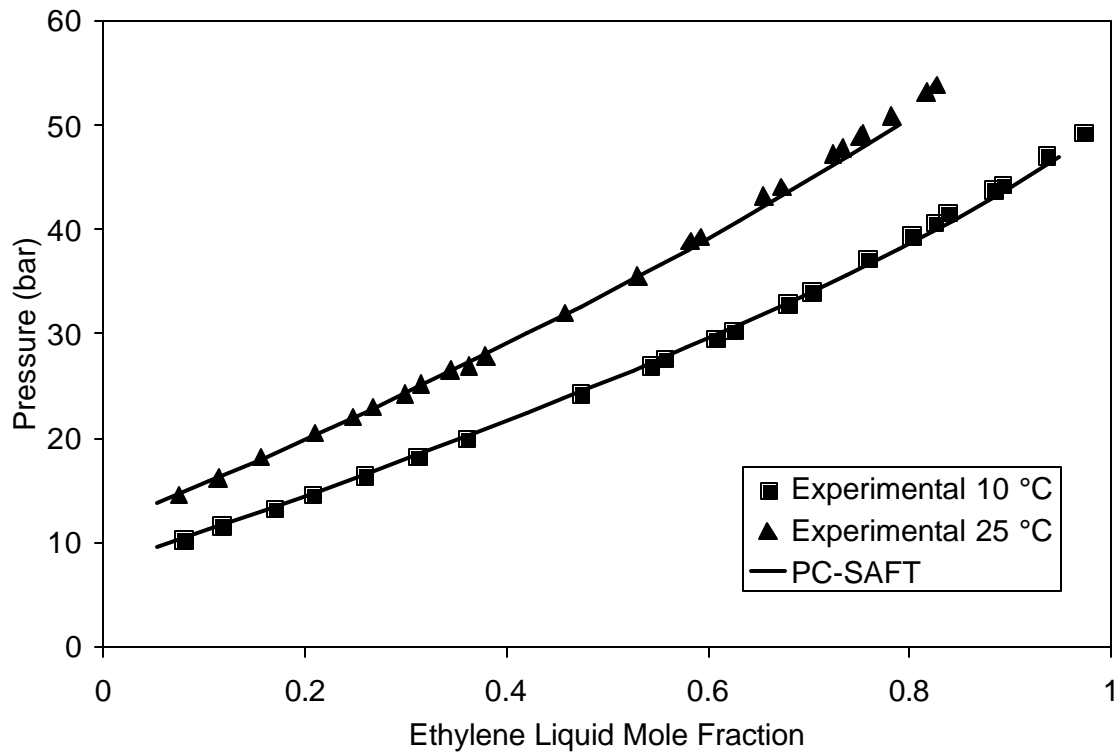
Figure 5-10. Comparing experimental data with PC-SAFT predictions for the solubility of ethylene in propylene. Data are from Ohgaki et al.[24]
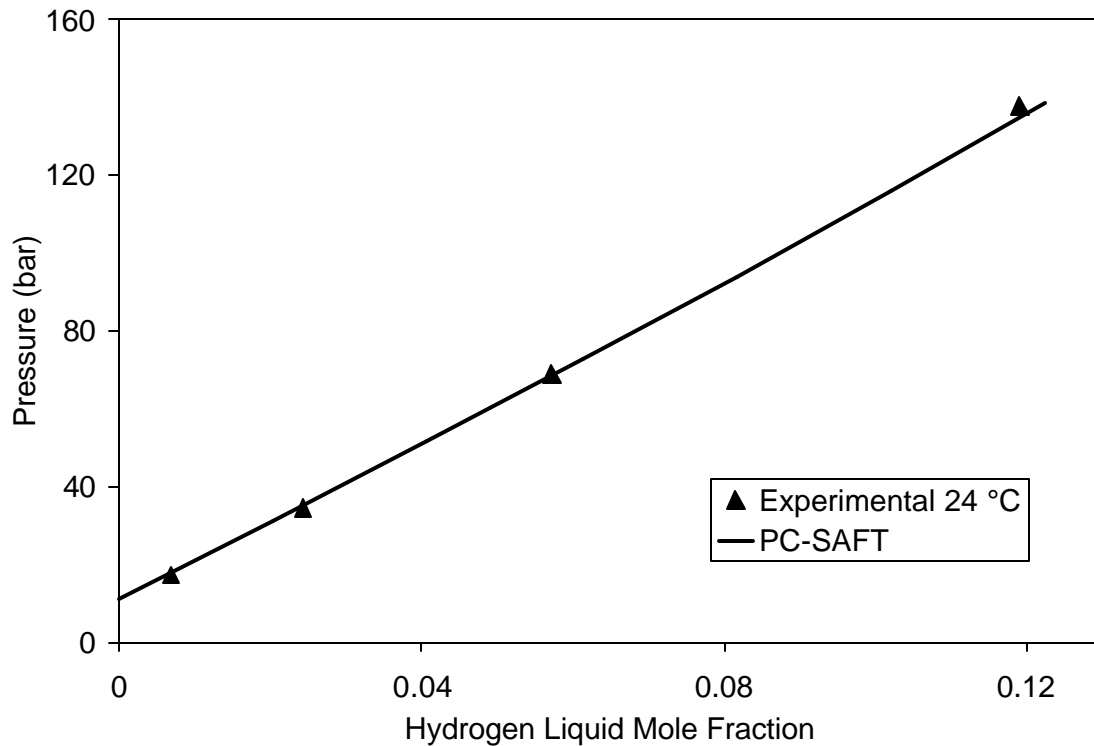
Figure 5-11. Comparing experimental data with PC-SAFT predictions for the solubility of hydrogen in propylene. Data are from Williams and Katz[25].

5.2.5 Polymer Properties

5.2.5.1 Heat of Polymerization

We compute the heat of polymerization by considering the difference between the enthalpies of gaseous propylene and solid polymer (propylene segment) at the same conditions[26]:

$$C_3H_{6(g)} \rightarrow \frac{1}{n}\left(C_3H_6\right)_{n(s)} \tag{7}$$

where *n* is the number of propylene segments in the polymer. Figure 5-12 illustrates the method we use to compute the heat of polymerization. We use the equation of state to compute each transition along the path.

ideal-gas monomer ———————— ideal-gas polymer

gas monomer – – – – – – → solid polymer
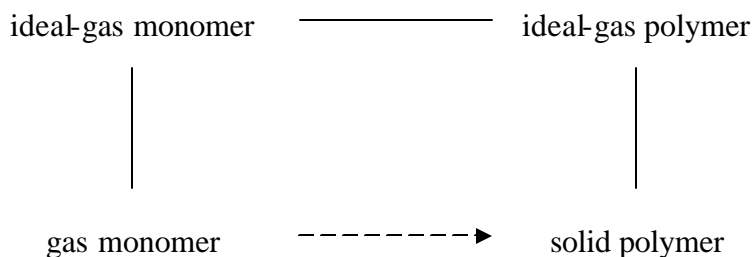
Figure 5-12. Method for computing the heat of propylene polymerization for the equation-of-state approach[26].

Table 5-4 compares PC-SAFT predictions with an experimental value for the heat of polymerization ΔH_f of -24.84 kcal/mol at 25 °C[26]. The computed values compare favorably with the literature value.

Table 5-4. Comparing PC-SAFT predictions for the heat of propylene polymerization with an experimental value of 24.84 kcal/mol at 25 °C[26].

T (°C)	P (bar)	$H_{propylene}$ (kcal/mol)	$H_{polypropylene}$ (kcal/mol)	ΔH_f (kcal/mol)
55	1.9	5.15	-20.05	-25.20
65	1.9	5.32	-19.77	-25.09
75	1.9	5.49	-19.49	-24.98
55	2.3	5.14	-20.05	-25.19
65	2.3	5.31	-19.77	-25.08
75	2.3	5.49	-19.49	-24.98

5.2.5.2 Molecular Weight from Method of Moments

We use the method of moments (population balance) to track the leading moments of the molecular weight distribution of the polymer. The moments are sums of the

concentrations of polymer species weighted by chain length. The moment expression for live polymer chains is

$$m_i = \sum_{n=1}^{\infty} n^i [P_n]$$ (8)

where m_i is the ith moment for live (growing) chains and $[P_n]$ is the concentration of polymer chains containing n segments. The expression for bulk (live plus dead) chains is

$$l_i = \sum_{n=1}^{\infty} n^i ([P_n] + [D_n])$$ (9)

where l_i is the ith moment for the all polymer chains and $[D_n]$ is the concentration of dead (inactive) polymer chains. Upon summing the rate equations over all n, they become functions of these moments, yielding a small number of closed expressions.

The zeroth, first, and second moments are sufficient for the computation of common molecular-weight properties of polypropylene. These include the number-average molecular weight (M_n), weight-average molecular weight (M_w), and the polydispersity index (PDI):

$$M_n = \frac{l_1}{l_0}$$ (10)

$$M_w = \frac{l_2}{l_1}$$ (11)

$$PDI = \frac{M_w}{M_n} = \frac{l_2 l_0}{l_1^2}$$ (12)

5.3 Reactor Modeling

5.3.1 Using CSTRs in Series

During steady-state operation, the polymer level remains constant along the reactor length[7]. The paddles along the reactor only mildly agitate the polymer and the solids are

not fluidized[7]. We can model this physical situation using several continuous stirred-tank reactors (CSTRs) configured in series. Experimental studies on the residence-time distribution (RTD) for polymer produced in horizontal stirred-bed reactors suggest that the polymer RTD is equivalent to that produced by three to five CSTRs[7]. Figure 5-13 compares the actual reactor to this modeling assumption. In our model, we use four CSTRs to represent the stirred-bed reactor. This approach has been used by other modelers as well[11]. Each CSTR receives liquid and vapor recycled from the overhead condenser, which includes fresh monomer and hydrogen. Only the first CSTR receives fresh catalyst and cocatalyst. The temperature and pressure are the same for all zones.

The polymer phase essentially undergoes plug-flow conditions along the reactor length. The concept of residence time is significantly different between this situation and that for multiple CSTRs in series. Furthermore, a residence-time calculation requires knowledge of the volumetric holdup in the reactor. This cannot be measured very accurately because the paddles are always agitating the polymer and there is a void fraction associated with the solid phase. We therefore do not use residence time as a simulation target in the model, and use reactor mass holdup instead. In the simulation, we constrain the CSTRs to the same polymer mass, in order to maintain the same level along the bed length. This results in monotonically decreasing residence times for the four CSTRs of a given stirred-bed reactor, which conforms to reported experimental results[7].

ACTUAL REACTOR

MODELING ASSUMPTION
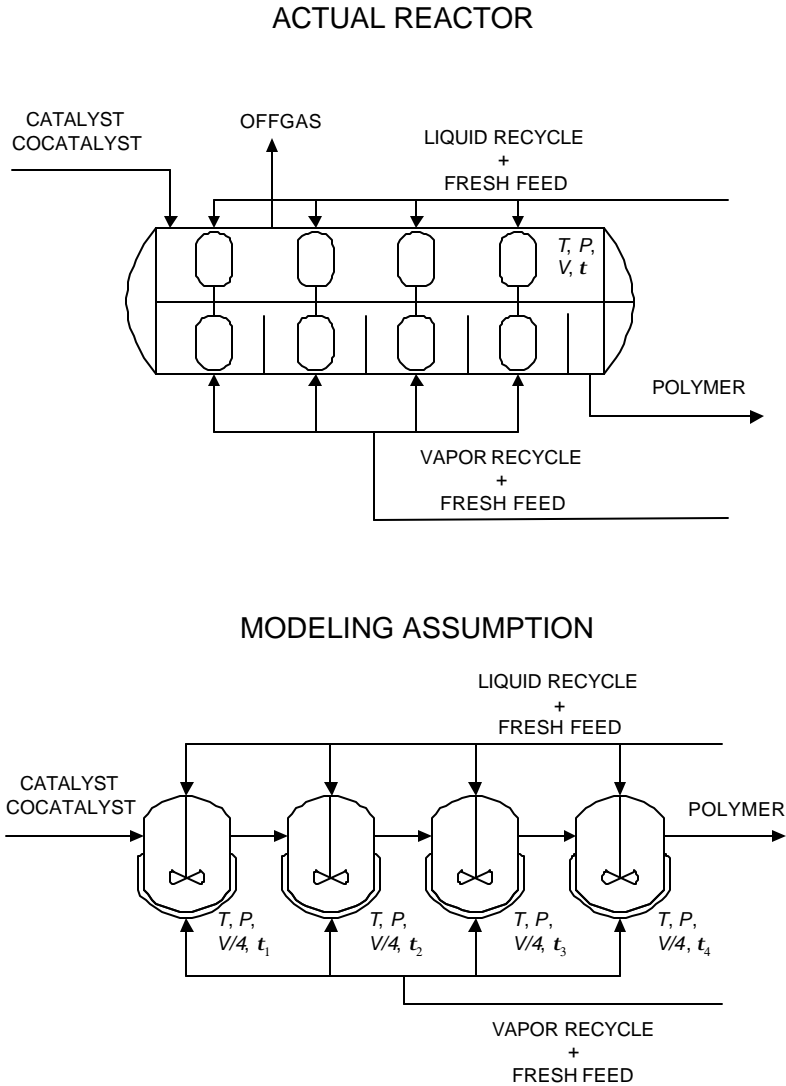
Figure 5-13. Comparing the actual reactor with the modeling assumption of four CSTRs in series.

5.3.2 Phase Equilibrium

The reaction mixture in the gas-phase process contains only solid and vapor. The liquid recycle essentially vaporizes instantly upon introduction into the reactor. The reactor temperature is well below the polymer melting point. We treat the solid polymer as a pseudo-liquid in the VLE calculations. As shown in Figure 5-7, this approach does not diminish the accuracy of the predictions for polymer density.

174

5.4 Polymerization Kinetics

5.4.1 Introduction

Many studies have been completed about the kinetics of olefin polymerization using Ziegler-Natta catalysts[27-33]. These catalysts tend to produce polymers with wide molecular-weight distributions (MWD). An accepted theory is that the catalyst contains several site types, each with its own relative reactivity[33]. We assume that each site type produces polymer with a most probable MWD. The resulting composite polymer produced by all of the site types together has a broad MWD.

We develop a kinetic model for a Ziegler-Natta catalyst containing multiple site types in order to describe the polymer production rate, molecular weight and its distribution, and copolymer composition. Sections 5.4.2 and 5.4.3 give the homo- and copolymerization kinetic schemes. Section 5.4.4 describes the process used to determine kinetic parameters for the model.

5.4.2 Homopolymerization Kinetic Scheme

We use a subset of the Ziegler-Natta reactions described in references 27-33. Table 5-5 lists the homopolymerization reactions. These reactions allow the model to describe the polymer properties for each grade. We describe these reactions next.

Table 5-5. Reaction subset used for the homopolymerization kinetics.

reaction	description
1	catalyst site activation
2	chain initiation
3	chain propagation
4	chain transfer
5	catalyst site deactivation

5.4.2.1 Catalyst Activation

For a typical Ziegler-Natta catalyst, a cocatalyst, such as triethyl aluminum[8], is typically used to activate the sites on a titanium catalyst

$$CAT_i + COCAT \xrightarrow{k_{act,i}} P_{0,i} \qquad (13)$$

where $k_{act,i}$ is the rate constant for catalyst activation of site type i by cocatalyst. Active sites undergo initiation and subsequent propagation by monomer to form the polymer chains. Since Ziegler-Natta catalysts tend to activate quickly, we use a relatively high rate constant for catalyst activation. We can also use activity profiles from semibatch reactor experiments to determine a value for the rate constant.

Hydrogen is known to enhance catalyst activity in gas-phase polypropylene processes[33]. The reaction is

$$CAT_i + H_2 \xrightarrow{k_{acth,i}} P_{0,i} \qquad (14)$$

where $k_{acth,i}$ is the rate constant for activation of catalyst site type i.

The model contains a "max sites" parameter representing the amount of catalyst sites per unit mass of catalyst. Parameter values usually range from 1.0E-5 to 1.0E-3 mol of sites per gram of catalyst (inverse of catalyst molecular weight). The utility of the max sites parameter is that it proportionally scales the rates of the reactions involving catalyst sites (propagation, chain transfer, etc.), allowing us to adjust the production rate without affecting the molecular weight or copolymer composition.

5.4.2.2 Chain Initiation

Monomer (M) can initiate chain growth by reacting with an active site

$$P_{0,i} + M \xrightarrow{k_{ini,i}} P_{1,i} \qquad (15)$$

where $k_{ini,i}$ is the rate constant for chain initiation at site type i and $P_{1,i}$ is an initiated catalyst site of type i with a single monomer attached to it. Since we cannot

experimentally determine individual values for chain initiation and propagation for a given monomer, we set their rate constants equal.

5.4.2.3 Chain Propagation

Chain propagation is the mechanism by which the polymer chains grow. Additional monomer adds to existing chains at the active catalyst sites

$$P_{n,i} + M \xrightarrow{k_{p,i}} P_{n+1,i} \tag{16}$$
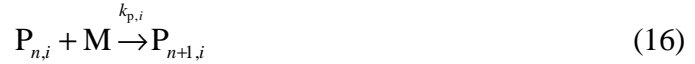
where $k_{p,i}$ is the rate constant for chain propagation at site type i, and $P_{n,i}$ and $P_{n+1,i}$ are polymer chains associated with site type i, of length n and $n+1$, respectively. Increasing the rate constants for propagation yields a linear increase in the polymer molecular weight. The reaction in eq (16) accounts for the total amount of polymer produced, including both isotactic and atactic formations.

We also include a propagation reaction to account for the small amount of atactic polymer produced

$$P_{n,i} + M \xrightarrow{k_{pa,i}} P_{n+1,i} \tag{17}$$

where $k_{pa,i}$ is the rate constant for atactic chain propagation at site type i. This reaction does not affect the total amount of polymer produced or the monomer conversions. We compute the atactic fraction by dividing the amount of polymer produced via total propagation by that for atactic propagation

$$\text{atactic fraction} = \frac{\text{rate of atactic propagation}}{\text{rate of total propagation}} \tag{18}$$

5.4.2.4 Chain Transfer

In chain transfer, a species, such as hydrogen or monomer, disengages the polymer chain from an active site, yielding a dead polymer chain. The empty catalyst site is then capable of producing a new polymer chain. This process limits the molecular weight of

the polymer. Hydrogen is used for controlling the molecular weight of the polypropylene in the gas-phase process[7].

Hydrogen reacts with an active catalyst site to disengage the polymer chain, rendering it inactive (dead), and leaving an empty catalyst site

$$P_{n,i} + H_2 \xrightarrow{k_{th,i}} D_n + P_{0,i} \tag{19}$$

where $k_{th,i}$ is the rate constant for chain transfer to hydrogen corresponding to site type i, and D_n is an inactive polymer chain.

Chain transfer to monomer yields a dead chain and an initiated catalyst site

$$P_{n,i} + M \xrightarrow{k_{tm,i}} D_n + P_{1,i} \tag{20}$$

where $k_{tm,i}$ is the rate constant for chain transfer to monomer corresponding to site type i. We adjust the rate constants for these two chain-transfer reactions to match the polymer M_n.

5.4.2.5 Catalyst Deactivation

The catalyst sites (both vacant and occupied) can undergo spontaneous deactivation

$$P_{0,i} \xrightarrow{k_{ds,i}} DCAT_i \tag{21}$$

$$P_{n,i} \xrightarrow{k_{ds,i}} DCAT_i \tag{22}$$

where $k_{ds,i}$ is the rate constant for deactivation for site type i, and $DCAT_i$ is the deactivated catalyst corresponding to site type i. An increase in this rate constant leads to a decrease in polymer production rate. It can also affect the polymer M_n if the rate of chain transfer is low.

The tacticity control agent can also participate in catalyst site deactivation[9]. The reaction is

$$P_{0,i} + TCA \xrightarrow{k_{dtca,i}} DCAT_i \tag{23}$$

where TCA is the tacticity control agent and $k_{dtca,i}$ is the rate constant for deactivation of site type i by the TCA. Theoretically, the TCA deactivates a portion of the catalyst sites that produce atactic polymer[9]. We account for this in the multi-site model, described in Section 5.4.4.4.

5.4.3 Copolymerization Kinetic Scheme

The introduction of comonomer disrupts the regularity along the polymer chain, reducing the polymer crystallinity and density. The modeled process uses ethylene as the comonomer. We include cross-propagation reactions to account for the comonomer incorporation. This approach follows the terminal model, where the rate of propagation for a specific monomer species depends on the last monomer species added to the chain. For a two-monomer system, we extend eq (16) as follows

$$P_{n,i}^1 + M_1 \xrightarrow{k_{p,i}^{11}} P_{n+1,i}^1 \tag{24}$$

$$P_{n,i}^1 + M_2 \xrightarrow{k_{p,i}^{12}} P_{n+1,i}^2 \tag{25}$$

$$P_{n,i}^2 + M_1 \xrightarrow{k_{p,i}^{21}} P_{n+1,i}^1 \tag{26}$$

$$P_{n,i}^2 + M_2 \xrightarrow{k_{p,i}^{22}} P_{n+1,i}^2 \tag{27}$$

where $P_{n,i}^j$ is a polymer chain of length n, associated with site type i, that has an active segment corresponding to monomer of type j, and $k_{p,i}^{jk}$ is the rate constant for propagation, associated with site type i, for a monomer of type k adding to a chain with an active segment of type j.

Since the amount of ethylene comonomer is small relative to propylene, there are far fewer chains with ethylene active segments than those with propylene active segments.

As a result, the primary reaction affecting propylene consumption is the propagation reaction involving propylene monomer and chains with propylene as the active segment. Similarly, the main reaction affecting ethylene conversion is the propagation reaction involving ethylene and chains with propylene as the active segment.

As with the propagation reactions, we also expand the chain-initiation and chain-transfer reactions for the copolymer case. For chain initiation

$$P_{0,i} + M_1 \xrightarrow{k_{\mathrm{ini},i}^1} P_{1,i}^1 \tag{28}$$

$$P_{0,i} + M_2 \xrightarrow{k_{\mathrm{ini},i}^2} P_{1,i}^2 \tag{29}$$

where M_j is monomer of type j and $k_{\mathrm{ini},i}^j$ is the rate of chain initiation for monomer j at site type i.

For chain transfer to hydrogen

$$P_{n,i}^1 + H_2 \xrightarrow{k_{\mathrm{th},i}^1} D_n + P_{0,i} \tag{30}$$

$$P_{n,i}^2 + H_2 \xrightarrow{k_{\mathrm{th},i}^2} D_n + P_{0,i} \tag{31}$$

where $k_{\mathrm{th},i}^j$ is the rate constant for chain transfer to hydrogen associated with a chain ending with a monomer unit of type j at site type i.

For chain transfer to monomer

$$P_{n,i}^1 + M_1 \xrightarrow{k_{\mathrm{tm},i}^{11}} D_{n,i}^1 + P_{1,i}^1 \tag{32}$$

$$P_{n,i}^1 + M_2 \xrightarrow{k_{\mathrm{tm},i}^{12}} D_{n,i}^1 + P_{1,i}^2 \tag{33}$$

$$P_{n,i}^2 + M_1 \xrightarrow{k_{\mathrm{tm},i}^{21}} D_{n,i}^2 + P_{1,i}^1 \tag{34}$$

$$P_{n,i}^2 + M_2 \xrightarrow{k_{tm,i}^{22}} D_{n,i}^2 + P_{1,i}^2 \qquad (35)$$

where $k_{tm,i}^{jk}$ is the rate constant for chain transfer to monomer of type k reacting with a chain with a terminal segment type j, associated with catalyst site type i.

5.4.4 Determination of Kinetic Parameters

5.4.4.1 Introduction

In this section, we describe how to use plant data to determine kinetic parameters for the gas-phase polymerization of propylene using a Ziegler-Natta catalyst. Since the polymerization reactions are highly coupled, adjusting a single kinetic parameter can affect several simulation variables. This makes parameter determination difficult. To simplify this process, we follow a procedure similar to that used recently for modeling an industrial slurry HDPE process with a Ziegler-Natta catalyst[34]. Using a two-step process, we establish a set of kinetic parameters that allows the model to accurately predict the polymer properties for several grades of polypropylene. In the first step, we assume that the catalyst contains a single site type. This allows us to model the polymer M_n but not the M_w, or equivalently, the PDI. In the second step, we assume the catalyst has multiple site types. We deconvolute GPC data for the polymer to determine the number of site types required to accurately describe the MWD, as well as the relative amount of polymer and M_n produced by each site type. It is much simpler to use this two-step process than to determine all of the parameters at once. Table 5-6 lists the simulation targets for the single- and multi-site models.

Section 5.4.4.2 describes parameter determination for the single-site approach. Section 5.4.4.3 provides a brief overview of the deconvolution method and the software that was used. Section 5.4.4.4 details the multi-site model. We manually implement iterative methodologies to adjust the kinetic parameters to match plant data in both the single- and multi-site approaches.

Table 5-6. Simulation targets for models for catalysts with single and multiple site types.

model for single-site catalyst	model for multi-site catalyst
polymer production rate	polymer production rate
polymer M_n	polymer M_n
ethylene content	ethylene content
isotacticity (homopolymer)	isotacticity (homopolymer)
	relative polymer production at each site type
	polymer M_n at each site type
	polymer PDI

5.4.4.2 Single-Site Kinetic Model

A kinetic model for a catalyst with a single site type allows us to model all simulation targets and polymer properties except the polymer PDI. It has significantly fewer kinetic parameters than a multi-site model. Since we must use iterative schemes to adjust the kinetic parameters to match plant data, this reduction greatly facilitates the process. Another advantage is that we can use the single-site parameters as the initial values in the multi-site model.

Table 5-7 shows a nominal set of kinetic parameters obtained from the open literature. We used an initial value of 0.0002 mol of sites/mol of Ti^{27}. Using these as initial values, we manually step through the methodology in Figure 4-14 to adjust the kinetic parameters to match plant data. The simulation targets for the single-site model appear in Table 5-6.

We begin by considering only the reactors that produce homopolymer. This allows us to disregard initially any reactions involving ethylene, thus simplifying the iterative procedure. We fit the rate constants for propylene-propylene propagation and catalyst activation to match the polymer production in all homopolymer reactors. During this iteration, if required, we adjust the max sites parameter to change the sensitivity of catalyst concentration on production and readjust the propagation and activation

parameters. We then adjust the kinetic parameters for atactic propagation to match the isotactic content of the polymer as closely as possible. Next, we fit the kinetic parameters for chain transfer to hydrogen and monomer to match the M_n for the homopolymer reactor grades having different hydrogen-to-monomer ratios.

We then move to the reactors that incorporate ethylene. We adjust the propagation parameters involving ethylene to match the ethylene conversion in these reactors. If we match total production in all reactors, we move on to adjust chain transfer parameters involving hydrogen and ethylene to match M_n produced in these copolymer reactors. If we do not match total production in all reactors, we vary the parameters for catalyst deactivation and return to the homopolymer reactors for another iteration loop.

The iterations are complete when the kinetic parameters allow the model to match all simulation targets, except polymer PDI, for all polymer grades. In the next section, we describe the deconvolution of GPC data to obtain information about the multi-site behavior of the catalyst.

Table 5-7. Nominal Set of Kinetic Parameters for the Single-Site Model.

reaction	reactant 1	reactant 2	k^a	ref	comments
cat-act	catalyst	cocatalyst	1	28	
cat-act	catalyst	hydrogen	1		b
chain-ini	catalyst	propylene	0.014		c
chain-ini	catalyst	ethylene	2.98		c
propagation	propylene	propylene	0.014	35	d
propagation	propylene	ethylene	0.668	35	d
propagation	ethylene	propylene	0.214	35	d
propagation	ethylene	ethylene	2.98	35	d
chat-agent	propylene	hydrogen	0.088	28	
chat-agent	ethylene	hydrogen	0.088	28	
spon-deact	catalyst	--	0.0001	28	
deact-agent	catalyst	tacticity control agent	0.0001		e

[a] General units are L/mol-s. [b] Assumed to be equal to that for activation by cocatalyst. [c] Assumed to be equal to that for homopropagation. [d] Evaluated at 70 °C using Arrhenius expression. [e] Assumed to be equal to that for spontaneous deactivation.
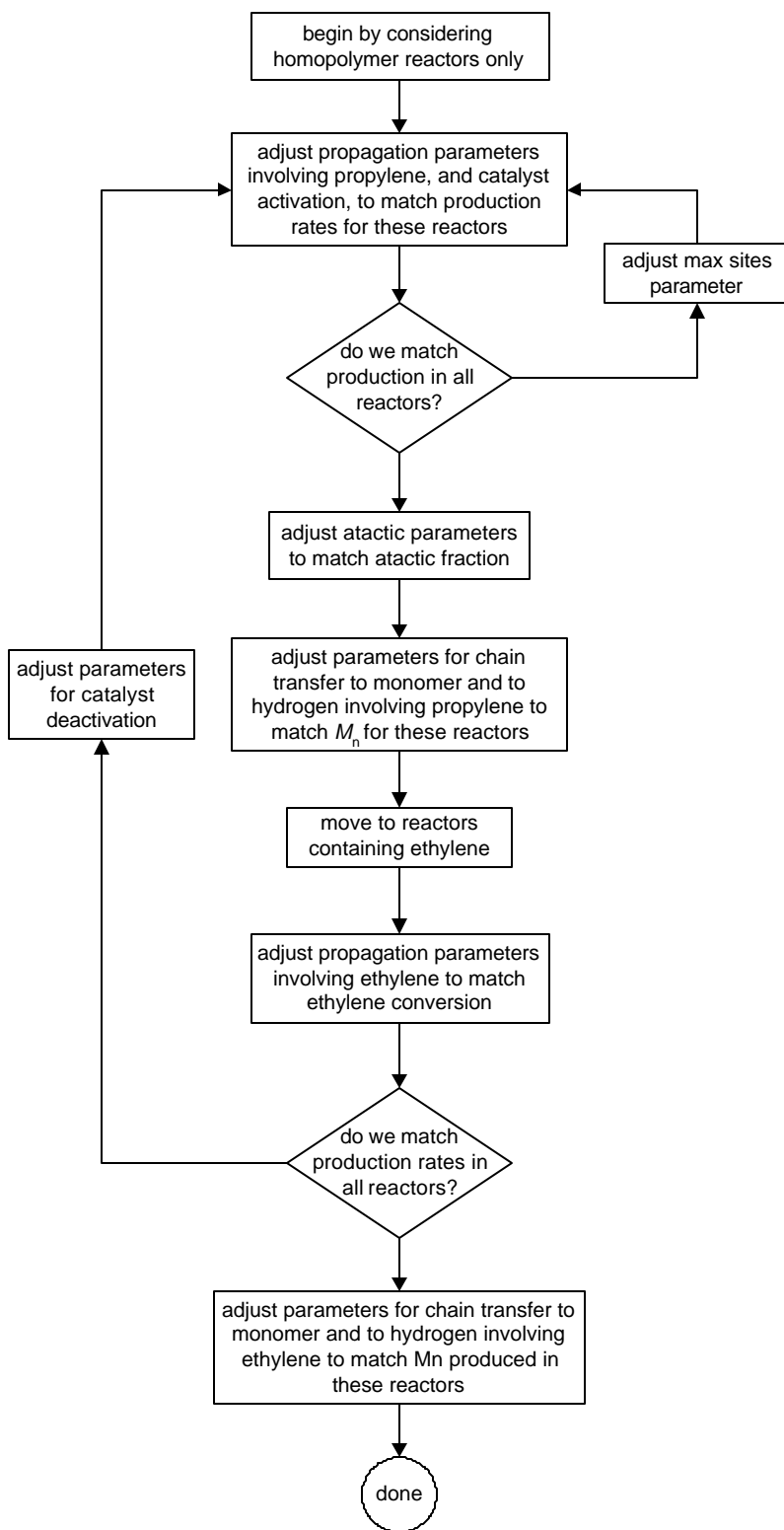
Figure 5-14. Iterative methodology used to determine kinetic parameters for the single-site model.

5.4.4.3 Deconvolution of Molecular Weight Distribution Data

185

We use a statistical algorithm developed by Soares and Hamielec[36], and implemented by Polythink Inc.[37], to deconvolute the polymer MWD obtained from gel-permeation chromatography (GPC). This procedure determines the minimum number of site types that accurately describes the polypropylene MWD. It is assumed that each site type produces a most-probable MWD. The algorithm also determines the polymer mass fraction and M_n produced by each site type.

Soares and Hamielec express the most-probable weight chain-length distribution produced by each site type as

$$w_i(n) = t_i^2 n \exp(-t_i n) \tag{36}$$

where $w_i(n)$ is the weight fraction of polymer of chain length n produced at site type i, and t_i is a fitting parameter for site type i. t_i represents the inverse of the polymer M_n produced at site type i. The chain-length distribution of the composite polymer is the sum of these distributions weighted by the mass fractions of polymer produced at each site type

$$W(n) = \sum_{i=1}^{j} m_i w_i(n) \tag{37}$$

where $W(n)$ is the total weight fraction of polymer of chain length n, m_i is the mass fraction of polymer produced at site type i, and j is the total number of site types.

Table 5-8 gives a representative set of deconvolution results for polypropylene. Figure 5-15 shows the corresponding experimental MWD distribution and the computed results. The algorithm indicates that a four-site model accurately describes the MWD of the polymer. The next section describes the development of the multi-site model.

Table 5-8. Deconvolution results for a representative polypropylene sample.

site type	polymer weight fraction	t_i (M_n^{-1})	t_i^{-1} (M_n)

1	0.04695	1.2459E-04	8026
2	0.24827	2.5198E-05	39686
3	0.41627	8.0231E-06	124640
4	0.28852	2.6116E-06	382907
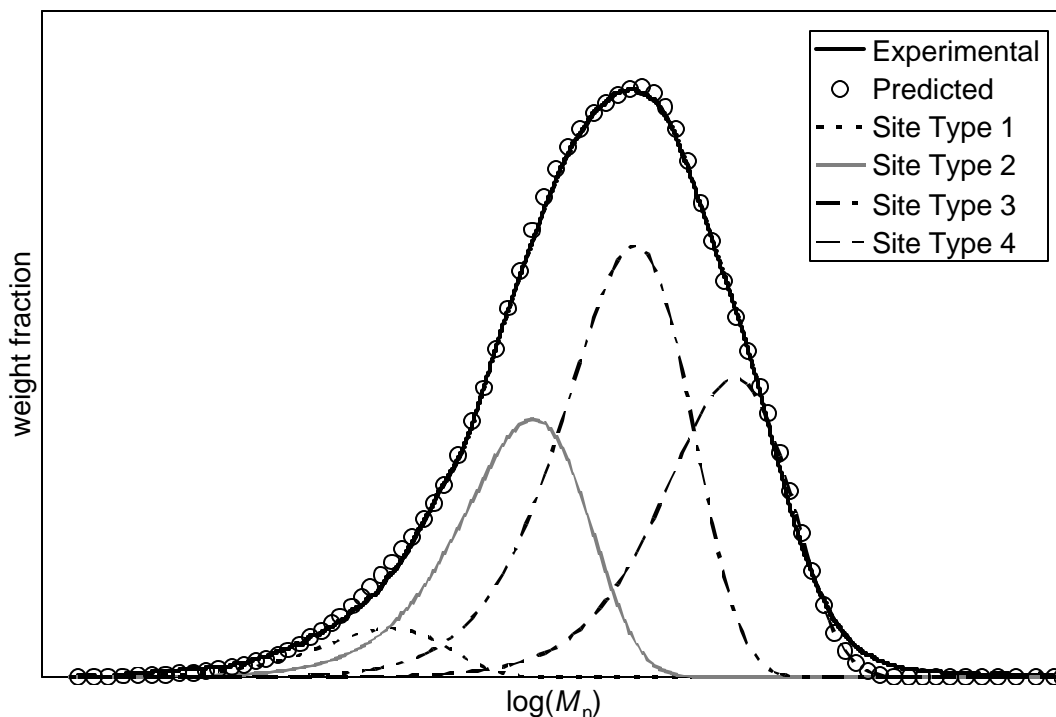
Figure 5-15. Representative MWD and deconvolution results indicating that a four-site kinetic model is sufficient.

5.4.4.4 Multi-Site Kinetic Model

Upon establishing kinetic parameters that allow the single-site model to match all the respective simulation targets listed in Table 5-6, we introduce multiple catalyst site types into the process model. The previous section describes the use of a GPC-deconvolution algorithm used to determine the optimal number of site types. The deconvolution results also provide two additional simulation targets for the multi-site model. These include the mass fraction of polymer and the M_n produced by each site type.

We obtain initial values for the propagation rate constants for each catalyst site type by multiplying the rate constant from the single-site model by the mass fraction of polymer produced at each corresponding site type

$$k_{p,i}^{ij} = n_{st} k_p^{ij} m_i \tag{38}$$

where n_{st} is the total number of catalyst site types. We must multiply the rate constant by the number of site types because the concentration of total sites is n_{st} times that of the individual sites. Note that we assume that the catalyst contains an equal number of moles of each site type. To match the M_n produced by each site type, we adjust the rate constants for chain transfer to monomer and to hydrogen.

Figure 5-16 shows the iterative scheme used to adjust the kinetic parameters in the multi-site model. In the model, the concentration of potential sites (CAT) is the same between the singe-site and multi-site models, but the concentration of vacant sites ($P_{0,i}$) must be divided by the number of site types. We resolve this by dividing the rate constants for both spontaneous catalyst activation and catalyst activation by hydrogen by the number of catalyst site types. We then use the deconvolution results and eq (38) to set the propagation rate constants to match the mass fraction of polymer produced at each site type. Next, we adjust the rate constants for chain transfer to hydrogen and to monomer to match the M_n produced by each site type. We maintain the same relative contribution of chain transfer to hydrogen and to monomer from the single-site model, so that we do not disrupt the sensitivity of these reactions to the concentrations of hydrogen and monomer. This ratio also permits the model to match the molecular weight and PDI for different hydrogen concentrations. If the observed data show an increase or decrease in molecular weight or PDI as hydrogen concentration changes, changing these ratios allows the model to capture the observed phenomena.

If we do not match M_n for all reactors, we increase the rate constant for deactivation of the catalyst site type that produces the lowest M_n. As mentioned in Section 5.4.2.5, the tacticity control agent is understood to deactivate some of the site types that produce

atactic polymer. Furthermore, atactic polymer that dissolves in solvent is mostly low molecular weight species. We return to the step for adjusting propagation rate constants for each site type. We repeat this loop until we match the production rate and M_n produced by each site type.

As initial guesses, we set the rate constant for isotactic propagation for each site such that the ratio of isotactic to total propagation is the same as that for the single-site model. If we do not match the isotactic content for polymer produced in each reactor, we increase the atactic propagation constant for the low- M_n site type, and make a downward adjustment for the remaining site types, while maintaining their relative ratios.
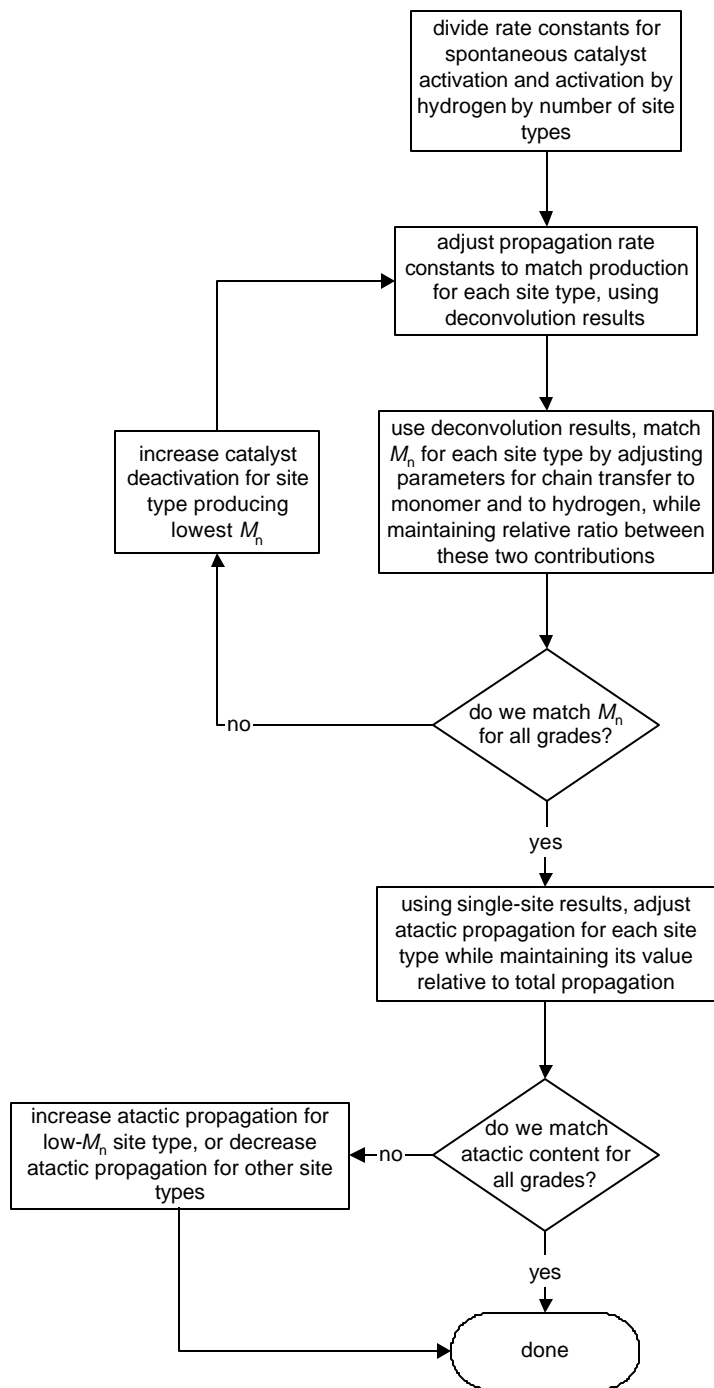
Figure 5-16. Iterative methodology used to adjust the kinetic parameters in the multi-site model.

5.5 Dynamic Modeling

5.5.1 Introduction

A dynamic model allows us to track changes in process variables and other disturbances as a function of time. Such models can be useful for determining the time required for a particular change to propagate through a process, or for planning and optimizing grade-change operations. Our aim is to illustrate the utility of a dynamic model by optimizing a grade-change operation. In Section 5.5.2, we give a general control scheme for the polypropylene process. In Section 5.6.2 we describe the optimization and present results.

We create a dynamic model by exporting a steady-state model from Polymers Plus into Aspen Dynamics. We provide additional information not required for steady-state simulation, such as vessel dimensions and geometries, to properly account for liquid levels in each vessel.

5.5.2 Control Scheme

We investigate a conceptual control scheme and its effect on grade changes. We include the following controllers in the model:

1. A level controller adjusts the flow of solids out of the reactor to maintain a constant powder level inside the reactor. Since we consider the solid polymer as a condensed phase, this level controller maintains the condensed-phase level in the reactor.
2. A temperature controller adjusts the flow rate of liquid recycle returning to the reactor to maintain the reactor temperature.
3. A pressure controller adjusts the flow rate of cooling medium to the overhead condenser to maintain the reactor pressure.
4. A flow controller adjusts the amount of vapor recycled to the reactor to maintain the ratio of vapor to liquid recycle.
5. A flow controller adjusts the feed rate of hydrogen to maintain a constant ratio of hydrogen to propylene in the reactor offgas.

6. Finally, a level controller adjusts the feed rate of propylene to the overhead flash vessel.

Table 5-9 summarizes the adjusted and manipulated variables.

Table 5-9. Controlled and manipulated variables in the control scheme.

controlled variable	manipulated variable
reactor solids level	solids outlet flow
reactor temperature	cooling medium flow
reactor pressure	liquid recycle flow
vapor/liquid recycle ratio	vapor recycle flow
hydrogen/propylene overhead ratio	hydrogen feed rate
flash unit liquid level	propylene feed rate

5.6 Simulation Results

5.6.1 Model Validation

We validate the model using data from four polymer grades produced in a commercial gas-phase polypropylene plant. Two grades are homopolymer and two grades are impact polymer with ethylene as the comonomer. These data were used to develop the polymerization kinetic parameters. Consequently, we can expect the model accuracy to be generally limited to conditions close to those of the four grades.

Figures 5-17 to 5-21 compare simulation results to plant data for polypropylene production rate, M_n, polydispersity index, atactic content, and reactor mass holdup, respectively. The model matches these process variables very well.
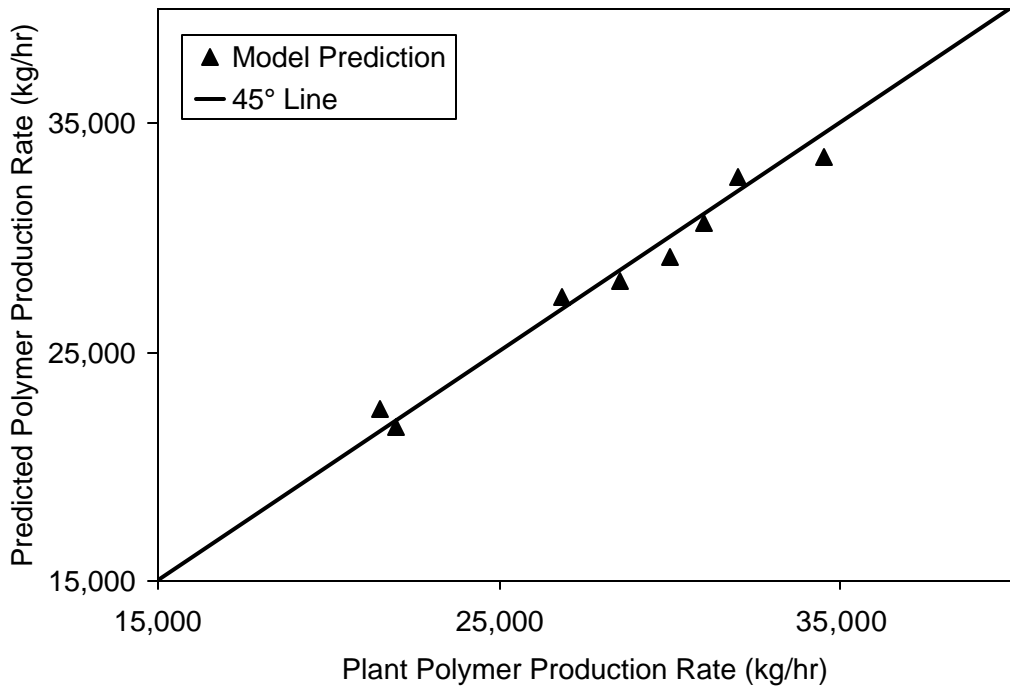
Figure 5-17. Comparison of model predictions with plant data for polypropylene production rate.

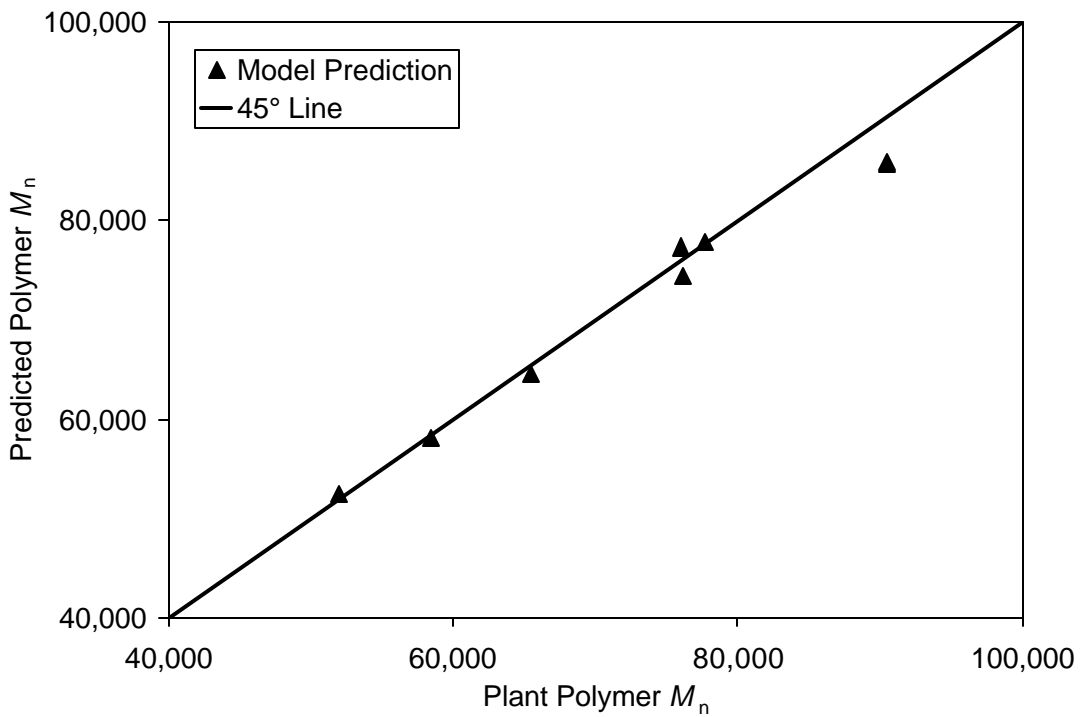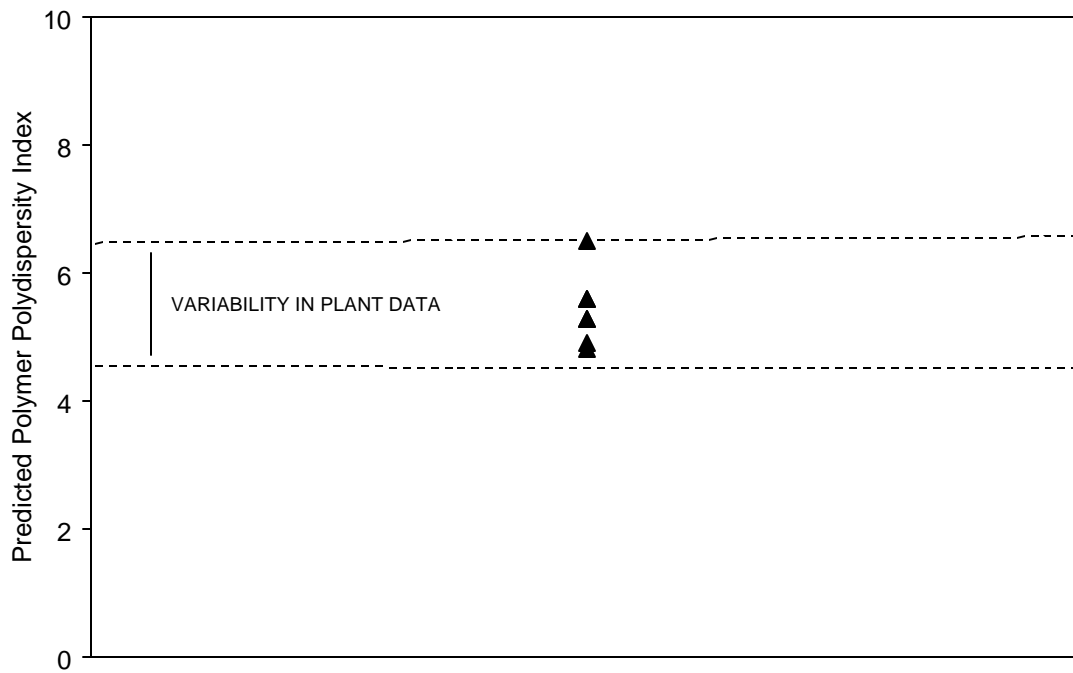**Figure 5-18. Comparison of model predictions with plant data for polypropylene M_n.**

Figure 5-19. Illustrating model predictions for polypropylene polydispersity index.
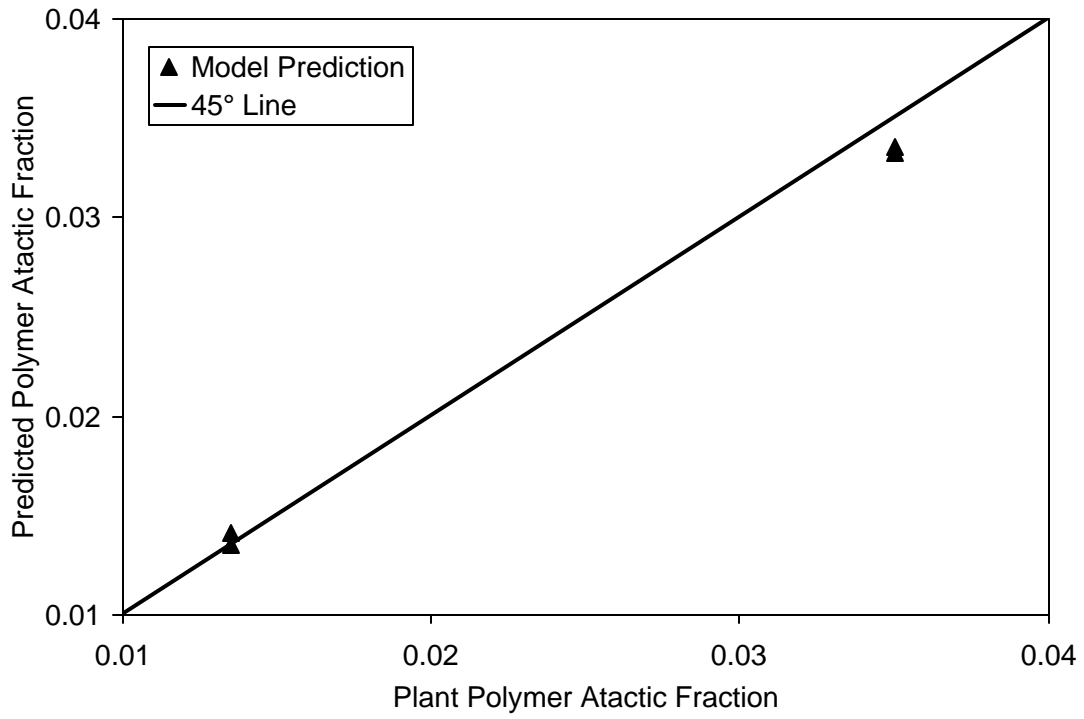
Figure 5-20. Comparing model results with plant data for polypropylene atactic fraction.

VARIABILITY IN PLANT DATA
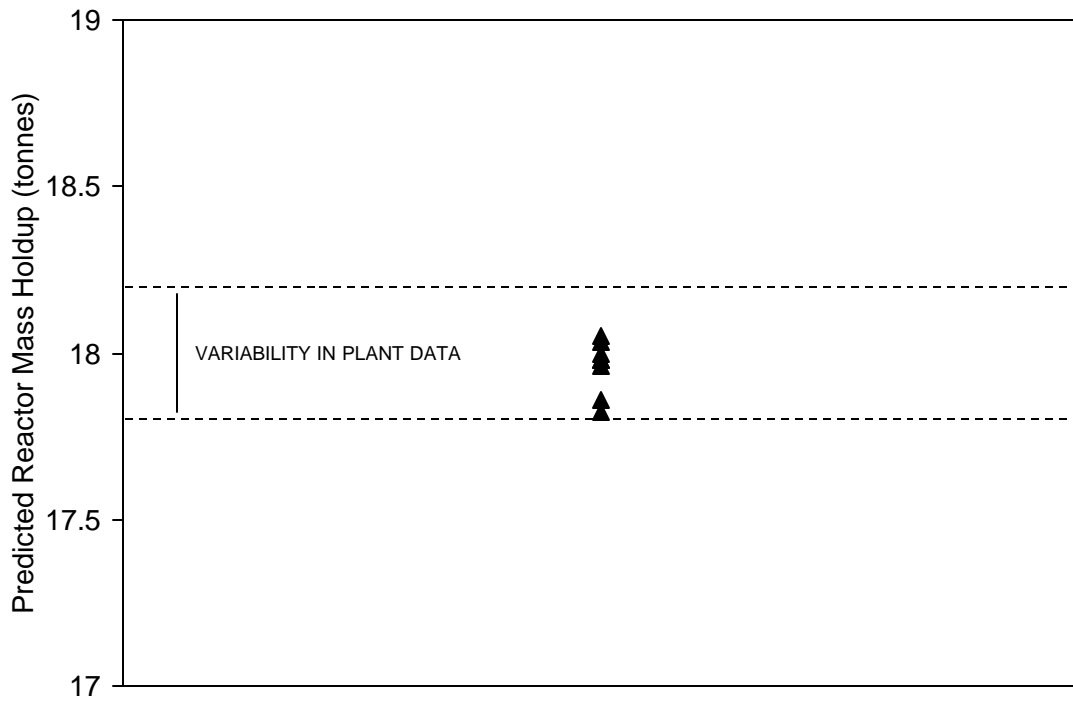
Figure 5-21. Illustrating model results for reactor mass holdup.

195

5.6.2 Model Application

We illustrate the utility of the dynamic model by simulating a typical grade change for the conceptual control scheme described in Section 5.5.2. Table 5-10 gives the key process variables. The unit-operation conditions remain the same between the two grades. We assume an instantaneous change to the new values.

Table 5-10. Specifications for the simulated grade change.

	grade 1	grade 2
propylene feed rate (kg/hr)	6,350	10,000
catalyst feed rate (kg/hr)	1.6	2.0
cocatalyst feed rate (kg/hr)	3.8	6.0
offgas H_2/C_3 molar ratio setpoint	0.0023	0.0018

Figure 5-22 shows the change in the H_2/C_3 molar ratio in the reactor overhead. The ratio initially increases due to the increase in catalyst feed rate to the reactor, yielding less propylene in the offgas. Figure 5-23 depicts the effect of the grade change on the polymer production rate. The production experiences a maximum as the system settles with the higher fresh feed rate of propylene. Figure 5-24 shows the effect of the grade change on the polymer M_n. The rate of chain transfer reduces with the lower hydrogen concentration, leading to an increase in molecular weight.
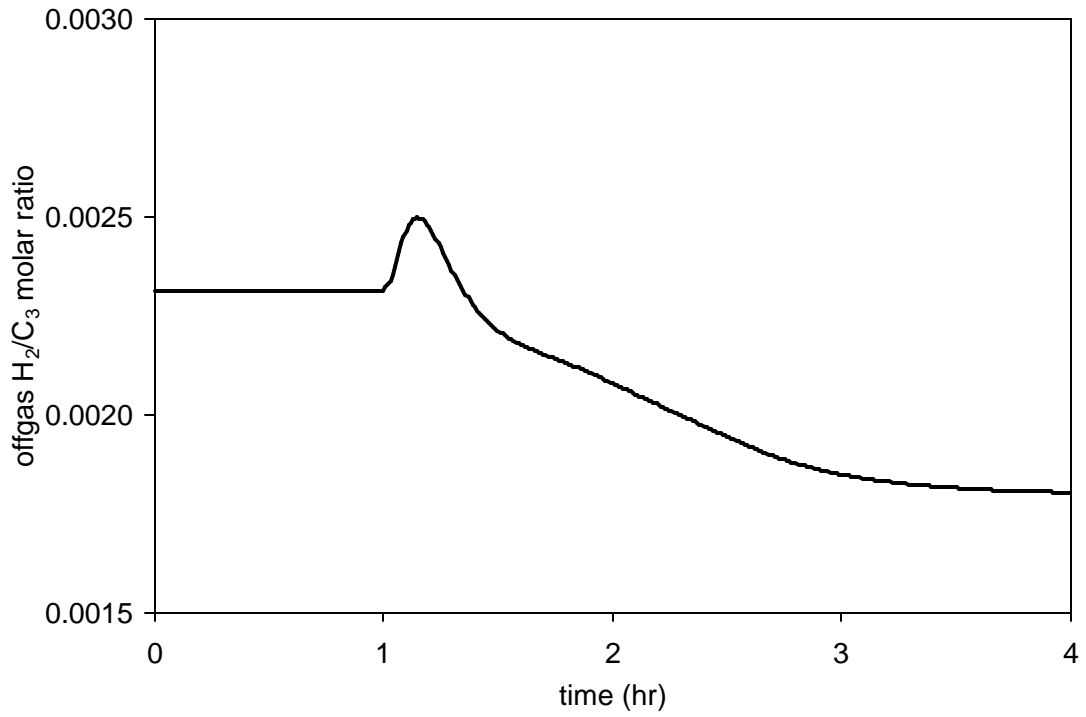
Figure 5-22. Change in the offgas H_2/C_3 molar ratio during the grade change.
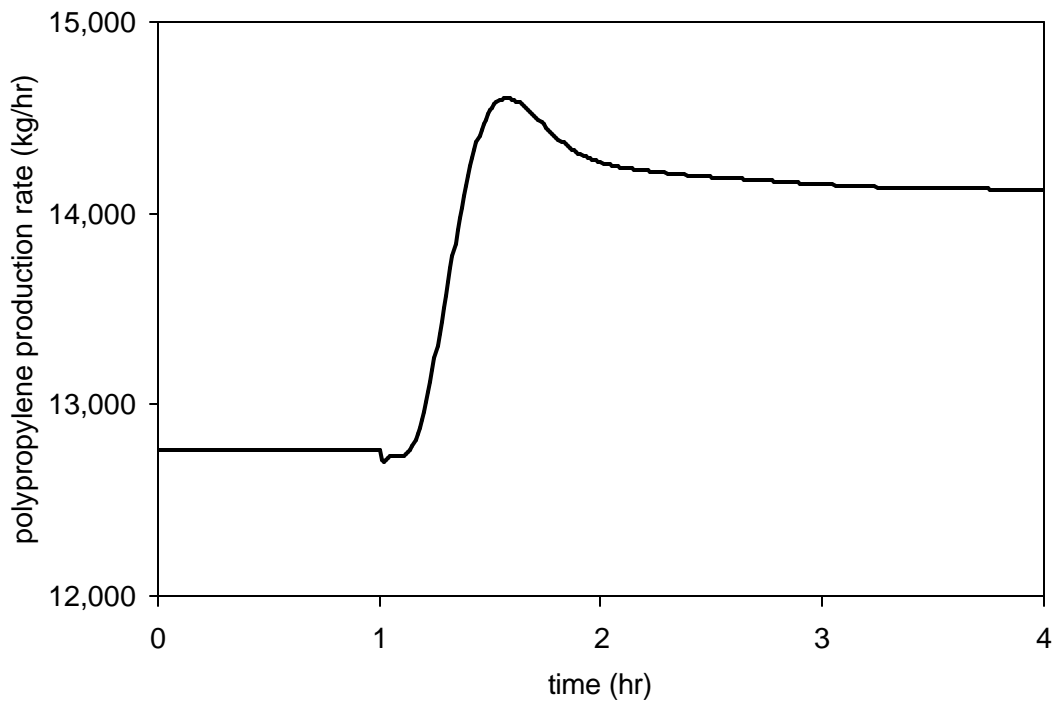
Figure 5-23. Effect of the grade change on the polypropylene production rate.
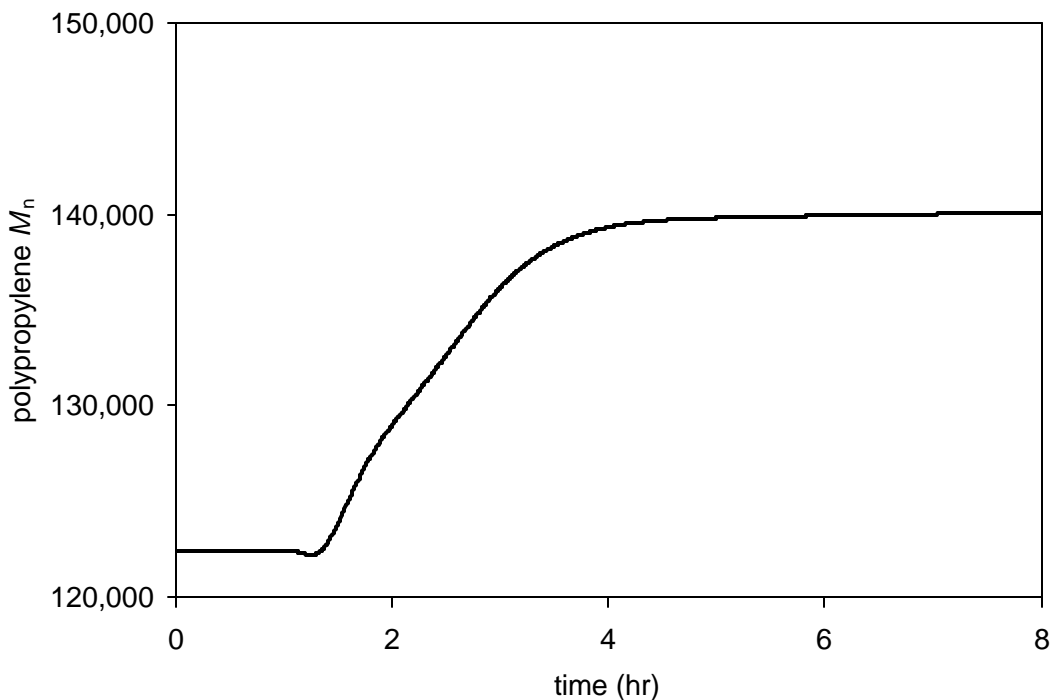
Figure 5-24. Effect of the grade change on the polypropylene M_n.

5.7 Conclusions

The PC-SAFT EOS does an excellent job of describing the physical and thermodynamic properties and phase equilibrium for the gas-phase polypropylene process. We can represent the behavior of the horizontal stirred-bed reactor using four CSTRs configured in series. We can describe a Ziegler-Natta catalyst used for polypropylene production by assuming the existence of multiple catalyst site types, each with its own relative reactivity. The steady-state model accurately predicts the major polymer properties and key process variables for four polymer trains.

There were several unique challenges during this modeling project. There were different stakeholders in the project, with different modeling objectives. We agreed to a common methodology and success criteria before the modeling began. Project communication was an issue, due to teams being in different geographical locations. This required

effective project management techniques. There is always a desire to model everything in the plant. However, modeling is an art of simplifying the complexity while still capturing the essential details.

A validated model, such as the one presented here, generates value for companies. It permits the exploration of different feed rates and operating conditions without wasting raw material or manpower. The model can also be used to debottleneck the process, test new catalysts and products, or design new polymer grades.

Acknowledgments

Symbols

English Symbols

A	parameter in polynomial for ideal-gas heat capacity, J/kmol-K
a^{res}	molar residual Helmholtz energy, J/kmol
a^{ref}	reference contribution to the molar residual Helmholtz energy, in the PC-SAFT EOS, J/kmol
a^{pert}	perturbation contribution to the molar residual Helmholtz energy, in the PC-SAFT EOS, J/kmol
B	parameter in polynomial for ideal-gas heat capacity, J/kmol-K^2
C	parameter in polynomial for ideal-gas heat capacity, J/kmol-K^3
C_p	constant-pressure heat capacity, J/kmol-K
C_p^{ig}	constant-pressure ideal-gas heat capacity, J/kmol-K

ΔC_{p}	EOS contribution to heat capacity, J/kmol-K
CAT_i	inactive catalyst of site type i
COCAT	cocatalyst
CSTR	continuous stirred-tank reactor
D	parameter in polynomial for ideal-gas heat capacity, J/kmol-K^4
D_n	inactive polymer chain containing n monomer segments
$[\mathrm{D}_n]$	concentration of inactive polymer chains containing n monomer segments, mol/L
DCAT_i	deactivated catalyst of site type i
EOS	equation of state
GPC	gel permeation chromatography
H_i^{l}	liquid enthalpy for species i, J/kmol
H_i^{v}	vapor enthalpy for species i, J/kmol
ΔH_{f}	heat of propylene polymerization, kcal/mol
$\Delta H_i^{\mathrm{vap}}$	heat of vaporization for species i, kJ/kg
HDPE	high-density polyethylene
k	rate constant with general units of L/mol-s
$k_{\mathrm{act},i}$	rate constant for activation of catalyst site type i, L/mol-s
$k_{\mathrm{acth},i}$	rate constant for activation by hydrogen of catalyst site type i, L/mol-s
k_{B}	Boltzmann's constant, J/K
$k_{\mathrm{ds},i}$	rate constant for spontaneous deactivation of catalyst site type i, s^{-1}
$k_{\mathrm{dtca},i}$	rate constant for deactivation of catalyst site type i by tacticity control agent, L/mol-s
$k_{\mathrm{ini},i}$	rate constant for chain initiation of site type i, L/mol-s
$k_{\mathrm{ini},i}^{j}$	rate constant for chain initiation of site type i by monomer type j, L/mol-s
$k_{\mathrm{p},i}$	rate constant for total chain propagation for catalyst site type i, L/mol-s
$k_{\mathrm{p},i}^{jk}$	rate constant for total chain propagation for monomer type j adding to segment type k for a chain attached to catalyst site type i, L/mol-s
$k_{\mathrm{pa},i}$	rate constant for atactic chain propagation for catalyst site type i, L/mol-s
$k_{\mathrm{th},i}$	rate constant for chain transfer to hydrogen for catalyst site type i, L/mol-s

$k_{\text{th},i}^{j}$	rate constant for chain transfer to hydrogen for chain ending in segment type j, attached to catalyst site type i, L/mol-s
$k_{\text{tm},i}$	rate constant for chain transfer to monomer for catalyst site type i, L/mol-s
$k_{\text{tm},i}^{jk}$	rate constant for chain transfer to monomer type j for chain ending in segment type k, attached to catalyst site type i, L/mol-s
m	characteristic chain length for conventional species in the PC-SAFT EOS
m_i	mass fraction of polymer produced at catalyst site type i
M	monomer
M_i	monomer of type i
M_n	number-average molecular weight, g/mol
M_w	weight-average molecular weight, g/mol
MWD	molecular weight distribution
n	number of monomer segments in the polymer (degree of polymerization)
n_{st}	number of catalyst site types
P	pressure, bar
$P_{0,i}$	activated catalyst site of type i
$P_{1,i}$	initiated catalyst site of type i
$P_{1,i}^{j}$	initiated polymer chain containing segment type j attached to catalyst site type i
P_c	critical pressure, bar
$P_{n,i}$	live polymer chain containing n segments attached to catalyst site type i
$P_{n,i}^{j}$	live polymer chain containing n segments, attached to catalyst site type i, ending in segment type j
PDI	polymer polydispersity index
$[P_n]$	concentration of active polymer chains containing n monomer segments, mol/L
PC-SAFT	perturbed-chain statistical associating fluid theory equation of state
r	size parameter for polymer species in the PC-SAFT EOS; ratio of the characteristic chain length to the number average molecular weight, mol/g
RTD	residence time distribution

SAFT	statistical associating fluid theory equation of state
T	temperature, °C
T_c	critical temperature, °C
TCA	tacticity control agent
V	volume, L
VLE	vapor-liquid equilibrium
$w_i(n)$	weight fraction of chains of length n produced at catalyst site type i
$W(n)$	total weight fraction of chains containing n segments
z	compressibility
z^{id}	ideal contribution to compressibility in the PC-SAFT EOS, equal to unity
z^{ref}	reference contribution to compressibility in the PC-SAFT EOS
z^{pert}	perturbation contribution to compressibility in the PC-SAFT EOS

Greek Symbols

ε	segment energy parameter in the PC-SAFT EOS, J
λ_i	i^{th} moment for all polymer chains
μ_i	i^{th} moment for active polymer chains
σ	segment characteristic diameter in the PC-SAFT EOS, Å
τ	residence time, hr
τ_i	adjustable parameter for chain length distribution function, mol/g

Literature Cited

(1) Choi, K. Y. Gas Phase Olefin Polymerization. In *Polymeric Materials Encyclopedia*; Salamone, J. C., Ed.; CRC Press: Boca Raton, 1996; p 2707.

(2) Shepard, J. W.; Jezl, J. L.; Peters, E. F.; Hall, R. D. Divided Horizontal Reactor for the Vapor Phase Polymerization of Monomers at Different Hydrogen Levels. U.S. Patent 3,957,488, 1976.

(3) Jezl, J. L.; Peters, E. F.; Hall, R. D.; Shepard, J. W. Process for the Vapor Phase Polymerization of Monomers in a Horizontal, Quench-Cooled, Stirred-Bed Reactor Using Essentially Total Off-Gas Recycle and Melt Finishing. U.S. Patent 3,965,083, 1976.

(4) Peters, E. F.; Spangler, M. J.; Michaels, G. O.; Jezl, J. L. Vapor Phase Reactor Off-Gas Recycle System for Use in the Vapor State Polymerization of Monomers. U.S. Patent 3,971,768, 1976.

(5) Jezl, J. L.; Peters, E. F. Horizontal Reactor for the Vapor Phase Polymerization of Monomers. U.S. Patent 4,129,701, 1978.

(6) Kissel, W. J.; Han, J. H.; Meyer, J. A. Polypropylene: Structure, Properties, Manufacturing Processes, and Applications. In *Handbook of Polypropylene and Polypropylene Composites*; Karian, H. G., Ed.; Marcel Dekker: New York, 1999; p 15.

(7) Caracotsios, M.; Theoretical Modelling of Amoco's Gas Phase Horizontal Stirred Bed Reactor for the Manufacturing of Polypropylene Resins. *Chem. Eng. Sci.* **1992**, *47*, 2591-2596.

(8) Moore, E. P. Polypropylene (Commercial) in *Polymeric Materials Encyclopedia*; Salamone, J. C., Ed.; CRC Press: Boca Raton, FL, 1996; p 6578.

(9) Seppälä, J. V.; Härkönen, M.; Luciani, L.; Effect of the Structure of External Alkoxysilane Donors on the Polymerization of Propene with High Activity Ziegler-Natta Catalysts. *Makromol. Chem.* **1989**, *190*, 2535.

(10) Balow, M. J. Growth of Polypropylene Usage as a Cost-Effective Replacement of Engineering Polymers. In *Handbook of Polypropylene and Polypropylene Composites*; Karian, H. G., Ed.; Marcel Dekker: New York, 1999; p 1.

(11) Zacca, J. J.; Debling, J. A.; Ray, W. H.; Reactor Residence Time Distribution Effects on the Multistage Polymerization of Olefins – I. Basic Principles and Illustrative Examples, Polypropylene. *Chem. Eng. Sci.*, **1996**, *51*, 4859.

(12) Gross, J.; Sadowski, G.; Perturbed-Chain SAFT: An Equation of State Based on a Perturbation Theory for Chain Molecules. *Ind. Eng. Chem. Res.* **2001**, *40*, 1244.

(13) Chapman, W. G., K. E. Gubbins, G. Jackson, and M. Radosz, "New Reference Equation of State for Associating Liquids," *Industrial and Engineering Chemistry Research*, **29**, 1709 (1990).

(14) Huang, S. H. and M. Radosz, "Equation of State for Small, Large, Polydisperse, and Associating Molecules," *Industrial and Engineering Chemistry Research*, **29**, 2284 (1990).

(15) Huang, S. H. and M. Radosz, "Equation of State for Small, Large, Polydisperse, and Associating Molecules: Extension to Fluid Mixtures," *Industrial and Engineering Chemistry Research*, **30**, 1994 (1991).

(16) DIPPR Online Database (2001).

(17) Sychev, V. V.; Vasserman, A. A.; Golovsky, E. A.; Kozlov, A. D.; Spiridonov, G. A.; Tsymarny, V. A. *Thermodynamic Properties of Ethylene*; Hemisphere Publishing Corp.: Washington, 1987.

(18) Zoller, P. Pressure-Volume-Temperature Relationships of Solid and Molten Polypropylene and Poly(butene-1). *J. App. Polym. Sci.* **1979**, *23*, 1057.

(19) Gaur, U.; Wunderlich, B. Heat Capacity and Other Thermodynamic Properties of Linear Macromolecules. IV. Polypropylene. *J. Phys. Chem. Ref. Data* **1981**, *10*, 1051.

(20) Smith, J. M.; Van Ness, H. C. *Introduction to Chemical Engineering Thermodynamics*, 4th Ed.; McGraw-Hill: New York, 1987, p. 571.

(21) Poling, B. E.; Prausnitz, J. M.; O'Connell, J. P. *The Properties of Gases and Liquids*, 5th Ed.; McGraw-Hill: New York, 2001.

(22) Gaur, U.; Wunderlich, B. Heat Capacity and Other Thermodynamic Properties of Linear Macromolecules. II. Polyethylene. *J. Phys. Chem. Ref. Data* **1981**, *10*, 119.

(23) Beaton, C. F.; Hewitt, G. F. *Physical Property Data for the Design Engineer*; Hemisphere Publishing Corp.: New York, 1989.

(24) Ohgaki, K.; Nakai, S.; Nitta, S.; Katayama, T. Isothermal Vapor-Liquid Equilibria for the Binary Systems Propylene-Carbon Dioxide, Propylene-Ethylene and Propylene-Ethane at High Pressure. *Fluid Phase Equil.* **1982**, *8*, 113.

(25) Williams, R. B.; Katz, D. L. Vapor Liquid Equilibria in Binary Systems. Hydrogen with Ethylene, Ethane, Propylene, and Propane. *Ind. Eng. Chem.* **1954**, *46*, 2512.

(26) Leonard, J. Heats and Entropies of Polymerization, Ceiling Temperatures, Equilibrium Monomer Concentrations, and Polymerizability of Heterocyclic Compounds.

In Polymer Handbook; Brandrup, J., Immergut, E. H., Grulke, E. A., Eds.; Wiley & Sons: New York, 1999; p II/363.

(27) Nagel, E. J.; Kirillov, V. A.; Ray, W. H. Prediction of Molecular Weight Distributions for High-Density Polyolefins. *Ind. Eng. Chem. Prod. Res. Dev*. **1980**, *19*, 372.

(28) McAuley, K. B.; MacGregor, J. F.; Hamielec, A. E. A Kinetic Model for Industrial Gas-Phase Ethylene Copolymerization. *AIChE J.* **1990**, *36*, 837.

(29) Xie, T.; McAuley, K. B.; Hsu, J. C. C.; Bacon, D. W. Gas Phase Ethylene Polymerization: Production Processes, Polymer Properties, and Reactor Modeling. *Ind. Eng. Chem. Res.* **1994**, *33*, 449.

(30) Arriola, D. J. Modeling of Addition Polymerization Systems. Ph.D. Dissertation, University of Wisconsin, Madison, WI, 1989.

(31) Cansell, F.; Siove, A.; Fontanille, M. Ethylene-Propylene Copolymerization Initiated with Solubilized Ziegler-Natta Macromolecular Complexes. I. Determination of Kinetic Parameters. *J. Polym. Sci., Part A: Polym. Chem.* **1987**, *25*, 675.

(32) Kissin, Y. V. *Isospecific Polymerization of Olefins with Heterogeneous Ziegler-Natta Catalysts*; Springer-Verlag: New York, 1985.

(33) Kissin, Y. V. Multicenter Nature of Titanium-Based Ziegler-Natta Catalysts: Comparison of Ethylene and Propylene Polymerization Reactions. *J. Polym. Sci., Part A: Polym. Chem.* **2003**, *41*, 1745.

(34) Khare, N. P.; Seavey, K. C.; Liu, Y. A.; Ramanathan, S.; Lingard, S.; Chen, C.-C. Steady-State and Dynamic Modeling of Commercial Slurry High-Density Polyethylene (HDPE) Processes. *Ind. Eng. Chem. Res*. **2002**, *41*, 5601.

(35) Ma, Q.; Wang, W.; Feng, L.; Wang, K.; Studies on Kinetics of Ethylene-Propylene Gas-Phase Copolymerization. *Gaofenzi Xuebao* **2001**, *6*, 746-750.

(36) Soares, J. B. P.; Hamielec, A. E. Deconvolution of Chain-Length Distributions of Linear Polymers Made by Multiple-Site-Type Catalysts. *Polymer* **1995**, *36*, 2257.

(37) Polythink Inc., 1005 Sydenham Rd., S.W., Calgary, Alberta, Canada T2T 0T3. http://www.polythink.com (accessed August 2002).

Chapter 6 Manuscript for the Solution Polymerization of Ethylene Using a Constrained-Geometry Catalyst

A Reactor Model for Metallocene-Catalyzed Ethylene Polymerizations

Neeraj P. Khare

Honeywell Center of Excellence in Computer-Aided Design and

SINOPEC/AspenTech Center of Excellence in Process Systems Engineering

Department of Chemical Engineering

Virginia Polytechnic Institute and State University

Blacksburg, VA 24061

*Phone: (540) 231-7800; Fax: (540) 231-5022; E-mail: design@vt.edu

To whom correspondence should be addressed.

Abstract

We present a reactor model for the continuous solution polymerization of ethylene using a metallocene catalyst system. Modeling considerations include mass and energy balances, physical properties, phase equilibrium, and polymerization kinetics. Predicted polymer properties include number- and weight-average molecular weights, number of long-chain branches, and number of terminal double bonds. Models for this type of system presented in the open literature focus only on polymerization kinetics, and do not include physical and thermodynamic properties, or phase equilibrium. We validate the model using literature data for two bench-scale polymerization experiments. We use values for kinetic parameters that are within the estimated ranges provided. The model matches experimental data for catalyst yield with an average error of 4.9% and 2.0%, for case studies 1 and 2, respectively. Predictions for polymer M_n are within 8.2% and 8.1%. For the number of long-chain branches, the average prediction errors are 22% and 36%. Finally, for number of terminal double bonds, the average errors are 17% and 14% for case studies 1 and 2, respectively. In light of the likely experimental error due to characterization techniques, and the lack of reproducibility data for any of the runs, we consider these predictions very good. Our model does a good job of describing the physical and kinetic phenomena for the runs in both case studies. We apply the validated model to investigate the effects of varying reactor conditions and the impact of physical properties and phase equilibrium on reactor performance and the reactor cooling duty.

Keywords: polyethylene; metallocene; simulation; model; physical properties; phase equilibrium; polymerization kinetics.

6.1 Introduction

Metallocene catalysts are used in all existing industrial polyolefin manufacturing plants. Constrained geometry catalysts, such as the version produced by Dow Chemical Co., are most suitable for producing *a*-olefins with long-chain branches. These catalysts contain an open metal active center, allowing the insertion of vinyl-terminated polymer molecules. Unlike traditional Ziegler-Natta catalysts, metallocene catalysts produce polymers with narrow molecular weight distributions, usually with a polydispersity index

close to the most-probable value of 2.0 [38]. When methylaluminoxane is used as the cocatalyst, metallocene catalysts can polymerize olefins 10 to 100 times faster than traditional Ziegler-Natta catalysts[39]. Another advantage to using metallocenes is the ability to more precisely control the polymer properties than with traditional Ziegler-Natta catalysts[39]. This is because metallocene catalysts have a single catalyst site type, whereas Ziegler-Natta catalysts contain multiple site types, each with its own relative rates of propagation, chain transfer, etc.

In this work, we develop a reactor model that incorporates mass and energy balances, physical properties, phase equilibrium, and polymerization kinetics. The model is capable of predicting polymer properties such as number- and weight-average molecular weights, number of long-chain branches, and number of terminal double bonds. We use Aspen Custom Modeler to implement and solve the model equations. We use Polymers Plus to perform calculations using the PC-SAFT equation of state. This software is part of Aspen Engineering Suite, offered by Aspen Technology, Inc., Cambridge, Massachusetts.

Physical and thermodynamic properties and phase equilibrium are important considerations for a polymerization model. For example, feed streams typically have differing molar volumes. In some processes, monomer enters as a vapor and solvent enters as a liquid. Changes in molar feed rates or molar inlet concentrations can correspond to large variations in volumetric flow. The change in volumetric flow influences the reactor residence time, which in turn affects the polymerization kinetics. Phase equilibrium can also play a role in model predictions. Changing the reactor temperature or pressure can result in different reactant concentrations in the polymer phase. Variations in these concentrations can affect the polymerization phenomena. A robust model must account for these changes.

---

[38] Hamielec, A. E.; Soares, J. B. P. Polymerization Reaction Engineering – Metallocene Catalysts. *Progress in Polymer Science* **1996**, *21*, 651.

[39] Kaminsky, W. New Polymers by Metallocene Catalysis. *Macromolecular Chemistry and Physics* **1996**, *197*, 3907.

A review of the models presented in the literature for the polymerization of ethylene using metallocene catalysts reveals a common focus on polymerization kinetics, with no consideration for physical and thermodynamic properties or phase equilibrium[40,41,42]. Yiannoulakis et al.[40] present a model that assumes that the reactor contains a single well-mixed phase. It considers reactor balances on molar concentrations. The user provides volumetric flow rates with inlet molar concentrations. The reactor residence time derives from the volumetric flow rate and the reactor volume. The model does not consider physical and thermodynamic properties, or phase equilibrium. Therefore, the model cannot capture the effect of vapor-liquid equilibrium on the reactor residence time and the polymerization kinetics. The model also does not include an energy balance, which is useful for computing the required cooling duty to maintain a constant reactor temperature.

Iedema and Hoofsloot[41] present a model that also considers a single, well-mixed phase with balances on molar concentrations. The user must specify the inlet molar concentrations and reactor residence time. There is no consideration for physical and thermodynamic properties or phase equilibrium. The resulting model therefore has the same limitations as mentioned in the previous paragraph. Additionally, it cannot account for the effect of differing molar volumes of the feed streams on the reactor residence time.

Beigzadeh et al.[42] develop a model that considers a single well-mixed phase. The model contains molar species balances. The user must supply inlet molar flow rates and the reactor residence time. Again, there is no consideration for any physical and thermodynamic properties or phase equilibrium. As with the other examples, this model

[40] Yiannoulakis, Y.; Yiagopoulos, A.; Pladis, P.; Kiparissides, C. Comprehensive Dynamic Model for the Calculation of the Molecular Weight and Long Chain Branching Distributions in Metallocene-Catalyzed Ethylene Polymerization Reactors. *Macromolecules* **2000**, *33*, 2757.

[41] Iedema, P. D.; Hoefsloot, H. C. J. Predicting Molecular Weight and Degree of Branching Distribution of Polyethylene for Mixed Systems with a Constrained Geometry Metallocene Catalyst in Semibatch and Continuous Reactors. *Macromolecules* **2003**, *36*, 6632.

[42] Beigzadeh, D.; Soares, J. B. P.; Hamielec, A. E. Recipes for Synthesizing Polyolefins with Tailor-Made Molecular Weight, Polydispersity Index, Long-Chain Branching Frequencies, and Chemical Composition Using Combined Metallocene Catalyst Systems in a CSTR at Steady State. *Journal of Applied Polymer Science* **1999**, *71*, 1753.

cannot consider the effect of molar volume or phase equilibrium on the reactor residence time and polymerization kinetics. It also does not include an energy balance for cooling-duty calculations.

The lack of consideration of phase equilibrium and physical and thermodynamic properties does not detract from the utility of these models in terms of polymerization kinetics. These previous models can be useful for predicting various polymer properties corresponding to a specific reactor composition and residence time. However, it can severely limit their usefulness when the user attempts to change the reactor conditions or feed rates, as is commonly the case in industrial applications.

A model that considers phase equilibrium and physical and thermodynamic properties, in addition to polymerization kinetics, is far more useful for exploring changes in feed composition and reactor conditions. To our knowledge, such a model has not been presented in the open literature.

6.2 Model Development

6.2.1 Overview

We develop a model for the solution polymerization of ethylene using a continuous stirred-tank reactor (CSTR). Figure 6-1 illustrates the essential elements required for a comprehensive polymer process model. Considerations include mass and energy balances, physical and thermodynamic properties, phase equilibrium, and polymerization kinetics. We use the method of moments (population-balance method) to quantify and track the polymer properties in the reactor. In the following sections, we describe each of these elements. We provide model code in the appendix.
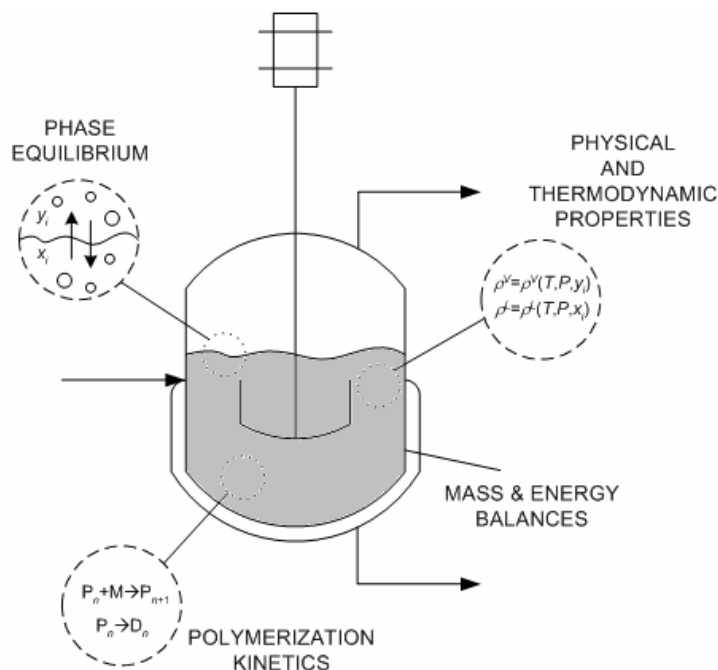
Figure 6-1. Essential elements of a robust polymer process model.

6.2.2 Modeled Process

We model the solution polymerization of ethylene using a constrained geometry catalyst. We consider a CSTR for the moderate-temperature, moderate-pressure system. Figure 6-2 illustrates the process. Catalyst and cocatalyst enter the reactor in solutions of solvent. Ethylene and hydrogen enter as vapor. There is a single outlet stream. Sufficient polymerization data at varying temperatures do not exist in the literature to justify adding temperature dependence to the reaction kinetics. We therefore focus on a single reaction temperature, 140 °C, to maintain a reasonable number of unknowns when fitting the kinetic parameters. We obtain two comprehensive sets of experimental data at this temperature[43,44]. The solvents used in references 43 and 44 are Isopar-E and toluene, respectively. Isopar-E is an industrial solvent consisting of a mixture of oligomeric hydrocarbons, and it is produced by ExxonMobil.

[43] Wang, W.-J.; Yan, D.; Zhu, S.; Hamielec, A. E. Kinetics of Long Chain Branching in Continuous Solution Polymerization of Ethylene Using Constrained Geometry Metallocene. *Macromolecules* **1998**, *31*, 8677.
[44] Kokko, E.; Wang, W.-J.; Seppala, J. V.; Zhu, S. Structural Analysis of Polyethene Prepared with rac-Dimethylsilylbis(indenyl)zirconium Dichloride/Methylaluminoxane in a High-Temperature, Continuously Stirred Tank Reactor. *Journal of Polymer Science: Part A: Polymer Chemistry* **2002**, *40*, 3292.
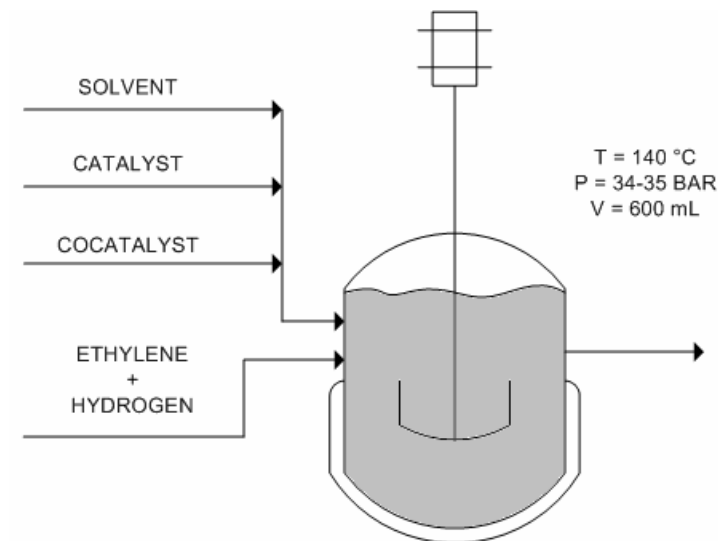
Figure 6-2. A schematic of the modeled process.

6.2.3 Phase Equilibrium and Physical and Thermodynamic Properties

6.2.3.1 Introduction

A robust reactor model must include physical and thermodynamic property calculations. We must incorporate accurate predictions for liquid density to permit the correct computation of volumetric throughput, reactor residence time, and molar concentrations. The polymerization kinetics are sensitive to residence time. Energy balances permit the calculation of the cooling duty required to maintain a constant reactor temperature. Small deviations in temperature can have large effects on the resulting polymer properties.

During steady-state operation, reactors for the solution polymerization of ethylene commonly contain a liquid solvent phase with a vapor overhead consisting of ethylene and hydrogen. Our reactor model must therefore consider phase equilibrium as well.

This directly affects the polymerization kinetics, which depend on the concentrations in the condensed phase.

We use the Perturbed-Chain Statistical Associating Fluid Theory (PC-SAFT) equation of state (EOS) for physical-property and phase-equilibrium predictions. The PC-SAFT EOS was developed specifically for polymeric systems, and is appropriate for the modeled process. A number of recent polymer process modeling articles have used the PC-SAFT EOS[45,46,47].

6.2.3.2 PC-SAFT EOS

Gross and Sadowski recently developed the PC-SAFT EOS[48], which is an extension of the well-known SAFT EOS[49,50,51]. Its development is based on perturbation theory, and it expresses the residual Helmholtz energy as sum of two contributions:

$$a^{\text{res}} = a^{\text{ref}} + a^{\text{pert}} \tag{1}$$

where a^{res} is the molar residual Helmholtz energy, and a^{ref} and a^{pert} are the reference and perturbation contributions, respectively. The reference term considers a fluid consisting of hard-sphere chains as a reference for the perturbation theory, and the perturbation term incorporates the attractive forces between the chains. The PC-SAFT model is valid for small molecules, such as monomer and solvent, and also chain-like polymers.

[45] Khare, N. P.; Lucas, B.; Seavey, K. C.; Liu, Y. A.; Sirohi, A.; Ramanathan, S.; Lingard, S.; Song, S.; Chen, C.-C. Steady-State and Dynamic Modeling of Gas-Phase Polypropylene Processes Using Stirred-Bed Reactors. submitted to *Industrial and Engineering Chemistry Research.*

[46] Bokis, C. P.; Ramanathan, S.; Franjione, J.; Buchelli, A.; Call, M. L.; Brown, A. L. Physical Properties, Reactor Modeling, and Polymerization Kinetics in Low-Density Polyethylene Tubular Reactor Process. *Industrial and Engineering Chemistry Research* **2002**, *41*,1017.

[47] Cheluget, E. L.; Bokis, C. P.; Wardhaugh, L.; Chen, C.-C.; Fisher, J. Modeling Polyethylene Fractionation Using the Perturbed-Chain Statistical Associating Fluid Theory Equation of State. *Industrial and Engineering Chemistry Research* **2002**, *41*, 968.

[48] Gross, J.; Sadowski, G.; Perturbed-Chain SAFT: An Equation of State Based on a Perturbation Theory for Chain Molecules. *Ind. Eng. Chem. Res.* **2001**, *40*, 1244.

[49] Chapman, W. G., K. E. Gubbins, G. Jackson, and M. Radosz, "New Reference Equation of State for Associating Liquids," *Industrial and Engineering Chemistry Research*, **29**, 1709 (1990).

[50] Huang, S. H. and M. Radosz, "Equation of State for Small, Large, Polydisperse, and Associating Molecules," *Industrial and Engineering Chemistry Research*, **29**, 2284 (1990).

[51] Huang, S. H. and M. Radosz, "Equation of State for Small, Large, Polydisperse, and Associating Molecules: Extension to Fluid Mixtures," *Industrial and Engineering Chemistry Research*, **30**, 1994 (1991).

The PC-SAFT EOS requires three pure component parameters for each species: m_i is the number of segments per chain for component i, $\mathbf{s}_i$ is the segment diameter (Å) for component i, and $\mathbf{e}_i/k_B$ is the segment energy parameter for component i (K). We can obtain parameters from the open literature, provided that they were determined using data measured near the conditions of interest. Alternatively, we can regress data along the saturation curve to obtain pure component parameters for conventional species. Ethylene is near supercritical state ($T_c = 9.25$ °C, $P_c = 50.4$ bar)[52] at the reactor conditions. Hydrogen is well into the supercritical region. We therefore use data from the superheated region to determine their parameters. For polyethylene, which is essentially nonvolatile, we typically use data for liquid density.

Little physical property data are publicly available for Isopar-E (a mixture of C_8-C_9 saturated hydrocarbons[53]). There is only a single data point available for its density[54]. We assume that Isopar-E has a segment diameter and segment energy parameter equal to that of *n*-octane, and we use the data point for Isopar-E density to determine its value for *m*, the number of segments per chain.

Table 6-1 lists the species we consider in the model. Table 6-2 shows the pure component PC-SAFT parameters and their sources.

Table 6-1. Species considered in the model.

species	function
catalyst	catalyst
cocatalyst	cocatalyst
ethylene	monomer
polyethylene	polymer

[52] Smith, J. M.; Van Ness, H. C. *Introduction to Chemical Engineering Thermodynamics*, 6th Ed.; McGraw-Hill: New York, 2001, p. 654.
[53] Web Site: http://www.exxonmobilchemical.com/Public_Products/Fluids/Aliphatics/Worldwide /FAQs/Fluids_Aliphatics_FAQ_Isopar.asp, accessed October 2003.
[54] ExxonMobil Chemical Product Properties Sheet for Isopar-E, March 2002. Web Site: http://www.exxonmobilchemical.com/Public_Files/Fluids/Aliphatics/NorthAmerica/Sales_Specification_Iso par_Fluid_E.pdf, accessed October 2003.

hydrogen	chain-transfer agent
toluene	solvent
Isopar-E	solvent

Table 6-2. Pure component parameters for the PC-SAFT EOS.

species	m (-)	s (Å)	e/k_B (K)	r (mol/g)	source
catalyst	25.0	2.67	198	--	a
cocatalyst	25.0	2.67	198	--	a
ethylene	1.59	3.45	176	--	48
polyethylene	--	4.02	252	2.63E-2	55
hydrogen	8.29E-1	2.97	12.5	--	b
toluene	2.81	3.72	285	--	48
Isopar-E	5.34	3.84	243	--	c

[a] We select parameters for catalyst and cocatalyst so that they remain in the liquid phase.

[b] Regressed using experimental data[56].

[c] Parameters s and e/k_B assumed to be equal to those of n-octane[48]. Parameter m regressed using experimental data[54].

6.2.3.3 Pure Component Properties

The primary physical properties we are concerned with include liquid and vapor densities. We consider the vapor densities of ethylene and hydrogen, since they are the key species that comprise the vapor phase. We focus on the liquid density of solvent, which is the primary species in the liquid phase. There is no need to examine the density predictions for Isopar-E because the pure component parameters were determined using a single data point for density. As a result, the PC-SAFT model predicts this data point exactly.

[55] Gross, J.; Sadowski, G. Modeling Polymer Systems Using the Perturbed Chain Statistical Associating Fluid Theory Equation of State. *Industrial and Engineering Chemistry Research* **2002**, *41*, 1084.

[56] Beaton, C. F.; Hewitt, G. F. *Physical Property Data for the Design Engineer*; Hemisphere Publishing Corp.: New York, 1989.

6.2.3.3.1 Molar Volume

Figures 6-3 and 6-4 compare experimental data with PC-SAFT predictions for the vapor molar volumes of ethylene and hydrogen, respectively. Note that both of these species are in the superheated state at the reactor conditions. Figures 6-5 and 6-6 give the saturated liquid and vapor molar volumes for toluene, respectively. The model provides excellent agreement in each case.
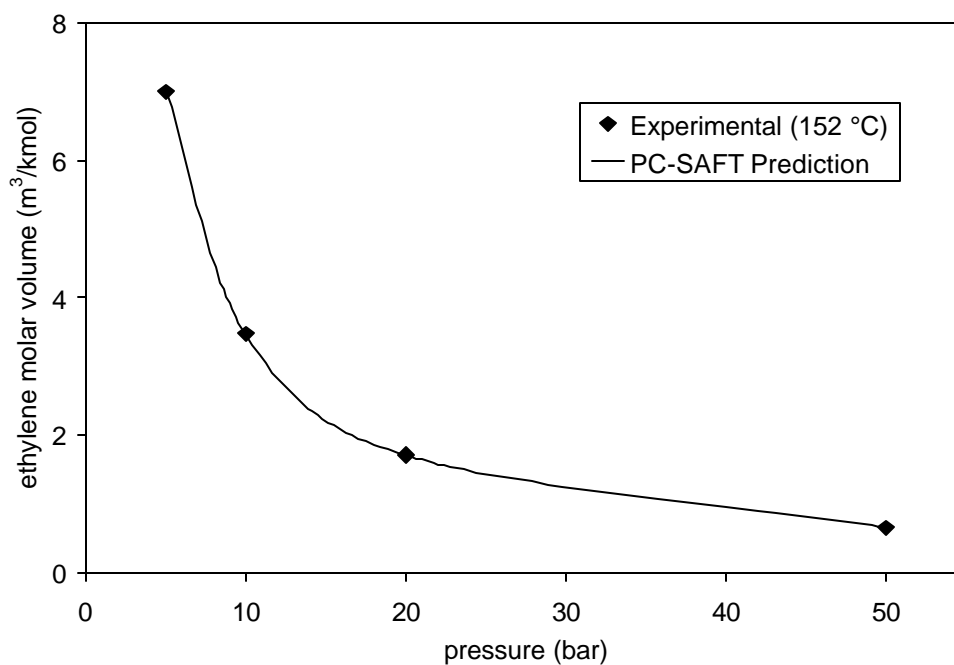

Figure 6-3. Comparing experimental data with PC-SAFT predictions for ethylene vapor molar volume. Data are from Beaton and Hewitt[56].
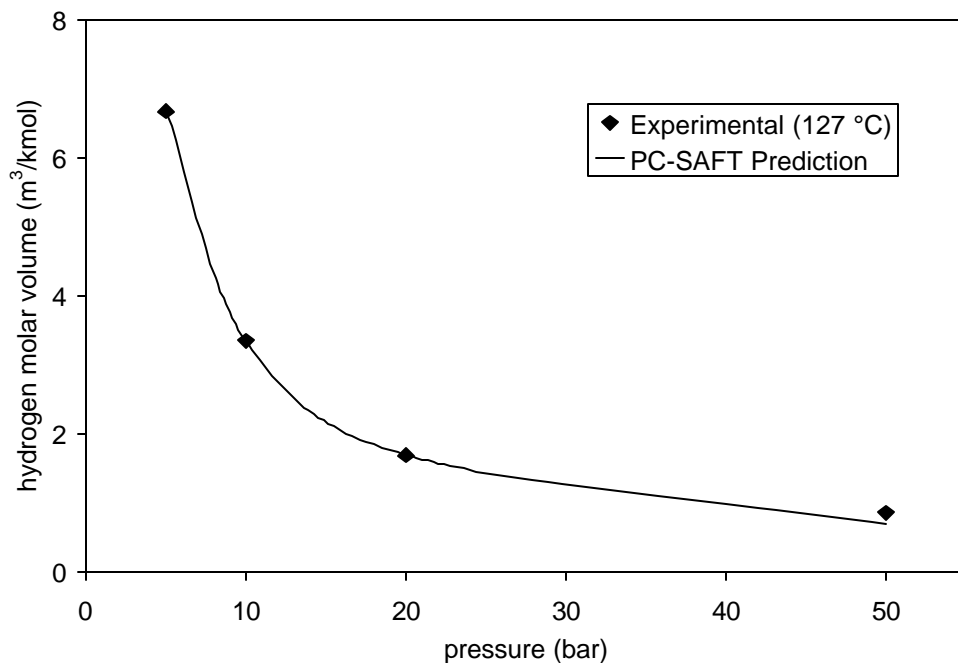
Figure 6-4. Comparing experimental data with PC-SAFT predictions for hydrogen vapor molar volume. Data are from Beaton and Hewitt[56].
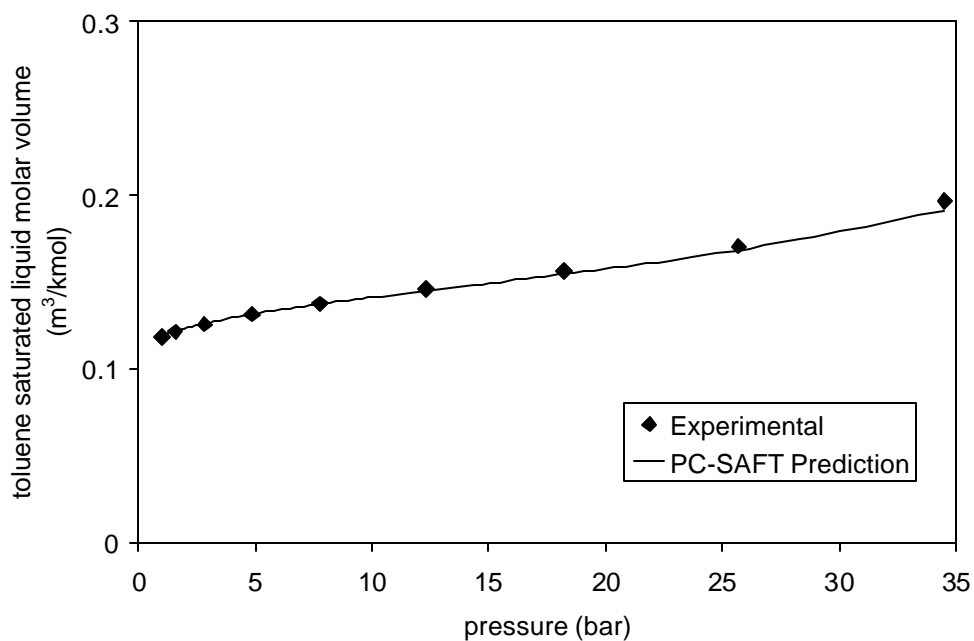

Figure 6-5. Comparing model predictions to experimental data for saturated liquid molar volume of toluene. Data are from Beaton and Hewitt[56].
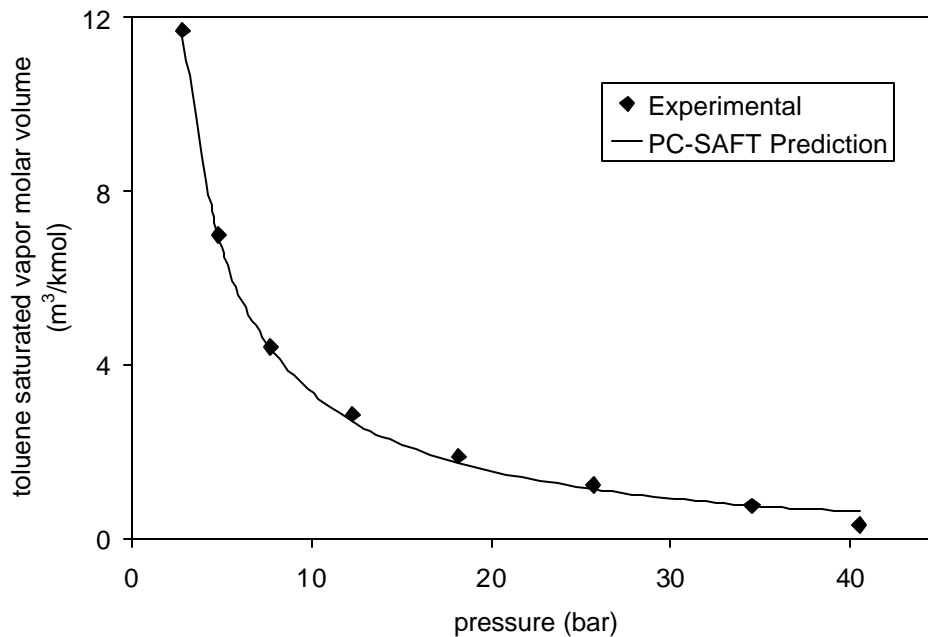
Figure 6-6. Comparing model predictions to experimental data for saturated vapor molar volume of toluene. Data are from Beaton and Hewitt[56].

6.2.3.3.2 Heat Capacity

Heat capacity is important for accurate energy-balance calculations. We can model the energy balance of the reactor to determine the cooling duty required to maintain a constant reactor temperature. Small changes in temperature can cause large changes in the polymer properties. We compute heat capacity by summing the ideal-gas and EOS contributions.

$$C_p(T,P) = C_p^{ig}(T) + \Delta C_p(T,P) \tag{2}$$

where $C_p^{ig}(T)$ is the ideal-gas term, evaluated at the system temperature, and $\Delta C_p(T,P)$ is the departure term, evaluated by the EOS at the system temperature and pressure. We model the ideal-gas heat capacity using a polynomial:

$$C_p^{ig}(T) = A + BT + CT^2 + DT^3 \tag{3}$$

where A, B, C, and D are adjustable parameters. Table 6-3 gives the regressed values for the major components in the modeled processes. Figures 6-7 to 6-9 compare experimental data with PC-SAFT predictions for the heat capacity of ethylene, toluene, and polyethylene, respectively. The predictions are excellent.

Table 6-3. Parameters for the ideal-gas heat capacity model.

species	A (J/kmol-K)	B (J/kmol-K^2)	C (J/kmol-K^3)	D (J/kmol-K^4)	reference
ethylene	3.51E4	-7.30E1	4.82E-1	-5.60E-4	[57]
toluene	7.06E4	1.10E3	-4.17	5.13E-3	a
polyethylene	1.79E4	4.33E1	0	0	b

^{a} Regressed using experimental data[56].

^{b} Regressed using experimental data[58].
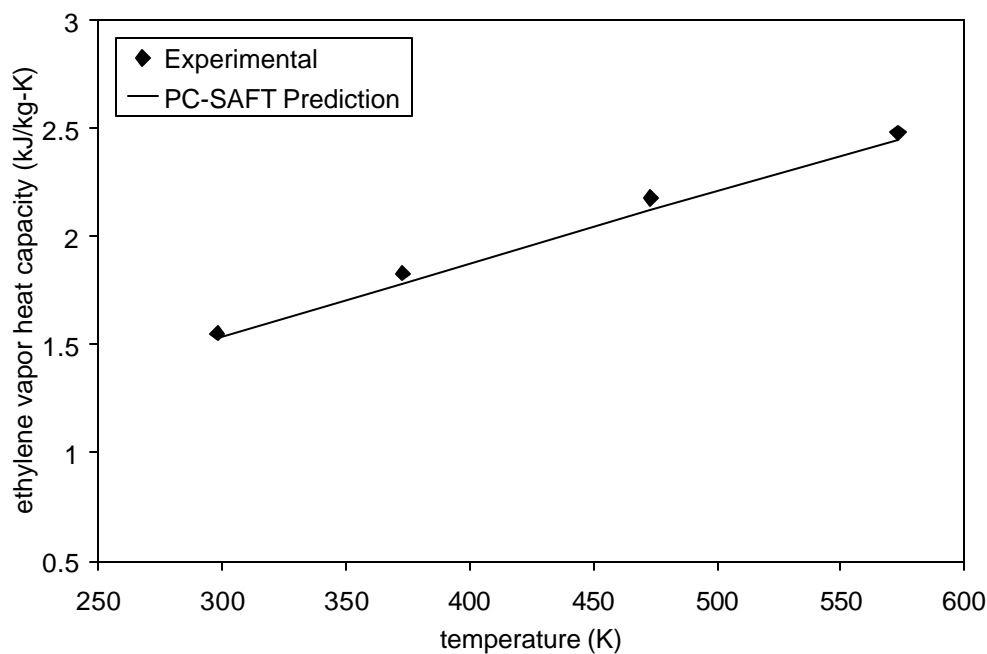
Figure 6-7. Comparing model predictions to experimental data for heat capacity of ethylene. Data are from Beaton and Hewitt[56].

[57] Poling, B. E.; Prausnitz, J. M.; O'Connell, J. P. The Properties of Gases and Liquids, 5th Ed.; McGraw-Hill: New York, 2001, p. A.36.

[58] Gaur, U.; Wunderlich, B. Heat Capacity and Other Thermodynamic Properties of Linear Macromolecules. II. Polyethylene. *J. Phys. Chem. Ref. Data* **1981**, *10*, 119.
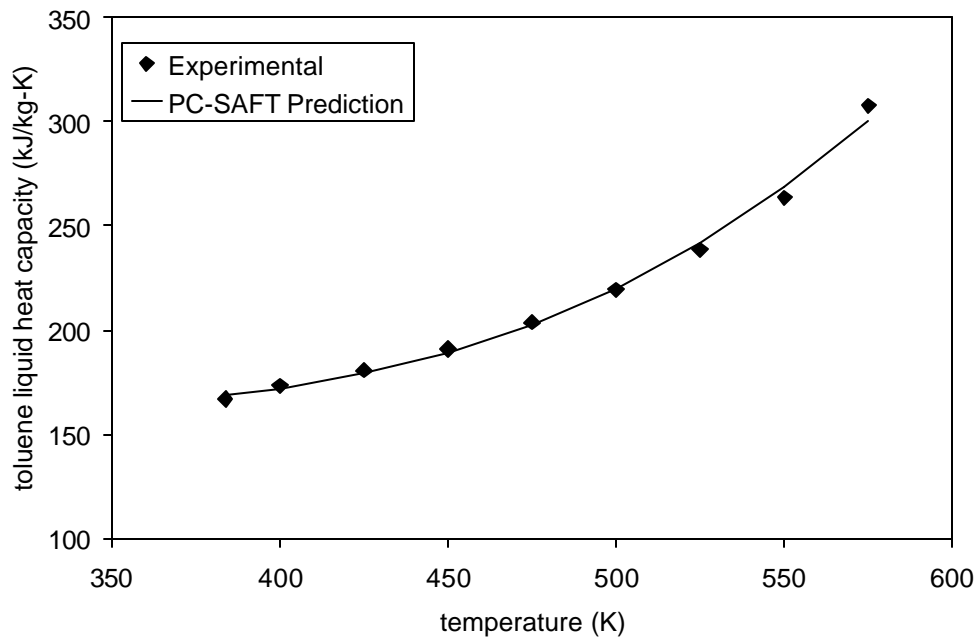
Figure 6-8. Comparing model predictions to experimental data for toluene heat capacity. Data are from Beaton and Hewitt[56].
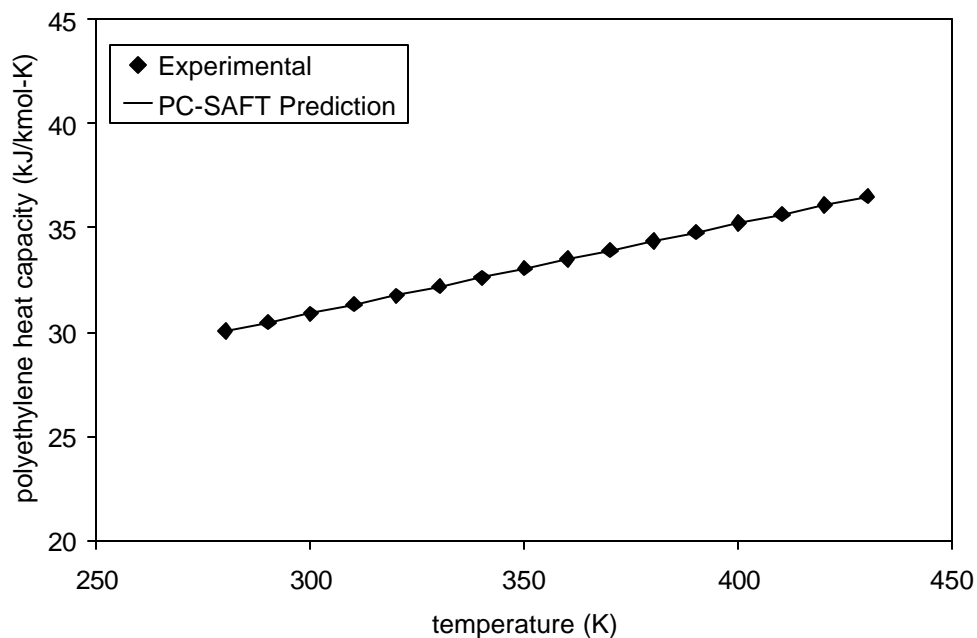
Figure 6-9. Comparing model predictions to experimental data for polyethylene heat capacity. Data are from Gaur and Wunderlich[58].

6.2.3.3 Vapor Pressure

Figure 6-10 compares experimental data with model predictions for toluene vapor pressure. The predictions are excellent.
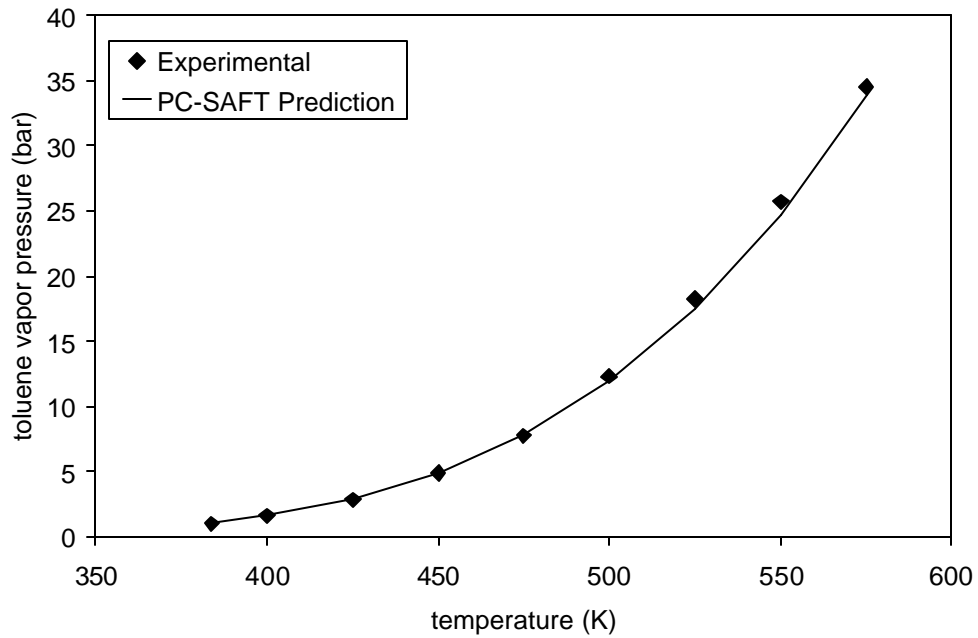
Figure 6-10. Comparing model predictions to experimental data for toluene vapor pressure. Data are from Beaton and Hewitt[56].

6.2.3.3.4 Heat of Vaporization

Figure 6-11 compares experimental data with model predictions for toluene heat of vaporization. The predictions are very good.
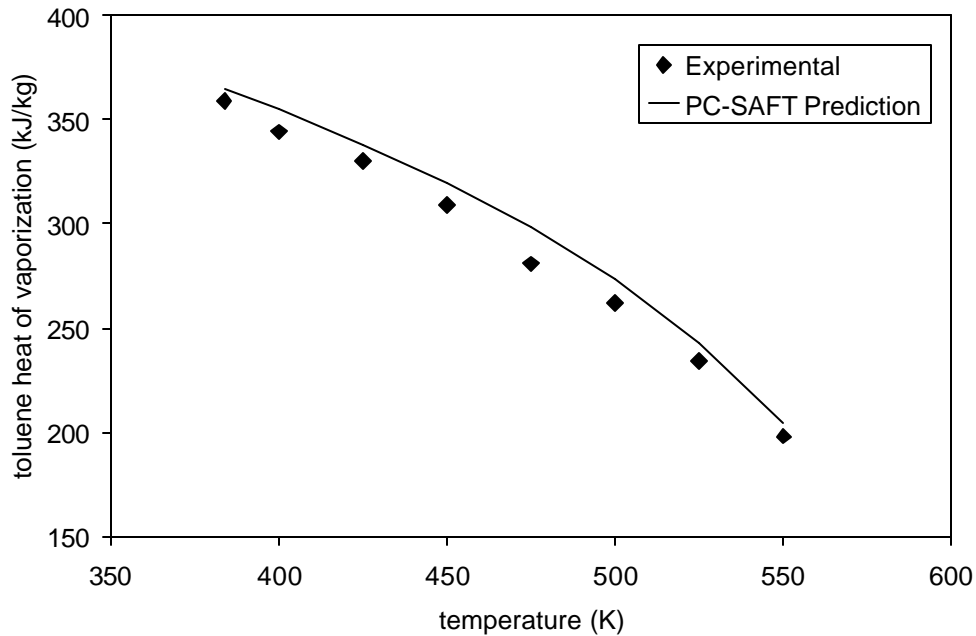
Figure 6-11. Comparing model predictions to experimental data for toluene heat of vaporization. Data are from Beaton and Hewitt[56].

6.2.3.4 Mixture Properties

We must account for the solubility of ethylene and hydrogen in the liquid phase because the polymerization kinetics are functions of their condensed-phase concentrations. Figures 6-12 and 6-13 compare experimental data to PC-SAFT predictions for solubility of ethylene and hydrogen in toluene, respectively. The model provides excellent agreement.
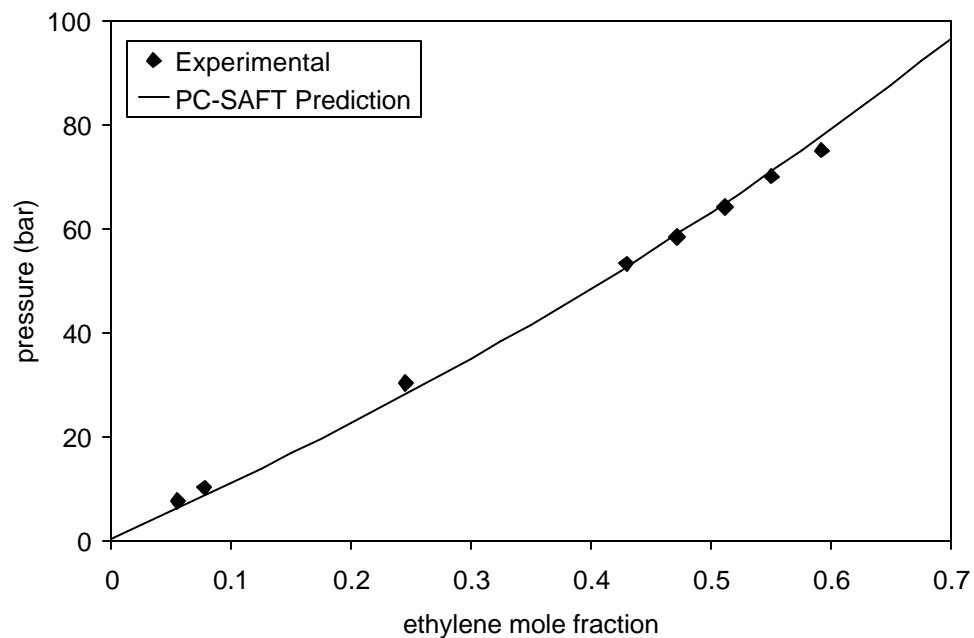
Figure 6-12. Comparing model predictions to experimental data for ethylene solubility in toluene. Data are from Fallaha[59].

---

[59] Fallaha, F. H. Ph.D. Dissertation, University of Birmingham, Birmingham, UK, 1974.
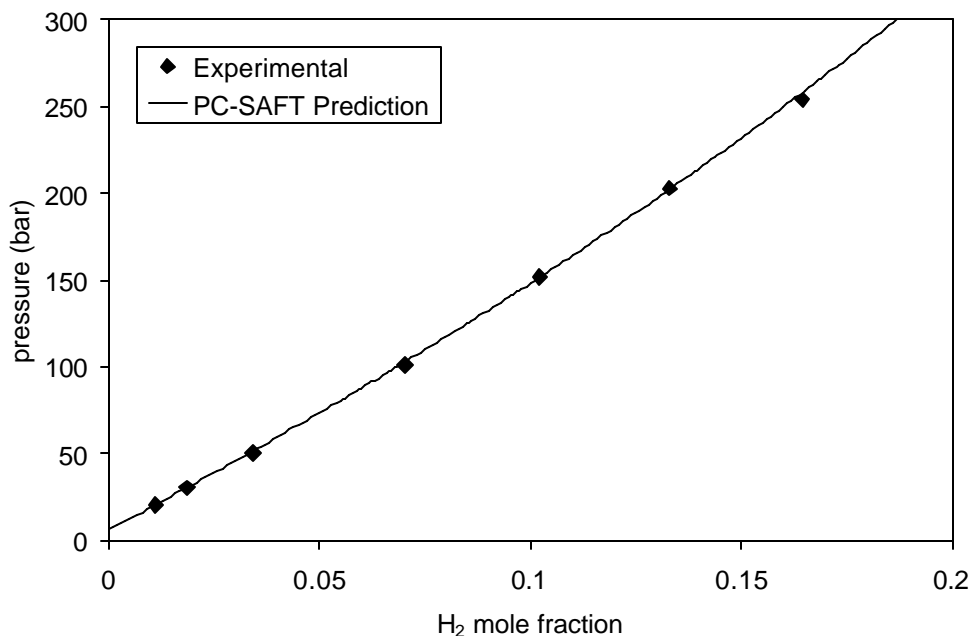
Figure 6-13. Comparing model predictions to experimental data for hydrogen solubility in toluene. Data are from Knapp et al.[60]

6.2.3.5 Polymer Properties

6.2.3.5.1 Heat of Polymerization

The heat of ethylene polymerization is the difference between the enthalpy of ethylene and polyethylene at the same temperature and pressure[61]

$$C_2H_{4(g)} \rightarrow \frac{1}{n}(C_2H_4)_{n \text{ (amorphous)}} \quad \Delta H = -24.3\text{kcal/mol} \tag{4}$$
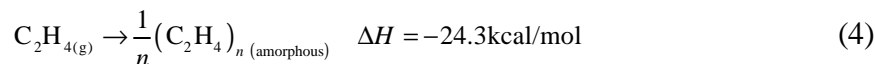
Table 6-4 gives model predictions for the heat of ethylene polymerization at various temperatures and pressures. The values compare favorably with the literature value.

---

[60] Knapp, H.; Doring, R.; Oellrich, L.; Plocker, U.; Prausnitz, J. M. *Vapor-Liquid Equilibria for Mixtures of Low-Boiling Substances*; Chemistry Data Series; DECHEMA: Frankfurt, Germany 1982; Vol VI, Part 1.
[61] Leonard, J. Heats and Entropies of Polymerization, Ceiling Temperatures, Equilibrium Monomer Concentrations, and Polymerizability of Heterocyclic Compounds. In Polymer Handbook; Brandrup, J., Immergut, E. H., Grulke, E. A., Eds.; Wiley & Sons: New York, 1999; p II/363.

Table 6-4. Computing the heat of ethylene polymerization using the PC-SAFT EOS. Results compare favorably with the experimental value of -24.3 kcal/mol[61].

T (°C)	P (bar)	$H_{ethylene}$ (kcal/mol)	$H_{polyethylene}$ (kcal/mol)	ΔH_f (kcal/mol)
130	30	13.5	-11.5	-25.0
140	30	13.7	-11.4	-25.1
150	30	13.8	-11.3	-25.1
130	40	13.5	-11.5	-25.0
140	40	13.6	-11.4	-25.0
150	40	13.8	-11.3	-25.0

6.2.3.5.2 Method of Moments

We use the *method of moments* (population-balance technique) to track the polymer properties in the reactor as a function of the polymerization kinetics. This treatment is a statistical technique that enables us to track various polymer properties without the need to include the very large number of equations and unknowns required to account for chains of every possible length. Common properties we can model include chain-length distributions, type and frequency of chain branching, and content of terminal double bonds.

The moments are averages of the numbers of polymer molecules that are weighted by their chain lengths. The moment expression for live polymer chains is

$$\boldsymbol{l}_i = \sum_{n=1}^{\infty} n^i \left(P_n \right) \tag{5}$$

where $\boldsymbol{l}_i$ is the ith moment of the molecular weight distribution of live chains, and P_n is the number of polymer chains containing n segments. We write a similar expression for dead chains:

$$\boldsymbol{m}_i = \sum_{n=2}^{\infty} n^i \left(D_n \right) \tag{6}$$

where m_i is the ith moment of the molecular weight distribution of dead chains and D_n is the number of dead polymer chains containing n segments. Finally, for dead chains with terminal double bonds, we have

$$m_i^= = \sum_{n=2}^{\infty} n^i \left(D_n^= \right) \tag{7}$$

the notation for which is analogous to that in eq (2).

The three leading moments, namely, the zeroth, first, and second, are sufficient for computing the common polymer properties. For the number-average molecular weight, we have[40]

$$M_n = MW_{seg} \times \frac{\lambda_1 + m_1 + m_1^=}{\lambda_0 + m_0 + m_0^=} \tag{8}$$

where MW_{seg} is the molecular weight of the ethylene segments (28.05 g/mol). The weight-average molecular weight is[40]

$$M_w = MW_{seg} \times \frac{\lambda_2 + m_2 + m_2^=}{\lambda_1 + m_1 + m_1^=} \tag{9}$$

The polydispersity is the ratio of M_w to M_n

$$PDI = \frac{M_w}{M_n} = \frac{\left(\lambda_2 + m_2 + m_2^= \right)\left(\lambda_0 + m_0 + m_0^= \right)}{\left(\lambda_1 + m_1 + m_1^= \right)^2} \tag{10}$$

Tracking the fraction of polymer chains with terminal double bonds is important because these affect the frequency of long-chain branching. We can compute this using

$$X_{TDB} = \frac{m_0^=}{m_0 + m_0^=} \tag{11}$$

where X_{TDB} is the molar fraction of polymer chains containing terminal double bonds.

We compute the number of long-chain branches per 1,000 carbon atoms[40]

$$\text{LCB per 1000 C} = 500 \frac{[\text{LCB}]}{\lambda_1 + m_1 + m_1^=} \tag{12}$$

228

where [LCB] is the molar concentration of long chain branches in the condensed phase ($kmol/m^3$). We multiply the right-hand side by 1,000 to account for each carbon atom, but we must then divide the result by 2 because each ethylene segment contains two carbon atoms. Similarly, we can compute the number of terminal double bonds per 1,000 carbon atoms

$$TDBper1000C = 500\frac{m_0^=}{l_1 + m_1 + m_1^=} \tag{13}$$

6.2.4 Polymerization Kinetics

6.2.4.1 Introduction

Metallocene catalyst systems are a subset of Ziegler-Natta catalyst systems. It is generally accepted that Ziegler-Natta catalysts produce polymers with broad molecular-weight distributions due to the presence of several catalyst site types, each with its own relative reactivity. Metallocene catalysts, on the other hand, produce polymers with a polydispersity close to the most-probable value of 2.0, indicating the presence of a single site type.

Constrained geometry metallocenes are designed so that the catalyst site is less hindered sterically. This facilitates the insertion of chains with terminal double bonds into the backbones of growing polymer chains, producing long-chain branches. Even very small amounts of long-chain branching can have a large impact on the rheological properties of the polymer[62]. It is therefore important to capture this catalyst behavior in the kinetic mechanism.

Section 6.2.4.2 discusses the kinetic scheme considered in the model. Section 6.2.4.3 describes the use of the method of moments to convert the reaction mechanisms to algebraic expressions.

---

[62] Doerpinghaus, P. J.; Bin Wadud, S. E.; Baird, D. G. Flow Behavior of Sparsely Branched Metallocene-Catalyzed Polyethylenes. *58th Annual Technical Conference – Society of Plastics Engineers* **2000**, *1*, 1101.

6.2.4.2 Kinetic Scheme

We incorporate a general kinetic mechanism based on our review of the open literature[40,41,42]. Sections 6.2.4.2.1 to 6.2.4.2.7 describe the reactions.

6.2.4.2.1 Catalyst Activation

We consider the activation of the metallocene catalyst by cocatalyst. The reaction is

$$CAT + COCAT \xrightarrow{k_{ac}} P_0 \qquad (14)$$

where CAT represents catalyst, COCAT is cocatalyst, k_{ac} is the rate constant for activation of catalyst by cocatalyst, and P_0 is an active catalyst site that is capable of polymerization. In the absence of information about catalyst-cocatalyst activity, we can consider spontaneous activation of catalyst

$$CAT \xrightarrow{k_{sact}} P_0 \qquad (15)$$

where k_{sact} is the rate constant for spontaneous catalyst activation.

6.2.4.2.2 Chain Initiation

The active sites react with monomer to initiate chain growth. This reaction is

$$P_0 + M \xrightarrow{k_{ini}} P_1 \qquad (16)$$

where M is monomer, P_1 is a polymer chain containing one monomer segment attached to a catalyst site, and k_{ini} is the rate constant for chain initiation for catalyst type i. We cannot experimentally determine the rate constants for initiation and propagation separately. We therefore set the rate constant for initiation equal to that for propagation. This is reasonable because they both involve the addition of an ethylene molecule to the catalyst site.

6.2.4.2.3 Chain Propagation

The addition of monomer species involves a complexation of the double-bond of the monomer at the catalyst site. The reaction is

$$P_n + M \xrightarrow{k_p} P_{n+1} \tag{17}$$

where P_n is a polymer chain attached to a catalyst site, and k_p is the rate constant for chain propagation. This reaction controls the monomer conversion in the reactor.

6.2.4.2.4 Chain Transfer

Metallocene catalysts require only trace amounts of hydrogen to achieve chain transfer, compared to Ziegler-Natta catalysts (Hamielec and Soares, 1996). Hydrogen is used almost exclusively as the chain transfer agent. The reaction is

$$P_n + H_2 \xrightarrow{k_{th}} D_n + P_0 \tag{18}$$

where D_n is a dead chain containing n segments, and k_{th} is the rate constant for chain transfer to hydrogen.

Monomer acts as a chain-transfer agent as well. This reaction is analogous to that for hydrogen given above:

$$P_n + M \xrightarrow{k_{tm}} D_n^= + P_1 \tag{19}$$

where $D_n^=$ is a dead polymer chain detached from the catalyst, and contains a terminal double bond, and k_{tm} is the rate constant for chain transfer to monomer.

In some cases, cocatalyst acts as a chain-transfer agent

$$P_n + COCAT \xrightarrow{k_{tc}} D_n + P_0 \tag{20}$$

where k_{tc} is the rate constant for chain transfer to cocatalyst.

6.2.4.2.5 Long-Chain Branching

A live chain can react with a chain containing a terminal double bond to form a single chain with a long branch:

$$P_n + D_m^= \xrightarrow{k_{tdb}} P_{n+m} \tag{21}$$
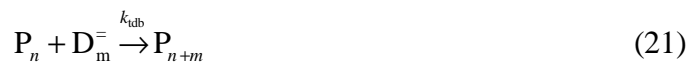
where k_{tdb} is the rate constant for incorporation of polymer chains with terminal double bonds. Constrained geometry metallocene catalysts are able to utilize this reaction to produce polymer with long-chain branches at moderate reactor conditions.

*6.2.4.2.6 **b**-Hydride Elimination*

We also include **b**-hydride elimination, where a polymer chain can detach from the active site, leaving it with a terminal double bond. The catalyst site remains active for reinitiation and polymerization. This reaction is important for the incorporation of long-chain branches, which requires chains with terminal double bonds. The reaction is

$$P_n \xrightarrow{k_b} D_n^= + P_0 \tag{22}$$

where k_b is the rate constant for **b**-hydride elimination. The M_n tends to be sensitive to temperature with the use of soluble metallocene catalysts, likely due to a higher rate of **b**-hydride elimination with increasing temperature[38].

6.2.4.2.7 Catalyst Deactivation

We consider spontaneous catalyst deactivation

$$P_0 \xrightarrow{k_{sd}} DCAT \tag{23}$$

$$P_n \xrightarrow{k_{sd}} D_n \tag{24}$$

where DCAT is deactivated catalyst, and k_{sd} is the rate constant for spontaneous catalyst deactivation. Table 6-5 summarizes the reactions we consider in the mechanism.

Table 6-5. The reactions considered in the kinetic mechanism.

reaction	stoichiometry	description
1	$CAT + COCAT \xrightarrow{k_{ac}} P_0$	catalyst activation
2	$CAT \xrightarrow{k_{sact}} P_0$	spontaneous catalyst activation
3	$P_0 + M \xrightarrow{k_{ini}} P_1$	chain initiation

4	$P_n + M \xrightarrow{k_p} P_{n+1}$	chain propagation
5	$P_n + H_2 \xrightarrow{k_{th}} D_n + P_0$	chain transfer to hydrogen
6	$P_n + M \xrightarrow{k_{tm}} D_n^= + P_1$	chain transfer to ethylene
7	$P_n + COCAT \xrightarrow{k_{tc}} D_n + P_0$	chain transfer to cocatalyst
8	$P_n + D_m^= \xrightarrow{k_{tdb}} P_{n+m}$	incorporation of long-chain branches
9	$P_n \xrightarrow{k_b} D_n^= + P_0$	*b*-hydride elimination
10	$P_0 \xrightarrow{k_{sd}} DCAT$	spontaneous catalyst deactivation (site)
11	$P_n \xrightarrow{k_{sd}} D_n$	spontaneous catalyst deactivation (chain)

6.2.4.3 Development of Rate Expressions

Table 6-6 gives the moment species contained in the model. These, along with the method of moments, allow the model to track the polymer properties.

Table 6-6. Moment species considered in the model.

moment species	description
l_0	zeroth live moment
l_1	first live moment
l_2	second live moment
m_0	zeroth dead moment
m_1	first dead moment
m_2	second dead moment
m_0^-	zeroth dead terminal-double-bond moment
m_1^-	first dead terminal-double-bond moment
m_2^-	second dead terminal-double-bond moment

233

6.2.4.3.1 Catalyst

For unactivated catalyst

$$r_{CAT} = -k_{ac} N_{cat} MW_{cat} [CAT][COCAT] \tag{25}$$

where N_{cat} is the moles of catalytic sites per unit mass of catalyst (kmol/kg). We have no specific information about the catalyst in either of the modeled processes. We assume a value of 2.0E-4 mol sites per mol metal[63].

6.2.4.3.2 Deactivated Catalyst

For deactivated catalyst, we have

$$r_{DCAT} = k_{sd} \left([P_0] + I_0 \right) \tag{26}$$

6.2.4.3.3 Cocatalyst

For cocatalyst

$$r_{COCAT} = -k_{ac} N_{cat} MW_{cat} [COCAT][CAT] - [COCAT] k_{tc} I_0 \tag{27}$$

6.2.4.3.4 Vacant Activated Catalyst Sites

For vacant activated catalyst sites, we have

$$r_{P_0} = k_{ac} N_{cat} MW_{cat} [CAT][COCAT] - k_{ini} [M][P_0]$$
$$+ k_{th} [H_2] I_0 + k_{tc} [COCAT] I_0 + k_b I_0 - k_{sd} [P_0] \tag{28}$$

6.2.4.3.5 Monomer

For ethylene

$$r_M = -k_{ini} [M][P_0] - k_p [M] I_0 - [M] k_{tm} I_0 \tag{29}$$

[63] Nagel, E. J.; Kirillov, V. A.; Ray, W. H. Prediction of Molecular Weight Distributions for High-Density Polyolefins. *Industrial and Engineering Chemistry Product Research and Development* **1980**, *19*, 372.

6.2.4.3.6 Hydrogen

For hydrogen, we have

$$r_{\mathrm{H}_2} = -\left[\mathrm{H}_2\right] k_{\mathrm{th}} \mathbf{l}_0 \tag{30}$$

6.2.4.3.7 Live Polymer Chains

For the zeroth live moment

$$r_{\mathbf{l}_0} = k_{\mathrm{ini}}\left[\mathrm{M}\right]\left[\mathrm{P}_0\right] - \left(k_{\mathrm{th}}\left[\mathrm{H}_2\right] + k_{\mathrm{tc}}\left[\mathrm{COCAT}\right] + k_b + k_{\mathrm{sd}}\right)\mathbf{l}_0 \tag{31}$$

For the first live moment

$$
\begin{aligned}
r_{\mathbf{l}_1} = {} & k_{\mathrm{ini}}\left[\mathrm{M}\right]\left[\mathrm{P}_0\right] + \left(k_{\mathrm{tm}}\left[\mathrm{M}\right]\right)\left(\mathbf{l}_0 - \mathbf{l}_1\right) + k_{\mathrm{p}}\left[\mathrm{M}\right]\mathbf{l}_0 \\
& + k_{\mathrm{tdb}}\,\mathbf{l}_0\,\overline{\mathbf{m}_1} - \left(k_{\mathrm{th}}\left[\mathrm{H}_2\right] + k_{\mathrm{tc}}\left[\mathrm{COCAT}\right] + k_b + k_{\mathrm{sd}}\right)\mathbf{l}_1
\end{aligned}
\tag{32}$$

For the second live moment

$$
\begin{aligned}
r_{\mathbf{l}_2} = {} & k_{\mathrm{ini}}\left[\mathrm{M}\right]\left[\mathrm{P}_0\right] + \left(k_{\mathrm{tm}}\left[\mathrm{M}\right]\right)\left(\mathbf{l}_0 - \mathbf{l}_2\right) + k_{\mathrm{p}}\left[\mathrm{M}\right]\left(\mathbf{l}_0 + 2\mathbf{l}_1\right) \\
& + k_{\mathrm{tdb}}\left(\mathbf{l}_0\,\overline{\mathbf{m}_2} + 2\mathbf{l}_1\,\overline{\mathbf{m}_1}\right) - \left(k_{\mathrm{th}}\left[\mathrm{H}_2\right] + k_{\mathrm{tc}}\left[\mathrm{COCAT}\right] + k_b + k_{\mathrm{sd}}\right)\mathbf{l}_2
\end{aligned}
\tag{33}$$

2.4.3.8 Dead Polymer Chains

For the zeroth dead moment

$$r_{\mathbf{m}_0} = k_{\mathrm{th}}\left[\mathrm{H}_2\right]\mathbf{l}_0 + k_{\mathrm{tc}}\left[\mathrm{COCAT}\right]\mathbf{l}_0 + k_{\mathrm{sd}}\mathbf{l}_0 \tag{34}$$

For the first dead moment

$$r_{\mathbf{m}_1} = k_{\mathrm{th}}\left[\mathrm{H}_2\right]\mathbf{l}_1 + k_{\mathrm{tc}}\left[\mathrm{COCAT}\right]\mathbf{l}_1 + k_{\mathrm{sd}}\mathbf{l}_1 \tag{35}$$

For the second dead moment

$$r_{\mathbf{m}_2} = k_{\mathrm{th}}\left[\mathrm{H}_2\right]\mathbf{l}_2 + k_{\mathrm{tc}}\left[\mathrm{COCAT}\right]\mathbf{l}_2 + k_{\mathrm{sd}}\mathbf{l}_2 \tag{36}$$

2.4.3.9 Dead Polymer Chains with Terminal Double Bonds

For the zeroth moment

$$r_{m_0^=} = \left(k_{tm}[M]\right)\boldsymbol{l}_0 + k_b\boldsymbol{l}_0 - k_{tdb}\boldsymbol{m}_0^=\boldsymbol{l}_0 \tag{37}$$

For the first moment

$$r_{m_1^=} = \left(k_{tm}[M]\right)\boldsymbol{l}_1 + k_b\boldsymbol{l}_1 - k_{tdb}\boldsymbol{m}_1^=\boldsymbol{l}_0 \tag{38}$$

For the second moment

$$r_{m_2^=} = \left(k_{tm}[M]\right)\boldsymbol{l}_2 + k_b\boldsymbol{l}_2 - k_{tdb}\boldsymbol{m}_2^=\boldsymbol{l}_0 \tag{39}$$

6.2.5 Model Equations

This section presents the model equations. We provide the actual code, written in Visual Basic Script, in the appendix.

6.2.5.1 Balance and Conversion Equations

The model considers vapor and liquid phases in equilibrium. We relate the total reactor volume to these phase volumes

$$V = V^V + V^L \tag{40}$$

where V is the reactor volume, V^V is the vapor-phase volume, and V^L is the condensed-phase volume (m^3).

Similarly, we track the phase mass holdups

$$m^{tot} = m^V + m^L \tag{41}$$

where m^{tot} is the total reactor mass holdup, and m^V and m^L are the vapor and liquid mass holdups, respectively.

The species mass balance in the CSTR is

$$F_{i,in} - F_i + r_i V^L = 0 \tag{42}$$

where $F_{i,in}$ and F_i are the molar flow rates of species i entering and exiting the reactor (kmol/hr), respectively, and r_i is the molar rate of formation for species i (kmol/m^3-hr).

We compute molar concentration in the condensed phase using molar flow rates and the condensed-phase volume

$$C_i = \frac{F_i}{V^L} \tag{43}$$

where C_i is the molar concentration of species i (kmol/m^3).

We interchange mass flows and molar flows using molecular weight

$$\dot{m}_i = F_i \times MW_i \tag{44}$$

where $\dot{m}_i$ is the mass flow rate of species i (kg/hr), and MW_i is the molecular weight of species i (kg/kmol).

There are three possible residence times to consider in a two-phase reactor: vapor, liquid, and total. The polymerization kinetics depend specifically on the liquid residence time. We compute this using

$$t^L = \frac{V^L}{Q^L} \tag{45}$$

where t^L is the condensed-phase residence time and Q^L is the liquid volumetric flow rate. We obtain the liquid volumetric flow rate using the liquid density and the liquid mass flow rate

$$Q^L = \frac{\dot{m}^L}{r^L} \tag{46}$$

where $\dot{m}^L$ is the mass flow rate of liquid exiting the reactor (kg/hr), and r^L is the liquid mass density (kg/m^3).

We use an overall mass balance and a species balance to compute the total inlet, vapor outlet, and liquid outlet flows

$$\dot{m}_{in} = \dot{m}^{V} + \dot{m}^{L} \tag{47}$$

where $\dot{m}_{in}$ is the total inlet mass flow rate, $\dot{m}^{V}$ is the vapor outlet mass flow rate, and $\dot{m}^{L}$ is the liquid outlet mass flow rate (kg/hr). For individual species, we have

$$\dot{m}_{in} z_{m,i\,in} = \dot{m}^{V} y_{m,i} + \dot{m}^{L} x_{m,i} \tag{48}$$

where $y_{m,i}$ and $x_{m,i}$ are the vapor and liquid mass fractions, respectively.

We include an energy balance for the reactor

$$\dot{m}_{out} h_{out} - \dot{m}_{in} h_{in} = Q_{duty} \tag{49}$$

where h_{in} and h_{out} are the mass-based enthalpies of the inlet and outlet streams (kJ/kg), respectively, and Q_{duty} is the cooling duty (kJ).

6.2.5.2 Subroutine Functions

We use an internal subroutine to flash the reaction mixture.

$$\text{INPUT}: T, P, z_{m,i} \quad || \quad \text{OUTPUT}: x_{m,i}, y_{m,i} \tag{50}$$

The subroutine takes in the system temperature, pressure, and total mass fractions, and returns the vapor and liquid mass fractions. Aspen Custom Modeler computes vapor-liquid equilibrium using the PC-SAFT EOS, as described in Section 6.2.3.2.

We use internal subroutines to compute the vapor and liquid mass densities

$$\text{INPUT}: T, P, y_{m,i} \quad || \quad \text{OUTPUT}: r^{V} \tag{51}$$

$$\text{INPUT}: T, P, x_{m,i} \quad || \quad \text{OUTPUT}: r^{L} \tag{52}$$

The inputs include temperature, pressure, and mass composition for the phase of interest. Mixture densities are computed using the equation of state, described in Section 6.2.3.2.

The rate expressions in the model appear exactly as presented in Section 6.2.4.3.

6.3 Model Validation

We validate the model using literature data for two bench-scale polymerization experiments. Each involves the polymerization of ethylene using a constrained geometry metallocene.

6.3.1 Case Study One

6.3.1.1 Process Description

We model a bench-scale reactor used for the continuous solution polymerization of ethylene using a constrained geometry metallocene catalyst, reported by Wang et al.[43]. Figure 6-2 illustrates the reactor system. The reactor volume is 600 mL. The catalyst and cocatalyst are fed in solutions of Isopar-E, the solvent for the system. Ethylene and hydrogen are premixed, and enter as a vapor. We only consider runs at a single reactor temperature, since sufficient data do not exist to justify adding temperature dependence to the reaction kinetics. Furthermore, a majority of the runs provided in this experimentation were performed at a single temperature.

6.3.1.2 Experimental Data

Table 6-7 gives the input data. The reactor conditions are 140 °C and 34.47 bar. Table 6-8 provides the characterization results.

Table 6-7. Experimental data for case study one[43]. Conditions for the CSTR reactor: $T = 140\ ^{\circ}C$, $P = 34$ bar.

run	$C_2H_4\ \dot{m}$	t (min)	ethylene conversion	yield (kg PE/g catalyst)

	(g/min)		(%)	
1	6.0	4.0	89.3	7.27
2	4.0	4.0	80.7	4.38
3	8.0	4.0	86.1	9.35
4	10.0	4.0	84.7	11.5
5	4.0	6.0	80.9	6.59
6	3.0	8.0	80.8	6.58

Table 6-8. Polymer characterization results for case study one[43].

run	M_n	LCB/1000 C	TDB/1000 C
1	50,980	0.035	0.065
2	50,746	--	--
3	56,373	0.038	0.079
4	54,500	0.040	0.084
5	56,784	--	--
6	54,067	0.044	0.135

6.3.1.3 Model Assumptions

We assume the reaction mixture is perfectly mixed, which is reasonable for such a small vessel. We also assume that all experimental data were gathered at steady-state conditions, as claimed[43]. We assume isothermal conditions. We adjust the solvent feed rates to match the reactor residence times, which are provided for the runs. We determine the catalyst feed rate using the catalyst yield. Since the reactors remain at constant temperature, we assume isothermal conditions in the model, and do not include a heat balance. There is no information about the liquid level in the reactor. Since ethylene and hydrogen remain in the vapor state at the reactor conditions, we assume a 5% vapor space.

No data are provided about the catalyst activity or the concentration of catalytic sites per unit mass of catalyst. We therefore cannot determine a unique rate constant for catalyst

activation. We assume a catalyst site concentration of 2E-4 mol sites per kg catalyst. In the absence of sufficient information about the catalyst activity, there is no reliable way to estimate the rate constant for catalyst activation by cocatalyst. Furthermore, the focus of the model is the prediction of polymer properties using a fundamental understanding of reaction mechanisms, not the specific activation method of the catalyst. We therefore assume that the catalyst activates completely spontaneously. Yiannoulakis et al.[40] further support this approach because they assume the catalyst is completely activated upon injection into the reactor, eliminating the need for any reaction for catalyst activation in that case. The model does contain the mechanism for catalyst activation by cocatalyst. If data become available in the future, the model has the ability to consider an experimental catalyst site concentration and rate constant for catalyst activation by cocatalyst.

It is not possible to determine the rate constants for chain initiation and propagation separately. We therefore assume these rate constants are always equal. This is reasonable because they both involve the addition of an ethylene molecule to an active catalyst site.

6.3.1.4 Model Results

It is important to mention that there are many possible sources of error in the experimental data. The largest relative source of error is typically in the characterization results. Results for molecular-weight determination, for example, can have significant error. The number of long-chain branches is usually very small, so the reported values likely have significant error associated with them. Other possible sources include fluctuating flow rates or reactor temperature. It is therefore unreasonable to expect any model to exactly match any set of data. Without repetition of each run, we cannot determine whether inconsistency between model prediction and experimental data is due to fluctuations in the reaction conditions, error in the characterization measurements, or a fundamental inability of the model to predict the reaction phenomena.

We use estimated kinetic constants as initial values in the model[43]. We then make small adjustments to the rate constants, within the estimated ranges, to match the experimental data. Figure 6-14 shows the methodology we use to fine-tune the constants. We begin by adjusting the rate constant for chain propagation to match the ethylene conversion. Next, we adjust the rate constants for chain transfer to monomer and hydrogen to match the number-average molecular weight of the polymer. We adjust these constants simultaneously because ethylene and hydrogen both contribute to lower the polymer molecular weight, and the relative amounts of these species are different in each run. We then adjust the rate constant for long-chain branching (LCB) formation. This reaction consumes polymer chains with terminal double bonds, so it affects the equilibrium concentration of terminal double bonds (TDBs). We must therefore follow its adjustment with a corresponding fine-tuning of the rate constant for b-hydride elimination, which is the primary source of chains with TDBs. The reaction for b-hydride elimination reduces the number of live polymer chains in the reactor, which affects the prediction for number-average molecular weight. We must return to adjust the rate constants for chain transfer to account for this. Since chain transfer to monomer, b-hydride elimination, and LCB formation all involve chains with terminal double bonds, they are highly correlated, and we must iterate between them until we match all of the observed reaction phenomena. Note that we do not need to adjust the rate constant for chain propagation. Also, we do not need to adjust the rate constant for catalyst deactivation because we assume a value for catalyst activation.
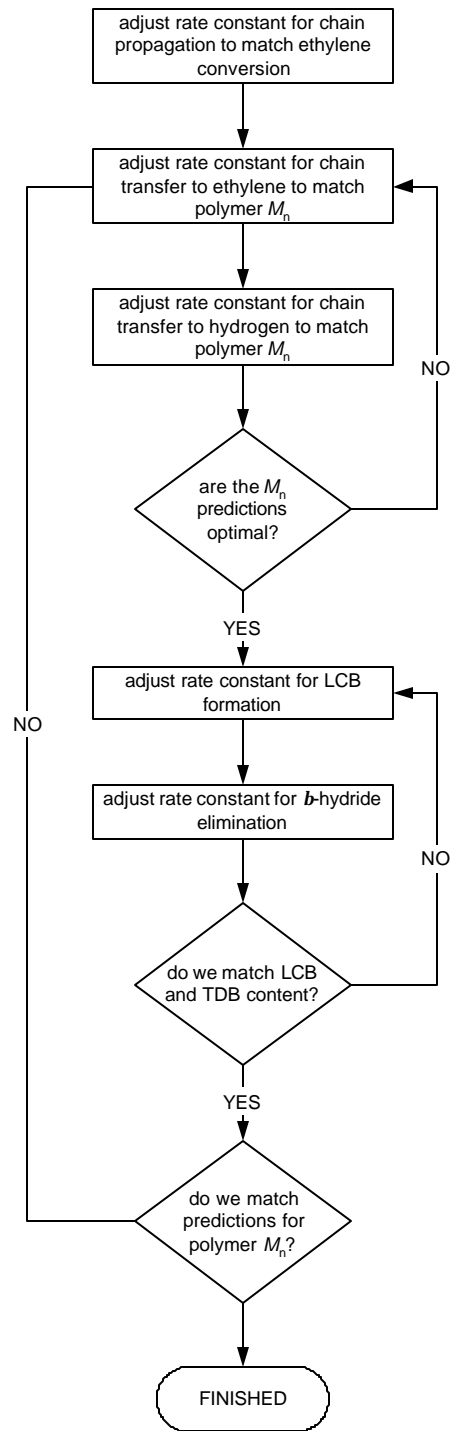
Figure 6-14. The methodology used to adjust kinetic parameters in case study one.

Table 6-9 compares estimated kinetic constants with the final values used in the model. The final model parameters are all within the estimate ranges given in Wang et al.[43]

except for the rate constant for long-chain branching (k_{tdb}), which is slightly below the lower range provided. However, it is of the same order of magnitude (1.0E5 m^3/kmol-hr). When using the lower estimate provided (7.59E5 m^3/kmol-hr), the predicted number of long-chain branches in the system is high. As we show in the figures that follow, the use of kinetic parameters close to the estimated values allows the model to provide excellent predictions for polymer properties.

Table 6-9. Comparing model rate constants to experimentally estimated values[43]. Model values are reasonably within the provided ranges.

rate constant	description	lower	upper	model value	units
k_{sact}	spontaneous catalyst activation	--	--	1.50E4	hr^{-1}
k_{ini}	chain initiation	--	--	2.0628E7	m^3/kmol-hr
k_p	chain propagation	1.22E7	3.49E7	2.0628E7	m^3/kmol-hr
k_{tm}	chain transfer to ethylene	9.37E2	1.46E4	1.367E3	m^3/kmol-hr
k_{th}	chain transfer to H_2	1.95E6	2.27E7	4.92325E6	m^3/kmol-hr
k_{tdb}	LCB formation	7.59E5	3.47E6	1.00E5	m^3/kmol-hr
k_b	b-hydride elimination	0	2.06E3	1.10E3	hr^{-1}
k_d	catalyst deactivation	13.6	23.9	18.792	hr^{-1}

Figure 6-15 compares experimental data to model predictions for yield, which is kg polymer produced per g catalyst fed. The model accurately predicts the yield for the six modeled runs in this case, with an average error of 4.9%. This indicates that the model properly accounts for the initiation and subsequent propagation of polymer chains, and the dependence of these reactions with ethylene concentration and reactor residence time.

Figure 6-16 compares experimental data to model predictions for polymer M_n. The average error is 8.2%. The predictions are very good, given the relatively large uncertainty typically associated with characterization of molecular weight. Wang et al.[43] do not provide error estimates for the characterization results. These results indicate the model properly considers the effect of ethylene and hydrogen concentrations on the rates of chain transfer.

Figure 6-17 compares experimental data to model predictions for the number of long-chain branches per 1,000 carbon atoms. The model predictions an average error of 22%. Figure 6-18 compares experimental data to model predictions for the number of terminal double bonds per 1,000 carbon atoms. The predictions have an error of 17%. In general, ^{13}CNMR spectroscopy, which was used for characterization in this study[43], cannot determine branching densities less than 0.1 LCB per 1000 carbon atoms[64]. This suggests that there may be significant error in the experimental values for LCB content, which range from 0.01 to 0.18 LCB per 1000 carbon atoms in this case. A test for reproducibility would allow us to verify the accuracy of the experimental results for each run. In light of the likely error in characterization techniques and the lack of reproducibility results, we consider these predictions very good.

In summary, the model does an excellent job of describing the physical and kinetic phenomena for the experimental runs in this case study.

---

[64] Bin Wadud, S. E.; Baird, D. G. Shear and Extensional Rheology of Sparsely Branched Metallocene-Catalyzed Polyethylenes. *Journal of Rheology* **2000**, *44*, 1151.
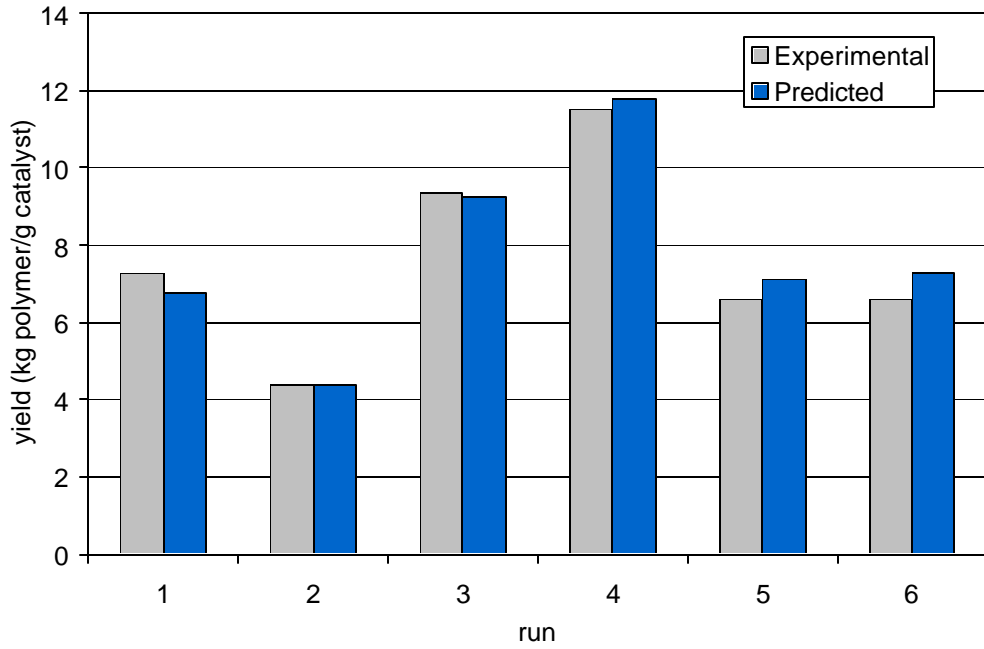
Figure 6-15. Comparing experimental data to model predictions for yield in case study one[43]. The average prediction error is 5.0%.
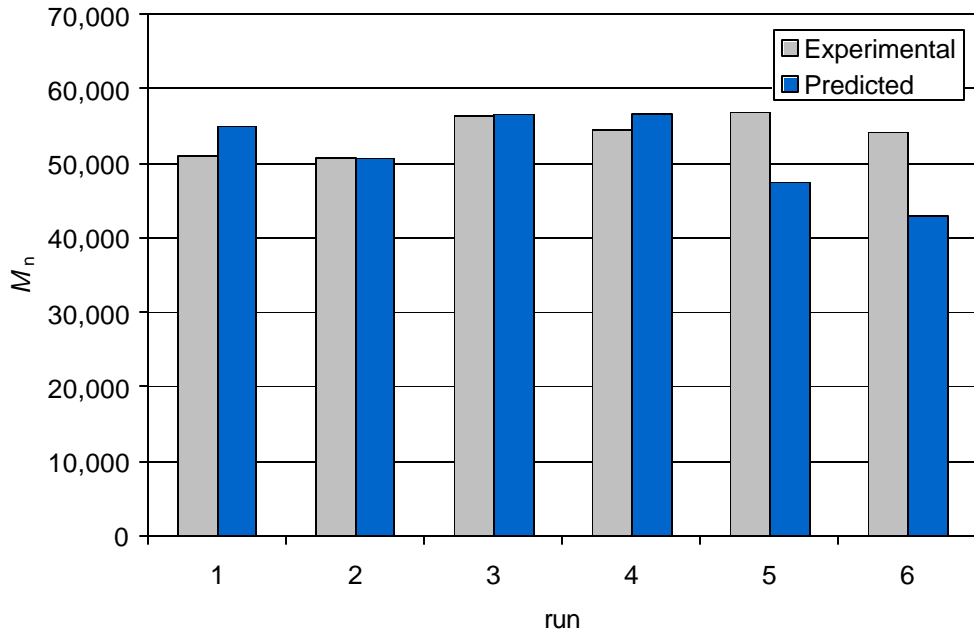

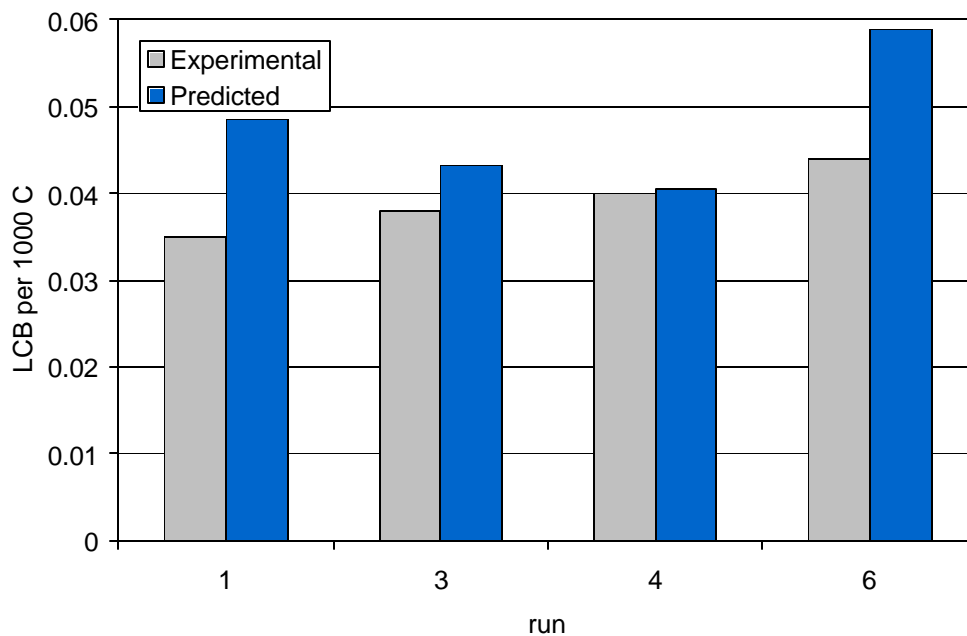**Figure 6-16. Comparing experimental data to model predictions for polymer M_n in case study one[43].**

Figure 6-17. Comparing experimental data to model predictions for number of long-chain branches per 1,000 carbon atoms in case study one[43].
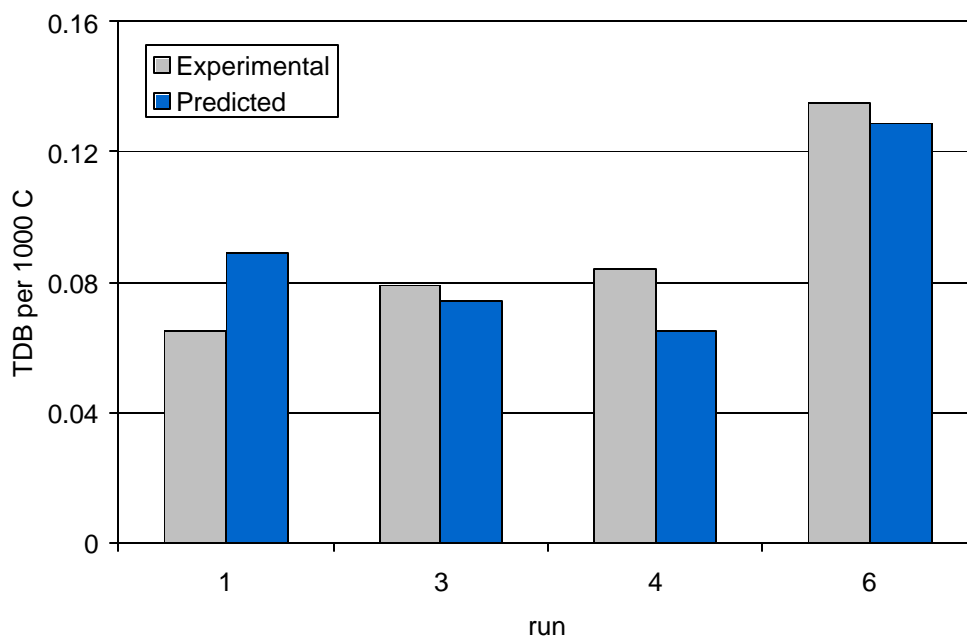

Figure 6-18. Comparing experimental data with model predictions for number of terminal double bonds per 1,000 carbon atoms in case study one[43].

6.3.2 Case Study Two

6.3.2.1 Process Description

In case study two, we model another bench-scale reactor used for the continuous solution polymerization of ethylene using a constrained geometry metallocene catalyst, as reported by Kokko et al.[44]. Figure 6-2 illustrates the reactor system. The reactor volume is 600 mL. The catalyst and cocatalyst are fed in solutions of toluene, the solvent for the system. Ethylene enters as a vapor. There is no hydrogen as chain-transfer agent in this case. All of the runs were performed at a single reactor temperature. We therefore do not consider temperature dependence for the reaction kinetics.

6.3.2.2 Experimental Data

Table 6-10 gives the input data. The reactor conditions are 140 °C and 34 bar, with a residence time of 4 min. Toluene enters at a constant rate of 150 mL/min.

Table 6-10. Input data for case study two[44]. Conditions for the CSTR reactor: $T = 140$ °C, $P = 34$ bar, $Q_{\text{toluene}} = 150$ mL/min, t=4 min.

run	C_2H_4 $\dot{m}$ (g/min)	ethylene conversion (%)	yield (kg PE/g catalyst)
1	4.0	70	67
2	4.0	84	40
3	4.0	80	38
4	4.0	95	23
5	4.0	93	11
6	2.5	88	6.5
7	8.0	98	23
8	8.0	85	81

Table 6-11. Polymer characterization results for case study two[44].

run	M_n	LCB/1000 C	TDB/1000 C
1	21,000	0.01	0.55
2	24,000	0.02	0.56
3	24,000	0.00	0.54
4	19,000	0.07	0.55
5	16,000	0.18	0.41
6	16,000	0.10	0.57
7	19,000	0.14	0.39
8	26,000	0.02	0.43

6.3.2.3 Model Assumptions

We apply the same model assumptions as in case study one (see Section 6.3.1.3).
Additionally, Kokko et al.[44] indicate that the specific cocatalyst used in the process
contributes to chain transfer reactions, affecting the polymer molecular weight. We
therefore include this reaction in the kinetic mechanism.

As in case study one, we assume the catalyst activates spontaneously because we have no
information about the activity of the employed catalyst system. A mentioned in Section
6.3.1.3, this is a reasonable assumption because the focus of the model is the prediction
of the polymer properties, not the specific activation method of the catalyst.

6.3.2.4 Model Results

Figure 6-19 shows the methodology we use to adjust the kinetic parameters to match the
experimental data. We assume that the rate constant for catalyst activation is the same as
that in case study one. We begin by adjusting the rate constant for catalyst deactivation
to match the relative amount of catalyst activated in the model for case study one. Next,
we vary the rate constant for chain propagation to match the yields. We then vary the

rate constant for chain transfer to ethylene to match the polymer M_n. We set the rate constant for chain transfer to cocatalyst equal to that for ethylene, since we have no other insight about its value. The remainder of the methodology is the same as that used for case study one.
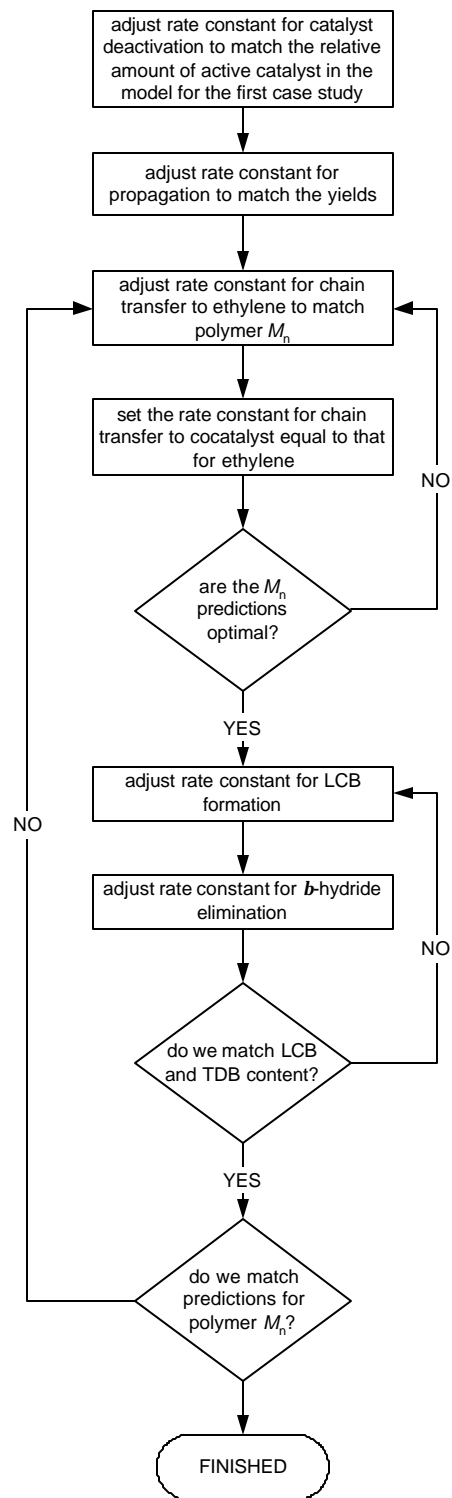
Figure 6-19. The methodology used to adjust the kinetic parameters in case study two.

Table 6-12 gives the final values for the kinetic parameters. The only insight provided in Kokko et al.[44] about kinetic parameters is the ratio of the rate constant for chain transfer to ethylene to the rate constant for chain propagation, k_{tm}/k_p. We compare the predicted value to the experimentally estimated range of values

$$\left(\frac{k_{tm}}{k_p}\right)_{experimental} = 0.00102 - 0.00118$$

$$\left(\frac{k_{tm}}{k_p}\right)_{predicted} = 0.00105$$

(53)

The model predicts a ratio that falls within the estimated range.

The catalyst systems in the two case studies are different, and it is therefore unreasonable to expect that the rate constants will be the same in both cases. The rate constants for chain initiation and propagation are of the same order of magnitude in the two case studies. The rate constants for chain transfer to ethylene, LCB formation, b-hydride elimination, and catalyst deactivation are not different by more than one order of magnitude. Given the large range of orders of magnitude among the kinetic parameters (1.0E0 – 1.0E7), the parameters in the two cases are quite similar.

Table 6-12. Rate constants used in case study two, compared to those used in case study one.

rate constant	description	model value (case study 2)	model value (case study 1)	units
k_{sact}	spontaneous catalyst activation	1.50E4	1.50E4	hr^{-1}
k_{ini}	chain initiation	8.02E7	2.0628E7	m^3/kmol-hr
k_p	chain propagation	8.02E7	2.0628E7	m^3/kmol-hr
k_{tm}	chain transfer to ethylene	8.40E4	1.367E3	m^3/kmol-hr
k_{tc}	chain transfer to cocatalyst	8.40E4	--	m^3/kmol-hr
k_{tdb}	LCB formation	3.43E4	1.00E5	m^3/kmol-hr
k_b	b-hydride elimination	7.00E2	1.10E3	hr^{-1}
k_d	catalyst deactivation	3.30	18.792	hr^{-1}

Figure 6-20 compares experimental data to model predictions for catalyst yield. The model predictions have an average error of 2.0% for the eight modeled runs. This value is lower than in case study one (4.9%), because the yields in case study two are relatively larger, so the relative contribution of error from possible fluctuations in the system is smaller. The monomer feed rate doubles between the first and last runs in this study. This indicates that the model does an excellent job of accounting for the concentration dependence of the rates of chain initiation and propagation.

Figure 6-21 compares experimental data to model predictions for polymer M_n. The average error for the eight runs is 8.1%. As mentioned in case study one, characterization of molecular weight typically has a large error associated with it, and Kokko et al.[44] do not provide estimates with the results. Nevertheless, these predictions are very good. The discrepancies in the figure appear larger than the corresponding values for case study one because the M_n values are roughly half in this case. Note that the average error is about the same as in case study one (8.2%). These results indicate that the model properly accounts for the concentration dependence of the rate of chain transfer to ethylene, which is the primary reaction affecting molecular weight. Cocatalyst contributes only slightly to chain transfer, as indicated by Kokko et al.[44]

Figure 6-22 compares experimental data to model predictions for the number of long-chain branches per 1,000 carbon atoms. The average prediction error is 36%. Figure 6-23 compares experimental data to model predictions for the number of terminal double bonds per 1,000 carbon atoms. The average prediction error is 14.0%. As mentioned in Section 6.3.1.4, when we consider the likely error associated with the characterization techniques and the lack of reproducibility data for the runs, we consider these predictions very good.

In summary, our model does an excellent job of describing the physical and kinetic phenomena for the runs in both case studies.
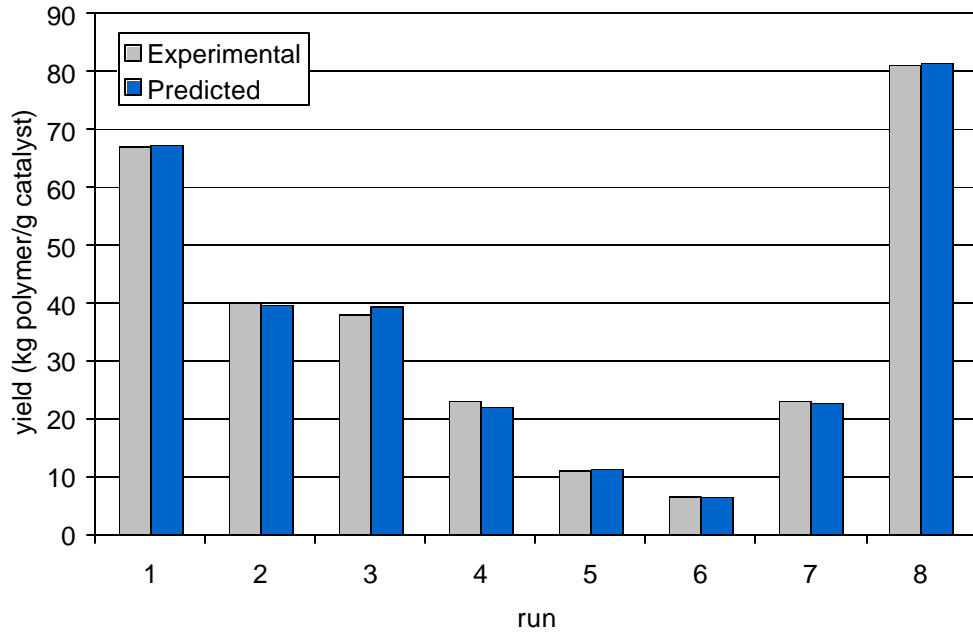
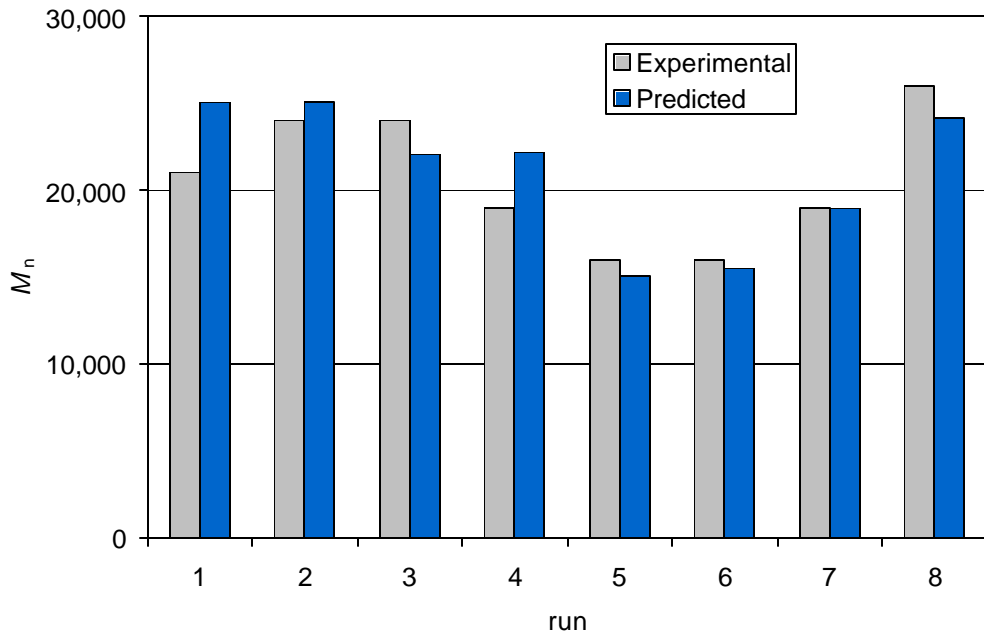**Figure 6-20. Comparing experimental data to model predictions for yield in case study two[44].**

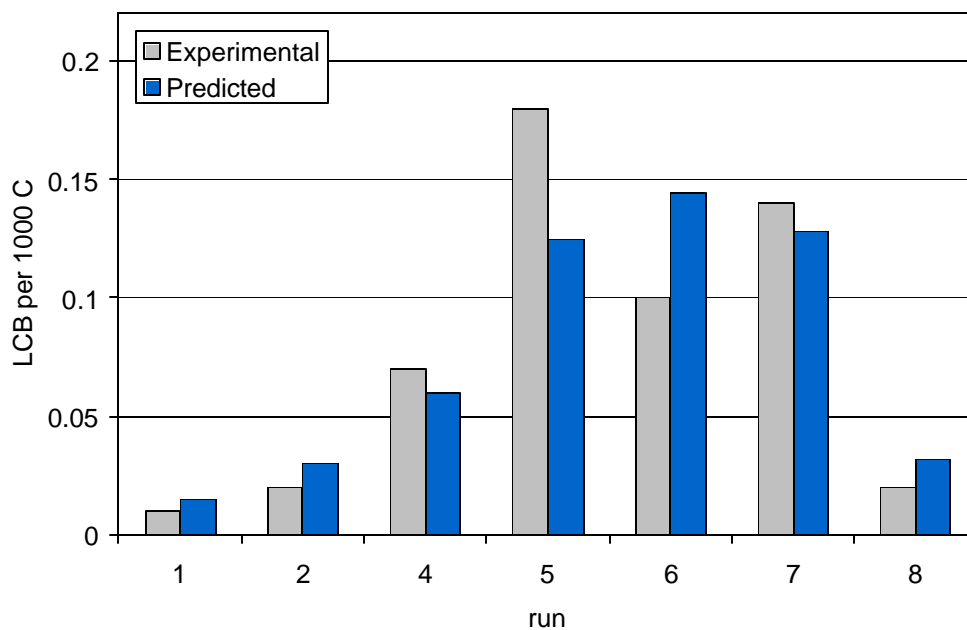**Figure 6-21. Comparing experimental data to model predictions for polymer molecular weight in case study two[44].**

Figure 6-22. Comparing experimental data to model predictions for number of long-chain branches per 1,000 carbon atoms in case study two[44].
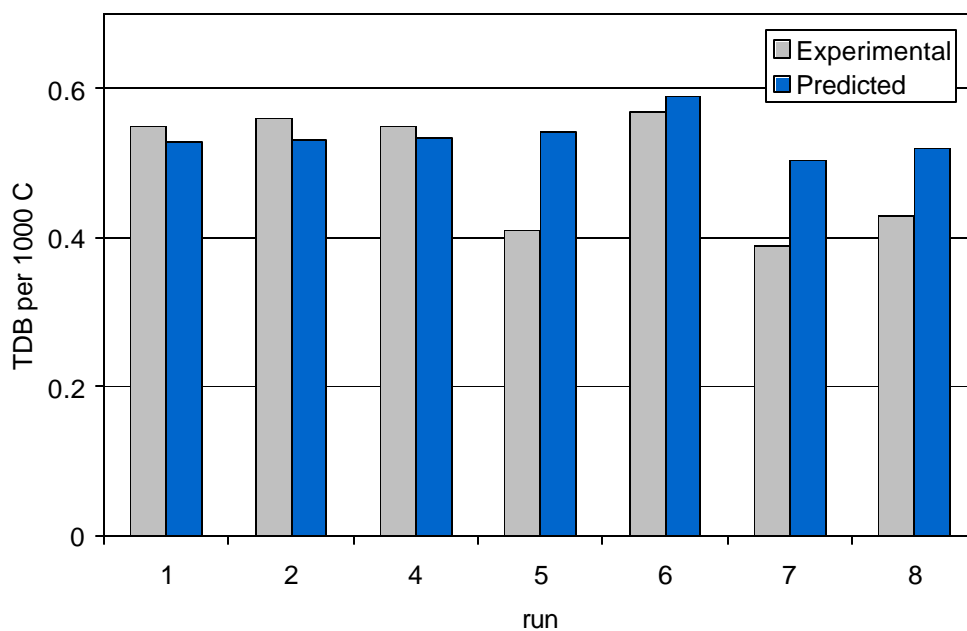

Figure 6-23. Comparing experimental data to model predictions for number of terminal double bonds per 1,000 carbon atoms in case study two[44].

6.4 Model Applications

Sections 6.4.1 and 6.4.2 discuss varying feed rates and reaction kinetics, respectively, for a typical ethylene polymerization. We use kinetic parameters from the validated model presented in case study two (see Table 6-12 in Section 6.3.2.4). Sections 6.4.3 and 6.4.4 quantify and discuss the impact of physical properties and phase equilibrium, respectively, on model predictions. Section 6.4.5 discusses energy-balance applications.

6.4.1 Varying Feed Composition

We vary the feed rates of ethylene, catalyst, hydrogen, and solvent, and illustrate trends in the model predictions. Figures 6-24 and 6-25 show the effect of changing the ethylene feed rate on M_n and ethylene conversion, respectively. The polymer molecular weight increases due to an increase in the rate of propagation. The ethylene conversion also increases, as a result of higher ethylene concentration in the liquid phase relative to other species.

Figures 6-26 and 6-27 illustrate the effect of varying the catalyst feed rate on M_n and ethylene conversion, respectively. Increasing the catalyst feed rate yields a greater number of active sites, leading to a greater number of polymer chains. Since the number of ethylene segments does not change as sharply as the number of polymer chains, the polymer molecular weight (number of segments per chain) decreases.

Figures 6-28 and 6-29 show the effect of changing the solvent feed rate on the polymer M_n and ethylene conversion, respectively. Increasing the solvent flow has a diluting effect on the concentrations of other species, and it also reduces the reactor residence time. A lower residence time yields a decrease in ethylene conversion. Hydrogen, present in trace amounts, is most affected by the dilution of solvent. As a result, chain transfer is reduced and the polymer molecular weight increases.
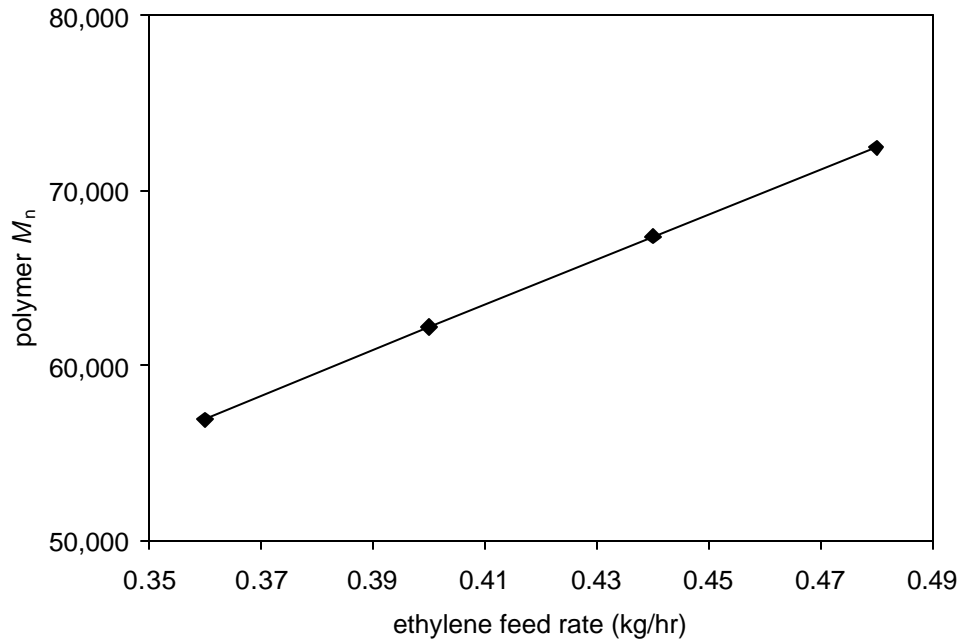
Figure 6-24. The effect of changing the ethylene feed rate on polymer M_n.
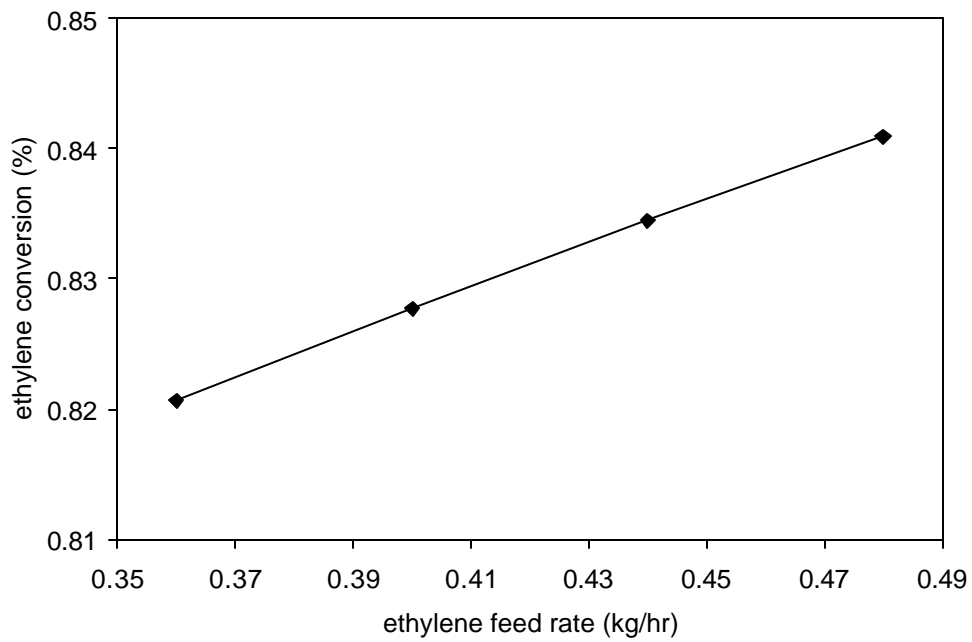

Figure 6-25. The effect of varying the ethylene feed rate on ethylene conversion.
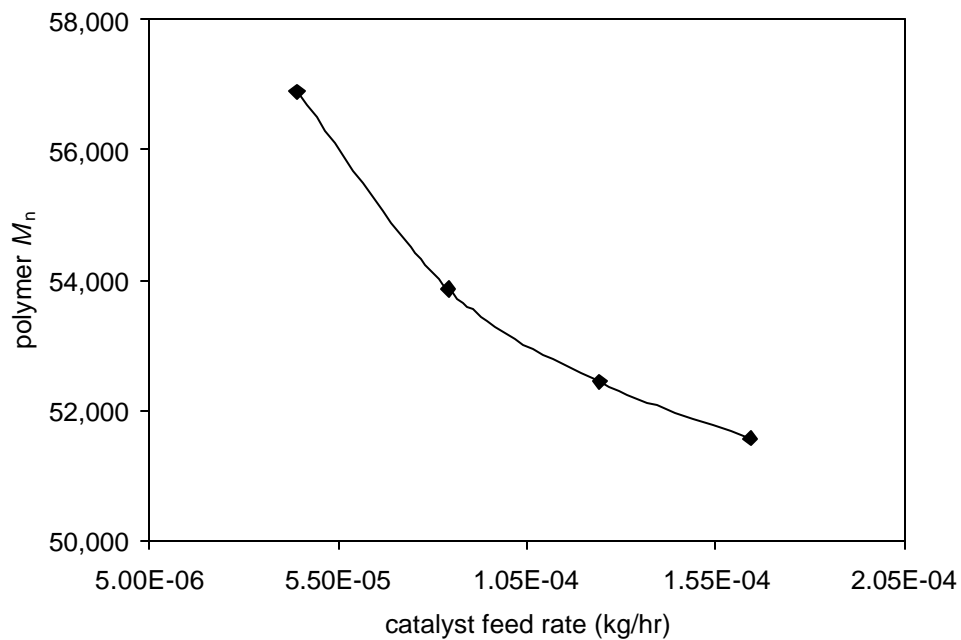
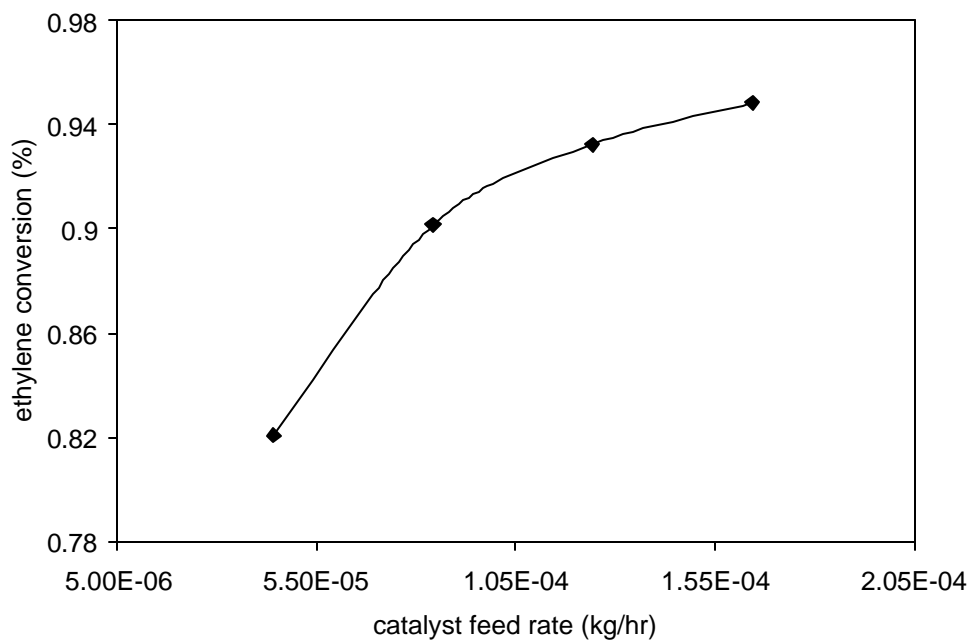**Figure 6-26. The effect of varying the catalyst feed rate on polymer M_n.**

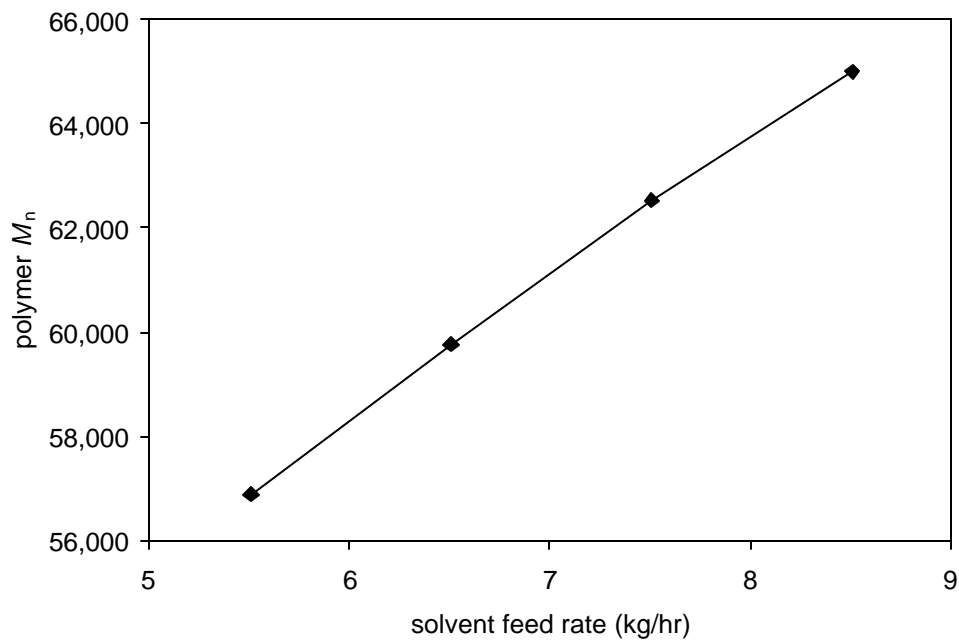**Figure 6-27. The effect of varying the catalyst feed rate on ethylene conversion.**

Figure 6-28. The effect of changing the solvent feed rate on the polymer M_n.
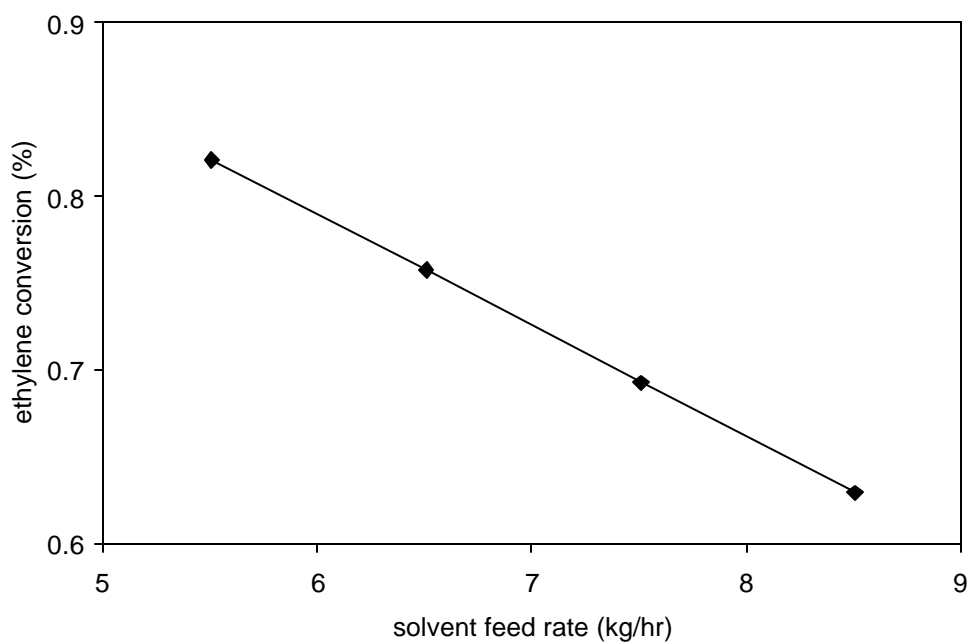

Figure 6-29. The effect of varying the solvent feed rate on ethylene conversion.

6.4.2 Varying Reaction Kinetics

We vary the rate constants for chain propagation, chain transfer to hydrogen, b-hydride elimination, and incorporation of terminal double bonds. Figure 6-30 shows the effect of changing the rate constant for chain propagation on ethylene conversion. As expected, the conversion increases with increasing k_p, leveling out asymptotically as the conversion approaches 100%.

Figure 6-31 illustrates the effect of changing the rate constant for chain transfer to hydrogen on the polymer M_n. Increasing this rate constant lowers the polymer molecular weight due to increased chain transfer.

Figure 6-32 shows the effect of changing the rate constant for b-hydride elimination on the fraction of polymer chains containing terminal double bonds. As b-hydride elimination becomes more frequent, the number of chains with terminal double bonds increases.

Figure 6-33 illustrates the effect of changing the rate constants for incorporation of chains with terminal double bonds and for b-hydride elimination. An increase in k_{tdb} leads to a higher number of long-chain branches due to increased frequency of this corresponding reaction. As the rate constant for b-hydride elimination increases, more chains are present that contain terminal double bonds. As a result, we see an increase in the number of long-chain branches at a given value of k_{tdb}.
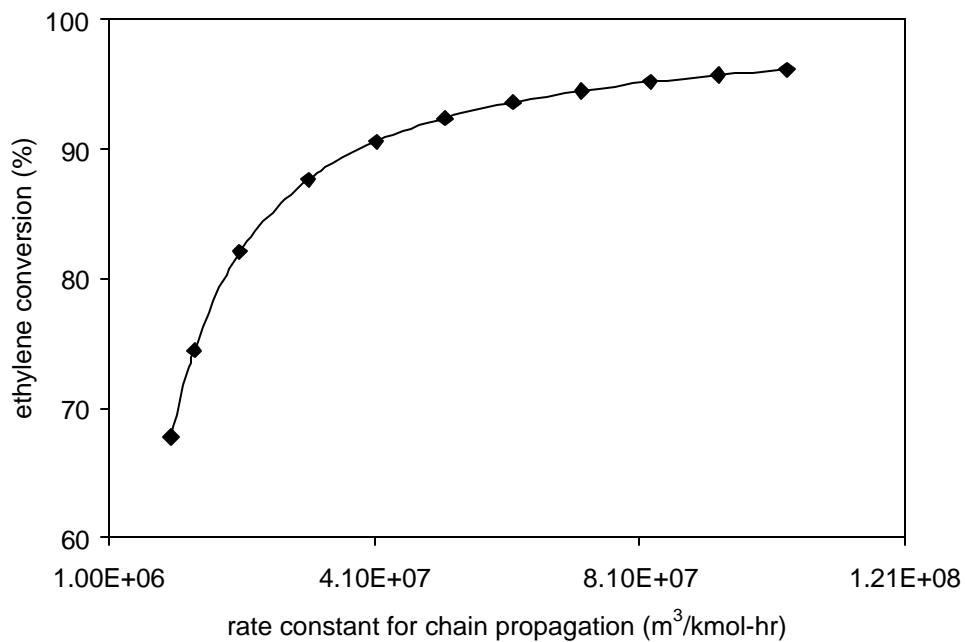
Figure 6-30. The effect of changing the rate constant for chain propagation on ethylene conversion.
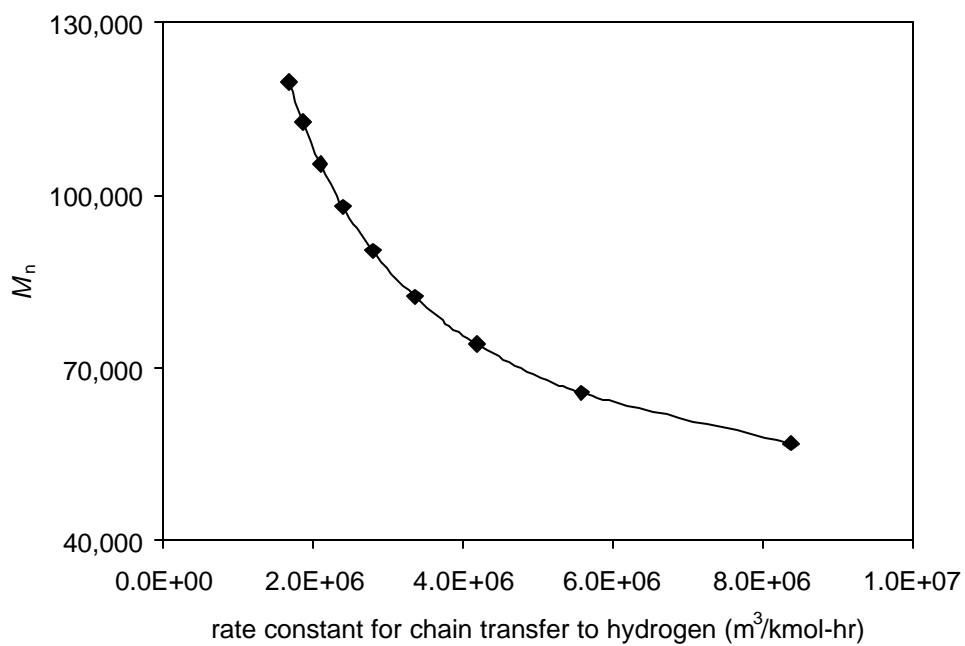
Figure 6-31. The effect of varying the rate constant for chain transfer to hydrogen on the polymer
M_n**.**
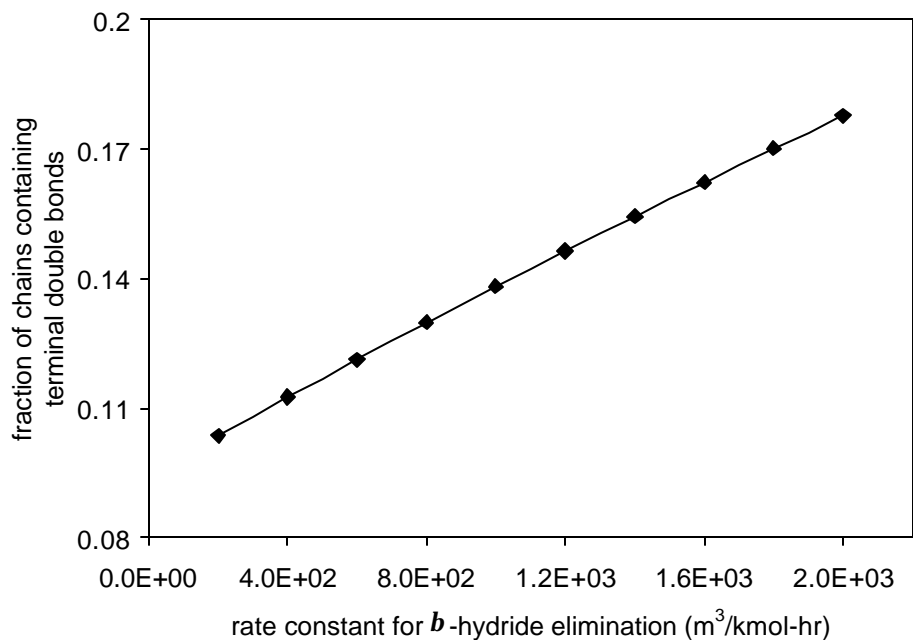
Figure 6-32. The effect of changing the rate constant for b-hydride elimination on the fraction of polymer chains containing terminal double bonds (k_b).
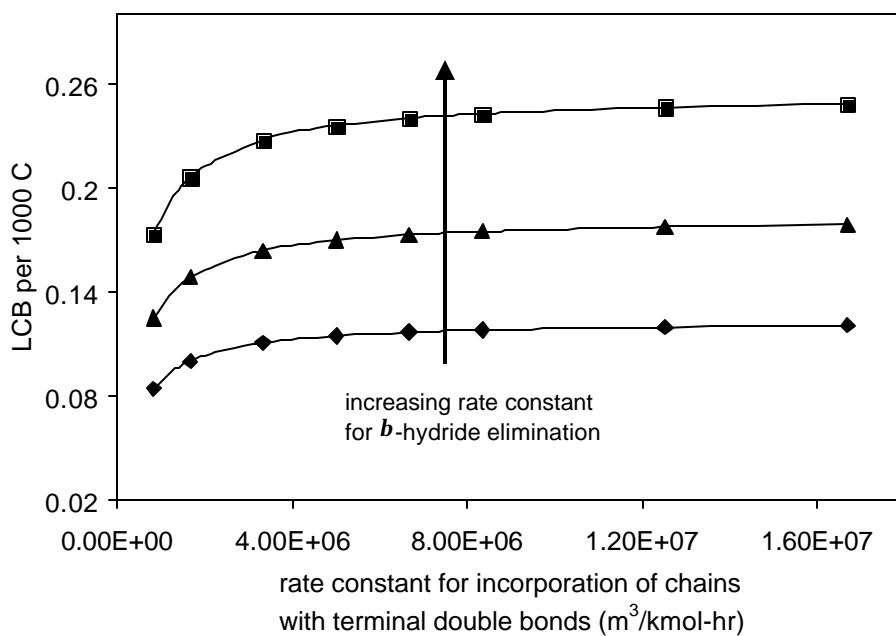
Figure 6-33. The effect of varying the rate constant for incorporation of chains with terminal double bonds on the number of long-chain branches (k_{tdb}).

6.4.3 The Impact of Physical Properties

Vapor and liquid molar volumes play a major role in reactor design because they affect the reactor mass holdup, residence time, and volumetric throughput. In the solution polymerization of ethylene, the solvent is the most abundant species. Figures 6-5 and 6-6 in Section 6.2.3.3.1 show the saturated liquid and vapor molar volumes of toluene, respectively, as a function of temperature. The values vary widely with changing conditions.

We consider an arbitrary mass holdup of 1,000 kg toluene. Figure 6-34 shows the liquid volume as a function of saturation temperature. Depending on the system temperature, the required vessel volume can range from 1.3 to 2.2 m^3, an increase of approximately 70%. In reactor design, we must therefore consider the system conditions when sizing the reactor.
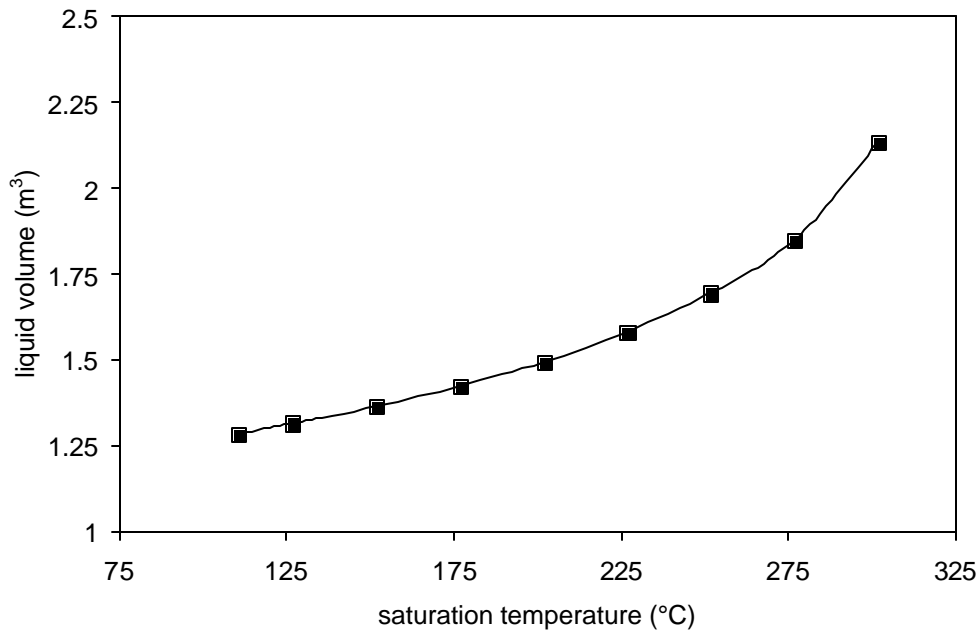
Figure 6-34. The volume displacement of 1,000 kg liquid toluene, as a function of saturation temperature.

We now assume that 5% of the toluene leaves the vessel as a vapor, at a rate of 50 kg/hr. Figure 6-35 shows the volumetric flow rate as a function of saturation temperature. The vapor molar volume changes dramatically with temperature. When designing overhead unit operations, such as compressors, we must take into account the volumetric throughput for proper sizing.
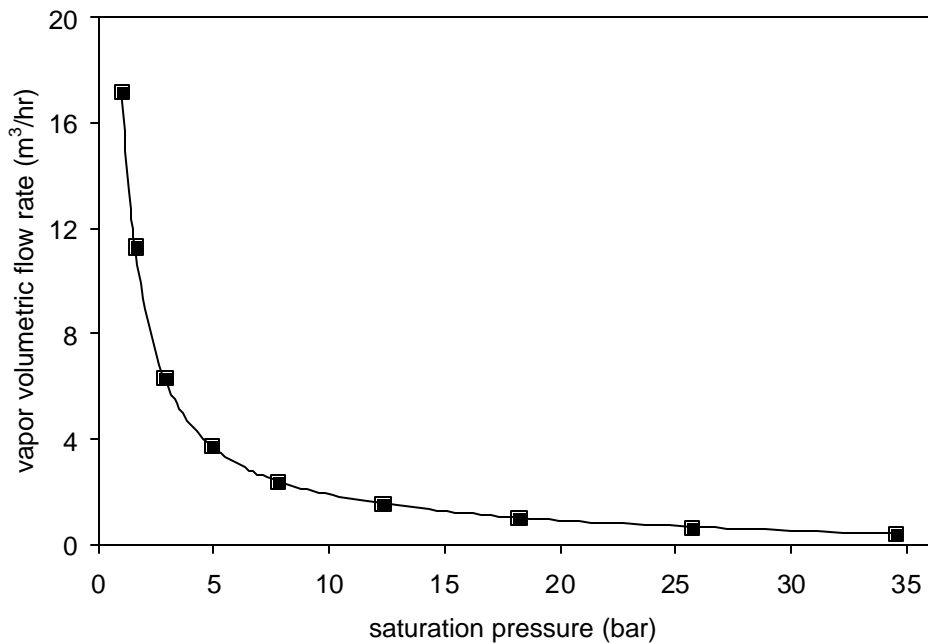
Figure 6-35. The volumetric flow rate of 50 kg/hr vapor toluene, as a function of saturation pressure.

6.4.4 The Impact of Phase Equilibrium

Depending on the system temperature and pressure, the reactor may contain a single liquid phase or both vapor and liquid in equilibrium. When there are two phases present, the solubility of the vapor species in the liquid phase can be important, especially if they are reactants. The polymerization kinetics are functions of the concentrations in the condensed phase. Furthermore, the amount of liquid present at equilibrium determines

the residence time of the condensed phase. A robust model must therefore consider phase equilibrium.

We illustrate the effect of vapor-liquid equilibrium on liquid holdup and residence time by flashing a mixture of ethylene and toluene at various temperatures and pressures. We use a feed rate of 0.36 kg/hr ethylene and 3.65 kg/hr toluene. We use a reactor volume of 600 mL.

Figures 6-36 and 6-37 show the effect of vessel conditions on the calculated liquid holdup and condensed-phase residence time, respectively. The liquid holdup decreases with increasing temperature, due to vaporization. As a result, the residence time also decreases with increasing temperature. Higher pressures force more material to remain in the liquid phase. This leads to higher liquid holdups and residence times, as shown in the figures.
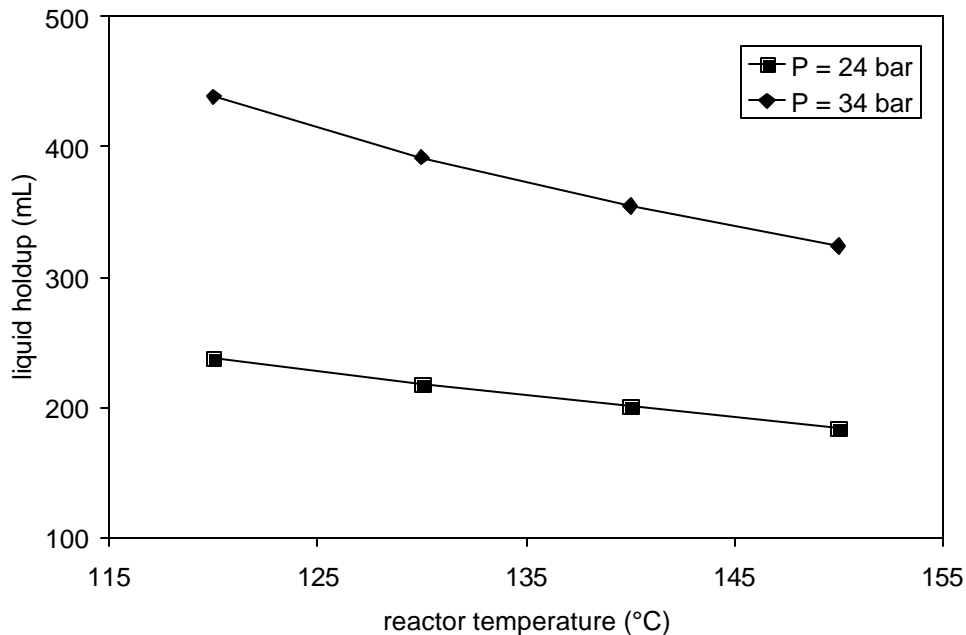
Figure 6-36. Illustrating the effect of reactor temperature on equilibrium liquid holdup.
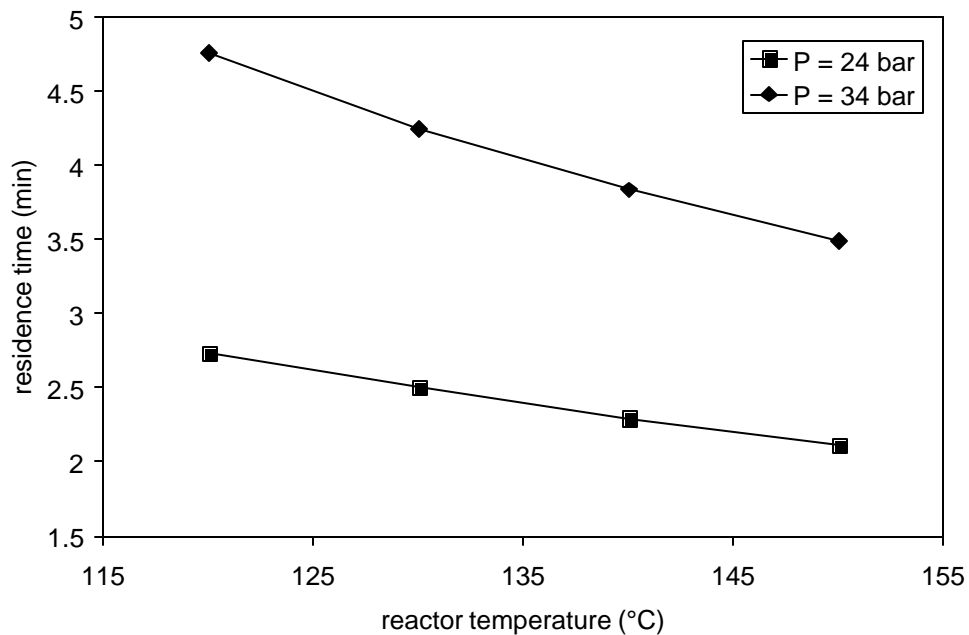
Figure 6-37. Showing the effect of temperature on residence time, corresponding to the results in Figure 6-36.

Next, we illustrate the effect of changing residence time on the predicted polymer properties. We consider run #1 from case study two (see Section 6.3.2). We vary the residence time by adjusting the solvent feed rate. Figure 6-38 shows that increasing the residence time yields a higher monomer conversion, as expected. The other polymer properties do not change considerably in this case because, in essence, we have diluted the reaction medium to varying degrees with the solvent, and therefore the concentrations of all species are affected equally.
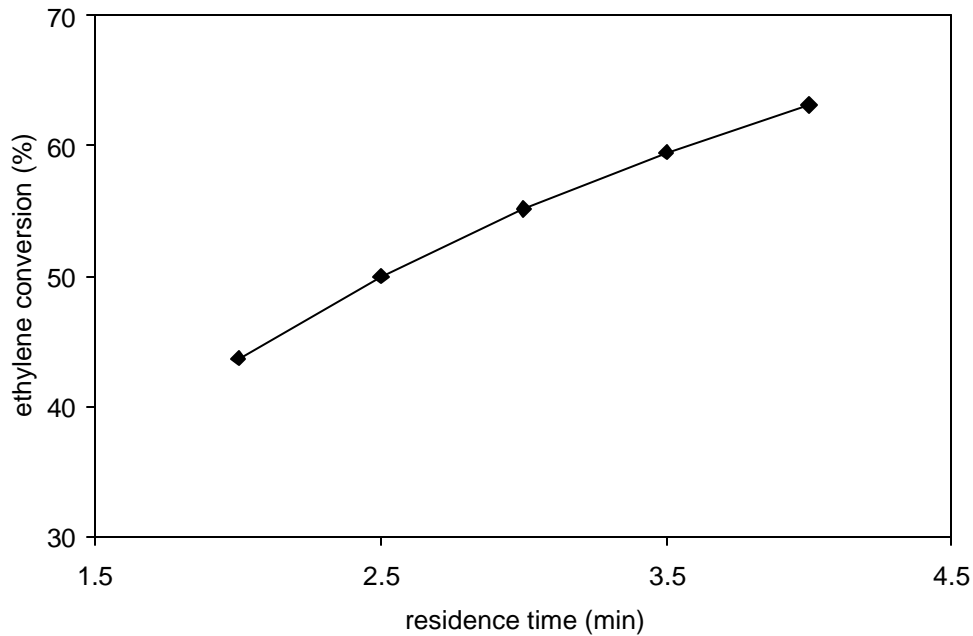
Figure 6-38. The effect of changing the reactor residence time on ethylene conversion.

Figure 6-39 shows the effect of changing the vessel conditions on the equilibrium mole fraction of ethylene in the liquid phase. Decreasing temperature and increasing pressure both increase the amount of ethylene in the liquid phase. Specifically, at a given temperature, a pressure increase of 10 bar yields an increase in the ethylene liquid mole fraction of more than 25%. This affects the rate of polymerization significantly. We compute the rate of polymerization using

$$r_{polymerization} = k_p [M] I_0 \tag{54}$$

This relation reveals that the rate of polymerization is proportional to the liquid mole fraction of ethylene

$$r_{polymerization} \propto x_{ethylene} \tag{55}$$

Therefore, at constant concentration of live polymer chains and rate constant for propagation, any change in the ethylene liquid mole fraction translates to the same percentage change in the rate of polymerization.
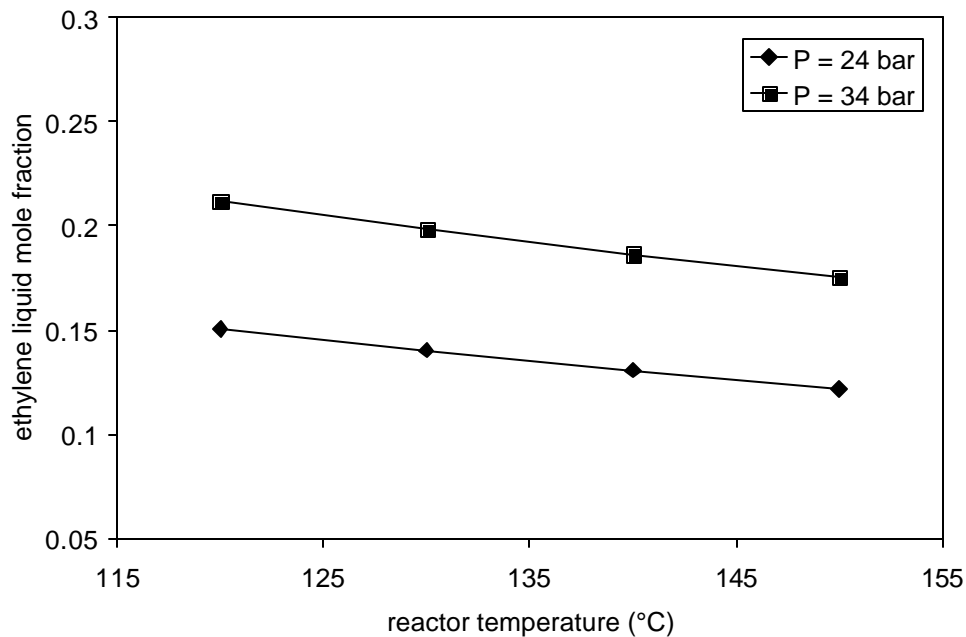
Figure 6-39. Illustrating the effect of changing the reactor temperature on the liquid mole fr action of ethylene.

6.4.5 Energy-Balance Applications

We illustrate the utility of energy-balance calculations by performing simulations and computing the cooling duty required to keep the reactor at a constant temperature. We use heat capacity to compute enthalpy values for the inlet and outlet streams. We validate the predictions for heat capacity in Section 6.2.3.3.2. Table 6-13 gives the stream flow rates and conditions for a simplified polymerization scheme. Ethylene enters as a vapor at 25 °C, and the toluene enters as a liquid, which is preheated to 100 °C. We assume complete conversion of the ethylene to polymer.

stream	kg/hr	T (°C)	P (bar)	phase
ethylene feed	0.36	25	35	vapor
toluene feed	3.65	100	35	liquid
product	4.01	reactor	35	liquid

Figure 6-40 shows the required cooling duty as a function of reactor temperature. The
model predicts that the cooling duty decreases as the reactor temperature increases. This
occurs because the polymerization is exothermic, and we require less removal of heat as
the steady-state reactor temperature increases.
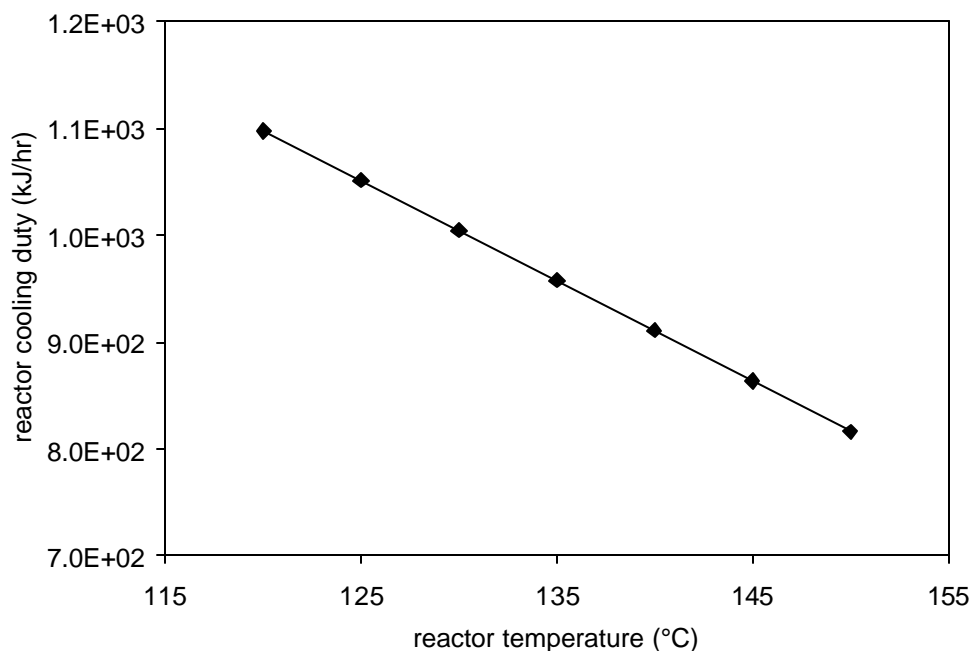
Figure 6-40. Illustrating the effect of reactor temperature on the reactor cooling duty.

Next, we vary the temperature of the solvent feed stream to determine the effect on the reactor cooling duty. Table 6-14 shows the feed flow rates and conditions. We again assume a complete conversion of ethylene.

Table 6-14. Stream flow rates and conditions for a simplified polymerization scheme. We vary the product temperature, which is equal to the reactor temperature.

stream	kg/hr	T (°C)	P (bar)	phase
ethylene feed	0.36	25	35	vapor
toluene feed	3.65	vary	35	liquid
product	4.01	140	35	liquid

Figure 6-41 illustrates the predicted trend. The reactor cooling duty decreases as the toluene feed temperature decreases. This occurs because the solvent absorbs the heat of polymerization. In order to save on energy costs, it is therefore desirable to feed the solvent at a lower temperature.
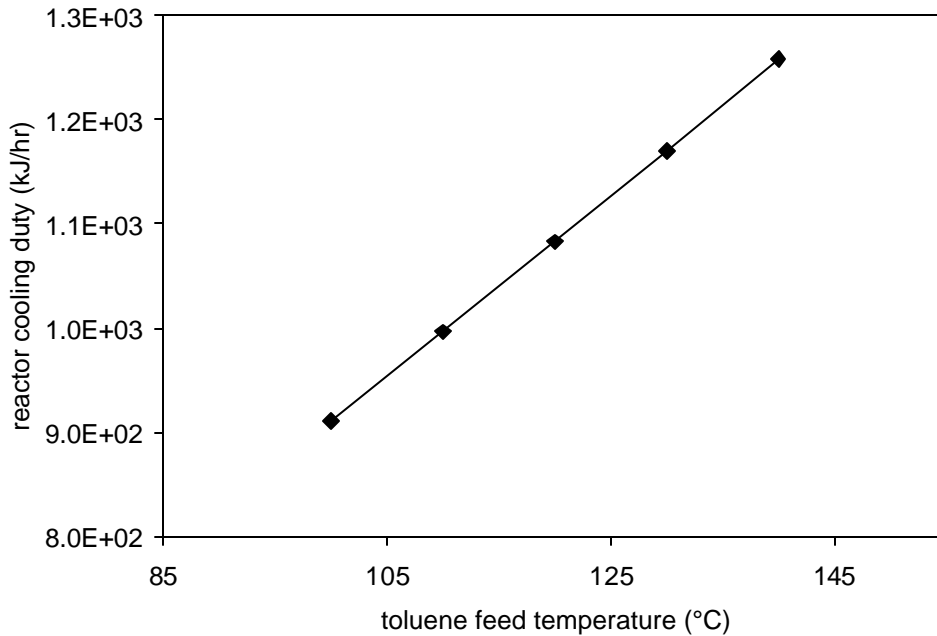
Figure 6-41. The effect of solvent feed temperature on the reactor cooling duty.

270

6.5 Conclusions

We present a reactor model for the continuous solution polymerization of ethylene using a metallocene catalyst system. Modeling considerations include mass and energy balances, physical properties, phase equilibrium, and polymerization kinetics. Predicted polymer properties include number- and weight-average molecular weights, number of long-chain branches, and number of terminal double bonds. Models for this type of system presented in the literature focus only on polymerization kinetics, and do not include physical and thermodynamic properties, or phase equilibrium. We validate the model using literature data for two bench-scale polymerization experiments. We use values for kinetic parameters that are within the estimated ranges provided. The model matches experimental data for catalyst yield with an average error of 4.9% and 2.0%, for case studies 1 and 2, respectively. Predictions for polymer M_n are within 8.2% and 8.1%. For the number of long-chain branches, the average prediction errors are 22% and 36%. Finally, for number of terminal double bonds, the average errors are 17% and 14% for case studies 1 and 2, respectively. In light of the likely experimental error due to characterization techniques, and the lack of reproducibility data for any of the runs, we consider these predictions very good. In summary, the presented model does an excellent job of describing the physical and kinetic phenomena for the runs in both case studies.

Recommendations for future study include the repetition of similar polymerization runs to determine the relative error due to fluctuations in the reactor conditions, and the extension of the current modeling considerations to include rheological properties of the polymer. By considering the flow properties of polymers with long-chain branches, a model can link catalyst behavior in the reactor to the resulting molecular architecture.

Symbols

English

a^{pert}	perturbation contribution to the residual molar Helmholtz energy, J/kmol
a^{ref}	reference contribution to the residual molar Helmholtz energy, J/kmol
a^{res}	residual molar Helmholtz energy, J/kmol
C	carbon atom
C_i	molar concentration of species i in liquid phase, kmol/m^3
CAT	catalyst
COCAT	cocatalyst
CSTR	continuous stirred-tank reactor
D_n	inactive polymer chain containing n monomer segments
$D_n^=$	inactive polymer chain with a terminal double bond, containing n monomer segments
DCAT	deactivated catalyst
EOS	equation of state
F_i	outlet molar flow rate of species i, kmol/hr
$F_{i,\text{in}}$	inlet molar flow rate of species i, kmol/hr
h	mass enthalpy, kJ/kg
k_{ac}	rate constant for catalyst activation by cocatalyst, m^3/kmol-hr
k_B	Boltzmann's constant, J/K
k_{ini}	rate constant for chain initiation, m^3/kmol-hr
k_{p}	rate constant for chain propagation, m^3/kmol-hr
k_{sact}	rate constant for spontaneous catalyst activation, hr^{-1}
k_{sd}	rate constant for spontaneous catalyst deactivation, hr^{-1}
k_{tc}	rate constant for chain transfer to cocatalyst, m^3/kmol-hr
k_{tdb}	rate constant for insertion of chain with terminal double bond, m^3/kmol-hr
k_{th}	rate constant for chain transfer to hydrogen, m^3/kmol-hr
k_{tm}	rate constant for chain transfer to monomer, m^3/kmol-hr
$k_{\boldsymbol{b}}$	rate constant for $\boldsymbol{b}$-hydride elimination, hr^{-1}
LCB	long-chain branch

[LCB]	molar concentration of long chain branches in liquid phase, kmol/m^3
m	characteristic chain length for conventional species in the PC-SAFT EOS
M	monomer
m^L	liquid mass, kg
m^V	vapor mass, kg
m^{tot}	total reactor mass, kg
M_n	number-average molecular weight, g/mol
M_w	weight-average molecular weight, g/mol
MW_i	molecular weight of species i, g/mol
MW_{seg}	segment molecular weight, g/mol
$\dot{m}_i$	mass flow rate of species i, kg/hr
$\dot{m}^L$	liquid mass flow rate, kg/hr
$\dot{m}_{in}$	inlet mass flow rate, kg/hr
$\dot{m}^V$	vapor mass flow rate, kg/hr
n	number of monomer segments in a given polymer chain
N_{cat}	moles of catalytic sites per unit mass of catalyst, kmol/kg
P	pressure, bar
P_0	activated catalyst site
P_1	initiated polymer chain
P_c	critical pressure, bar
P_n	polymer chain containing n segments
PC-SAFT	Perturbed-Chain Statistical Associating Fluid Theory equation of state
PDI	polydispersity index
PE	polyethylene
Q_{duty}	reactor cooling duty, kJ
Q^L	liquid-phase volumetric flow rate, m^3
r	size parameter for polymer species in the PC-SAFT EOS; ratio of the characteristic chain length to the number average molecular weight, mol/g
r_i	molar rate of reaction of species i, kmol/m^3-hr
T	temperature, °C

T_c	critical temperature, K
TDB	terminal double bond
V	reactor volume, m^3
V^L	liquid-phase volume, m^3
V^V	vapor-phase volume, m^3
$x_{m,i}$	liquid mass fraction of species i
$y_{m,i}$	vapor mass fraction of species i
X_{TDB}	fraction of polymer chains containing a terminal double bond
$z_{m,i}$	mass fraction of species i
$z_{m,i,in}$	inlet mass fraction of species i

Greek

$\boldsymbol{e}$	segment energy parameter in the PC-SAFT EOS, J
$\boldsymbol{l}_i$	i^{th} moment for active polymer chains
$\boldsymbol{m}_i$	i^{th} moment for dead polymer chains
$\boldsymbol{\bar{m}_i}$	i^{th} moment for dead polymer chains containing a terminal double bond
$\boldsymbol{r}^L$	liquid mixture mass density, kmol/m^3
$\boldsymbol{r}^V$	vapor mixture mass density, kmol/m^3
$\boldsymbol{s}$	segment characteristic diameter in the PC-SAFT EOS, Å
$\boldsymbol{t}$	residence time, hr
$\boldsymbol{t}^L$	liquid-phase residence time, hr

6.6 Appendix

Code implemented in Aspen Custom Modeler, using Visual Basic Script language.

```
Model CSTR
//Written by Neeraj P. Khare
//Department of Chemical Engineering
//Virginia Polytechnic Institute and State University
//Blacksburg, VA 24061
```

```
//****************************************
//Variable Declarations
//****************************************
Available_Sites    as pos_large        (Description:"Total Moles Available Catalyst Sites");
C_EmptyLiveSite as pos_large           (scale:1e-8,Description:"Empty Live Catalyst Site Concentration");
C_EmptyLiveSite_in as pos_large        (scale:1e-8,fixed,Description:"Empty Live Catalyst Site Concentration");
C_Lambda0      as pos_large            (scale:1e-5,0.0001,Description:"Zeroth Live Moment Concentration");
C_Lambda0_in    as pos_large (scale:1e-5,fixed,0.0001,Description:"Zeroth Live Moment Concentration");
C_Lambda1      as pos_large            (0.1,Description:"First Live Moment Concentration");
C_Lambda1_in    as pos_large          (fixed,0.1,Description:"First Live Moment Concentration");
C_Lambda2      as pos_large            (scale:1e4,100,Description:"Second Live Moment Concentration");
C_Lambda2_in    as pos_large          (scale:1e4,fixed,100,Description:"Second Live Moment Concentration");
C_in(Componentlist) as pos_large (scale:1e-5,Description:"Inlet Molar Concentration");
C_LCB  as flow_mol        (scale:1e-5,Description:"Number of LCBs per Chain");
LCBper1000C     as pos_large          (scale:1e-5,Description:"Number of LCBs per 1000 Cs");
C_Liq(ComponentList)      as conc_mole      (scale:1e-4,Description:"Liquid Molar Concentration");
C_Mu0   as pos_large      (scale:1e-5,0.001,Description:"Zeroth Dead Moment Concentration");
C_Mu0_in as pos_large      (scale:1e-5,fixed,0.001,Description:"Zeroth Dead Moment Concentration");
C_Mu1   as pos_large      (10.0,Description:"First Dead Moment Concentration");
C_Mu1_in as pos_large      (fixed,10.0,Description:"First Dead Moment Concentration");
C_Mu2   as pos_large      (scale:1e3,1000,Description:"Second Dead Moment Concentration");
C_Mu2_in as pos_large      (scale:1e3,fixed,1000,Description:"Second Dead Moment Concentration");
C_Mu3   as pos_large      (100000,Description:"Third Dead Moment Concentration");
C_Mu3_in as pos_large      (fixed,100000,Description:"Third Dead Moment Concentration");
C_MuTDB0 as pos_large      (scale:1e-5,0.001,Description:"Zeroth Dead TDB Moment Concentration");
C_MuTDB0_in as pos_large (scale:1e-5,fixed,0.001,Description:"Zeroth Dead TDB Moment
Concentration");
C_MuTDB1 as pos_large      (0.2,Description:"First Dead TDB Moment Concentration");
C_MuTDB1_in    as pos_large      (fixed,0.2,Description:"First Dead TDB Moment Concentration");
C_MuTDB2 as pos_large      (scale:1e3,200,Description:"Second Dead TDB Moment Concentration");
C_MuTDB2_in as pos_large (scale:1e3,fixed,200,Description:"Second Dead TDB Moment Concentration");
C_Vap(ComponentList)      as conc_mole      (scale:1e-5,Description:"Vapor Molar Concentration");
comp_mass_out(componentlist) as flow_mass          (scale:1e-3);
conversion        as pos_small      (Description:"Monomer Conversion");
denominatorx                 as pos_large;
denominatory                 as pos_large;
denominatorz                 as pos_large;
denomPcx(ComponentList) as pos_large                            (scale:1e-8);
denomPcy(ComponentList) as pos_large                            (scale:1e-8);
denomPcz(ComponentList) as pos_large                            (scale:1e-8);
density          as dens_mol;
Eaact                        as pos_large                            (Fixed,0);
```

```
Eaactm            as pos_large                    (Fixed,0);
Eabeta            as pos_large                    (Fixed,0);
Eadp              as pos_large                    (Fixed,0);
Eai               as pos_large                    (Fixed,0);
Eap               as pos_large                    (Fixed,0);
Easact            as pos_large                    (Fixed,0);
Easd              as pos_large                    (Fixed,0);
Eatdb             as pos_large                    (Fixed,0);
Eath              as pos_large                    (Fixed,0);
Eatm              as pos_large                    (Fixed,0);
hml               as enth_mass_liq    (Description:"Liquid mass enthalpy");
hmv               as enth_mass_vap    (Description:"Vapor mass enthalpy");
kact              as pos_large                    (scale:1e5);
kact0             as pos_large                    (scale:1e5,Fixed);
kactm             as pos_large;
kactm0            as pos_large                    (Fixed);
kbeta             as pos_large                    (/*lower:0,upper:2063.03976*/);
kbeta0            as pos_large                    (Fixed);
ki                as pos_large                    (scale:1e7);
ki0               as pos_large                    (scale:1e7,Fixed);
kp                as pos_large         (scale:1e7/*lower:12168000,upper:34884000*/);
kp0               as pos_large                    (scale:1e7,Fixed);
ksact             as pos_large                    (scale:1e7);
ksact0            as pos_large                    (scale:1e7,Fixed);
ksd               as pos_large                    (scale:10/*lower:13.644,upper:23.94*/);
ksd0              as pos_large                    (scale:10,Fixed);
ktc               as pos_large                    (free);
ktc0              as pos_large                    ;
ktdb              as pos_large                    (/*lower:759283.2,upper:3467469.6*/);
ktdb0             as pos_large                    (Fixed);
kth               as pos_large                    (/*lower:1946880,upper:22744368*/);
kth0              as pos_large                    (Fixed);
ktm               as pos_large                    (/*lower:936.936,upper:14616.396*/);
ktm0              as pos_large                    (Fixed);
LCBD              as pos_large         (Description:"Number of branching points per carbon atom");
LCBDDiff          as pos_large;
LCBDTarget        as pos_large                    (fixed,1);
LCBperChain       as pos_large;
Liq_Flow_Out      as flow_Vol                     (Description:"Liquid Volumetric Flow Out");
Liq_Mass          as pos_large                    (Description:"Liquid Mass Holdup");
liq_mol_Cat       as flow_mol                     (Description:"SS Catalyst Molar Flowrate");
liq_mol_Cocat     as flow_mol            (Description:"SS Cocatalyst Molar Flowrate");
```

```
liq_mol_Ethylene as flow_mol                        (Description:"SS Ethylene Molar Flowrate");
liq_mol_H2              as flow_mol                  (Description:"SS H2 Molar Flowrate");
liq_mol_Solvent         as flow_mol                  (Description:"SS Solvent Molar Flowrate");
liq_mol_PE              as flow_mol                  (Description:"SS PE Molar Flowrate");
Liq_Moles               as pos_large                 (Description:"Liquid Molar Holdup");
Liq_Vol        as volume                 (fixed,Description:"Liquid Volume");
Liq_Vol2       as volume                 (fixed);
mass_Cat_in             as flow_mass                 (scale:1e-5);
mass_Cat2_in            as flow_mass;
mass_Cocat_in           as flow_mass                 (scale:1e-5);
mass_Ethylene_in        as flow_mass;
mass_H2_in              as flow_mass                 (scale:1e-5);
mass_Solvent_in as flow_mass;
mass_in(Componentlist)    as flow_mass(fixed);
mass_out(Componentlist) as flow_mass;
mass_liq_out(Componentlist) as flow_mass;
mass_PE_in              as flow_mass;
mass_vap_out(Componentlist) as flow_mass;
max_sites as pos_small    (scale:1e-4,fixed,0.0001,Description:"kmol Potential Sites per kg Catalyst");
Mn                      as pos_large      (scale:1e5,Description:"Number Average Molecular Weight");
MnDiff                  as realvariable;
MnTarget                as pos_large                  (scale:1e5);
mol_Cat_in              as flow_mol       (scale:1e-5,1,fixed,Description:"Inlet Catalyst Molar Flowrate");
mol_Cat2_in             as flow_mol       (1,fixed,Description:"Inlet Catalyst2 Molar Flowrate");
mol_Cocat_in    as flow_mol        (scale:1e-5,1,fixed,Description:"Inlet Cocatalyst Molar Flowrate");
mol_Ethylene_in as flow_mol        (1,fixed,Description:"Inlet Ethylene Molar Flowrate");
mol_H2_in               as flow_mol       (scale:1e-5,1,fixed,Description:"Inlet H2 Molar Flowrate");
mol_Solvent_in          as flow_mol       (1,fixed,Description:"Inlet Solvent Molar Flowrate");
mol_PE_in               as flow_mol       (0,fixed,Description:"Inlet PE Molar Flowrate");
moles_in(Componentlist) as flow_mol;
MolWt(ComponentList)    as molweight;
Mw                      as pos_large      (Description:"Weight Average Molecular Weight");
P                       as pressure       (1.01325,Fixed);
P_fake                  as pressure       (1,fixed);
Pbar                    as pressure;
PDI                     as pos_large      (Description:"Polydispersity Index");
PDIDiff                 as realvariable;
R                       as constant       (8.314,Fixed,Description:"Gas Constant");
rate_Cat                as realvariable   (scale:1e-4);
rate_Lambda0            as realvariable   (scale:1e-6);
rate_Lambda1            as realvariable   (scale:1e-2);
rate_Lambda2            as realvariable   (scale:1e2);
```

277

```
rate_Cat2              as realvariable;
rate_Cocat             as realvariable;
rate_EmptyLiveSite     as realvariable   (scale:1e-9);
rate_Ethylene          as realvariable   (scale:1e2);
rate_H2        as realvariable           (scale:1e-3);
rate_Solvent           as realvariable                   (scale:1);
rate_LCB               as realvariable                   (scale:1e-4);
rate_Mu0               as realvariable                   (scale:1e-2);
rate_Mu1               as realvariable                   (scale:1e2);
rate_Mu2               as realvariable                   (scale:1e4);
rate_MuTDB0            as realvariable                   (scale:1e-3);
rate_MuTDB1            as realvariable                   (scale:1);
rate_MuTDB2            as realvariable                   (scale:1e4);
rate_PE               as realvariable                   (scale:1e2);
Reac_mass             as pos_large                      (Description:"Total Mass Holdup");
Reac_moles            as pos_large                      (Description:"Total Molar Holdup");
Reac_Vol              as volume                         (fixed,Description:"Reactor Volume");
rho_L                 as dens_mol;
rho_V                 as dens_mol;
rhom_L                as dens_mass;
rhom_L_fake           as dens_mass;
rhom_V                as dens_mass;
scale                 as pos_large                      (fixed,1);
Segments              as hidden stringset               (ComponentList.Option("Segments"));
sflowc(Segments)      as seg_mass                       (5.092257143,Description:"segment flow");
smomc          as smom_mass                      (Fixed,0,Description:"second moment");
T                     as temperature                    (30,Fixed);
T_fake                as temperature                    (77,fixed);
Tau                   as time_          (Description:"Total Residence Time");
Tau_Liq        as time_                 (900,Description:"Liquid Residence Time");
Tau_Vap               as time_          (900,Description:"Vapor Residence Time");
Tbar                  as temperature;
TDBDiff               as pos_large;
TDBper1000C           as pos_large                      (Description:"Number of TDBs per 1000 Cs");
TDBperC               as pos_large                      (Description:"Number of TDBs per C");
TDBTarget             as pos_large            (fixed,1);
temp                  as realvariable;
tmomc                  as tmom_mass            (fixed,0,Description:"third moment");
tot_mass_in           as flow_mass;
tot_mass_liq_out      as flow_mass;
tot_mass_out          as flow_mass;
tot_mass_vap_out      as flow_mass;
```

```
V                         as volume                        (Fixed);
Vaact                     as pos_large                     (Fixed,0);
Vaactm                    as pos_large                     (Fixed,0);
Vabeta                    as pos_large                     (Fixed,0);
Vadp                      as pos_large                     (Fixed,0);
Vai                       as pos_large                     (Fixed,0);
Vap                       as pos_large                     (Fixed,0);
Vap_Flow_Out              as flow_Vol                      (Description:"Vapor Volumetric Flow Out");
Vap_Mass                  as pos_large                     (Description:"Vapor Mass Holdup");
vap_mol_Cat               as flow_mol                      (Description:"SS Catalyst Molar Flowrate");
vap_mol_Cat2              as flow_mol                      (Description:"SS Catalyst2 Molar Flowrate");
vap_mol_Cocat             as flow_mol                      (Description:"SS Cocatalyst Molar Flowrate");
vap_mol_Ethylene          as flow_mol                      (Description:"SS Ethylene Molar Flowrate");
vap_mol_H2                as flow_mol                      (Description:"SS H2 Molar Flowrate");
vap_mol_Solvent           as flow_mol                      (Description:"SS Solvent Molar Flowrate");
vap_mol_PE                as flow_mol                      (Description:"SS PE Molar Flowrate");
Vap_Moles                 as pos_large                     (Description:"Vapor Molar Holdup");
Vap_Vol                   as volume                        (Description:"Vapor Volume");
Vasact                    as pos_large                     (Fixed,0);
Vasd                      as pos_large                     (Fixed,0);
Vatdb                     as pos_large                     (Fixed,0);
Vath                      as pos_large                     (Fixed,0);
Vatm                      as pos_large                     (Fixed,0);
vf                        as output vapmassfraction        (Description:"Mass based Vapor fraction");
x(ComponentList)          as molefraction;
xm(componentlist)         as output massfraction           (Description:"Liquid Mass fractions");
Xtdb                      as pos_small;
y(ComponentList)          as molefraction;
yield                     as pos_large                     (Description:"kg pol/g cat");
yieldDiff                 as realvariable;
yieldTarget               as pos_small;
ym(componentlist)         as output massfraction           (Description:"Vapor Mass fractions");
z(ComponentList)          as molefraction;
zm(ComponentList)         as massfraction                  (1/7);
zmfake(componentlist)     as massfraction;
zmomc                     as zmom_mass                     (0.014285714,Description:"zeroth moment");
Lambda0                   as pos_large;
Lambda1                   as pos_large;
Lambda2                   as pos_large;
Mu0                       as pos_large;
Mu1                       as pos_large;
Mu2                       as pos_large;
```

```
MuTDB0                    as pos_large;
MuTDB1                    as pos_large;
MuTDB2                    as pos_large;
EmptyLiveSite             as pos_large;
LCB                       as pos_large;
convDiff        as pos_large;
convTarget                as pos_large;
//-------------------------------------------------------------------------------------------------
//Model Equations
//-------------------------------------------------------------------------------------------------

MnDiff/(MnDiff + 1e-10) = abs(Mn - MnTarget)/MnTarget*100/(MnDiff + 1e-10);
LCBDDiff/(LCBDDiff + 1e-10) = abs(LCBD - LCBDTarget)/LCBDTarget*100/(LCBDDiff + 1e-10);
YieldDiff/(YieldDiff + 1e-10) = abs(yield - yieldTarget)/yieldTarget*100/(YieldDiff + 1e-10);
TDBDiff/(TDBDiff + 1e-10) = abs(TDBperC - TDBTarget)/TDBTarget*100/(TDBDiff + 1e-10);
convDiff/(convDiff + 1e-10) = abs(conversion - convTarget)/convTarget*100/(convDiff + 1e-10);

//Arrhenius Expressions
kact/(kact + 1e-10) = kact0/(kact + 1e-10);
kactm/(kactm + 1e-10) = kactm0/(kactm + 1e-10);
ksact/(ksact + 1e-10) = ksact0/(ksact + 1e-10);
ki/(ki + 1e-10) = ki0/(ki + 1e-10);
kp/(kp + 1e-10) = kp0/(kp + 1e-10);
kth/(kth + 1e-10) = kth0/(kth + 1e-10);
ktc/(ktc + 1e-10) = ktc0/(ktc + 1e-10);
ktm/(ktm + 1e-10) = ktm0/(ktm + 1e-10);
kbeta/(kbeta + 1e-10) = kbeta0/(kbeta + 1e-10);
ktdb/(ktdb + 1e-10) = ktdb0/(ktdb + 1e-10);
ksd/(ksd + 1e-10) = ksd0/(ksd + 1e-10);
ki0/(ki + 1e-10) = kp0/(ki + 1e-10);

//Moment Concentrations
EmptyLiveSite/(EmptyLiveSite + 1e-15) = C_EmptyLiveSite*Liq_vol/(EmptyLiveSite + 1e-15);
Lambda0/(Lambda0 + 1e-15) = C_Lambda0*Liq_vol/(Lambda0 + 1e-15);
Lambda1/(Lambda1 + 1e-10) = C_Lambda1*Liq_vol/(Lambda1 + 1e-10);
Lambda2/(Lambda2 + 1e-10) = C_Lambda2*Liq_vol/(Lambda2 + 1e-10);
Mu0/(Mu0 + 1e-10) = C_Mu0*Liq_vol/(Mu0 + 1e-10);
Mu1/(Mu1 + 1e-10) = C_Mu1*Liq_vol/(Mu1 + 1e-10);
Mu2/(Mu2 + 1e-10) = C_Mu2*Liq_vol/(Mu2 + 1e-10);
MuTDB0/(MuTDB0 + 1e-10) = C_MuTDB0*Liq_vol/(MuTDB0 + 1e-10);
MuTDB1/(MuTDB1 + 1e-10) = C_MuTDB1*Liq_vol/(MuTDB1 + 1e-10);
MuTDB2/(MuTDB2 + 1e-10) = C_MuTDB2*Liq_vol/(MuTDB2 + 1e-10);
```

LCB/(LCB + 1e-10) = C_LCB*Liq_vol/(LCB + 1e-10);

//Species Concentrations
for i in ComponentList do
C_Liq(i)/(C_Liq(i) + 1e-10) = x(i)*rho_L/(C_Liq(i) + 1e-10);
C_Vap(i)/(C_Vap(i) + 1e-10) = y(i)*rho_V/(C_Vap(i) + 1e-10);
endfor

//Species Mass Balances
(mass_in("Ethylene")   + rate_Ethylene*MolWt("Ethylene")*Liq_vol)/(mass_in("Ethylene") + 1e-10)
        = tot_mass_out*zm("Ethylene")/(mass_in("Ethylene") + 1e-10);
(mass_in("CAT")   + rate_Cat*MolWt("Cat")*Liq_vol)/(mass_in("CAT") + 1e-10)
        = tot_mass_out*zm("Cat")/(mass_in("CAT") + 1e-10);
mass_in("Solvent")/(mass_in("Solvent") + 1e-10) = tot_mass_out*zm("Solvent")/(mass_in("Solvent") + 1e-10);
(mass_in("H2")   + rate_H2*MolWt("H2")*Liq_vol)/(mass_in("H2") + 1e-10)
        = tot_mass_out*zm("H2")/(mass_in("H2") + 1e-10);

(mass_in("Cocat")   + rate_Cocat*MolWt("Cocat")*Liq_vol)/(mass_in("Cocat") + 1e-10)
        = tot_mass_out*zm("Cocat")/(mass_in("Cocat") + 1e-10);

mass_out("PE")/(mass_out("PE") + 1e-10)
        = (mass_in("Ethylene")   - mass_out("Ethylene"))/(mass_out("PE") + 1e-10);

//Moment Mass Balances
EmptyLiveSite   =   rate_EmptyLiveSite*Liq_vol;
Lambda0   =   rate_Lambda0*Liq_vol;
Lambda1   =   rate_Lambda1*Liq_vol;
Lambda2   =   rate_Lambda2*Liq_vol;
Mu0   =   rate_Mu0*Liq_vol;
Mu1   =   rate_Mu1*Liq_vol;
Mu2   =   rate_Mu2*Liq_vol;
MuTDB0   =   rate_MuTDB0*Liq_vol;
MuTDB1   =   rate_MuTDB1*Liq_vol;
MuTDB2   =   rate_MuTDB2*Liq_vol;
LCB   =   rate_LCB*Liq_vol;

//Polymer Properties

Mn = (C_Mu1 + C_MuTDB1 + C_Lambda1)/(C_Mu0 + C_MuTDB0 + C_Lambda0 + 1e-10)*28.05376;

Mw = (C_Mu2 + C_MuTDB2 + C_Lambda2)/(C_Mu1 + C_MuTDB1 + C_Lambda1 + 1e-10)*28.05376;

PDI*Mn = Mw;

LCBperChain/(LCBperChain + 1e-10) = C_LCB/(C_Lambda0 + C_Mu0 + C_MuTDB0)/(LCBperChain + 1e-10);

LCBper1000C/(LCBper1000C + 1e-10) = 500*C_LCB/(C_Lambda1 + C_Mu1 + C_MuTDB1)/(LCBper1000C + 1e-10);

TDBper1000C/(TDBper1000C + 1e-10) = 500*C_MuTDB0/(C_Lambda1 + C_Mu1 + C_MuTDB1)/(TDBper1000C + 1e-10);

TDBperC/(TDBperC + 1e-10) = 0.5*C_MuTDB0/(C_Lambda1 + C_Mu1 + C_MuTDB1)/(TDBperC + 1e-10);

LCBD/(LCBD + 1e-10) = C_LCB/(C_Lambda1 + C_Mu1 + C_MuTDB1)/(LCBD + 1e-10);

conversion*mass_in("Ethylene")/(conversion + 1e-10) = mass_out("PE")/(conversion + 1e-10);

yield/(yield + 1e-10) = mass_out("PE")/mass_in("CAT")/1000/(yield + 1e-10);

sflowc("C2-SEG")*mass_out("PE") = (mass_out("PE")/MolWt("Ethylene"))*1000;

zmomc/(zmomc + 1e-10) = (Lambda0 + Mu0 + MuTDB0)*1000/(zmomc + 1e-10)/(mass_out("PE") + 1e-10);

Xtdb = C_MuTDB0/(C_MuTDB0 + C_Mu0);

//PCSAFT Predictions
Two_Phase_Flash: call (ym, xm, vf, hmv, hml) = pFlashP (T,P,zm,zmomc,sflowc,smomc,tmomc);
Liquid_Molar_Density: call (rho_L) = pDens_Mol_Liqp (T,P,xm,zmomc,sflowc,smomc,tmomc);
Vapor_Molar_Density: call (rho_V) = pDens_Mol_Vap (T,P,y);
Liquid_Mass_Density: call (rhom_L) = pDens_Mass_Liqp (T,P,xm,zmomc,sflowc,smomc,tmomc);
Vapor_Mass_Density: call (rhom_V) = pDens_Mass_Vap (T,P,y);

//Mass to Moles
moles_in("CAT")/(moles_in("CAT") + 1e-10) = mass_in("CAT")/MolWt("CAT")/(moles_in("CAT") + 1e-10);
moles_in("COCAT")/(moles_in("COCAT") + 1e-10) =
mass_in("COCAT")/MolWt("COCAT")/(moles_in("COCAT") + 1e-10);
moles_in("Ethylene")/(moles_in("Ethylene") + 1e-10) =
mass_in("Ethylene")/MolWt("Ethylene")/(moles_in("Ethylene") + 1e-10);
moles_in("Solvent")/(moles_in("Solvent") + 1e-10) =
mass_in("Solvent")/MolWt("Solvent")/(moles_in("Solvent") + 1e-10);
moles_in("H2")/(moles_in("H2") + 1e-10) = mass_in("H2")/MolWt("H2")/(moles_in("H2") + 1e-10);
moles_in("PE")/(moles_in("PE") + 1e-10)   = mass_in("PE")/MolWt("PE")/(moles_in("PE") + 1e-10);

//Species Mass Out
for i in componentlist do
mass_out(i) = tot_mass_out*zm(i);
endfor

```
//Flow Calculations
tot_mass_in = sigma(mass_in);
tot_mass_in = tot_mass_out;
Liq_Vol + Vap_Vol = Reac_Vol;
Liq_mass + Vap_mass = Reac_mass;
Liq_Vol = rhom_L*Liq_mass;
Vap_Vol = rhom_V*Vap_mass;


//Two Equations to Solve for Two Outlet Flows
tot_mass_out*zm("Ethylene")        = tot_mass_vap_out*ym("Ethylene")        +
tot_mass_liq_out*xm("Ethylene");
tot_mass_out*zm("Solvent")         = tot_mass_vap_out*ym("Solvent")  + tot_mass_liq_out*xm("Solvent");


//Liquid Residence Time
Liq_flow_out      = tot_mass_liq_out/rhom_L;
Tau_liq  = Liq_vol/Liq_flow_out;


//Molecular Weights
MolWt("CAT")            = 327.42126;
MolWt("COCAT")          = 50.0;
MolWt("H2")             = 2.01588;
MolWt("ETHYLENE")       = 28.05376;
MolWt("Solvent")        = 160;
MolWt("PE")             = Mn;


//Convert mass fractions to mole fractions
for i in ComponentList do
denomPcx(i)*MolWt(i) = xm(i);
denomPcy(i)*MolWt(i) = ym(i);
denomPcz(i)*MolWt(i) = zm(i);
endfor
denominatorx = sigma(denomPcx);
denominatory = sigma(denomPcy);
denominatorz = sigma(denomPcz);
for i in ComponentList do
x(i)*denominatorx = xm(i)/MolWt(i);
```

```
y(i)*denominatory = ym(i)/MolWt(i);
z(i)*denominatorz = zm(i)/MolWt(i);
endfor
```

```
//Compute Rates
rate_PE/(rate_PE + 1e-10) = kp*C_Liq("Ethylene")*C_Lambda0/(rate_PE + 1e-10);


rate_Ethylene/(rate_Ethylene + 1e-10) = (-ki*C_Liq("Ethylene")*C_EmptyLiveSite -
kp*C_Liq("Ethylene")*C_Lambda0 - ktm*C_Liq("Ethylene")*C_Lambda0)/(rate_Ethylene + 1e-10);


rate_H2/(rate_H2 + 1e-10) = -kth*C_Liq("H2")*C_Lambda0/(rate_H2 + 1e-10);


rate_Cocat = -kact*C_Liq("Cocat")*C_Liq("Cat")*max_sites - ktc*C_Liq("Cocat")*C_Lambda0;


rate_Cat/(rate_Cat + 1e-10) = (-kact*C_Liq("Cat")*max_sites*C_Liq("Cocat") -
ksact*C_Liq("Cat")*max_sites)/(rate_Cat + 1e-10);


rate_EmptyLiveSite/(rate_EmptyLiveSite + 1e-12) = (kact*C_Liq("Cat")*max_sites*C_Liq("Cocat") +
ksact*C_Liq("Cat")*max_sites - ki*C_Liq("Ethylene")*C_EmptyLiveSite
 + kth*C_Liq("H2")*C_Lambda0 + ktc*C_Liq("Cocat")*C_Lambda0 + kbeta*C_Lambda0 -
ksd*C_EmptyLiveSite)/(rate_EmptyLiveSite + 1e-12);


rate_Lambda0/(rate_Lambda0 + 1e-12) = (ki*C_Liq("Ethylene")*C_EmptyLiveSite - (kth*C_Liq("H2") +
ktc*C_Liq("Cocat") + kbeta + ksd)*C_Lambda0)/(rate_Lambda0 + 1e-12);


rate_Lambda1/(rate_Lambda1 + 1e-10) = (ki*C_Liq("Ethylene")*C_EmptyLiveSite - (kth*C_Liq("H2") +
ktc*C_Liq("Cocat") + kbeta + ksd)*C_Lambda1
 + (ktm*C_Liq("Ethylene"))*(C_Lambda0 - C_Lambda1) + kp*C_Liq("Ethylene")*C_Lambda0 +
ktdb*C_Lambda0*C_MuTDB1)/(rate_Lambda1 + 1e-10);


rate_Lambda2/(rate_Lambda2 + 1e-10) = (ki*C_Liq("Ethylene")*C_EmptyLiveSite - (kth*C_Liq("H2") +
ktc*C_Liq("Cocat") + kbeta + ksd)*C_Lambda2
 + (ktm*C_Liq("Ethylene"))*(C_Lambda0 - C_Lambda2) + kp*C_Liq("Ethylene")*(C_Lambda0 +
2*C_Lambda1)
 + ktdb*(2*C_Lambda1*C_MuTDB1 + C_Lambda0*C_MuTDB2))/(rate_Lambda2 + 1e-10);


rate_Mu0/(rate_Mu0 + 1e-10) = ((C_Liq("H2")*kth + ktc*C_Liq("Cocat"))*C_Lambda0 +
ksd*C_Lambda0)/(rate_Mu0 + 1e-10);


rate_Mu1/(rate_Mu1 + 1e-10) = ((C_Liq("H2")*kth + ktc*C_Liq("Cocat"))*C_Lambda1 +
ksd*C_Lambda1)/(rate_Mu1 + 1e-10);
```

rate_Mu2/(rate_Mu2 + 1e-10) = ((C_Liq("H2")*kth + ktc*C_Liq("Cocat"))*C_Lambda2 + ksd*C_Lambda2)/(rate_Mu2 + 1e-10);

rate_MuTDB0/(rate_MuTDB0 + 1e-10) = ((C_Liq("Ethylene")*ktm)*C_Lambda0 + kbeta*C_Lambda0 - C_MuTDB0*ktdb*C_Lambda0)/(rate_MuTDB0 + 1e-10);

rate_MuTDB1/(rate_MuTDB1 + 1e-10) = ((C_Liq("Ethylene")*ktm)*C_Lambda1 + kbeta*C_Lambda1 - C_MuTDB1*ktdb*C_Lambda0)/(rate_MuTDB1 + 1e-10);

rate_MuTDB2/(rate_MuTDB2 + 1e-10) = ((C_Liq("Ethylene")*ktm)*C_Lambda2 + kbeta*C_Lambda2 - C_MuTDB2*ktdb*C_Lambda0)/(rate_MuTDB2 + 1e-10);

rate_LCB/(rate_LCB + 1e-10) = ktdb*C_Lambda0*C_MuTDB0/(rate_LCB + 1e-10);

End

Chapter 7 Conclusions and Future Work

Robust polymer process models must include consideration for physical and thermodynamic properties, in addition to polymerization kinetics. Physical properties are important because they can affect calculations for volumetric throughput and reactor residence time. Thermodynamic properties are important because they can affect predictions for reactant concentrations in the polymer phase and the reactor heat duty. Models that consider all of these properties are more useful for exploring changes in feed composition or reactor conditions than models that only focus on polymerization kinetics.

Chain-like equations of state, such as the recently developed Perturbed-Chain Statistical Associating Fluid Theory model, provide excellent predictions for physical and thermodynamic properties of polyolefin systems. These include vapor and liquid densities, enthalpies, heat capacities, heats of polymerization, heats of vaporization, and vapor-liquid equilibrium.

We can determine unique sets of kinetic parameters for metal-catalyzed polymerizations using iterative methodologies. The reaction expressions for these systems are highly coupled, and as a result, changing the value for one rate constant can affect several polymer properties simultaneously. We present methodologies for the slurry polymerization of ethylene and the gas-phase polymerization of propylene using Ziegler-Natta catalysts, and the solution polymerization of ethylene using a constrained-geometry metallocene catalyst.

We can model a slurry polyethylene reactor by assuming the polymer is dissolved in the liquid solvent. This allows the model to contain a single reacting phase. Most commercial simulators do not allow the consideration of species that are thermodynamically inert. This approach does not significantly affect the phase behavior of the other species in the reaction mixture.

We can model a stirred-bed reactor for the gas-phase polymerization of propylene using several continuous stirred-tank reactors in series. This approach allows the model to capture the plug-flow behavior of the solids phase, and the constant vapor composition along the reactor length.

There is a need for establishing the reproducibility of experimental data for polymerization phenomena. This would reveal the relative variation in the data due to either fluctuations in reactor conditions or characterization error. Insight about these variations would allow us to more accurately judge discrepancies between model predictions and experimental data.

A recommended area of future work is the consideration of the rheological properties of polymers created using metal-based catalysts. A model that considers the flow properties of a polymer can relate the catalyst behavior in the reactor to the molecular architecture of the resulting polymer. This would be useful in the areas of catalyst and product design.

Acknowledgments

Vita

Neeraj was born and raised in Framingham, Massachusetts, and is the oldest of four brothers. While at Framingham High School, he recognized that he had both talent and interest in the subjects of mathematics and chemistry. It was at this point in time that he decided to pursue a career in chemical engineering. He was inducted into the National Honor Society in his senior year.

In May of 1996, he received a Bachelor of Science in chemical engineering from Worcester Polytechnic Institute in Worcester, Massachusetts. In addition to coursework, he completed a junior-year project on the mitigation of radon gas in the home, and a senior-year project involving gas separation using glass membranes. He maintained weekend and summer jobs throughout his college years to pay for tuition and his car, and through very hard work he achieved an overall grade point average of 3.9. By virtue of his academic excellence, he was inducted into the Tau Beta Pi Honor Society, the Phi Lambda Upsilon Honorary Chemical Society, and the Tau Kappa Lambda Society of Chemical Engineers. He also became a member of the American Institute of Chemical Engineers.

Neeraj felt that his education would be incomplete if he stopped at just a Bachelor's degree. In August of 1997, he enrolled in the Ph.D. program in the Department of Chemical Engineering at Virginia Polytechnic Institute and State University. He joined the research group of Dr. Y. A. Liu, and completed a variety of academic and industrial projects relating to fundamental modeling of polymerization processes. He successfully defended his dissertation, which focused on the modeling of metal-catalyzed polyolefin processes, and received his Ph.D. in December 2003. During his Ph.D. studies, he led three modeling projects involving industrial polymerization processes.

Soon after arriving at Virginia Tech, Neeraj became actively involved with the Graduate Honor System. He served one year as a student panel member, one year as an investigator, and two years as the Chief Justice. Neeraj received a variety of awards and

commendations for his work with the Graduate Honor System. He was elected to Who's Who Among Students in American Colleges and Universities in 2001, and again in 2002. He received an award from the Virginia Tech Center of Excellence in Undergraduate Teaching in 2001 for his participation in the Winter Workshop for Academic Integrity. Finally, he received the Graduate Student Service Commendation Award in 2003.